PATTERN RECOGNITION OF NEURAL DATA: METHODS AND ALGORITHMS FOR SPIKE SORTING AND THEIR OPTIMAL PERFORMANCE IN PREFRONTAL CORTEX RECORDINGS

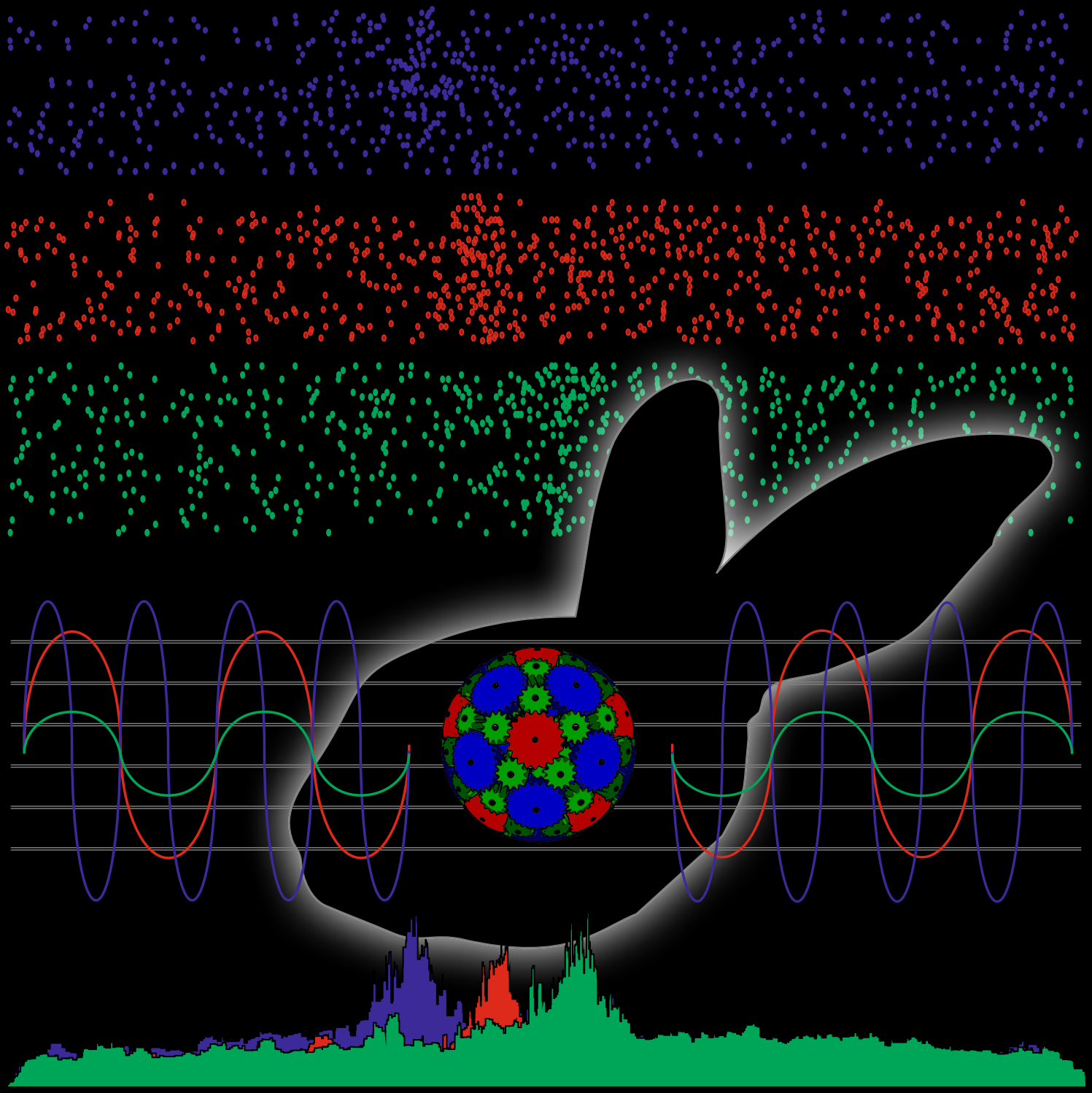

CARMEN ROCÍO CARO MARTÍN

Seville, 2017

Pablo de Olavide University
Department of Physiology, Anatomy and Cell Biology

CARMEN ROCÍO CARO MARTÍN

PATTERN RECOGNITION OF NEURAL DATA: METHODS AND ALGORITHMS FOR SPIKE SORTING AND THEIR OPTIMAL PERFORMANCE IN PREFRONTAL CORTEX RECORDINGS

Doctoral Thesis co-directed by **Dr. Raudel Sánchez Campusano** and **Dr. Agnès Gruart i Massó**

Seville, Spain 2017

Abbreviations: CS, conditioned stimulus; US, unconditioned stimulus; ISI, inter-stimulus interval (or CS–US interval); D_{US}, duration of the US; $ISID_{US} = ISI + D_{US}$, time interval between the beginning of the CS and the end of the US; EMG, electromyographic; O.O., orbicularis oculi muscle; rmPFC, rostro-medial prefrontal cortex

CONTENTS

INDEX

FIGURES

TABLES

EQUATIONS

RESUMEN

El reconocimiento de patrones de descarga neuronales constituye la base electrofisiológica de la caracterización funcional de los procesos cerebrales, por lo que la implementación de un algoritmo de clasificación de espigas es un paso imprescindible para el análisis de los códigos neurales y sus interacciones en una red o en un circuito cerebral. La información extraída de potenciales de acción neurales puede usarse para caracterizar eventos de actividad neural y correlacionarlos con procesos conductuales y cognitivos, incluyendo diferentes tipos de tareas de aprendizaje, como el aprendizaje asociativo. En particular, la extracción de características es un paso crítico en el procedimiento de selección de espigas, que es anterior a la etapa de agrupación y posterior a su detección e identificación en algoritmos de clasificación.

En la presente Tesis Doctoral se propone la implementación de un algoritmo computacional no supervisado, para la detección, identificación y clasificación de potenciales de acción neurales obtenidos a través de registros electrofisiológicos. Los potenciales de acción fueron clasificados en función de características tales como su forma, fase y distribución, las cuales se extrajeron de la derivada de primer orden de los potenciales en estudio. Para implementar el algoritmo, se desarrolló un método alternativo y eficiente de clasificación de espigas que integra el conocido método de clasificación *'K-mean'* con dos medidas de validez de la clasificación (el índice de validación y el índice de error) que permiten verificar tanto la cohesión–dispersión entre los potenciales de acción durante la clasificación, como la agrupación errónea de estos potenciales, respectivamente. Tanto el método como el algoritmo, se integraron en un programa informático personalizado de clasificación de eventos neurales, denominado *VISSOR* (por sus siglas en inglés, *Viability of Integrated Spike Sorting of Real Recordings*). Adicionalmente, se implementó un método de agrupación supervisado para el reconocimiento de patrones específicos de los perfiles de las frecuencias instantáneas de las descargas neurales.

La validez y eficacia del método y del algoritmo desarrollado en esta Tesis Doctoral se puso a prueba mediante la clasificación de potenciales de acción obtenidos en registros extracelulares de la corteza prefrontal rostro-medial de conejos durante el condicionamiento clásico del reflejo corneal. Al comparar el método de clasificación de espigas propuesto en este trabajo con otros métodos también basados en la extracción de características de los potenciales de acción, se observó que éste tuvo un mejor rendimiento durante la clasificación. Es decir, el método y el algoritmo propuestos aquí

permitieron obtener: (1) el número óptimo de grupos de espigas neuronales (gracias al criterio del máximo valor del índice de cohesión-dispersión); y (2) el agrupamiento óptimo de estas espigas (gracias al criterio del mínimo valor del índice de error). La implicación analítica de estos resultados fue que la extracción de características basadas en la forma, la fase y la distribución de las amplitudes de los potenciales de acción, junto con la aplicación de un método alternativo de clasificación no supervisado con índices de validez y de error; garantizan una eficiente clasificación de los eventos neurales, especialmente aquellos detectados desde registros extracelulares o multi-unitarios.

Se empleó un paradigma de demora que consistió en la asociación de un estímulo condicionado (un tono) que comenzó 50, 250, 500, 1000 o 2000 ms antes de otro estímulo incondicionado (un soplo de aire) que co-termina con el primero. Los resultados obtenidos mostraron que la tasa de disparo de cada neurona registrada presentó un solo pico de actividad con una frecuencia dependiente del intervalo entre estímulos (es decir, ≈12 Hz durante 250 ms, ≈ 6 Hz durante 500 ms, y ≈ 3 Hz durante 1000 ms). Curiosamente, las neuronas identificadas de la corteza prefrontal rostro-medial presentaron sus picos de actividad máxima en tres momentos distintos distribuidos uniformemente con respecto al inicio del estímulo condicionado, y también dependiendo de la duración del intervalo entre estímulos (sólo para los intervalos entre estímulos de 250, 500 y 1000 ms). No se registraron respuestas neuronales significativas a intervalos entre estímulos de corta (50 ms) o larga (2000 ms) duración. Los movimientos palpebrales que se registraron con la técnica del seguidor magnético de la posición y la actividad electromiográfica del músculo orbicular de los párpados permitieron constatar que las aceleraciones de las respuestas reflejas y condicionadas del parpadeo presentaron una frecuencia dominante de ≈ 12 Hz. La implicación experimental de este estudio fue que las neuronas de la corteza prefrontal rostro-medial parecen no codificar las propiedades oscilatorias que caracterizan las respuestas condicionadas del parpadeo en conejos. Como conclusión experimental, se podría decir que estas neuronas están muy relacionadas con la determinación del intervalo entre estímulos, específicamente para intervalos de duración definidas en rangos intermedios entre 250-1000 ms.

ABSTRACT

Pattern recognition of neuronal discharges is the electrophysiological basis of the functional characterization of brain processes, so the implementation of a Spike Sorting algorithm is an essential step for the analysis of neural codes and neural interactions in a network or brain circuit. Extracted information from the neural action potential can be used to characterize neural activity events and correlate them during behavioral and cognitive processes, including different types of associative learning tasks. In particular, feature extraction is a critical step in the spike sorting procedure, which is prior to the clustering step and subsequent to the spike detection-identification step in a Spike Sorting algorithm.

In the present doctoral thesis, the implementation of an automatic and unsupervised computational algorithm, called 'Unsupervised Automatic Algorithm', is proposed for the detection, identification and classification of the neural action potentials distributed across the electrophysiological recordings; and for clustering of these potentials in function of the shape, phase and distribution features, which are extracted from the first-order derivative of the potentials under study. For this, an efficient and unsupervised clustering method was developed, which integrate the *K*-means method with two clustering measures (validity and error indices) to verify both the cohesion-dispersion among neural spike during classification and the misclassification of clustering, respectively. In additions, this algorithm was implemented in a customized spike sorting software called *VISSOR* (*Viability of Integrated Spike Sorting of Real Recordings*). On the other hand, a supervised grouping method of neural activity profiles was performed to allow the recognition of specific patterns of neural discharges.

Validity and effectiveness of these methods and algorithms were tested in this doctoral thesis by the classification of the detected action potentials from extracellular recordings of the rostro-medial prefrontal cortex of rabbits during the classical eyelid conditioning. After comparing the spike-sorting methods/algorithms proposed in this work with other methods also based on feature extraction of the action potentials, it was observed that this one had a better performance during the classification. That is, the methods/algorithms proposed here allowed obtaining: (1) the optimal number of clusters of neuronal spikes (according to the criterion of the maximum value of the cohesion-dispersion index) and (2) the optimal clustering of these spike-events (according to the criterion of the minimum value of the error index). The analytical

implication of these results was that the feature extraction based on the shape, phase and distribution features of the action potential, together with the application of an alternative method of unsupervised classification with validity and error indices; guaranteed an efficient classification of neural events, especially for those detected from extracellular or multi-unitary recordings.

Rabbits were conditioned with a delay paradigm consisting of a tone as conditioned stimulus. The conditioned stimulus started 50, 250, 500, 1000, or 2000 ms before and co-terminated with an air puff directed at the cornea as unconditioned stimulus. The results obtained indicated that the firing rate of each recorded neuron presented a single peak of activity with a frequency dependent on the inter-stimulus interval (i.e., ≈ 12 Hz for 250 ms, ≈ 6 Hz for 500 ms, and ≈ 3 Hz for 1000 ms). Interestingly, the recorded neurons from the rostro-medial prefrontal cortex presented their dominant firing peaks at three precise times evenly distributed with respect to conditioned stimulus start, and also depending on the duration of the inter-stimulus interval (only for intervals of 250, 500, and 1000 ms). No significant neural responses were recorded at very short (50 ms) or long (2000 ms) conditioned stimulus-unconditioned stimulus time intervals. Furthermore, the eyelid movements were recorded with the magnetic search coil technique and the electromyographic (EMG) activity of the orbicularis oculi muscle. Reflex and conditioned eyelid responses presented a dominant oscillatory frequency of ≈ 12 Hz. The experimental implication of these results is that the recorded neurons from the rostro-medial prefrontal cortex seem not to encode the oscillatory properties characterizing conditioned eyelid responses in rabbits. As a general experimental conclusion, it could be said that rostro-medial prefrontal cortex neurons are probably involved in the determination of CS-US intervals of an intermediate range (250-1000 ms).

1. INTRODUCTION

The performing of an analytical approach in Neuroscience involves deepening in biophysical-mathematical/computational methods and/or models which help to understand neural processes, and therefore to understand different meaningful aspects about the functional states of the brain (Silva, 2011). However, the analytical approach alone does not guarantee direct applicable results in the experimental framework; therefore, it is essential to link this together with the experimental approach. In other words, it is necessary that the proposed biophysical-mathematical method operates directly on the experimental data (i.e., a phenomenological model); otherwise, it would be a mere simulation (i.e., a computational model). In summary, it is an effective way of integrating both tendencies (analytical and experimental) into a single optimized analytical-experimental approach (Sánchez-Campusano, 2007).

In Neuroscience, an analytical-experimental approach must provide relevant information about: (1) how the organism detects sensory information; (2) how such information is integrated and processed in the brain; and (3) how the output of each processing results in meaningful decision-making and behaviors by the organism to allow it to function and thrive in interaction with its environment (Silva, 2011). Therefore, the analytical-experimental approach should help to corroborate empirically obtained results, to verify previous hypotheses and to provide improvements to the experimental design, and raise new questions and answer them more effectively. The main advantages of this type of approach (analytical and experimental) consist in to integrate all these aspects (Sánchez-Campusano et al., 2012).

1.1. Electrophysiological aspects of the analytical-experimental approach

It is known that in *in vivo* neurophysiology studies, involving chronic experiments in alert behaving animals, there have still not specific electrophysiological tools to record a single neuronal action potential (or unitary spike) and isolate it from background noise in a specific time window. Nevertheless, there are simultaneous strategies of intracellular and extracellular recording from the same neuron, which allow the characterization of their discharge pattern by correlating both type of recordings (Harris et al., 2000; Henze et al., 2000). However, this procedure is performed at a very low scale and it is not possible to extend it to study neuronal populations.

Notice that chronically recording from each neuron of the brain to understand its functioning is an unreasonable idea since the electrical recording of individual neurons is an invasive process and causes a noticeable damage in the brain tissue, greatly

affecting the functional dynamics of established circuits (Buzsáki, 2004). Therefore, the unitary/intracellular recording presents clear limitations for the study of cooperative activity of different neurons in the same area or among different brain areas, and therefore to understand the processes of synchronization among neuronal populations that determine most of the cognitive states and of behavior.

In absence of unitary/intracellular recordings during experiments *in vivo* or *in vitro* (slice studies), it is only possible to record extracellular electrical potentials that represent the simultaneous electrical activity of an unknown number of neurons (Thakur et al., 2007). This is because the physical properties (conductivity and resistivity/impedance) of the electrodes are limited and the spatial resolution of them (sensor diameter, mechanical stability, distance and orientation relative to the source) is not sufficient to detect unit activity. In this way, the activity of the neuron closest to the electrode and of its nearest neighbours is recorded, plus the background noise of the extracellular recording which generally occurs in a mid-low signal-to-noise ratio (Kim and Kim, 2003; Quian-Quiroga, 2004; Scanziani and Häusser, 2009).

The basic hypotheses that should be taken into account for the characterization of the action potentials of extracellular recordings are:

(1) Neurons which are at the same distance from the electrode and with an equivalent orientation produce action potentials of equal magnitude.
(2) All the spikes of the same neuron are characterized by a similar amplitude-time waveform.
(3) The shape of the action potential is unique and is preserved in magnitude and duration for each neuron from a noise-free stationary recording.

However, the shape of an action potential depends on the distance and orientation relative to the exact position of the electrode, its mechanical stability and its electrical properties. Also depends on other factors, no less important, such as the morphology of the dendritic tree, the electrical properties of the neuronal membrane, the presence and distribution of glia cells, as well as, the stationarity of the extracellular recording and the resulting signal-to-noise ratio. In addition to the external electronic noise, extracellular and intracellular noises that produce intrinsic variations in the shape of the action potential and slow-wave noises present in the recordings when the subject moves freely or due to the generation of evoked potentials are recorded. Note that if the extracellular recording is stationary and free of noise, it implies assuming that the shape and magnitude of the action potential is well-preserved over time, but this affirmation

cannot be verifiable for an electrophysiological recording. Cellular properties evolve temporarily causing neuronal ensembles to change over time and in relation to stimuli, therefore it cannot be guaranteed experimental conditions in the absence of background noise. All these factors make the contaminated/masked recorded spike not fit exactly to its true waveform (Buzsáki, 2004; Brown et al., 2004; Quian-Quiroga et al., 2007a).

In this way, a new problem arises when extracellular activity is recorded in a particular brain area, which involves taking from the raw recording (signal + noise) the trains of individual action potentials corresponding to the different neurons. In this experimental situation, the action potentials must be identified, the number of involved neurons must be determined, and each detected spike must be assigned to the neuron that produces it. This procedure that may seem simple, certainly leads to new difficulties (Lewicki, 1998; Constantinidis and Goldman-Rakic, 2002; Klausberger et al., 2003; Ison et al., 2011), which raise the following questions:

(1) What happens when the neurons that are firing their action potentials are at a similar distance and orientation from the electrode?
(2) How to classify spikes with similar peak amplitudes but with different time-amplitude waveforms?
(3) How to classify spikes with similar waveforms but with different peak amplitude?
(4) What happens when several neurons discharge simultaneously or with a small delay among them?
(5) How to identify overlapping discharges generated by the sum of the simultaneous spikes from different neurons?
(6) How can be extracted a determined action potential from the overlapping recording or from a complex spike pattern of multiunitary activity?
(7) How to distinguish action potentials between principal neurons (pyramidal cells) and non-principal neurons (interneurons) based on the waveform and temporal course of the spikes from the extracellular recording?
(8) How can one specific neuron class be differentiated from another class?
(9) How to assign different spikes to neurons of similar cellular morphology if the extracellular recordings are performed with multiple electrodes where the relative positions between neurons and electrodes are changing?

1.2. Spike sorting for extracellular/multi-unitary recordings

The aforementioned problem is still unresolved from a pure electrophysiological approach, therefore for some years (Aksenova et al., 2003; Zhang et al., 2004; Chibirova et al., 2005; Chan et al., 2008a; 2008b) a number of analytical approaches (biophysical-mathematical/computational methods and/or models) has been developed. The integration of these methods/models into a common mathematical/computational tool known as spike-sorting, allows the detection, identification and classification of multi-unitary activity in a specific and limited brain area. In addition, the spike-sorting methods enable the characterization of the different neural activity patterns of the registered neurons in different brain areas (Vargas-Irwin and Donoghue, 2007; Porras-García et al., 2010). Currently, the pattern recognition of different neuronal discharges constitutes the electrophysiological base of the functional characterization of the cerebral processes. Therefore, the implementation of a spike-sorting algorithm is an essential step for the analysis of neural codes and the neural interactions in a network or cerebral circuit (**Figure 1**). In summary, the accuracy of the implemented spike-sorting algorithm critically affects the accuracy of all successive analyses relative to the electrophysiological characterization of the neural process, as well as the reliability of the results and their interpretations (Brown et al., 2004; Ventura, 2009a; Quian-Quiroga, 2012).

At present several spike-sorting algorithms are used but there is not a consensus about which of them is better, since it depends on the adaptability of the algorithm to the studied experimental situation. Different algorithms applied on the same electrophysiological recording provide different results during the classification, and on the other hand, different algorithms applied to different electrophysiological recording can provide similar clustering results. In general, spike-sorting algorithms encompass from non-parametric approaches such as *K*-means (Salganicoff et al., 1988) and neural networks (Ohberg et al., 1996) to probabilistic and Bayesian approaches based on clustering using mixed distributions (Lewicki, 1994; Wood et al., 2006; Ventura, 2009b).

All the spike-sorting approaches can be grouped in two blocks. In the first block, the spike separation is performed based on the variation of the waveform of the action potential (amplitude-time profile of the spike) under the assumption that neighbouring neurons generate spikes with invariant features (Aksenova et al., 2003; Zhang et al., 2004; Chibirova et al., 2005; Chan et al., 2008a; 2008b; Paraskevopoulou et al., 2013).

In the second block, the spikes of the extracellular recording emanate from point sources (McNaughton et al., 1983; Gray et al., 1995) and not from the complex geometry of neurons. This assumption is controversial and is based on: (1) the extracellular action potential results from the sum of the integrated micro-potentials from the soma and from the long proximal dendrites; and (2) the parameters of the extracellularly recorded spike change with the magnitude of the action potential propagation and with other variations of the membrane potential which are dependent on specific states and behaviors (Buzsáki, 2004; Pedreira et al., 2012).

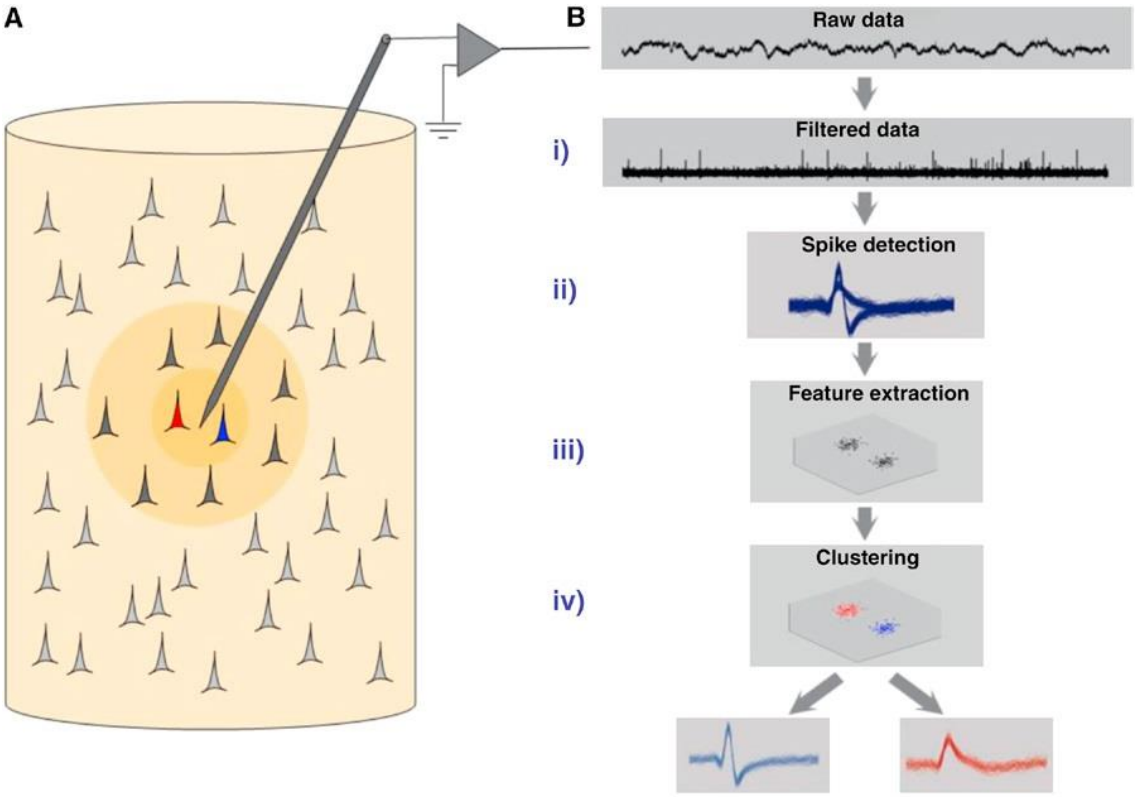

Figure 1. Extracellular recordings and spike sorting. (**A**) The extracellular activity of neurons is recorded with microwires inserted in the brain. The spikes of neurons close-by the electrode tip (in red and blue) can be separated via spike sorting; neurons further away (in dark grey) can be detected but not sorted, thus generating the multiunit activity; more distant neurons (in light gray) contribute to the background noise. (**B**) Steps of a standard Spike Sorting algorithm: i) obtaining the filtered register (for example, bandpass FIR of [400, 3000] Hz) from the raw extracellular recording, ii) detection of the spikes after the application of an amplitude threshold or a winding algorithm, iii) extraction of the most relevant features with reduction of dimensionality and formation of feature vectors (FV), and iv) classification of the different spikes based on the variability of the amplitude, duration and shape of the action potential. Modified and adapted from Quian-Quiroga et al. (2004).

In other words, the extent of the somatodendritic propagation of the action potential varies depending on the excitatory and inhibitory inputs/outputs of the neurons. Therefore, the point source model is a questionable idea because according to

this, different parts of the neuronal membrane are able to generate action potentials that emanate from different point sources, when in fact; they are different neuronal events (discharges) from the same neuron (Llinás, 1988; Buzsáki and Kandel, 1998).

1.3. Spike sorting based on the waveform of the action potential

Spike sorting approaches have received intensive attention in neurophysiology and multiple alternative solutions have been proposed during the past few years (Balasubramanian and Obeid, 2011; Bestel et al., 2012; Kamboh and Mason, 2013; Jahanmiri-Nezhad et al., 2014; Rey et al., 2015; Fournier et al., 2016; Leibig et al., 2016; Werner at al., 2016).

Some studies on spike sorting have been concerned with simplifying the common steps of sorting processes based on mathematical transformations of the raw neural recording to obtain a new signal that would discriminate among spike waveforms originating from different neurons, which presumably correspond to different groups (Charbiwala et al., 2011; Thorbergsson et al., 2014; Petrantonakis and Poirazi, 2015).

According to that approach, the common spike-detection and spike-identification steps have been simplified, reducing the computational costs in function of their execution times, but other non-common steps (e.g., raw signal segmentation, local maxima selection, and noisy spike discrimination) were inevitably introduced in the spike-sorting process.

In other published works, the focus of attention has been on the feature extraction methods (see **Table 1** for details). These methods are mainly focused on extracting various features in relation to the spike waveform (waveform-based features) to be able to interpret physiologically the obtained results.

Table 1. Overview of other spike sorting algorithms based on feature extraction. Note that, in general, the authors cited here have only used three (F_{14}, F_{18} and F_{19} common features) of the 24 features (F_1 – F_{24}) proposed in the unsupervised automatic algorithm (**Table 2**).

Author / Year	Number of Features / Description	Classification
Gibson et al. (2008, 2012)	2 Areas under the positive (integral I_P) and negative (integral I_N) phases of the action potential, that is – the Integral Transform (IT).	Fuzzy C-means clustering.
Jahanmiri-Nezhad et al. (2014)	2 Peak-to-valley amplitude of the action potential, and the area under the curve (sum of absolute values).	*K*-means clustering and Gaussian mixture model estimation.
Kamboh and Mason (2013); Saeed and Kamboh (2013)	2 Zero Crossing Features (ZCF) of the spike. ZC1 (the sum of all the values before zero-crossing) and ZC2 (the sum of values after zero-crossing).	*K*-means and Mahalanobis distance.
Zviagintsev et al. (2005)	2 Integral Transform (IT). Discrete and normalized spike integrals I_P and I_N.	Segmented Principal Component (PC) algorithm and PC Analysis (PCA).
Lewicki (1998)	3 Positive peak amplitude of the spike, peak-to-valley amplitude, and the waveform duration.	*K*-means with Euclidean distance and Scaled PC score.
Yang et al. (2008)	3 Positive peak amplitude of the spike, and the positive [F_{14}] and negative peaks of the spike first derivative (FD).	WaveClus – PCA.
Paraskevopoulou et al. (2013; 2014)	3 Positive peak [F_{14}] of the spike FD, and the positive [F_{18}] and negative [F_{19}] peaks of the spike second derivative (SD).	10-iteration *K*-means with Squared Euclidean metric.
Yang et al. (2014)	3 Integral of repolarization (IR) of the spike, and the positive [F_{14}] and negative peaks of the spike FD.	20-iteration *K*-means using Euclidean metric.
Balasubramanian and Obeid (2011)	5 Spike power, spike amplitude range, negative and positive deflections, and the spike gradient slope.	Fuzzy logic-based feature extraction system.
Sonoo and Stalberg (1993)	5 Peak-to-valley amplitude of the spike, waveform duration, negative Integral Transform (nIT), ratio (nIT/maximum peak), and the logarithm of the maximum rise of the spike.	Nearest neighbor methods for discriminant analysis.
Su et al. (2013)	6 Spike peak amplitude, peak roundness (i.e., the spike peak [F_{19}] of the SD), the root-mean-square of pre-spike amplitude, the highest repolarization rate, the afterhyperpolarization (i.e., afterspike minimum), and the correlation coefficient between the spike and the reference waveform.	*K*-means clustering and PCA.
Bestel (2012)	7 Positive and negative peaks of the action potential, left and right spike angles, negative and positive signal energy of a continuous-time signal, and the core spike duration.	Expectation maximization (EM) method using Gaussian basis functions.
Stewart et al. (2004)	7 Peak-to-valley amplitude of the spike, waveform duration, trailing waveform duration, leading waveform aspect ratio, trailing waveform aspect ratio, waveform transition slope, and event duration.	Nearest neighbor methods for discriminant analysis.

Most of the features used by different authors in previous works can be separated in the following blocks:

(1) Shape-based features: these physiological features were directly extracted from the detected action potential (Sonoo and Stalberg, 1993; Lewicki, 1998; Stewart et al., 2004; Balasubramanian and Obeid, 2011; Bestel, 2012; Su et al., 2013; Jahanmiri-Nezhad et al., 2014; Yang et al., 2014). In this block, the most common shape-based features were the peak-to-valley amplitude, the waveform duration, and the maximum rise of the action potential (**Figure 2**). After studying the algebraic definitions of these features and the correlations among them, many authors began to apply the logarithm as a way to prevent dependencies (multi-collinearity) among the shape-based features (Sonoo and Stalberg, 1993).

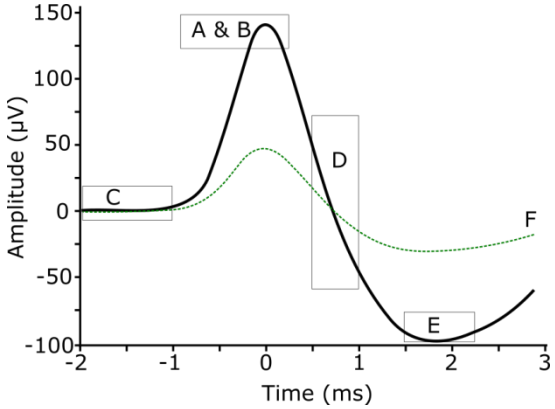

Figure 2. Extraction of spike waveform features. Squares enclose the waveform segments (solid line) that are used to evaluate spike peak amplitude (A), peak roundness (B), prespike amplitude (C), repolarization rate (D), afterhyperpolarization (E), and correlation coefficient (F) with a reference spike waveform (dashed line) are showed. Modified and adapted from Su et al. (2013).

(2) Phase-based features: these physiological features were extracted of the trajectory of the action potential in the phase-space, which was obtained as the representation of the second-order derivative versus first-order derivative of the amplitudes each neuronal spike (Yang et al., 2008; Paraskevopoulou et al., 2013; 2014; Su et al., 2013; Yang et al., 2014). In this block, the features more highlighted were the positive and negative peaks of the first-order and second-order derivatives of the spike-event (**Figure 3**).

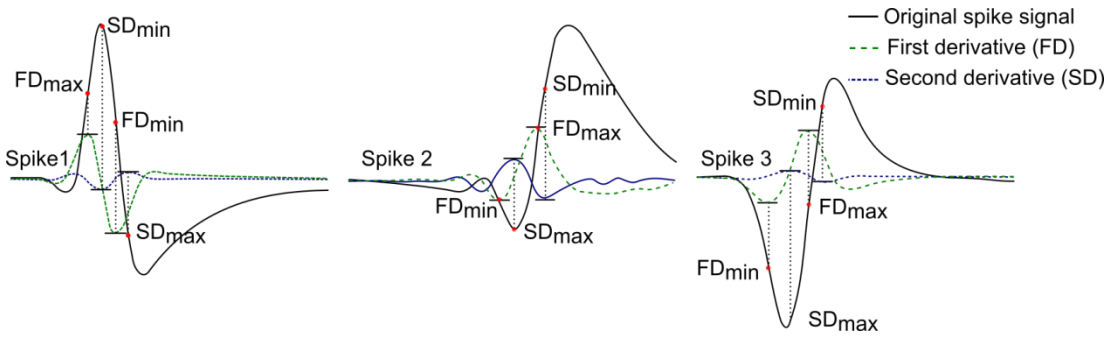

Figure 3. Typical action potential waveforms with their first-order and second-order derivatives. Annotated onto the original spike waveforms are the points corresponding to the extrema (i.e. minimum and maximum) of the first-order and second-order derivatives (FD and SD, respectively). Modified and adapted from Paraskevopoulou et al. (2013; 2014).

(3) Geometric-based features: these features were based on the calculation of the area under the curve of the spike waveform (Zviagintsev et al., 2005; Kamboh and Mason, 2013; Saeed and Kamboh, 2013; Jahanmiri-Nezhad et al., 2014). The most used were the areas under the positive (integral I_P) and negative (integral I_N) phases of the action potential, called Integral Transform (IT) (Gibson, 2008; 2012), and the Zero Crossing Features (ZCF) (Kamboh and Mason, 2013; Saeed and Kamboh, 2013; Yang et al., 2014) of the action potential (**Figure 4**). In this block, the features more highlighted were ZC1 (the sum of all the values before zero-crossing) and ZC2 (the sum of values after zero-crossing).

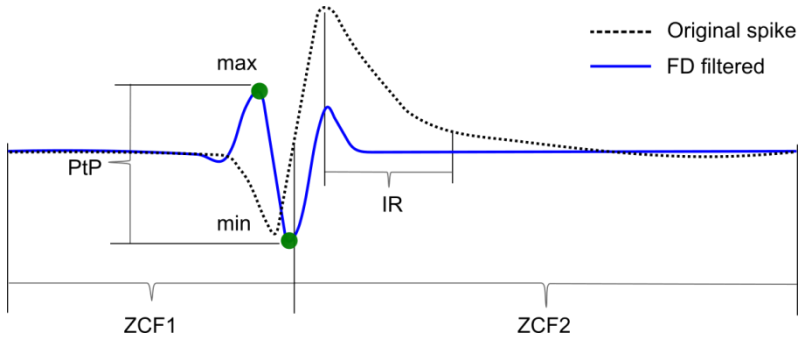

Figure 4. Graphical representation of zero crossing features for an original spike and for the first-order derivative (FD) of the same filtered spike. The features: peak-to-peak (PtP) amplitude, integral of repolarization (IR) and the minimum and maximum peaks are showed. A spike is detected when either threshold is crossed. A ZCD detects when the zero level is crossed. ZCF1 is the sum of all the values before zero-crossing and ZCF2 is the sum of values after zero-crossing. Since the spikes are aligned according to their onset as detected by the spike detector, different spike shapes have different zero-crossing locations. Thus, the number of samples in ZCF1 and ZCF2 varies for all the spikes. Modified and adapted from Yang et al. (2014).

(4) Transformation-based features: these features were based on coefficients, factors, or components extracted of different mathematical transformations. The wavelet transform was one of the most popular transformation-based features, which is directly applied on the points of the spike waveform. Normally, the resulting wavelet coefficients of the third iteration were used (Quian-Quiroga, 2004; Bestel,

2012). Another transformation used directly on the points of the spike waveform was the principal components analysis (PCA). In previous works (Zviagintsev et al., 2005; Su et al., 2013), the second or third principal components were used for forming the feature vectors. The resulting vectors were an uncorrelated orthogonal basis set. However, principal components analysis was sensitive to the relative scaling of the original variables. Therefore, the transformation-based features were very useful for spike detection and classification but require analytical expertise for an appropriate because those coefficients and/or components were not directly recognizable electrophysiological features of the spike-event.

On the other hand, there are features based on the amplitude distributions of the spike-event that have not been applied for spike sorting from neuronal activity recordings and that usually give good results when these have been employing to other neural signals (neurograms). In particular, some of the distribution-based features may be useful in detecting wavelet coefficients related to neural bursts of raw muscle sympathetic nerve activity (MSNA neurogram). For example, local kurtosis was an optimal method to separate pure noise wavelet coefficients from those associated with MSNA bursts (Brychta et al., 2007). In general, during period of moderate and high burst rates, the tails of the probability density function become progressively heavier and the amplitude distribution was non-normal, but during periods of neural silence (noise-related epochs), the distribution was nearly normal (or Gaussian). However, to our knowledge, the distribution-based features have not been applied to spike sorting from extracellular recordings of neuronal activity. As supported by a previous study (Caro-Martín et al., 2015) and according to the present Doctoral Thesis, the distribution-based features were very powerful during the spike-classification from the rostro-medial prefrontal cortex (rmPFC) extracellular activity.

In general, the extracted features get together for forming high-dimensionality vectors. Too often, misapplication of the feature extraction step leads to an extreme reduction of dimensionality of these feature vectors, and therefore, the resulting feature matrices correspond with “abstract” mathematical entities (based on coefficients, factors, or components) that do not reflect the meaningful functional properties of the neural events under study. One of the most applied transformations to reduce the feature vector dimensionality is the Principal Component Analysis (Yang et al., 2008).

However, some of the most cited works (Letelier and Weber, 2000; Jarvis and Mitra, 2001; Buzsáki, 2004; Quiroga et al., 2004; Ventura, 2009; Einevoll et al., 2012)

and many recent studies (Kapucu et al., 2016; Knieling et al., 2016; Leibig et al., 2016; Regalia et al., 2016; Swindale and Spacek, 2016) on the spike sorting continue to emphasize in the effort to develop robust and non-redundant spike-sorting algorithms based on the exhaustive extraction of features with a clear physiological description of the spike-event. This physiological information of the spike-event is highly appreciated in the qualitative and quantitative characterization of the neuronal activity (intracellular, extracellular or multi-electrode-array recordings) and have practical uses in neurophysiology beyond the mere spike classification (Sánchez-Campusano et al., 2007; 2009; Porras-García et al., 2010; Caro-Martín et al., 2015; Kapucu et al., 2016). In particular, extracellular microelectrode recordings can include action potentials from multiple neurons. As the microelectrode tip is surrounded by many neurons, it detects the occurrence of the electrical events generated by all nearby neurons. To separate spikes from different neurons, they can be sorted according to a systematic comparison among spike feature vectors.

1.4. Application of a spike sorting approach on an experimental model

An important aspect in electrophysiological studies is the classification of principal and non-principal neurons from an extracellular recording. These two general types of neurons are very well characterized anatomically, but their anatomy-functional correlates are subject to the exhaustive characterization of the discharges generated by each of them and by the precise identification and classification of their action potentials. In order to do so, different electrophysiological features determined by the shape of the action potentials, their fundamental amplitudes and peaks, the spikes timing latencies, their refractory periods and the magnitude of their instantaneous frequencies (neuronal firing rates) are studied and considered in a spike sorting approach (Stevenson and Kording, 2011).

The most important studies on the recognition of specific discharge patterns for principal (pyramidal) and non-principal (interneuron) neurons have been performed in brain regions such as the neocortex and the medial temporal lobe. In the neocortex, the firing rates of pyramidal neurons and interneurons of the motor cortex (Buzsáki and Kandel, 1998), and in the somatosensory and prefrontal cortex (Barthó et al., 2004) of rats, as well as, in the somatosensory bark of rabbits (Swadlow, 2003) and in the dorsolateral prefrontal cortex of primates (Constantinidis and Goldman-Rakic, 2002). In the medial temporal lobe, firing patterns of pyramidal neurons and interneurons have

been identified by spike sorting approaches in the amygdala, the entorhinal cortex, the posterior parahippocampal cortex, and in the human hippocampus (Harris et al., 2000; Viskontas et al., 2007), and rats (Csicsvari et al., 1999; Harris et al., 2000; Henze et al., 2000; Klausberger et al., 2003).

1.4.1. Structure under study: rostro-medial prefrontal cortex

The prefrontal cortex occupies part of the frontal lobe centred in front of the motor area and represents the highest level in the hierarchical organization of the cortex (**Figure 5**). In addition, three topographic regions are distinguished in it: (1) ventrolateral, (2) medial and orbital, and (3) dorsal, which is divided in two regions: dorsolateral and dorsomedial regions. The prefrontal cortex is involved in the proper timing, representation, selection, and execution of intentional behaviors and in a set of cognitive processes such as anticipation, choice of objectives, planning, behaviour selection, self-regulation, self-control and feedback (Damasio, 1994; Fuster, 1997; 2001; Kolb and Whishaw, 1999). In additions, Fuster (1988; 1995) in his general theory on the prefrontal cortex considered the temporal structuring of behavior as fundamental. Therefore, he proposed three subordinate functions that must be coordinated: (1) a provisional retrospective short-term memory function; (2) a prospective behaviour-planning function; and (3) a function of controlling and suppressing internal and external influences which interfere with behaviour.

Although functions of the prefrontal cortex cannot be easily ascribed to specific sites, the dorsolateral aspects of the prefrontal cortex seem to be more related to the sustained neuronal firing underlying working memory processes, to the discriminative components of cognitive phenomena and two-interval discrimination (Romo et al., 1999). In contrast, both medial and orbital prefrontal cortex are involved in the emotional component of selected behaviours, including associative (pavlovian/classical and instrumental) conditionings (Powell et al., 1996; Corbit and Balleine, 2003; Weiss and Disterhoft, 2011; Jurado-Parras et al., 2012).

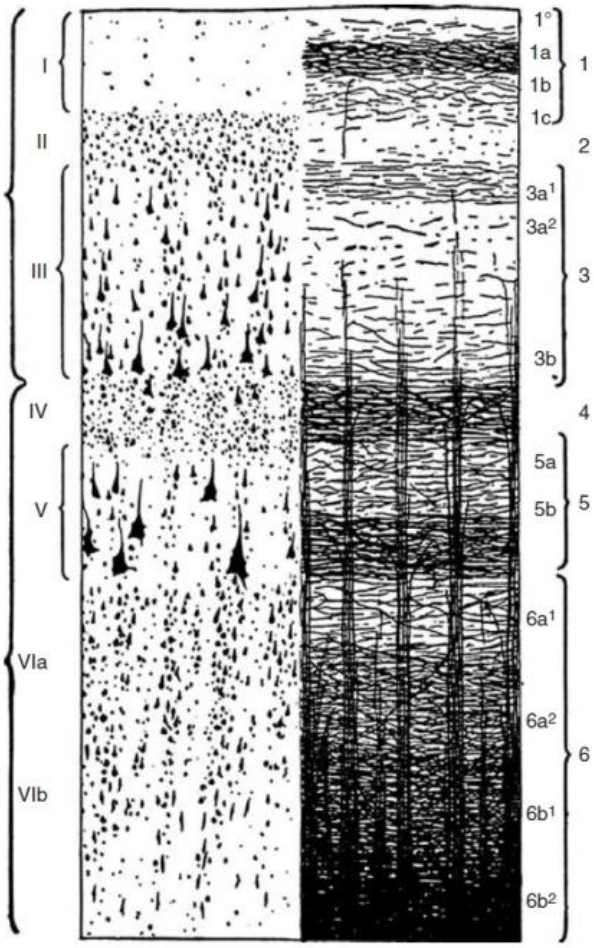

Figure 5. The cellular and myelin structure of the cortex. The structure is showed according to Brodmann (1909) and Vogt (1906). Modified and adapted from Fuster (2008).

In particular, the medial prefrontal cortex is involved in stimulus salience, sustained attention (Weible et al., 2003), and/or the integration of learned emotional changes (Powell et al., 1996), whereas the orbital prefrontal cortex participates in the selection of appropriate motor actions, exerting an inhibitory control on general motility (Sauerland et al., 1967; Fuster, 1997).

Although the involvement of the medial prefrontal cortex in associative learning is well documented, the specific roles of its rostral and caudal parts are not yet well established. The involvement of caudal-medial prefrontal cortex areas in different aspects of the acquisition, reversal, and retrieval of classical eyeblink conditioning using trace paradigms is well established (Kronforst-Collins and Disterhoft, 1998; Powell et al., 2005). Moreover, the caudal-medial prefrontal cortex seems to be necessary when weak unconditioned stimuli are used and during partial reinforcement, trace conditioning reversal and conditioning retrieval (Powell et al., 1996; Kronforst-Collins and Disterhoft, 1998; Weible et al., 2003).

In contrast, it has been reported that the rostro-medial prefrontal cortex inhibits the expression of reflex and conditioned eyelid responses potently without affecting the latent acquisition of conditioned responses (Leal-Campanario et al., 2007) and be involved in different motor, emotional, and/or cognitive functions (Leal-Campanario, 2007). Earlier studies indicated that the electrical stimulation of the orbital prefrontal cortex inhibits spinal reflexes in cats (Sauerland et al., 1967) and that lesions of the medial prefrontal cortex evoke hyperactivity and resistance to extinction of acquired motor abilities in rabbits (Weible et al., 2000; Kolb et al., 2004). Therefore, the rostro-medial prefrontal cortex could play an important role in the expression of motor responses, including reflexively evoked blinks and conditioned responses. In addition, the neuronal firing which underlies to the functions of the rostro-medial prefrontal cortex could be related to the classical eyeblink conditioning, as is the case for the caudal-medial prefrontal cortex areas.

1.4.2. Experimental context: classical eyeblink conditioning

The physiological mechanisms that underlie learning have been successfully addressed and in a large extent by classical conditioning. The classical conditioning is one of the simplest forms of associative learning, which is based on the assumption that ideas and experiences reinforce one another and can be linked to enhance the learning process.

Classical conditioning was first demonstrated by Ivan Pavlov, which developed a procedure for surgically implanting a tube, called a fistula, into living animals (**Figure 6A**). This allowed him to discover that the animal varied the amount of salivary secretion in function of different experimental situations. Specifically, Pavlov observed that gastric secretions were produced with the contact of the food during the digestion process and also with the only presences of the collaborator which gave him to eat (Pavlov, 1927). After developing various experiments, Pavlov understood that (1) by repeating the food (meat) presentations several times, the dog salivated to all of them; and (2) by repeatedly touching a bell just before presenting the meat (the sound slightly preceded the presentation of the food), the animal came to associate the sound of the bell with the presentation of the meat, and it would begin to salivate when the bell started to ring. In addition, for a while the dog would even salivate if the bell was rung but no food was presented (**Figure 6B**). In the paradigm of Pavlov, he used a stimulus capable of producing a response by himself. This stimulus was the meat which normally elicits salivation without experimenter intervention (it is a reflex response) and was called unconditioned stimulus (US) which causes an unconditioned response. He also

used a stimulus that did not produce any response in the animal for itself which was the bell. This stimulus elicits salivation only if repeatedly paired with the meat and it is termed the conditioned stimulus (CS). In addition, the salivation evoked by the sound of the bell is termed the conditioned response (**Figure 6B**). This is the basis of classical conditioning: the association of a conditioned stimulus with an unconditioned stimulus so that the first stimulus produces a similar response to the produced by the second stimulus alone.

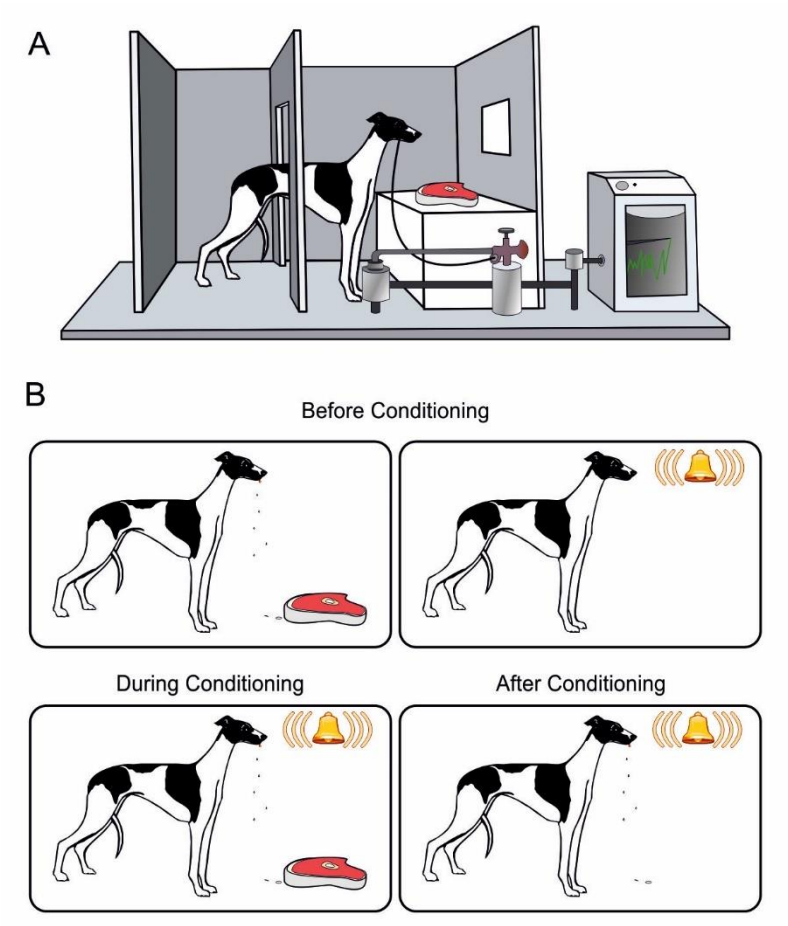

Figure 6. Representation of the experiments performed by Ivan Pavlov. (**A**) Dogs were taken into a room for the training session and they were prepared for the extraction of the salivary fluids. (**B**) The classical conditioning paradigm proposed by Pavlov had three blocks: (1) Before Conditioning, in which the dogs received a stimulus (unconditioned stimulus) that evoked a reflex (unconditioned) response. He used food that produced salivation and a neutral stimulus for this response (bell sound); (2) During Conditioning, both stimuli closely paired and dogs salivated; and finally (3) After Conditioning, only the bell sound that now produced the salivation of the animals. This last step demonstrated that the tone had become a conditioned stimulus that produced salivation (now a conditioned response).

Since Pavlov, various forms of classical conditioning have been developed. One of the most used for the study of the physiology of learning is the classic conditioning of eyelid responses which was initially proposed by Gormezano in the mid-20th century in rabbits (Moore and Gormezano, 1961; Gormezano et al., 1962). The contribution of Gormezano and his collaborators is noteworthy in this field, since they performed the

necessary modifications in the Plexiglas restraining box and in the stimuli system to improve the recordings of classical conditioning in the albino rabbit model. In their experiments they measured eyeball retraction (Deaux and Gormezano, 1963), nictitating membrane movement (Moore and Gormezano, 1961; Gormezano et al., 1962), and developed very accurate protocols for classical eyeblink conditioning in albino rabbit (Schneiderman et al., 1962). The passive response of nictitating membrane movements, in opposition to the active and complex character of the response of the eyelid motor system, makes this latter more suitable for the study of the neural system which subjacent to the generation of the conditioned responses.

In a typical experiment of classical eyeblink conditioning, the conditioned stimulus is a tone (sound) and the unconditioned stimulus is an air puff directed towards the cornea of the animal which produces a reflex response that consists of a vigorous and rapid closure of the eyelids. These two stimuli are paired and the tone precedes the air-puff presentation. Upon several paired trials presented, the animal starts to show conditioned responses, closing the eyelid immediately after the tone (CS; conditioned stimulus) appears and before presentation of the air puff (US; unconditioned stimulus). Usually, an air puff directed towards the cornea, of 3kg/cm^2 intensity and 100 ms duration, is used as an unconditioned stimulus. Other types of stimulus have been used by other authors such as mechanical stimulation or an electrical stimulus in the trigeminal nerve (Woody et al., 1992) for unconditioned stimulus and a weak air puff (Gruart et al., 1997) or a flash of light (Welsh and Harvey, 1991) for conditioned stimulus. The stimuli that have gave better results in the classic eyeblink conditioning have been a tone as a conditioned stimulus and an air puff as an unconditioned stimulus, particularly in rabbits and cats.

On the other hand, there are several types of paradigms during a classical eyeblink conditioning but the most used are of delay and trace.

(1) Delay paradigm: the unconditioned stimulus is applied after the onset of the conditioned stimulus and both stimuli overlap (coexist for a short period of time) to end at the same time (co-terminate). Although, the conditioned stimulus can also end before the unconditioned stimulus finishes. The conditioned response occurs in the conditioned stimulus - unconditioned stimulus time interval (CS-US interval) as well as inter-stimulus interval. In this paradigm, the conditioned stimulus is always present; therefore it is possible that the presence of this conditioned stimulus serves to the animal of reference for the execution of the conditioned response. In the last

years, the duration of the inter-stimulus interval has been optimized. The conditioned response rate after the presentation of the conditioned stimulus is maximal when the inter-stimulus interval is between 200 and 400 ms (Deaux and Gormezano, 1962). On the contrary, if the interval exceeds 2 seconds or is less than 50 ms, it is impossible to generate conditioned responses since the association of the stimuli cannot be given. Therefore, the pairs of stimuli must have a temporal contiguity and to guard a contingency among them (Rescorla, 1988).

(2) Trace paradigm: the conditioned stimulus ends before the unconditioned stimulus begins, therefore the stimuli are temporally separated by a gap in which there is no stimulus present. After several presentations of these stimuli, the conditioned stimulus begins to generate a conditioned response, even in those trials in which the conditioned stimulus is presented in isolation. In this type of paradigm the optimal inter-stimulus interval is approximately 300 ms. Above this value is very difficult to obtain a conditioned response and completely impossible in intervals greater than 1 second. When the conditioned stimulus is a tone, it must have a duration not more than 700 ms, and must be more intense for obtaining an optimum conditioning (Woodruff-Pak et al., 1985; Gruart, 1993)

Furthermore, the generated eyeblink movement is studied thanks to the technique of the electromagnetic follower of the position of the eyelid. This technique is very precise and useful for the analysis of the kinetics of the conditioned response and its subsequent anatomical, electrophysiological or behavioral comparison (Gruart and Delgado-García, 1994; Domingo et al., 1997; Carretero-Guillén, 2015). In addition, the conditioned response frequency is usually used to indicate the degree of conditioning achieved (percentage of conditioned responses), both in relative and absolute values. An description of the kinetics and the frequency domain properties of spontaneous, reflex, and conditioned eyelid responses (Evinger et al., 1984; Gruart et al., 1995; 2000; Sánchez-Campusano et al., 2011); and the underlying neural mechanisms that maintain a basal oscillation allowing a correct and gradual response to sensory stimuli (Welsh, 1992; Domingo et al., 1997; Trigo et al., 1999; 2003) can be found in previous works. These already available studies and the docile nature of rabbits offer a good experimental system for the study of the neural basis of associative learning.

1.4.3. Kinematic of conditioned eyelid responses and their neuronal correlates

It is commonly accepted that associative learning processes such as the classical eyeblink conditioning require the participation of the cerebellum during a delay paradigms, or the hippocampus during a trace paradigms, as unique structures (Thompson, 2005; Gerwig et al., 2007; Green and Arenos, 2007; Thompson and Steinmetz, 2009). However, in several previous studies, authors have been concluded that the neural correlates of this special type of associative learning could be dependent on the functional activity of multiple brain structures (**Figure 7**).

The performed studies in the laboratories of the Division of Neurosciences at the Pablo de Olavide University have been of great importance to advance in understanding the neural correlates of classical eyeblink conditioning. In this regard, it has been proposed that the eyelid motor system is a suitable biological model for to study the functional role of the cerebellar-interpositus/red-nucleus-motoneuron network and their nodal structures (**Figure 7A**), in different animal models, including experiments in cats (Trigo et al., 1999; Gruart et al., 2000; Sánchez-Campusano et al., 2007), mice (Porras-García et al., 2010), and rabbits (Pacheco-Calderón et al., 2012). Moreover, the cerebellar-interpositus/red-nucleus-motoneuron pathway has been reported (Sánchez-Campusano et al., 2011) as being involved in the generation, control, and expression of conditioned eyeblinks, or at least in the proper performance of reflex and acquired eyelid responses.

In addition to the cerebellum and the brainstem nuclear centers, many other cerebral cortical and subcortical structures (**Figure 7B**) have been reported as involved as well in different aspects of acquisition, retrieval, and extinction processes.

Figure 7. Summary of different experimental designs in relation to classical eyeblink conditioning. (**A**) Diagrammatic representation of the electrophysiological approaches that involve the cerebellum and the brainstem nuclear centers: the cerebellar interpositus nucleus (IP n), the red nucleus (RN), and the motor nuclei (V n, trigeminal nucleus; VI n, abducens nucleus; Acc VI n, accessory abducens nucleus; VII n, facial nucleus). (**B**) Diagrammatic representation of the electrophysiological approaches that involve the hippocampus (Hi.), the motor cortex (MC), and the rostro-medial prefrontal cortex (rmPFC). The diagrams also illustrate the recording (Rec.) sites, as well as the eyelid coil and electromyographic (EMG) electrodes implanted in the upper eyelid. Other abbreviations: OO, orbicularis oculi muscle; MN, motoneurons; CS, conditioned stimulus; US, unconditioned stimulus. Modified and adapted from Sánchez-Campusano et al. (2007; 2011).

SUMMARY OF DIFFERENT EXPERIMENTAL DESIGNS IN RELATION TO CLASSICAL EYEBLINK CONDITIONING

A

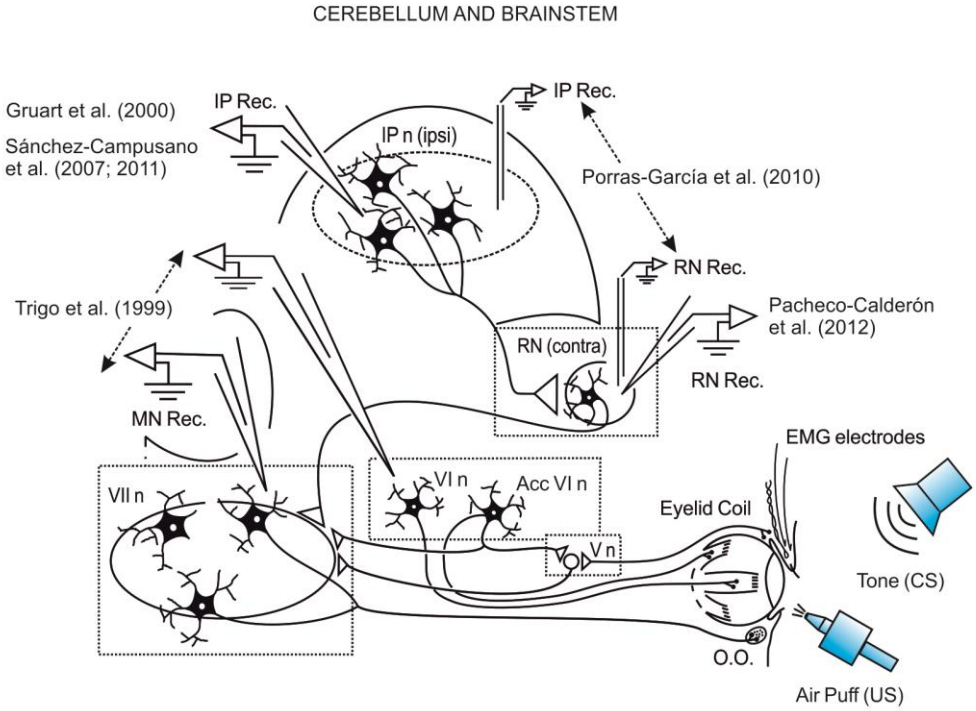

B

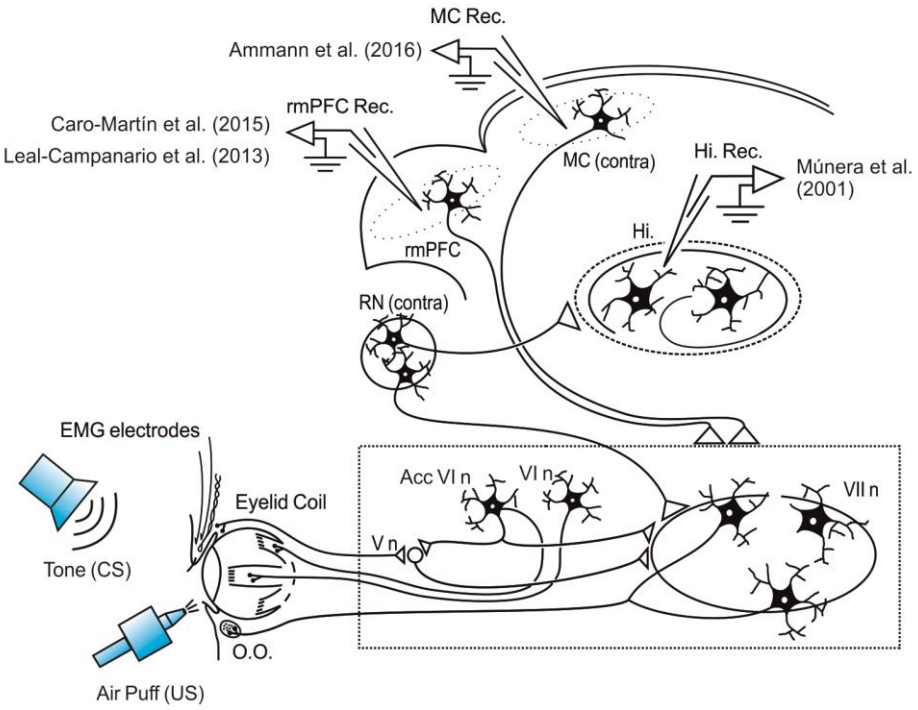

For example, it has been demonstrated that hippocampal pyramidal cell activity encodes conditioned stimulus predictive value during classical conditioning in alert cats (Múnera et al., 2001). According to this study, the hippocampal pyramidal evoked firing appeared restricted to a narrow time window closely related to the time of paired stimulus presentations. In addition, in a recent study (Ammann et al., 2016), it has been observed that the motors cortex is involved in the generation of classically conditioned eyelid responses in behaving rabbits. The motor cortex neurons were identified as projecting to the red or facial nuclei and encoded the kinematic of conditioned eyelid responses.

In the same way, the rostro-medial prefrontal cortex (Leal-Campanario et al., 2013) has been shown to participate as a potent inhibitor of reflex and conditioned eyeblinks, controlling the release of newly acquired eyelid responses during a delay paradigm (250 ms of inter-stimulus interval). Furthermore, Caro-Martín et al. (2015) have chronically recorded the neuronal activity of the rostro-medial prefrontal cortex during the classical eyeblink conditioning in delay paradigms with different inter-stimulus intervals (50, 250, 500, 1000, and 2000 ms). According to this study, the rostro-medial prefrontal cortex neurons seem not to encode the oscillatory properties characterizing conditioned eyelid responses in rabbits, but are probably involved in the determination of inter-stimulus interval of an intermediate range (250-1000 ms).

In this regard, the oscillatory properties of the kinematic of conditioned eyelid responses and their neuronal correlates were studied. In a previous study of the kinematic properties of cat eyelids, Gruart et al. (1995) suggested the existence of a 20-25 Hz oscillator underlying reflex and classical eyeblink responses. Indeed, published records note the easily seen presence of oscillations in eyelid movements or in the EMG activity of involved facial or retractor bulbi muscle (Berthier, 1992; Welsh, 1992). In particular, eyelid oscillations in rabbits present a dominant frequency of 4-15 Hz (Gruart et al., 2000). In this regard, it was shown that oscillatory activities of the eyelid are tuned to its size and viscoelastic properties, as determined in different (mouse, rat, rabbit, cat, and human) species of mammals (Domingo et al., 1997; Gruart et al., 2000; Koekkoek et al., 2002).

Oscillations in a range similar to those presented by the lids have also been described in the resting membrane potentials and firing properties of cat facial motoneurons (Trigo et al., 1999) and motor cortex neurons (Aou et al., 1992) during the

performance of conditioned eyeblinks. In a recent study of the firing activities of the neurons of the rostro-medial prefrontal cortex in rabbits during the classical conditioning of eyelid responses, the presence of dominant peaks in the discharge rate of recorded neurons at different latencies with respect to conditioned stimulus presentations, but always within the inter-stimulus interval was reported (Leal-Campanario et al., 2013; Caro-Martín et al., 2015). This observation raised the possibility that neural firing of rostro-medial prefrontal cortex neurons could be related to the oscillatory properties and timing of conditioned eyeblinks or, on the contrary, be involved in the determination of inter-stimulus intervals, associative strength of conditioning stimuli, or related matters.

In accordance, the firing activities of the neurons of the rostro-medial prefrontal cortex during classical eyeblink conditioning of behaving rabbits were recorded. For conditioning, a delay was used, since it has been reported that cerebral cortical areas are not involved in its proper acquisition and retrieval (Clark et al., 1984; Takehara-Nishiuchi et al., 2005; Oswald et al., 2006). Thereby, we could check whether rostro-medial prefrontal cortex activity during this type of associative learning is engaged in additional neural processing of associative learning tasks. To properly determine the oscillatory properties of conditioned eyelid responses, lid movements were recorded with the magnetic search coil technique (Gruart et al., 2000). The EMG activity of the ipsilateral orbicularis oculi muscle was also recorded. Firing activities of contralateral pyramidal neurons of the rostro-medial prefrontal cortex were recorded across the successive conditioning sessions. Collected results allow suggesting that the rostro-medial prefrontal cortex plays an important role in cognitive processes related to associative learning tasks, such as the determination of conditioned stimulus – unconditioned stimulus time intervals. In contrast, the rostro-medial prefrontal cortex seems not to be directly involved in the acquisition process or in the execution of the acquired eyelid responses.

In this Doctoral Thesis, an unsupervised spike-sorting approach based on shape (spike waveform in time domain), phase (spike phase-space representation) and distribution (direct statistical inferences) features of each spike-event is presented, all of them with a proper physiological description. In accordance with these features, spikes can be grouped automatically by *K*-means clustering, followed by internal validation indices to verify the homogeneity or dissimilarity among spikes during the classification. In addition, this spike-sorting algorithm/method based on shape, phase,

and distribution features was compared with other published algorithm/methods of feature extraction (see **Table 1** for details).

The unsupervised off-line spike-sorting algorithm was implemented here by examining their performances in sorting of spike-events from extracellular recordings of the rostro-medial prefrontal cortex of rabbits during a paradigm of classical eyelid conditioning (a special type of associative learning). Finally, the spiking events were clustered employing *K*-means method with three different internal validation indices (Silhouette, Davies-Bouldin, and Dunn). For an objective assessment of the spike-sorting capabilities of the present method and algorithm on real extracellular recordings, two integrative measures (cohesion-dispersion, *CD*-index; and clustering error, *CE*-index) were also implemented. Therefore, the present spike-sorting method and algorithm are suitable for the off-line analysis of neuronal recordings. Moreover, they could substantially improve the quality of data evaluation based on microelectrode recordings for several applications in neurophysiology.

2. HYPOTHESIS AND OBJECTIVES

Hypothesis: An automatic and unsupervised computational algorithm should be the best option for detecting, identifying and classifying the action potentials involved in the neural electrophysiological recordings, as well as for accurately clustering these action potentials. The methods and algorithms created could be tested in electrophysiological recordings acquired in the rostral medial prefrontal cortex trying to see the role of this neural structure in determining the inter-stimulus interval during a classical conditioning task.

General Objective: To understand how and under what biophysical-mathematical/computational assumptions is it possible to design, develop and implement a single optimized analytical-experimental approach of spike sorting, which allows analytically processing real (not simulated) electrophysiological recordings and guarantees the optimal detection, identification and classification of the neuronal action potentials distributed across the recordings, as well as the efficient pattern recognition and clustering of the different firing rate profiles of the involved neurons.

To carry out both the preceding hypothesis and the general objective, the following specific objectives were proposed in this Doctoral Thesis.

Specific Objectives:

1. To perform an exhaustive review of the main spike sorting methods based on the recognition of the waveform (amplitude-time) of the action potentials and determine the mathematical and computational requirements necessary for the optimal implementation of an unsupervised automated algorithm for pattern recognition of neural spikes from real electrophysiological recordings.
2. To design and develop customized spike sorting methods and algorithms which detects, identifies and classifies the neural spikes distributed across the real electrophysiological recordings, and clusters these spiking events in function of their physiological features (shape, phase and distribution features from each spike-event). In addition to implement and fine-tuning a spike-sorting software called *VISSOR* (*Viability of Integrated Spike Sorting of Real Recordings*) which integrates in a single computational package these spike sorting methods and algorithms.
3. To design and develop a method for the extraction of an optimal frequency range which allows optimally filtering neural recordings and differentiate action potentials from different types (principal and non-principal) of neurons. In addition, to

implement and fine-tuning a software called ERFo (Extractor of Range for Filtering optimization). Furthermore, to explore the integration of the ERFo methods into the *VISSOR* preprocessing block.

4. To design and develop a supervised and hierarchical clustering method for the neural pattern recognition and classification of the firing rate profiles from the electrophysiological recordings under study.
5. To develop the proposed methods and algorithms with the general purpose of characterizing the neuronal activation patterns during classical eyeblink conditioning, and applying these methods and algorithms specifically for the pattern recognition of the firing rate profiles obtained from the rostro-medial prefrontal cortex (rmPFC) neurons.
6. To find out the relationships between the activity patterns of the rostro-medial prefrontal cortex (rmPFC) neurons and the level of expression of the conditioned eyelid responses, expressed in kinematic parameters such as the eyelid position, velocity and acceleration. In addition, to study the oscillatory properties of these neurons, the relationship with the regular eyeblink oscillations, and how these neuronal oscillations depend on the duration of the inter-stimulus interval during a delay paradigm.

3. MATERIALS AND METHODS

3.1. *Unsupervised Automatic Algorithm* based on feature extraction for spike-sorting method

For the analysis of the neuronal activity, a features extraction and clustering method (SS-SPDF) was designed and developed on MATLAB (The MathWorks, Natick, MA, USA; version 7.12.0; R2011a) platform. This method detects, identifies and classifies the neuronal spikes distributed across the electrophysiological recordings, and clusters these spiking events in function of the shape, phase and distribution features. In additions, the *Unsupervised Automatic Algorithm*, in which was integrated SS-SPDF method, was implemented in the customized spike-sorting software *VISSOR*. This software was designed and developed in the same platform.

3.2. Structure of Unsupervised Automatic Algorithm

The proposed spike-sorting methodology is graphically illustrated in **Figure 8**. This methodology was developed in two different blocks: (1) Data Preprocessing block which includes data filtering, the calculation of the derivative and interpolation of data filtering, the application of the adaptive threshold of amplitude; and the spike detection and alignment steps; and (2) Spike Classification block which contains the SS-SPDF method for the features extraction and spike-events clustering of the neural recording.

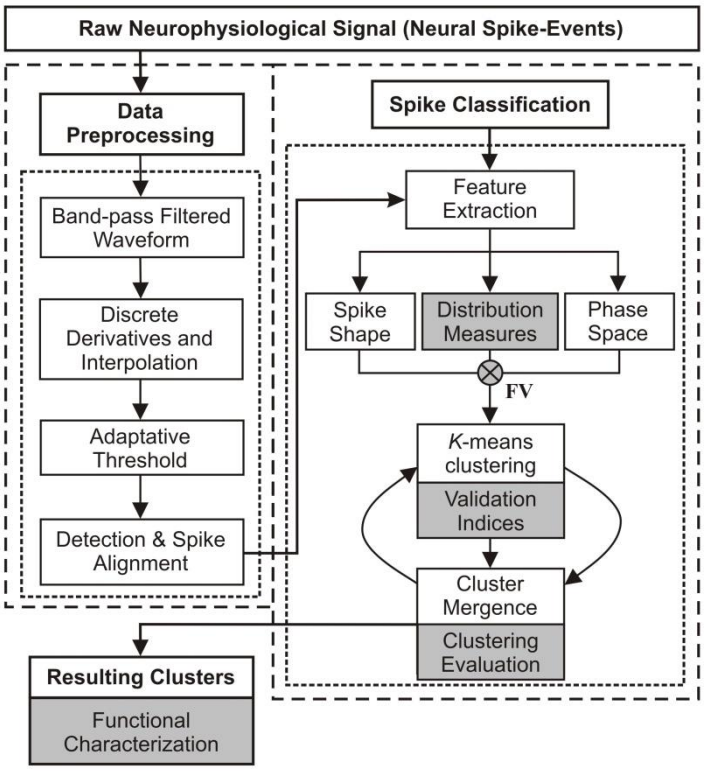

Figure 8. Overall structure of the proposed unsupervised automatic algorithm. Step-by-step illustration of the spike sorting process based on shape, phase and distribution features, and *K*-means clustering with internal validation indices. White blocks represent the common steps of a spike-sorting algorithm. Gray sub-blocks indicate the main methodological contributions of the proposed algorithm. Notice that each feature vector (FV) included shape, phase and distribution measures of each spike-event. Resulting clusters, a summary sub-block (also in gray) for reporting the relevant information of the whole process was implemented. This approach facilitates the physiological interpretation of the extracted spike features, the assessment of the modulating properties of the involved neurons, and the functional characterization of the neural process under study.

In the Spike Classification block, a vector of twenty-four physiological parameters was determined for each spike-event. From now on, the term spike-event will be used to referring to both the detected spike from the filtered recording and its first or second derivative. This twenty-four dimensional vector (24D-vector) included shape (spike-event waveform in time domain), phase (spike-event phase-space representation) and distribution (direct statistical inferences) spike features (see **Figure 9** for details). Those feature vectors were the input to an unsupervised *K*-means clustering method (MacQueen, 1967) with three internal validation measures: Silhouette (Rousseeuw et al., 1987), Davies Bouldin (Davies and Bouldin, 1979) and Dunn (Dunn, 1970) indices. This unsupervised clustering method was used to determine the number of classified spike-events distributed across time and the neuronal identity of them. In this way, spike waveforms originated from different neurons were discriminated. Moreover, the cohesion-dispersion among and within clusters during the neural events classification was studied.

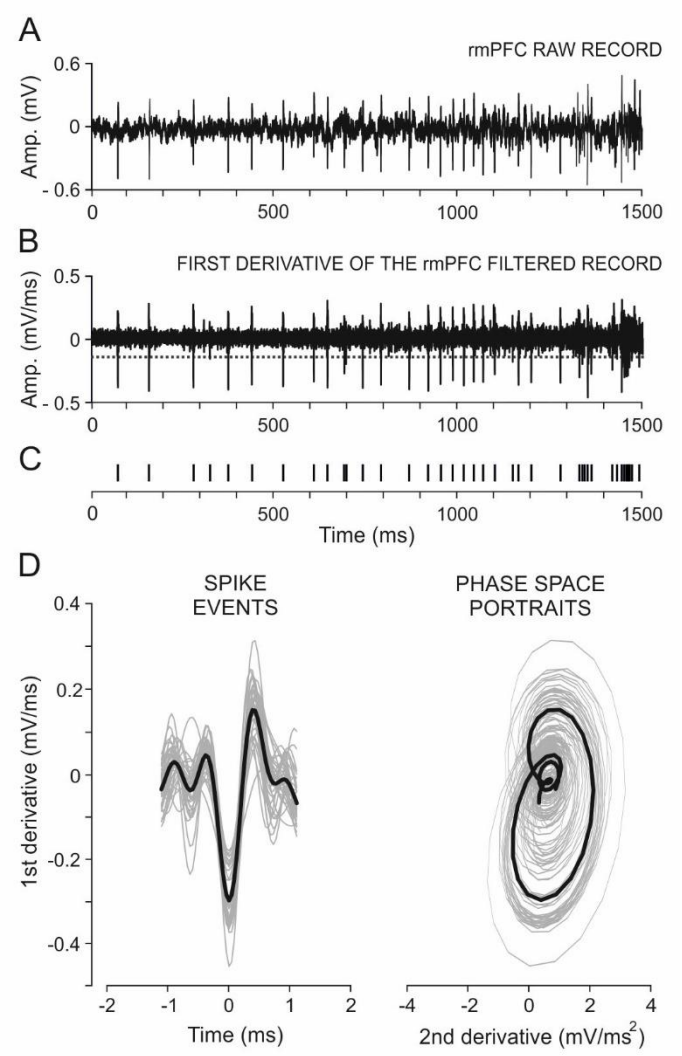

Figure 9. An example illustrating the preprocessing steps. (**A**) rostro-medial prefrontal cortex (rmPFC) raw record, with 37500 time points that corresponds to 1.5 s at a sampling rate of 25 kHz. (**B**) First derivative of the rmPFC band-pass (FIR filter, 450–2000 Hz) filtered record. The horizontal dotted line indicates an alternative amplitude threshold for direct spike-event detection. (**C**) Distribution in time of the spikes detected in B. (**D**) Left, resulting spike-events (gray traces) in the time domain (time vs. first derivative) and their corresponding mean event profile (black trace). Right, phase space portraits (second derivative vs. first derivative; gray traces) of the spikes and their corresponding mean phase trajectory (black trace).

Furthermore, the proposed spike-sorting algorithm included a modified index of clustering error taken from Letelier and Weber (2000) upon completion of the classification process.

3.2.1. Preprocessing of electrophysiological recording

The first step in the Preprocessing block was the filtering of the electrophysiological recordings (**Figure 9A**). These recordings were filtered (**Figure 9B**) with a bandpass (450 to 2050 Hz) FIR filter (Vogelstein et al., 2004; Yang et al., 2014). The applied frequency range allowed the detection of spikes whose durations (absolute refractory periods) were in the range [0.5 – 2.2] ms. Afterwards, the regular differentiations (first-order and second-order derivatives) of the filtered records were calculated to stabilize the resulting record (Yang et al., 2008). Additionally, if the sampling frequency was < 20 kHz, the recording was interpolated applying a cubic splines to improve the calculation of the regular differentiations of the filtered recording.

The subsequent preprocessing steps were the selection of the amplitude threshold (horizontal dotted line in **Figure 9B**) for the preliminary spike-events detection and identification (**Figure 9C**). The amplitude threshold could be selected automatically (always the same amplitude threshold regardless of the recording) or could be selected following the investigator's choice. In this later case, multiple thresholds could be chosen, as there are multiple neurons with similar-shaped waveforms but different amplitudes and the spike amplitude distribution could be multimodal. To avoid this problem, an adaptive threshold was applied to the first-order derivative of the filtered records. This threshold was adjusted to the data points of this recording once the possible artifacts and rejected the contaminated segments by them were removed. The artifacts of these recordings were atypical waveforms or oscillations caused by an increase in the connection resistance between the recording electrode and the tissue impedance. They were evident because their peak-to-valley amplitudes were significant ($P < 0.001$) with respect to the mean peak-to-valley amplitudes of the recording. The adaptive threshold (*Thr*) was set automatically to three times the median absolute deviation of the first-order derivative $\dot{V}(t)$ of the band-pass filtered record.

$$Thr = \pm q \cdot \sigma_n; \qquad \sigma_n = median\left\{\frac{|\dot{V}(t)|}{0.6745}\right\} \qquad [1]$$

The value of the constant q was typically between 3 and 5. The denominator in the last formula is the inverse of the cumulative distribution function for the standard

normal distribution evaluated at 0.75. In general, the median absolute deviation σ_n of the filtered recording is an estimate of the standard deviation of the background noise (Donoho and Johnstone, 1994; Quiroga et al., 2004; Rey et al., 2015).

After this process, all detected spike-events were aligned (**Figure 9D**, Left) based on their negative peak positions and the phase-space portraits (Aksenova et al., 2003) of all the aligned spike-events were calculated and reconstructed (**Figure 9D**, Right). Four millisecond windows, centered on these negative peaks, were identified as segments of spiking activity in the first derivative of the filtered electrophysiological recording.

For each detected spike-event, twenty-four physiological features (**Figure 10** and **Table 2**) were extracted and assembled for further process. Details of other steps are described in the following subsections.

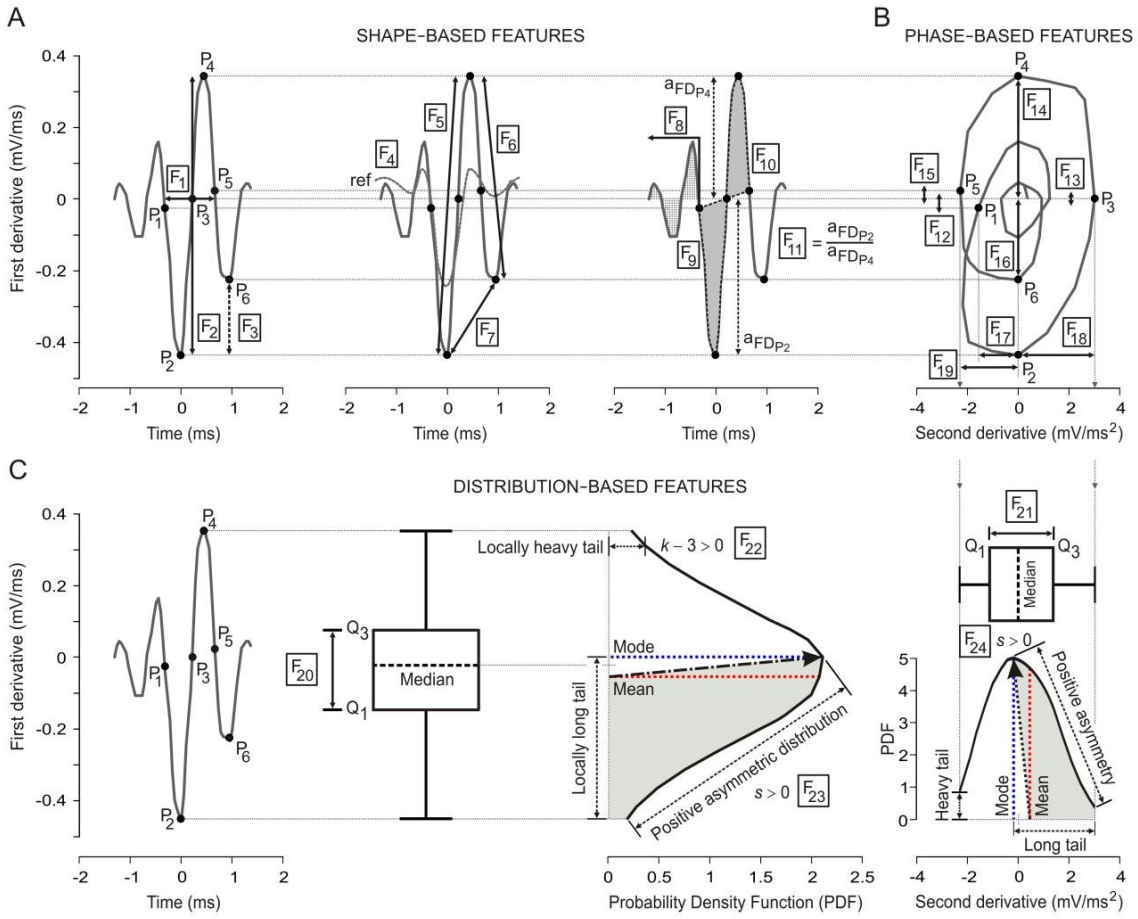

Figure 10. Schematic representation of the extracted features. (**A**) Six fundamental points (P_1 – P_6) and 11 shape-based features (F_1 – F_{11}) from each spike-event in the time domain of the spike first derivative (FD). (**B**) Eight phase-based features (F_{12} – F_{19}) from each spike trajectory in the phase space (second derivative (SD) versus FD). (**C**) Five distribution-based features (F_{20} – F_{24}) for the statistical amplitude distribution of the FD (F_{20}, F_{22}, and F_{23}) and SD (F_{21} and F_{24}) of the spike-event. Note that, for each spike-event amplitude distribution (probability density function, PDF), the mean, median, mode, interquartile range (Q_3 – Q_1), kurtosis and asymmetry are indicated. In summary, a vector of 24 features (F_1 – F_{24} in Table 2) was determined for each spike-event. Notice that P_2 and P_4 are valley and peak of the FD of the action potential; P_1, P_3 and P_5 are first, second and third zero crossing of the FD of the action potential; and P_6 is valley of the FD after the action potential (see **Table 3** for details).

Table 2. Neurophysiological features of each spike-event characterizing the process of creating 24D feature vectors. List of shape ($F_1 - F_{11}$), phase ($F_{12} - F_{19}$), and distribution ($F_{20} - F_{24}$) features and their algebraic definition (**Figure 10**), considering the first-order derivative (FD) and the second-order derivative (SD) of the action potential. The three common features (F_{14}, F_{18} and F_{19}) proposed also by other authors (**Table 1**) are marked with an asterisk.

	Number	Name	Algebraic definition
SHAPE	**F_1**	Waveform duration of the FD of the action potential	$t_{P5} - t_{P1}$
	F_2	Peak-to-valley amplitude of the FD of the action potential	$a_{FD_{P4}} - a_{FD_{P2}}$
	F_3	Valley-to-valley amplitude of the FD of the action potential	$a_{FD_{P6}} - a_{FD_{P2}}$
	F_4	Correlation coefficient between the FD of the action potential (ap) and the reference spike-waveform (ref), considering their corresponding standard deviation σ_{FD}	$\frac{\sigma^2_{FD_{ap,ref}}}{\sigma_{FD_{ap}} \cdot \sigma_{FD_{ref}}}$
	F_5	Logarithm of the positive deflection of the FD of the action potential	$\log\left(\frac{a_{FD_{P4}} - a_{FD_{P2}}}{t_{P4} - t_{P2}}\right)$
	F_6	Negative deflection of the FD of the action potential	$\frac{a_{FD_{P6}} - a_{FD_{P4}}}{t_{P6} - t_{P4}}$
	F_7	Logarithm of the slope among valleys of the FD of the action potential	$\log\left(\frac{a_{FD_{P6}} - a_{FD_{P2}}}{t_{P6} - t_{P2}}\right)$
	F_8	Root-mean-square of pre-event amplitudes of the FD of the action potential	$\sqrt{\frac{a_{FD_{P1}} + \sum_{i=m-1}^{1} a_i}{m}}$
	F_9	Negative slope ratio of the FD of the action potential	$\left(\frac{a_{FD_{P2}} - a_{FD_{P1}}}{t_{P2} - t_{P1}}\right) \Big/ \left(\frac{a_{FD_{P3}} - a_{FD_{P2}}}{t_{P3} - t_{P2}}\right)$
	F_{10}	Positive slope ratio of the FD of the action potential	$\left(\frac{a_{FD_{P4}} - a_{FD_{P3}}}{t_{P4} - t_{P3}}\right) \Big/ \left(\frac{a_{FD_{P5}} - a_{FD_{P4}}}{t_{P5} - t_{P4}}\right)$
	F_{11}	Peak-to-valley ratio of the FD of the action potential	$\frac{a_{FD_{P2}}}{a_{FD_{P4}}}$
PHASE	**F_{12}**	Amplitude of the FD of the action potential relating to P_1	$a_{FD_{P1}}$
	F_{13}	Amplitude of the FD of the action potential relating to P_3	$a_{FD_{P3}}$
	F_{14}*	Amplitude of the FD of the action potential relating to P_4	$a_{FD_{P4}}$
	F_{15}	Amplitude of the FD of the action potential relating to P_5	$a_{FD_{P5}}$
	F_{16}	Amplitude of the FD of the action potential relating to P_6	$a_{FD_{P6}}$
	F_{17}	Amplitude of the SD of the action potential relating to P_1	$a_{SD_{P1}}$
	F_{18}*	Amplitude of the SD of the action potential relating to P_3	$a_{SD_{P3}}$
	F_{19}*	Amplitude of the SD of the action potential relative to P_5	$a_{SD_{P5}}$
DISTRIBUTION	**F_{20}**	Inter-quartile range $(Q_3 - Q_1)$ of the FD of the action potential, considering the percentiles $P_{75_{FD}}$ and $P_{25_{FD}}$	$P_{75_{FD}} - P_{25_{FD}}$
	F_{21}	Inter-quartile range $(Q_3 - Q_1)$ of the SD of the action potential, considering the percentiles $P_{75_{SD}}$ and $P_{25_{SD}}$	$P_{75_{SD}} - P_{25_{SD}}$
	F_{22}	Kurtosis coefficient of the FD of the action potential, considering the fourth sampling moment of n amplitudes a_{FD_i} about its mean $\overline{a_{FD}}$, and the standard deviation σ_{FD}	$\frac{\sum_{i=1}^{n}\left(a_{FD_i} - \overline{a_{FD}}\right)^4}{n \cdot \sigma^4_{FD}}$
	F_{23}	Fisher asymmetry of the FD of the action potential, considering the third sampling moment of n amplitudes a_{FD_i} about its mean $\overline{a_{FD}}$, and the standard deviation σ_{FD}	$\frac{\sum_{i=1}^{n}\left(a_{FD_i} - \overline{a_{FD}}\right)^3}{n \cdot \sigma^3_{FD}}$
	F_{24}	Fisher asymmetry of the SD of the action potential, considering the third sampling moment of n amplitudes a_{FD_i} about its mean $\overline{a_{SD}}$, and the standard deviation σ_{SD}	$\frac{\sum_{i=1}^{n}\left(a_{SD_i} - \overline{a_{SD}}\right)^3}{n \cdot \sigma^3_{SD}}$

3.2.2. Features extraction process of the SS-SPDF method

The feature extraction process is a critical step in the spike-sorting methods after detection of the spike in a real recording. In this work, the feature extraction process consisted in the extraction of twenty-four features based on shape, phase and distribution measures of each spike-event. These features (n = 24, see **Table 2** for details) were selected independent of each other to guarantee a best description and separation the neuronal spikes, removing the multi-collinearity and simplify the classification process. The independent features (F_1 – F_{24}) proposed ensure that the features vector in a 24D space (R^{24}) did not hold redundant information and therefore deleted the need to further reduce the dimensionality. Furthermore, these independent features (**Figure 10**) were quickly and easily calculated and represented no imminent threat to the computational cost and complexity of the algorithm.

In summary, in the feature extraction process was used twenty-one new features (**Table 2**) in addition to the three common features (F_{14}, F_{18} and F_{19}) used by other authors (**Table 1**).

Shape-based features

After fixing the six fundamental points (P_1 – P_6; **Table 3**) of the spike-waveform in the time domain of the first-order derivative of the action potential (**Figure 10A**), the feature extraction process returns 11 shape-based features. These new features (F_1 – F_{11}, **Table 2**) were self-explanatory and provided essential information of the spike-event during the spike-classification of real neural data. The shape-based features (F_1, F_2, F_4, F_5, F_6, F_8, and F_{11}, from the spike first-order derivative) were used with similar algebraic definitions to those used by other authors (Sonoo and Stalberg, 1993; Lewicki, 1998; Stewart et al., 2004; Balasubramanian and Obeid, 2011; Bestel, 2012; Su et al., 2013; Jahanmiri-Nezhad et al., 2014; Yang et al., 2014) during the feature extraction directly from the spike and not from its first-order derivative.

Phase-based features

In this step, the first and second order derivatives (Aksenova et al., 2003; Chibirova et al., 2005) of the filtered electrophysiological recording were calculated. Eight features (F_{12} – F_{19}; **Table 2**) of the spike trajectory in phase space (second-order derivative against first-order derivative, **Figure 10B**) were extracted. Five of these phase-based features were proposed as new features: amplitudes F_{12}, F_{13}, F_{15}, and F_{16} of the first-

order derivative of the action potential corresponding to the points P_1, P_3, P_5, and P_6, respectively; and the amplitude F_{17} of the second-order derivative of the action potential corresponding to P_1. These new phase-based features (F_{12}, F_{13}, F_{15}, F_{16}, and F_{17}) allowed preserving the independence in this set of features and resolving better the overlapping problem of the spikes. The remaining phase-based features (F_{14}, F_{18}, and F_{19}) were common features used with good results by some of the authors (Yang et al., 2008; Paraskevopoulou et al., 2013; 2014; Su et al., 2013; Yang et al., 2014) cited in the **Table 1** of the Introduction section.

Table 3. List of the selected waveform components. Six fundamental points (P_1 – P_6) determined each detected spike-events. These points were graphically identified in both time domain (**Figure 10A**) and phase space (**Figure 10B**), considering the first-order derivative (FD) and the second-order derivative (SD) of the action potential.

Spike-points number	Definition
P_1	First zero crossing of the FD before the action potential has been detected.
P_2	Valley of the FD of the action potential.
P_3	Second zero crossing of the FD of the action potential that has been detected.
P_4	Peak of the FD of the action potential.
P_5	Third zero crossing of the FD after the action potential has been detected.
P_6	Valley of the FD after the action potential.

Distribution-based features

The features directly related to distribution measures of each spike-event were one of the most important contributions of the feature vector, considering the sample of amplitude values of the spike. Using basic inter-quartile ranges, kurtosis coefficient and Fisher asymmetry measures of the first-order and second-order derivatives, five distribution-based features (F_{20} – F_{24}; **Table 2**) from each spike-event were extracted (Caro-Martín et al., 2017). For the calculation of these distribution measures, two tests were performed: (1) selecting only the points of the positive and negative components of the spike-waveform; and (2) selecting all the points of the spike-waveform. The better results were obtained with all the points of the spike-waveform. In particular, the kurtosis coefficient (DeCarlo, 1997) was calculated from first-order and second-order derivatives, obtaining similar results, therefore, the feature F_{22} was extracted of the first-order derivative of the action potential.

Notice that, the inter-quartile range F_{20} (or F_{21}) is the difference between the 75th percentile and the 25th percentile of the amplitude values from the first-order derivative (or second-order derivative) of each action potential, and is the most significant basic

robust measure of scale to quantify the statistical dispersion of the amplitude values of a spike. Therefore, spikes of different sizes will have different inter-quartile ranges. In the same way, the kurtosis coefficient (F_{22}) measures the critical changes in the tail weights and peakedness of the probability density function for the amplitudes of each spike-event. In this situation, kurtosis largely reflects tail behavior of the amplitude distribution; therefore, the distribution will have a high kurtosis coefficient if there is a concentration of values near its tails (heavy tailed distribution). Therefore, the presence of action potentials with large positive and negative values leads to locally heavy tails of the amplitude distribution.

Finally, the features F_{23} and F_{24} (Fisher asymmetries) measure the relative deviation of the distribution mode respect to mean value of amplitude distribution of the spike of the first-order derivative (**Figure 10C**). For a unimodal distribution, negative asymmetry coefficient indicates that the tail on the left side of the probability density function is longer or fatter than the right side – it does not distinguish these two kinds of shape, but it was a reliable geometric measurement. Conversely, positive asymmetry coefficient indicates that the tail on the right side of the probability density function is longer or fatter than the left side.

3.2.3. Spike-event clustering process according to the SS-SPDF method

In the process of spike-events clustering, the different feature vectors that described all detected neuronal spikes in the before process were comprised and compared to obtain the classification most relevant. Therefore, the well-known *K*-means clustering method (MacQueen, 1967; Jin and Han, 2010) was implemented, as its name indicates, using the means of each group of feature vectors to detect the similarities among them and the formed centers by clusters of similar feature vectors.

K-means clustering method had the purpose of maximizing the similarity of feature vectors within each clustering and of minimizing the similarity among feature vectors of different clustering (Lewicki, 1998). This method was previously described by Tou and González (1974) in the following steps:

1. *Establish the initial conditions of the classification centers*. By default, values of the feature vectors array were chosen as initial values of classification centers. In additions, the number of chosen centers was equal to the number of final clustering obtained from the classification.

2. *Apply distance and metric measurement criteria among the different feature vectors and among the centroids*. Four different measures of distance (sqEuclidean, Cityblock, Cosine and Correlation; see **Table 4** for details) among clusters and seven clustering metrics (sqEuclidean, Euclidean, Cityblock, Cosine, Correlation, Hamming and Jaccard; see **Table 5** for details) were considered. Therefore, a total of twenty-eight (4 distances x 7 metrics) different combinations were applied in the classification.

Table 4. Summary of the available distance measures by *K*-means. *K*-means computes centroid clusters differently for the different supported distance measures. In the formulae, x is an observation (that is, a row of the matrix X) and c is a centroid (a row vector).

Distance	Description	Formule
sqEuclidean	Squared Euclidean distance (default). Each centroid is the mean of the points in that cluster.	$d(x,c) = (x-c)(x-c)'$
Cityblock	Sum of absolute differences. Each centroid is the component-wise median of the points in that cluster.	$d(x,c) = \sum_{j=1}^{p} \lvert x_j - c_j \rvert$
Cosine	One minus the cosine of the included angle between points (treated as vectors). Each centroid is the mean of the points in that cluster, after normalizing those points to unit Euclidean length.	$d(x,c) = 1 - \frac{xc'}{\sqrt{(xx')(cc')}}$
Correlation	One minus the sample correlation between points (treated as sequences of values). Each centroid is the component-wise mean of the points in that cluster, after centering and normalizing those points to zero mean and unit standard deviation.	$d(x,c) = 1 - \frac{(x-\vec{x})(c-\vec{c})'}{\sqrt{(x-\vec{x})(x-\vec{x})'}\sqrt{(c-\vec{c})(c-\vec{c})'}}$ where $\vec{x} = \frac{1}{p}(\sum_{j=1}^{p} x_j)\overrightarrow{1_p}$ $\vec{c} = \frac{1}{p}(\sum_{j=1}^{p} c_j)\overrightarrow{1_p}$ $\overrightarrow{1_p}$ es a row vector of p ones

Table 5. Summary of the available metric measures. The algorithm calculates the internal validation indices using the inter-point distance function specified as metric.

Metric	Description
Euclidean	Euclidean distance.
sqEuclidean	Squared Euclidean distance (default).
Cityblock	Sum of absolute differences.
Cosine	One minus the cosine of the included angle between points (treated as vectors).
Correlation	One minus the sample correlation between points (treated as sequences of values).
Hamming	Percentage of coordinates that differ.
Jaccard	Percentage of nonzero coordinates that differ.

3. *Calculate the membership of the feature vectors to a cluster until convergence criteria.* Given an initial but not optimal clustering, relocated each features vector to its new nearest center, updated the clustering centers by calculating the mean of the feature vectors clustered, and repeated the relocating-and-updating process until that the convergence criteria (such as predefined number of iterations) were satisfied.
4. Finally, *K*-means clustering method returned the most pertinent *K* value (optimal number of clusters) and the most suitable classification (optimal clustering) of the feature vectors for each distance-metric combination and for the indicated number of centroids.

K-means clustering method requires *K* inputs and is based on distance metrics calculation. In the spike-events clustering process, *K*-means clustering method was unsupervised because it did not depend on a number *K* of clusters introduced by the researcher and completely automatic as the input *K* was iterated from two to root-square of the number of detected spikes (**Figure 11**). The maximum number of clusters (K_{max}) which could be presented in a neural dataset having *s* spikes should not exceed the value $\sqrt{s}$. The K_{max} value is considered as a rule of thumb in clustering literature (Pal and Bezdek, 1995; Pakhira et al., 2004).

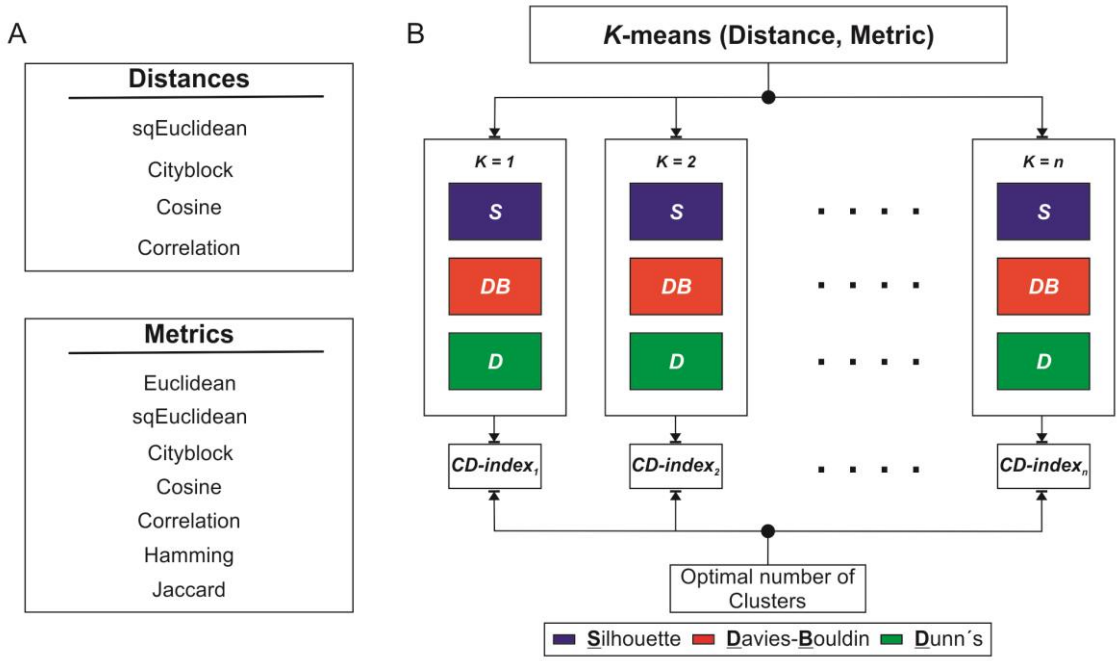

Many indices have been developed and compared for determining clustering validity (Bezdek and Pal, 1998; Ray and Turi, 2000; Maulik and Bandyopadhyay, 2002; Pakhira et al., 2004; Handl et al., 2005; Petrovic, 2006; Yanchi et al., 2010; Platzer, 2013). As the goal of clustering is to make feature vectors within the same cluster similar and feature vectors in different clusters distinct, internal validation index measures are often based on two criteria: (1) compactness (it measures how closely related the objects in a cluster are); and (2) separation (it measures how distinct or well-separated a cluster is from other clusters).

The goal of the Spike Classification block was to find the best partition and the optimal number of clusters. Thus, the following internal validation measures were used: Silhouette (*S*), Davies-Bouldin (*DB*) and Dunn indices (*D*).

Silhouette (S) index

The Silhouette (*S*) index value for each point *i* is a measure of the similarity of a point to points in its own cluster compared to points in other clusters (Rousseeuw, 1987). For a given grouping $\mathcal{A}_j$ $j \in [1, \dots, c]$; c = number of classes, the method assigns each object $\mathcal{A}_j$ a quality measure $\mathcal{S}_i$ $(i = 1, \dots, m)$; m = number of objects of $\mathcal{A}_j$. The Silhouette index value is defined as:

$$\mathcal{S}(i) = \frac{b(i) - a(i)}{max\{a(i), b(i)\}} \qquad [2]$$

In the above expression *a*(i) is the average distance between the *i-th* object and all the objects included in $\mathcal{A}_j$, while *b*(i) is the minimum distance between the *i-th* object and all objects classified in $\mathcal{A}_k$ $k \in [1, \dots, c]$, $k \neq j$.

Figure 11. Unsupervised *K*-means method and internal validation indices to obtain the optimal number of clusters. (**A**) *K*-means method uses four different measures of distance (sqEeuclidean, Cityblock, Cosine and Correlation, in Table 4) and seven clustering metrics (sqEuclidean, Euclidean, Cityblock, Cosine, Correlation, Hamming and Jaccard, in Table 5) for all possible values of *K*. (**B**) In this diagram *K*-means method (for a selected distance-metric combination) uses the internal validation indices: Silhouette (S), Davies-Bouldin (DB) and Dunn (D). Also, a general index for measuring the cohesion and dispersion of the clustering (called *CD*-index) for each classification is calculated. The higher value of the *CD*-index allows determining the optimal number of clusters. Note that, the maximum number of clusters n should not exceed the value $\sqrt{s}$ where *s* is the number of detected spikes in the neural recording.

Index's value will range $-1 \leq \mathcal{S}(i) \leq 1$, and being poorly grouped any object with an index value between $-1 \leq \mathcal{S}(\mathrm{i}) \leq 0$. The index for a group $\mathcal{A}_j$ is defined as:

$$\mathbb{S}_j = \frac{1}{m}\sum_{i=1}^{m} \mathcal{S}(i) \qquad [3]$$

Here m is the number of objects within $\mathcal{A}_j$ y c is the total number of classes. Therefore, the average value of the Silhouette index overall indicating whether the classification made is optimal, adequate and well separated as to provide optimal number of classes is as follows:

$$S = \frac{1}{c}\sum_{j=1}^{c} \mathbb{S}_j \qquad [4]$$

Davies-Bouldin (DB) index

Index measures the average similarity of groups of objects (classes) within a classification. A small value of the Davies-Bouldin (*DB*) index indicates that a class is grouped by similar objects and compact and has each class centers far from each other (Davies and Bouldin, 1979). The average values of the index for different classes determine the final value of *DB*. This index is defined with the following formulation:

$$DB = \frac{1}{c}\sum_{j=1}^{c} max_{i\neq j}\left\{\frac{\Delta(\mathcal{A}_j) + \Delta(\mathcal{A}_i)}{\delta(\mathcal{A}_j, \mathcal{A}_i)}\right\} \qquad [5]$$

In the above expression $\mathcal{A}_j$ and $\mathcal{A}_i$ represent the class j and i, respectively; $\mathcal{A}_i$ represent the class i; $\delta(\mathcal{A}_j, \mathcal{A}_i)$ the distance between classes $\mathcal{A}_j$ and $\mathcal{A}_i$, the term $\Delta(\mathcal{A}_k)$ represents the distances within the class $\mathcal{A}_k$ and finally c is the number of similar classes of objects within the classification $\mathrm{C}\{\cup\mathcal{A}_j \; j \in [1, \ldots, c]\}$.

Dunn (D) index

This index maximizes the distances within each class of similar objects while minimizing the distances between the remaining classes of the classification – i.e., identifies compact and well separated classes (Dunn, 1970). Therefore, large values of Dunn's index indicate the presence of very compact classes and separate objects within a classification. The number of classes that maximizes the *D*-index is taken as number

of optimal classes. For any classification, $\mathrm{C}\{\cup\mathcal{A}_j \ j \in [1,\ldots,c]\}$ the *D*-index is defined as:

$$D(\mathrm{C}) = min_{1\le j\le c}\left\{min_{1\le i\le c}\left\{\frac{\delta(\mathcal{A}_j,\mathcal{A}_i)}{max_{1\le k\le c}\{\Delta(\mathcal{A}_k)\}}\right\}\right\} \quad [6]$$

Here, $\delta(\mathcal{A}_j,\mathcal{A}_i)$ denotes the distance between classes $\mathcal{A}_j$ and $\mathcal{A}_i$; $\Delta(\mathcal{A}_k)$ represents the distances within the class $\mathcal{A}_k$ and *c* is the number of similar classes of objects within the classification $\mathrm{C}\{\cup\mathcal{A}_j \ j \in [1,\ldots,c]\}$.

For determining the optimal cluster number, the internal validation indices were homogenized of different form. Silhouette index validated the clustering performance based on the pairwise difference of between and within-cluster distances. Dunn's index used the minimum pairwise distance between objects in different clusters as the inter-cluster separation and the maximum diameter among all clusters as the intracluster compactness. The optimal cluster number was determined by maximizing the values of both Silhouette and Dunn indices. However, the Davies-Bouldin index was calculated as follows. For each cluster C, the similarities between C and all other clusters were computed, and the highest value was assigned to C as its cluster similarity. Then, the Davies-Bouldin index was obtained by averaging all the cluster similarities. The smaller the Davies-Bouldin index was, the better the clustering result was. By minimizing this index, clusters were the most distinct from each other, and therefore achieve the best partition (**Figure 11B**).

3.2.4. Clustering validity measure '*CD*-index'

For objectively evaluate the performance of the clustering classification by *K*-means clustering method, in conjunction with the three internal validation indexes, a unified validity index for determining the cohesion and dispersion of the clustering was proposed. This cohesion-dispersion index (*CD*-index) for each clustering was calculated using the probabilities (p_S, p_{DB}, p_D) of the three internal validation indices (Silhouette, *S*; Davies-Bouldin, *DB*; and Dunn, *D*) and their respective weight contributions $w_s, w_{DB}\ y\ w_D$:

$$CD = w_s * p_S + w_{DB} * p_{DB} + w_D * p_D \quad [7]$$

For computation, the score of each index was homogenized. For Silhouette and Dunn indices, the optimum score was obtained of the maximum value of the index that produces a greater separation among all possible clusters. On the other hand, for Davies-Bouldin index, the optimum score was obtained of the minimum value of the index that returned the more compact cluster. Each index evaluated its score between the maximum (*max*) and minimum (*min*) values, such that Silhouette and Dunn indices assigned a probability of 1 at *max* and 0 at *min*, while Davies-Bouldin index assigned a probability of 1 at global *min* and 0 at *max*, defined as follows:

$$p_S(\lambda) = \frac{S(\lambda) - min(S)}{max(S) - min(S)} \quad [8]$$

$$p_{DB}(\lambda) = \frac{DB(\lambda) - max(DB)}{min(DB) - max(DB)} \quad [9]$$

$$p_D(\lambda) = \frac{D(\lambda) - min(D)}{max(D) - min(D)} \quad [10]$$

Note that the above expressions allowed to calculate the probability values for each combination (λ, from 1 to 28). The *min* and *max* values were the global extremes of each internal validation index among all the combinations (distance versus metric). Thus, when *CD*-index is close to 1 (or 100%) the three indices interact to produce the maximal cohesion-dispersion of the clustering and therefore the optimal number of clusters (**Figure 11B**). The *CD*-index was a proper validity measure for quantifying the success of the Spike Classification block (**Figure 8**) in the SS-SPDF method.

3.2.5. Clustering error measure '*CE*-index'

To validate the classification a clustering error index, called *CE*-index, which measures the misclassification of the clustering, was implemented. *CE*-index was defined as the root-mean-square difference between expected and observed values (Letelier and Weber, 2000):

$$CE = \sqrt{\frac{\sum_{i=1}^{n}(d_i - \bar{d})^2 + \sum_{k=1}^{m} r_k^2}{\sum_{i=1}^{n} d_i + \sum_{k=1}^{m} r_k}} \quad [11]$$

In the above expression, d_i is the number of spike-events of each *i*-cluster, r_k is the correlation coefficients between the template of the spike-events corresponding to *i*-cluster and the spike-events of other *j*-cluster (when $i \neq j$). The integers *n* and *m* are the number of clusters and combinations, respectively. A lower *CE*-index indicated less

misclassified and unclassified events, and therefore a better spike-sorting performance. Finally, notice that in accordance with the **equation [11]**, the value of the *CE*-index did not depend on the number of features used in the spike-sorting algorithm. For more details, an example for three clusters was showed.

Example for three clusters

CE-index quantifies the similitude between the observed matrix (OM) and the expected matrix (EM), and is an adaptation of the index proposed by Letelier and Weber (2000). Here, OM was defined as:

$$\begin{matrix} & T1 & T2 & T3 \\ Cluster\ 1 \\ Cluster\ 2 \\ Cluster\ 3 \end{matrix} \begin{pmatrix} d1 & r1 & r2 \\ r3 & d2 & r4 \\ r5 & r6 & d3 \end{pmatrix} \quad [12]$$

In the case of the existence of three clusters resulting of the classification, *T*1, *T*2 and *T*3 represent the templates belonging to each cluster, while the clusters (1, 2 and 3) represent the groups distinguished by the automatic clustering algorithm. d_i is the number of spike-events of each *i*-cluster, r_k is the correlation coefficient between the template of the spike-event corresponding to *i*-cluster and all the spike-events of other *j*-cluster (when $i \neq j$). The positive integers *n* and *m* are the number of clusters and cross-correlations, respectively.

On the other hand, a sorting procedure should produce the following expected matrix (EM):

$$\begin{matrix} & T1 & T2 & T3 \\ Cluster\ 1 \\ Cluster\ 2 \\ Cluster\ 3 \end{matrix} \begin{pmatrix} \bar{d} & 0 & 0 \\ 0 & \bar{d} & 0 \\ 0 & 0 & \bar{d} \end{pmatrix} \quad [13]$$

In the above expression $\bar{d} = \frac{\sum_{i=1}^{3} di}{3}$. Note that, $r_k = 0$, with k = 1,… 6; and therefore there is no linear relationship between the clusters. Finally, *CE*-index for three clusters was defined as the root-mean-square difference between expected and observed values:

$$CE = \sqrt{\frac{\sum_{i=1}^{3}(d_i - \bar{d})^2 + \sum_{k=1}^{6} r_k^2}{\sum_{i=1}^{3} d_i + \sum_{k=1}^{6} r_k}} \quad [14]$$

3.3. Supervised and hierarchical clustering method for the classification of the firing rate profiles

Once the stage of classification and validation of the spike-events of the neural recording were finished, a supervised and hierarchical clustering method was applied. This method was supervised because it was implemented taking into account a fixed number of clusters. The formation of these groups depended on physiological parameters extracted from each class of firing rate profile. **Table 6** summarizes the physiological parameters that were used for the pattern recognition of the firing rates. Notice that, the selected parameters (**Table 6** and **Figure 12**) combine the numerical characteristics of the spike-events (parameters 3 and 4) with the modulating properties of the neural discharges (parameters 1, 2, 5 and 6). Parameters 3 and 4 allowed to identify the temporal patterns of the spike-events both in all the time-window of the trial and within the time interval between the beginning of the CS and the end of the US.

Table 6. Definition of the physiological parameters for the pattern recognition of the firing rates. These parameters were used in the supervised clustering method. Abbreviations: CS, conditioned stimulus; US, unconditioned stimulus; ISI, inter-stimulus interval (or CS–US interval); D_{US}, duration of the US; $ISID_{US}$ = ISI + D_{US}, time interval between the beginning of the CS and the end of the US.

Number	Symbols	Definition
1	f_{max}	Peak firing rate in the $ISID_{US}$ interval (in spikes/s).
2	ℓ_{max}	Latency of the peak firing rate with respect to the CS (in ms).
3	η_{total}	Total number of detected spike-events in all the time-window of the trial.
4	η_{inter}	Number of detected spike-events in the $ISID_{US}$ interval.
5	$\overline{f}$	Average of the peak firing rates in the $ISID_{US}$ interval (in spikes/s).
6	f_{sem}	Standard error of the mean for the peak firing rates in the $ISID_{US}$ interval (in spikes/s).

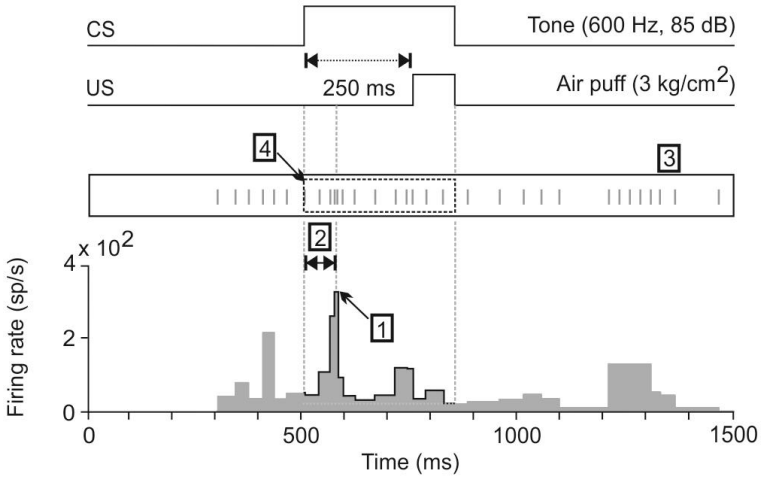

Figure 12. Physiological parameters taken for the pattern recognition of the firing rates. In this diagram, it is shown a delay-conditioning paradigm with 250 ms inter-stimulus interval and the representation of the physiological parameters needed for the supervised and hierarchical clustering method of the firing rate profiles (**Table 6**).

This Doctoral Thesis referred to this last interval as $ISID_{US}$ = ISI + D_{US}, where ISI was the inter-stimulus interval (or CS–US interval) and D_{US} was the duration of the US. In addition, these parameters (3 and 4) enable to study the inter-trials variability in a particular conditioning session (with n = 60 trials) by mean of the raster representations of the spike-events. Peak firing rate (or the maximum instantaneous frequency, in spike/s) was calculated as 1/*rrp*, where *rrp* was the relative refractory period (in s) of the detected neuron.

Classification of the firing rate profiles was implemented in two fundamental steps:

(1) Firing rate profiles were separated in three different levels after applying two amplitude thresholds (in spike/s) for the instantaneous frequency. These thresholds were: Thr 1 (the mean firing rate values in the $ISID_{US}$ interval); Thr 2 (the mean minus three times the standard error of mean (SEM) of the firing rate values in the $ISID_{US}$ interval). Maximum values of the firing rate (parameter 1, **Table 6** and **Figure 12**) were analyzed taking into account the amplitude thresholds (Thr 1 and Thr 2). If the maximum value of the firing rate exceeded the amplitude threshold Thr 1, the firing rate profile was showed in the top level. If the maximum value of the firing rate was between the amplitude thresholds Thr 1 and Thr 2, then the firing rate profile was located in the middle level. Finally, if the maximum value of the firing rate did not exceed the amplitude threshold Thr 2, the firing rate profile was placed in the bottom level.

(2) Latencies corresponding to the peak firing rate with respect to the CS (parameter 2 in **Table 6,** and **Figure 12**) were sorted for fixing three subintervals of the $ISID_{US}$ interval: (I) [CS, CS+D1] ms; (II) [CS+D1, CS+D1+D2] ms; and (III) [CS+D1+D2, CS+D1+D2+D3] ms. In general, these subintervals were depending on the values of D1, D2 and D3, which must satisfy that D1+D2+D3 = $ISID_{US}$.

In addition, in each raster representation the total number of detected spike-events in all the time-window of the trial (parameter 3), and the number of detected spike-events in the $ISID_{US}$ interval (parameter 4); were taken into account to refine the supervised classification and the pattern recognition of firing rate profiles.

Finally, considering the amplitude thresholds (Thr 1 and Thr 2) and the defined subintervals (I, II and III), nine groups (groups 1–3 in the bottom level; groups 4–6 in the middle level, and groups 7–9 in the top level) were formed to classify the firing rate profiles (**Figure 13**).

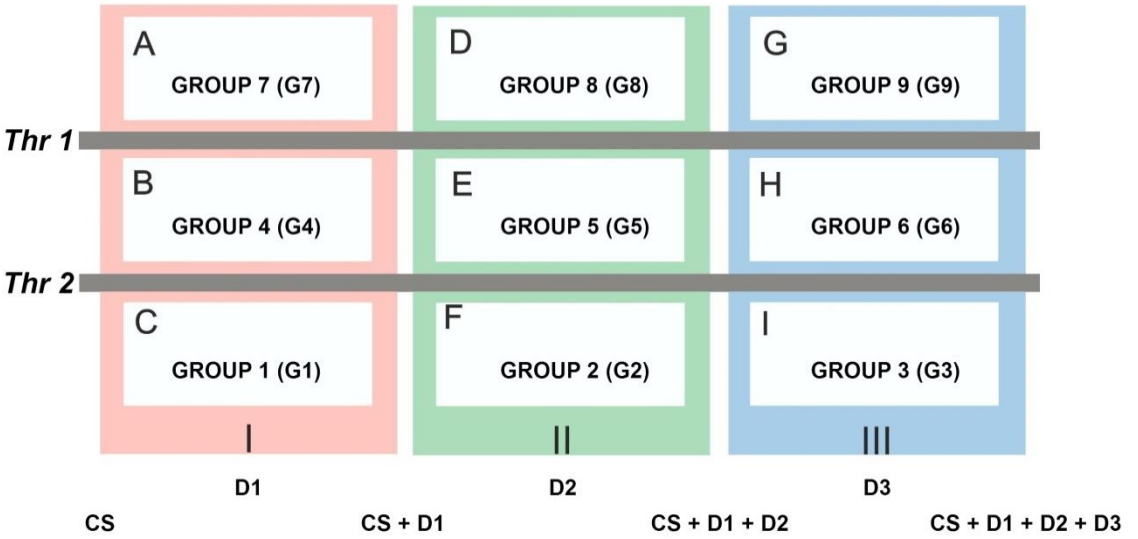

Figure 13. Scheme showing the formation of groups (G1–G9) corresponding to the supervised and hierarchical clustering method of the firing rate profiles. Peak firing rates (parameter 1 in **Table 6**) were analyzed taking into account the amplitude thresholds Thr 1 (the mean firing rate values) and Thr2 (the mean minus three time the standard error of mean (SEM) of the firing rate values). Groups 7–9 are in the top level (i.e., peak firing rate > the amplitude thresholds Thr 1); groups 4–6 are in the middle level (i.e., Thr 2 < peak firing rate < Thr 1); and groups 1–3 are in the bottom level (i.e., peak firing rate < the amplitude thresholds Thr 2). The latencies corresponding to the peak firing rates (parameter 2 in **Table 6**) were sorted for fixing three subintervals of the $ISID_{US}$ interval: (I) [CS, CS+D1] ms; (II) [CS+D1, CS+D1+D2] ms; and (III) [CS+D1+D2, CS+D1+D2+D3] ms. These subintervals were depending on the values of D1, D2 and D3, which must satisfy that D1+D2+D3 = $ISID_{US}$. Abbreviations: CS, conditioned stimulus; US, unconditioned stimulus; ISI, inter-stimulus interval (or CS–US interval); D_{US}, duration of the US; $ISID_{US}$ = ISI + D_{US}, time interval between the beginning of the CS and the end of the US.

3.4. Extractor of Range for Filtering optimization, 'ERFo'

Electrophysiological recording filtering was a crucial step in pre-processing of the recordings. This process was important to eliminate frequency components associated with noise and possible recorded artefacts. For performing the most optimal filtering of the neural recording, a customized algorithm called ERFo (Extractor of Range for Filtering optimization) was designed and developed on MATLAB platform. This algorithm determines the frequency range boundaries (extreme values, maximum and minimum) meant to be optimal for the observation of the recording power spectrum with the largest power in the range of interest.

The proposed methodology for the extraction of an optimal frequency range was based on the analysis of regular differentiations of the electrophysiological recording.

For calculating these regular differentiations were used the first-order and second-order derivatives of a kernel function (Aksenova et al., 2003; Asai et al., 2005; Chibiroba et al., 2005) which was generated by a Gaussian curve with the mean and the standard deviation of the electrophysiological recording (**Figure 14**).

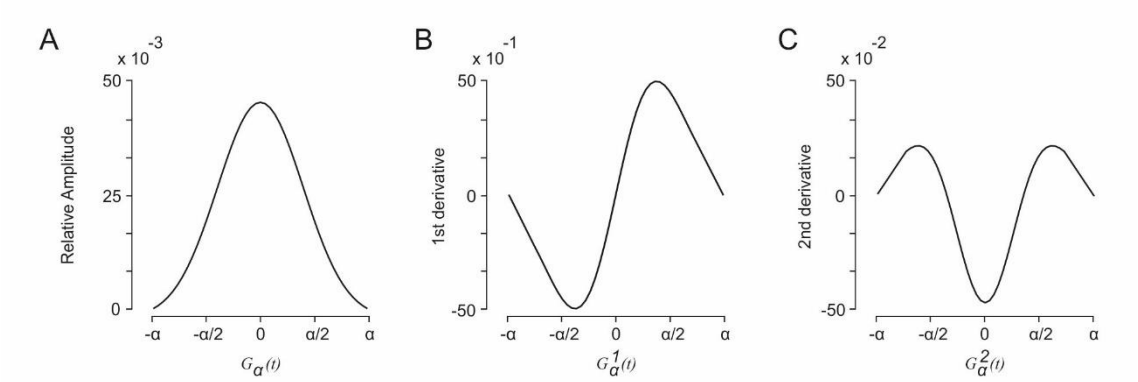

Figure 14. Kernel function and its regular differentiations. (**A**) Kernel function, which is used to estimate the first-order and second-order derivatives of the electrophysiological neural recording. First-order (**B**) and Second-order (**C**) derivatives of the Kernel function. Note that, α is a dummy variable of time (in ms) that indicates the displacement of the Kernel function across the neural recording.

The first-order $D_{\propto}^{1}f(t)$ and second-order $D_{\propto}^{2}f(t)$ derivatives of the recording were calculated through a convolution between the derivatives of the kernel function $G_{\propto}^{j}(t)$ and the recording $f(t)$.

$$D_{\alpha}^{j}f(t) = \left(f * G_{\alpha}^{j}\right)(t) = \sum_{\alpha} f(\alpha)G(t-\alpha) \qquad [15]$$

Where α was a dummy variable of the convolution that reflected the displacement of $G_{\alpha}^{j}(t)$ across of $f(t)$ and j was the order of the derivative (1, first-order; and 2, second-order). The study of these regular differentiations (based on the convolution) provided much more exhaustive results during the computation of the frequency ranges.

Selection of both the kernel function $G_{\alpha}^{j}(t)$ and the value of the parameter α depend on the order of the derivative to be calculated, the level of additive noise, and the required smoothness of the recording.

Once the regular differentiations were calculated (**Figure 15**), two adaptive thresholds were applied which were set automatically to ± 3σ (σ is the standard deviation of the first-order and second-order derivatives of the recording). This strategy assured that the optimal power spectrum was included in the interest range (extracted range).

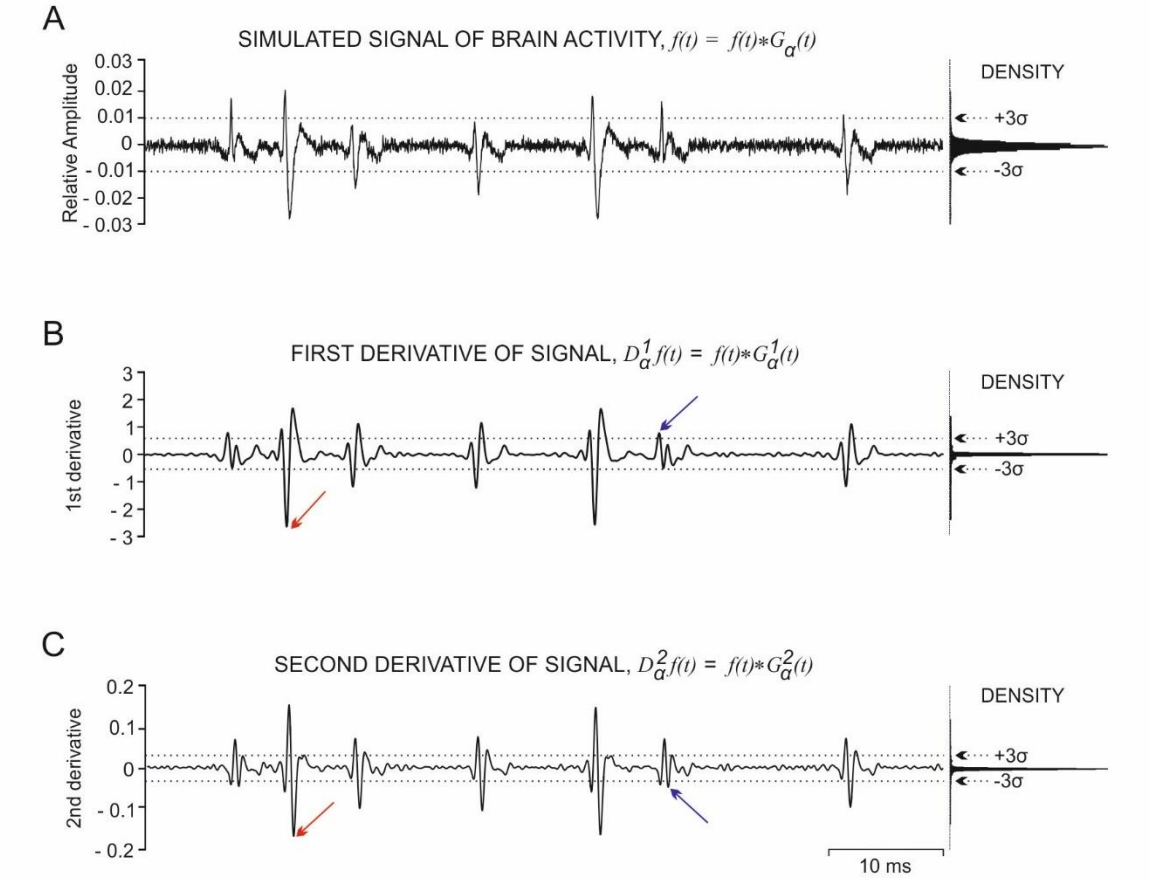

Figure 15. An example illustrating the process of extraction of the frequency range in a simulate recording. (**A**) Simulate recording with low noise [SNR 3.55 dB; see Asai et al. (2005)] is shown during 60 ms at a sampling rate of 44 kHz. (**B**) First-order derivative of the simulate recording shown in A for convolution, $D_{\propto}^{1}f(t)$. (**C**) Second-order derivative of the simulate recording shown in A for convolution, $D_{\propto}^{2}f(t)$. Note that, the horizontal dotted lines in each signal (panels A, B and C) indicate two adaptive amplitude thresholds (± 3σ) for direct spike-events detection. In each panel (A, B and C), σ is the standard deviation of the corresponding signal. On the right of each panel (A, B and C) is shown the probability density function (PDF) for the signal amplitudes. The red arrows indicate the biggest spike-event (with maximum amplitude) and the blue arrows indicate the smallest spike-event (with minimum amplitude).

After applying the thresholds, the extreme values of frequency were obtained (**Figure 16**) by determining the cycle properties of the detected spike-events (e.g., $1/\tau^{1}_{min}$ where τ is the period or duration of the spike-events). Note that, the maximum frequency of the range was in correspondence with the minimum period (τ^{1}_{min} or τ^{2}_{min}) and the minimum frequency of the range was in correspondence with the maximum period (τ^{1}_{max} or τ^{2}_{max}).

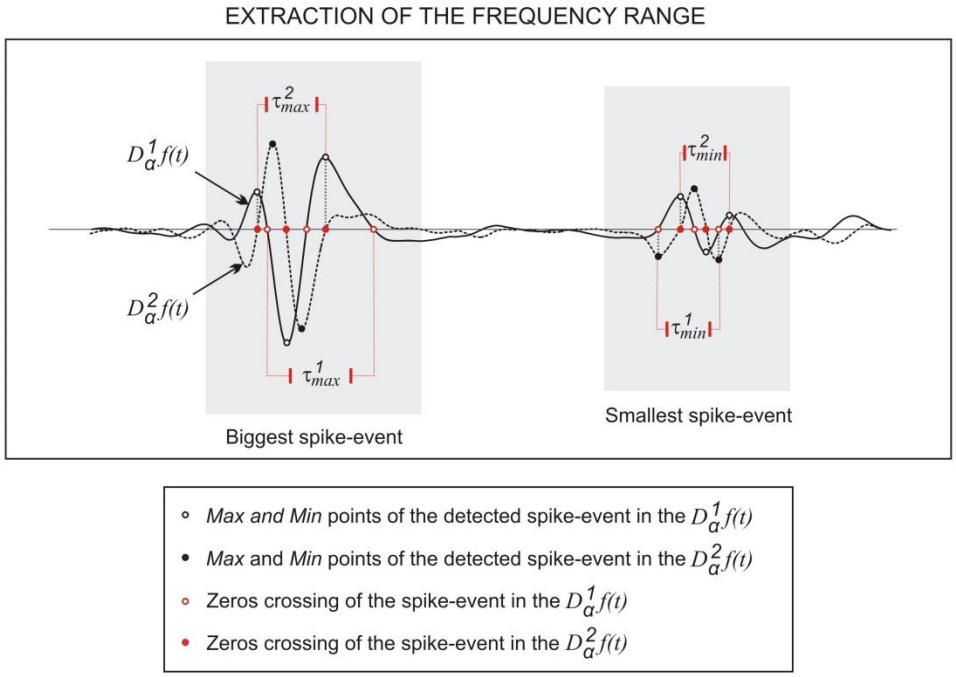

Figure 16. Diagram illustrating the extraction of the frequency range. It is shown the detected spike-events with maximum amplitude (biggest spike-event; on the right) and with minimum amplitude (smallest spike-event; on the left). Notice that, the solid line signal indicates the first-order derivative $[D^1_\alpha f(t)]$ and the dotted line signal indicates the second-order derivative $[D^2_\alpha f(t)]$ of a simulate recording. τ^1_{min} and τ^1_{max} (for the first-order derivative) are the periods corresponding to the spike-events (solid line) with minimum and the maximum amplitudes, respectively. τ^2_{min} and τ^2_{max} (for the second-order derivative) are the periods corresponding to the spike-events (dotted line) with minimum and maximum amplitudes, respectively.

3.5. Application of *Unsupervised Automatic Algorithm* to real experimental data

Finished the design and development of the proposed *Unsupervised Automatic Algorithm* based on the SS-SPDF method, a validate process was performed. The validations were implemented for both simulated data (**Figure 15**) and experimental recordings (e.g., **Figure 9A**). The experimental recordings were acquired from a particular area (the rostro-medial prefrontal cortex) of the circuit of classical eyeblink conditioning. In a first approximation, we implemented the algorithm to extracellular recordings from rostro-medial prefrontal cortex registered by other authors (Leal-Campanario et al., 2007; 2013), specifically, during classical eyeblink conditioning of rabbits with a delay paradigm of 250 ms of CS–US interval.

Once the validation of the algorithm for a delay paradigm of 250 ms was performed and the obtained results were satisfactory; then, it was proceeded to perform a series of experiments where the neuronal activity in the rostro-medial prefrontal cortex of rabbits was recorded during delay paradigms with different CS-US intervals (50, 250, 500, 1000 and 2000 ms; Caro-Martín et al., 2015).

3.5.1. Experimental subjects

Experiments were carried out on 24 adult male rabbits (New Zealand white albino) weighing 2.5-3 kg on arrival, obtained from an authorized supplier (Isoquimen, S.L., Barcelona, Spain). Animals were housed in individual cages for the whole experiment, and kept on a 12/12 h light/dark cycle with constant ambient temperature (21 ± 1 ºC) and humidity (50 ± 7%). Food and water were available ad libitum. All experimental procedures were carried out in accordance with European Union (2010/63/EU) guidelines and Spanish (BOE 34/11370-421, 2013) regulations for the use of laboratory animals in chronic experiments. In addition, all experimental protocols were approved by the local University Ethics Committee.

3.5.2. Experimental preparation

3.5.2.1. Pre-surgery

A daily handling protocol was started the week prior to surgery. The rabbits underwent an intense period of manipulation by the researcher herself for its habituation to the experimental conditions and to the movement restriction box. Only rabbits which did not present problems under these conditions, as stressing signals, were chosen for the following experimental phase.

3.5.2.2. Surgery

Rabbits were pre-anesthetized with a ketamine-xylazine cocktail (Ketaminol®, 25 mg/mL; Rompun®, 3 mg/mL). In addition, atropine sulfate (0.1 mg/kg) was injected them to prevent secretions. The frontal, occipital, and parietal zones of the head, the margin of the right ear and a small perimeter of the anterior left leg were shaved after the rabbits were anesthetized. Finally, an antiseptic solution (Dermozel®, Schering-Plough S.A., Spain) was applied to the rabbit's skin to prevent infections and were moved to the operating room.

Once there, the rabbits were cannulated in the marginal vein of the right ear using an intravenous catheter of gauge 24G (Abbocath®). The infusion flow consisted of 100 ml of physiological serum with a concentration of 10 mg/ml ketaminol (Imalgene®, 25 mg/kg of animal weight) and 3mg/ml xylazine (Rompun®).

The heart rate and oxygen saturation of the rabbits were monitored with a pulsioximeter (Canal- 425SV, MED Associates INC.) and the temperature was continuously monitored and controlled thanks to a temperature control system (TR-200, Fine Science Tools INC.). The body temperature of rabbits was kept within physiological values (39.0 ± 0.5 ºC).

The head of the rabbit was placed in a stereotaxic frame (David Kopf Instruments 1204, Tujunja, CA, USA) and immobilized with a buccal support located under the incisors. In addition, two lateral brackets were fixed in both zygomatic bones. By last, a transparent gel was applied on both corneas (Methocel® 2%, CIBA vision) to prevent desiccation ocular.

All surgery material was sterilized applying heat (≈ 150ºC) during 60 min in a sterilizer (Dryterm, Cod. 2000787, J.P, Selecta S.A, Barcelona, Spain) prior to use. Surgery process was started performing a medial frontal-occipital incision of the head skin and subcutaneous tissues. Temporal muscles were retracted and periosteum was removed with the help of a scalpel and a palette knife to achieve the correct exposure of cranial bones. The exposed area was cleaned with a Ringer solution at 38 ºC and any bleeding was stopped with bone wax (Ethicon®, Johnson & Johnson Intl., Beerse, Belgium).

The head of the rabbit was positioned correctly in order to get an accurate system of coordinates and to locate the desired points on the surface of the skull. Bregma and lambda positions were determined for adjusting the sagittal plane with a stereotaxic manipulator arm. The difference between bregma and lambda was looked for equal to 1.5 mm depth and 18.5 mm anteroposterior (lambda is deeper and caudal to bregrma). Also, with the stereotaxic manipulator arm was located the points where the screws were fixed and the zone of the recording of the neural activity of the prefrontal cortex centred around the 9-11 mm anteroposterior, -1 mm lateral and 2.1-3.8 mm depth respect to bregma (Girgis and Shih-Chang, 1981; Shek et al., 1986). These points and a 5 mm x 5 mm window were drawn.

Four perforations were performed in the cranial bone of the rabbit with a dental drill (NE 120, NSK Dental-Spain, Madrid, Spain).

In the perforations, it was inserted a screw together with a silver wire (**Figure 17E**) which was used like reference electrode and a silver ring with two free extremes (**Figure 17C**), of which one was winded to a screw (**Figure 17D**), and the other was placed in contact with the dura-mater meninge (which served as ground). In the rest of perforations, it was tightened screws as anchoring (**Figure 17F**). All elements were fixed with a layer of cyanoacrylate (Superglue 3, Loctite®) and of dental cement (Duralay®, Dental Mfg. Co., IL, USA). In addition, the 5 mm × 5 mm window was drilled in the frontal bone, centered above the right the rostro-medial prefrontal cortex (Girgis and Shih-Chang, 1981; Shek et al., 1986).

The dura mater was removed, and an acrylic recording chamber was constructed around the window. The brain surface was protected with a piece of silicone sheet, and the chamber was filled with sterile gauze and capped with a plastic cover. A needle tip was implanted stereotaxically in one corner of the chamber for reference purposes during unitary recordings.

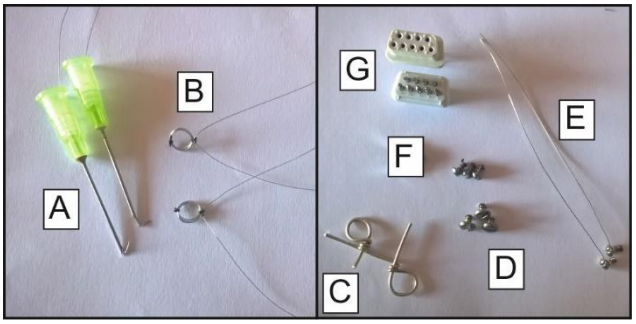

Figure 17. Material used during the surgery procedure. (**A**) Teflon®-coated stainless steel wire (7 strands) electrodes inserted into 23G needles to record the electromyography of the orbicularis oculi muscle. (**B**) Coil of the same thread for recording palpebral movements. (**C**) Ring of silver wire with two different endings of which one is inserted into a hole performed in the rabbit's skull and the other one is attached to a screw placed into the skull and used as one of the grounds. (**D**) Screw fixed in rabbit's skull for holding the silver ring C. (**E**) Screw with silver thread that worked like earth. (**F**) Screws attached to the rabbit's skull to support the female DB-9 connector by means of dental cement. (**G**) 9-way connectors (DB-9) female and male.

In the center of the left upper eyelid, close to the lid margin, a five-turn coil was inserted to measure, study and analyze the palpebral position (**Figure 17B**). Stitches were applied at the ends of the incision to avoid the movement of the coil. Coils were made from Teflon®-coated stainless steel wire (7 strands, A-M Systems, WA, USA) with an external diameter of 50 μm, and weighed 10-15 mg.

Rabbits were also implanted with recording bipolar hook electrodes (**Figure 17A**) in the ipsilateral orbicularis oculi muscle of both eyelids to record the electromyography activity (EMG). These electrodes were made from the same stainless steel wire. In the free ends of the coils and electrodes the Teflon® was removed 2 mm.

Finally, a head-holding system consisting of three bolts cemented to the skull perpendicular to the stereotaxic plane was implanted. A silver electrode (1 mm in diameter) was attached to the skull as a ground. Terminals of the coil and EMG and ground electrodes were soldered to a nine-pin socket (**Figure 17G**). All wire connections were covered with cyanoacrylate glue (Superglue 3, Loctite®), and the whole system was attached to the skull with the aid of three small screws fastened and cemented with an acrylic resin (Duralay®, Dental Mfg. Co., IL, USA) to the bone (for further details, see Leal-Campanario et al., 2013; Caro Martín et al., 2015).

3.5.2.3. Post-surgery

Rabbits were injected with a dose of 1000000 of U.I. of penicillin (Penilevel Retard®, ERN S.A. Laboratory, Spain) and also, a healing cream (Blastoestimulina®, Almirall Prodesfarma, Spain) was applied to the edges of the wounds to prevent infections. Rabbits were recovering for a period of two week in their individual cages.

Weight of the rabbits, the water ingested and the food eaten were checked daily and carefully to prevent signs of discomfort during recovery period. After this period, each rabbit was placed in Plexiglass® restrainer (**Figure 18**) designed for limiting the animal's movements (Gruart et al., 2000) and adapted to the experimental conditions; no stimulus was presented during these sessions. The box was placed on the recording table and was surrounded by a black cloth.

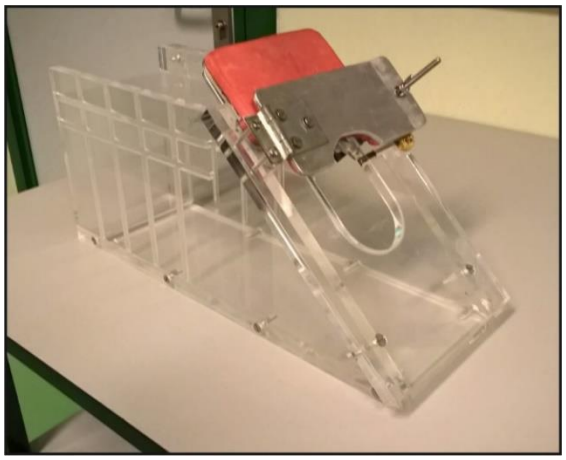

Figure 18. Movement restraining box for rabbits. This box was used for transportation of the rabbit to the recording room and to prevent movement during the experimental protocols. The restraining box made of Plexiglas® allowed to adjust the internal space depending on the size of the rabbits and to fixe with a padded clamp the position of the head.

3.5.3. Experimental protocols

After the recovery and adaptation phase, it was initiated an experimental protocol of classical eyelid conditioning in different groups of rabbits (**Figure 19**). This protocol was carried out during a period of several consecutive sessions (days) and always respecting the hour of beginning of these sessions. The recording room was kept softly illuminated and a 60 dB back-ground white noise was switched on during the experiments. In addition, this room was maintained to a temperature between 20ºC and 22ºC.

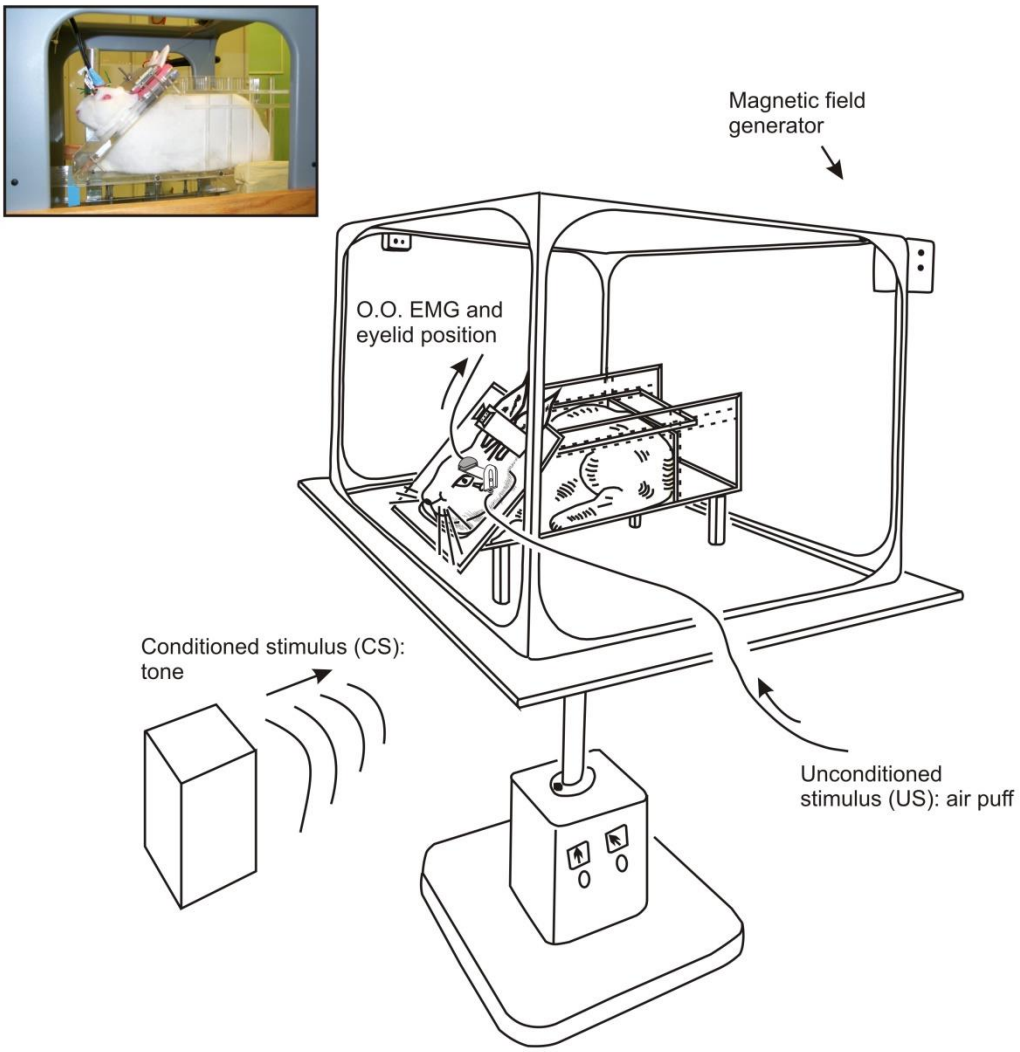

Figure 19. Diagram of the setup used for training the rabbits during the classical eyeblink conditioning using a magnetic field generator frame. The movement of the rabbits was limited by a Plexiglas® restraining box. A tone (conditioned stimulus, CS) was presented to the rabbit before the air puff (unconditioned stimulus, US), which elicited a reflex eyeblink response (unconditioned response). After several paired stimuli, the rabbits responded to the tone with the closing of the eye (conditioned response). The tone was presented through a loudspeaker located in front of the rabbit, and the air puff was directed at the cornea using a plastic tube to 2 cm of its eye. Eyelid movements (position, in degree) were recorded with the magnetic field search coil technique.

3.5.3.1. General procedures

Protocol of a classical eyelid conditioning was carried out in three groups of sessions: habituation, conditioning and extinction sessions with a total of 15 sessions. An experimental session consisted in 66 trials presented with an interval of 60 ± 10 secs among consecutives trials. The 66 trials were showed in 6 blocks of 11 trials. The complete duration of a session was approximate of 1 hour and 10 minutes (**Figure 20**).

Habituation sessions were the first two sessions of the experimental protocol. In these sessions, the conditioned stimulus was presented in isolation into the 66 trials. In the case of conditioning sessions were performed 10 sessions. The first trial of each block belonging to a session was presented as an isolated conditioned stimulus. In the rest of trials, stimuli were presented in pairs (conditioned and unconditioned stimulus). Finally, the rabbits were submitted to three sessions called extinction sessions. In these sessions the conditioned stimulus were presented alone into the 66 trials as in the habituation sessions.

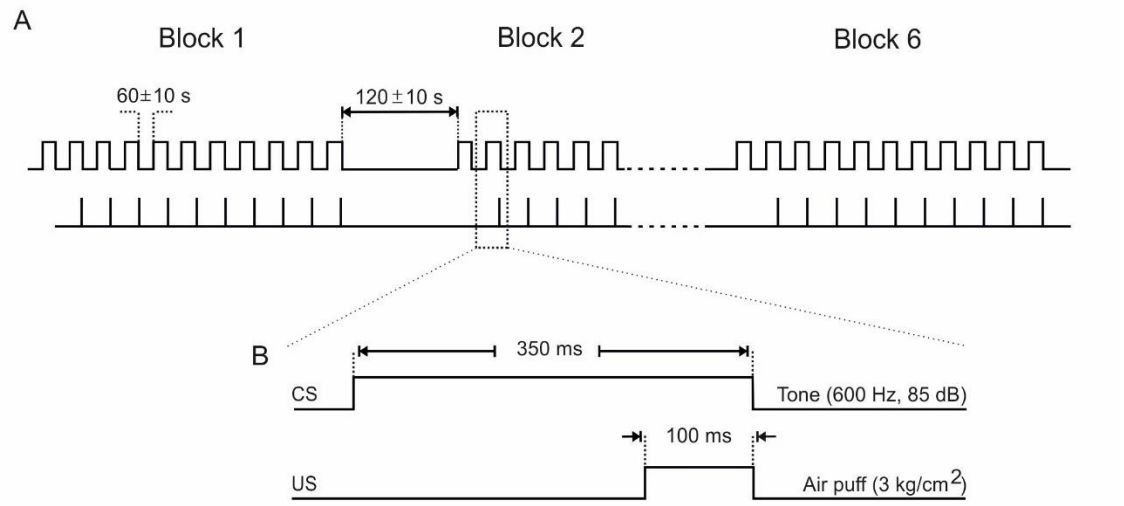

Figure 20. General structure of a conditioning session during the classical eyelid conditioning of rabbits. (A) A session consists of 6 blocks with 11 trials in each block. The interval among trials was 60 ± 10 ms and among blocks it was 120 ± 10 ms. The inter-stimuli interval (conditioned stimulus (CS) - unconditioned stimulus (US) interval) depended on the experimental protocol carried out. The first trial of each block was formed by the conditioned stimulus alone. (**B**) Scheme showing one of the delay paradigms (e.g., inter-stimuli interval of 250 ms) uses to study the prefrontal cortex activity during classical eyelid conditioning of rabbits.

3.5.3.2. Classical eyeblink conditioning: the delay paradigm

Classical eyeblink conditioning was achieved by the use of a delay conditioning paradigm as described in detail previously (Caro-Martín et al., 2015). For this, rabbits were presented with a tone (600 Hz and 85 dB) as conditioned stimulus followed 50, 250, 500, 1000, or 2000 ms from its beginning by an air puff (100 ms and 3 kg/cm^3) aimed at the left cornea as unconditioned stimulus.

In all paradigms, the unconditioned stimulus co-terminated with the conditioned stimulus. Four rabbits were used for each of these five paradigms with different conditioned stimulus - unconditioned stimulus time intervals (**Figure 21**). In addition, tones as conditioned stimulus were applied from a loudspeaker located 80 cm below the animal's head and air puffs as unconditioned stimulus were delivered through the opening of a plastic pipette (3 mm in diameter) attached to a metal holder fixed to the animal's nine-pin socket (dual-channel air-puff device; Biomedical Engineering).

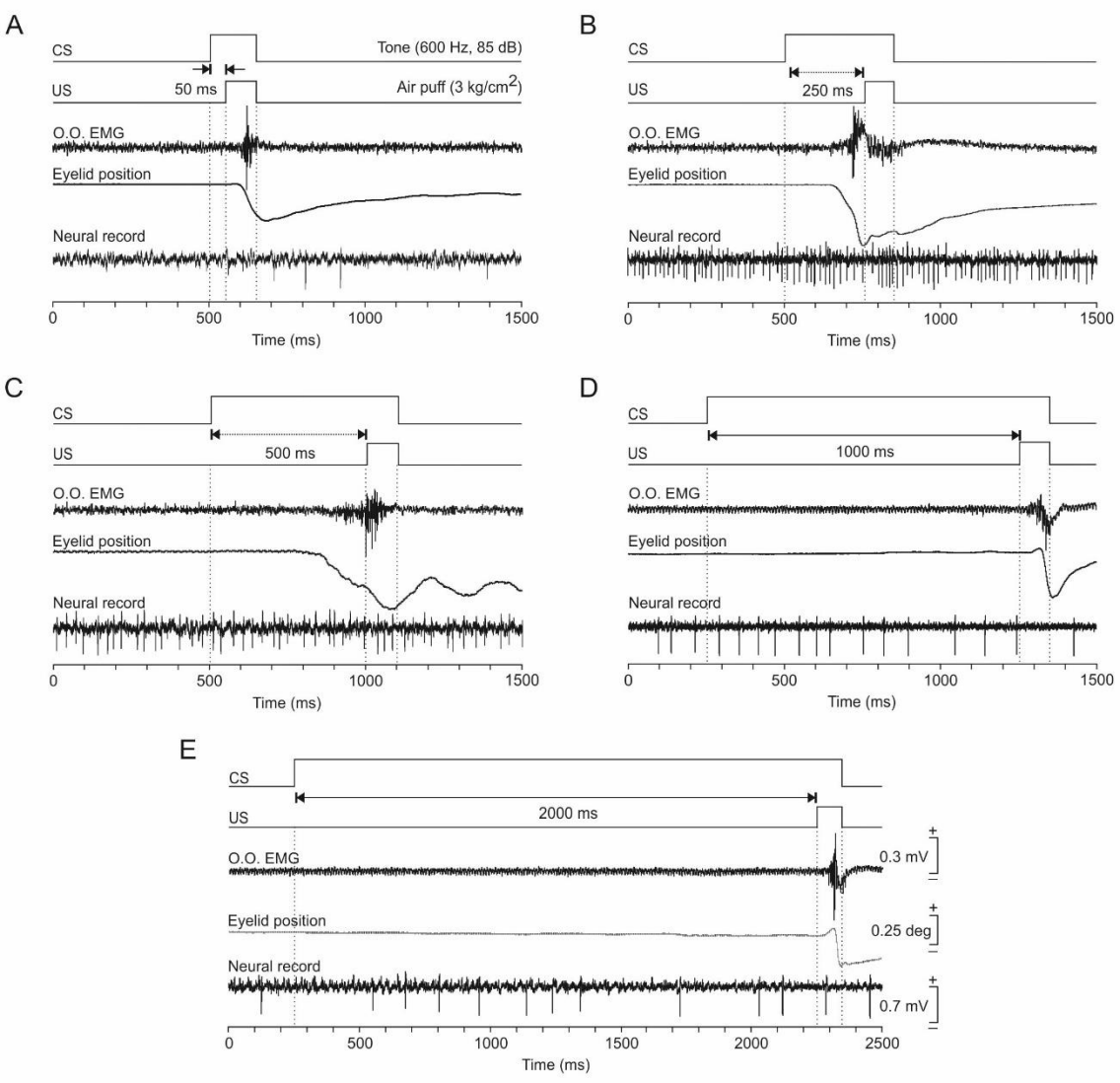

After this protocol, the rabbits were subjected to a paradigm of pseudoconditioning for controlling that the observed changes were a direct consequence of the animal's learning. Pseudoconditioning sessions, performed in four additional animals, also consisted of 66 trials separated at random by intervals of 50–70 secs. For each trial, the conditioned stimulus was presented unpaired in relation to the unconditioned stimulus, the only restriction being that no more than two conditioned stimulus or unconditioned stimulus trials occurred sequentially (Gruart et al., 2000). The total training per session for pseudoconditioning was the same as for conditioning.

3.5.4. Recorded activity

3.5.4.1. Electrical activity of the prefrontal cortex

Neuronal electrical activity was recorded in the rostro-medial prefrontal cortex area with the help of a NEX-1 preamplifier (Biomedical Engineering). These recordings were performed with a glass micropipette of 2 – 3 µm of tip diameter which was manufactured with a micropipette puller (Narishigue, SR-20, Japan). The micropipettes were filled with a 2M solution of NaCl (3–6MΩ of resistance).

Rabbits were introduced in the box of movement restriction and transferred to the recording room. His head was fixed to a bar attached to the experimental table and connected nine-pin socket, after was removed the occlusive dressing from the cranial window. The glass pipette was wrapped with aluminum foil to minimize electrical noise and connected to a ground through a silver wire.

Figure 21. Representation of the experimental protocols using different inter-stimulus intervals (ISI) during a delay paradigm. (**A**) ISI = 50 ms [Conditioned stimulus (CS, Tone, 600 Hz, 85 dB) duration was of 150 ms followed 50 ms from its beginning by the unconditioned stimulus (US, Air-puff, 3 kg/cm^2)]. (**B**) ISI = 250 ms [CS duration was of 350 ms followed 250 ms from its beginning by the US]. (**C**) ISI = 500 ms [CS duration was of 600 ms followed 500 ms from its beginning by the US]. (**D**) ISI = 1000 ms [CS duration was of 1100 ms followed 1000 ms from its beginning by the US]. (**E**) ISI = 2000 ms [CS duration was of 2100 ms followed 2000 ms from its beginning by the US]. In each panel (from A to E), the electromyographic (EMG) activity of the orbicularis oculi muscle (O.O. EMG, in mV), the direct recording of the eyelid position (in degree), and the raw neural record (e.g. from the rostro-medial prefrontal cortex, in mV) are represented.

The recording area was approached with the help of stereotaxic coordinates (**Figure 22**; Girgis and Shih-Chang, 1981; Shek et al., 1986). At the end of each recording session, the recording micropipette was always removed and the recording chamber sterilized and closed.

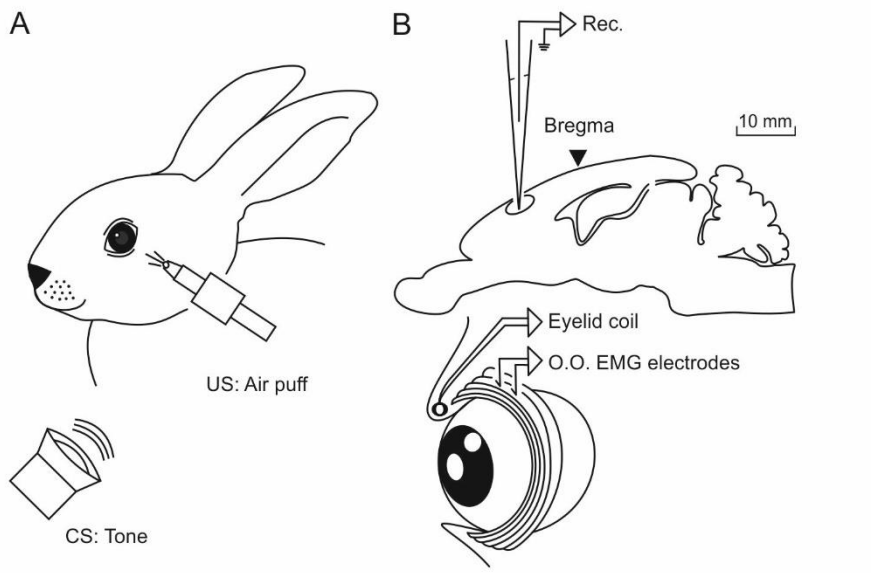

Figure 22. A diagram illustrating the electrodes implantation and the stimuli presented. (**A**) For the classical conditioning of eyelid responses, with a delay paradigm, rabbits were presented with a tone (600 Hz, 85 dB) as conditioned stimulus (CS) followed at different inter-stimulus intervals (50, 250, 500, 1000, or 2000 ms) by an air puff (100 ms, 3 kg/cm^2) directed at the left cornea as a unconditioned stimulus (US). The two stimuli terminated simultaneously. (**B**) Diagram illustrating the rostro-medial prefrontal cortex (rmPFC) recording (Rec.) area. Eyelid movements were recorded using the magnetic field search coil technique with the help of a coil chronically implanted in the left upper lid. Animals were also implanted with electromyographic (EMG) recording electrodes in the ipsilateral orbicularis oculi (O.O) muscle.

Unitary recordings in the rostro-medial prefrontal cortex area were made during habituation, conditioning, extinction and pseudoconditioning sessions. The recording micropipette was approached to the selected recording site with the help of the implanted reference needle. The recording site was changed in the horizontal plane in steps of 0.1 mm until a suitable unit was recorded and identified (Pacheco-Calderón et al., 2012; Leal-Campanario et al., 2013; Caro-Martín et al., 2015). Neuron isolation was performed during the time intervals in which the pairs of stimuli were not presented. Usually, a range of 1–6 neurons was recorded per conditioning session.

3.5.4.2. Eyeblink movements and electromyographic activity of the orbicularis oculis muscle

Eyelid movements were recorded with the magnetic field search coil technique (**Figure 23A;** coil system from C-N-C Engineering). Eyelid coils were calibrated with a transparent protractor placed sagittally to the rabbit's head and with its center located at the external canthus of the lids. Eyelid closures were evoked with air puffs. Upper eyelid maximum opening ranged from 30° to 40° for the 24 rabbits. For the sake of homogeneity, the gain of the recording system was adjusted to yield 1 V per 10° (Gruart et al., 2000).

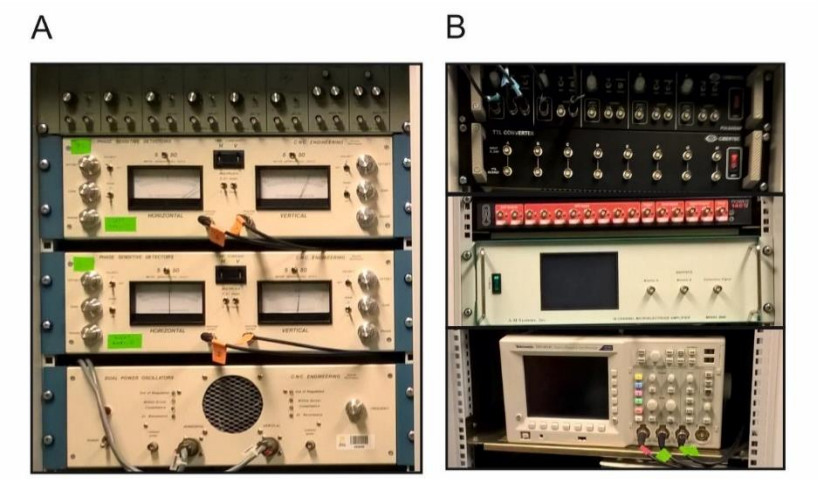

Figure 23. Monitoring and acquisition equipment for the recorded signals. (**A**) Coil system from C-N-C Engineering for the measurement of the eyelid position with the search coil in a magnetic field technique. Eyelid coils were calibrated with a transparent protractor placed sagittally to the rabbit's head and with its center located at the external canthus of the lids. The gain of the recording system was adjusted to yield 1V per 10° (Gruart et al., 2000). (**B**) Above, it is shown a pulse generator and a Transistor-Transistor Logic (TTL) compatible signal converter. Just below, it is shown an analogic-to-digital card converter (Power 1401 MKII with an expansion ADC16 from Cambridge Electronic Design) which constitutes the acquisition system of the neural and electromyography recording signals. Below, it is shown an oscilloscope to properly visualize the signals on-line.

The electromyographic activity of the orbicularis oculi muscle was recorded using a Grass P511 differential amplifier with a bandwidth of 0.1 Hz to 10 kHz. When the electromyographic activity was initiated > 50 ms after conditioned stimulus onset and with peak amplitude at least 2 times greater than the electromyography amplitude recorded 50 ms before the conditioned stimulus onset was considered the presence of a conditioned response during the conditioned stimulus – unconditioned stimulus time interval. In additions, a rabbit was considered conditioned when it was able to produce 80% of conditioned responses per session to the stimulus-paired presentation (Gruart et al., 2000; Leal-Campanario et al., 2007; 2013; Caro-Martín et al., 2015).

3.5.4.3. Digitization and storage

The horizontal and vertical position of the upper eyelid, the unrectified EMG activity of the orbicularis oculi muscle, the unitary activity recorded in the rostro-medial prefrontal cortex, and 1 V rectangular pulses corresponding to conditioned stimulus and unconditioned stimulus presentations were acquired online through an 8-channel analog-to-digital converter (1401-plus; CED), and transferred to a computer for quantitative offline analysis (**Figure 23B**). Data were sampled at 5000 Hz for electromyographic activity and 25000 Hz for unitary activity, with an amplitude resolution of 12 bits.

Computer programs (Spike2 and SIGAVG from CED) were used to display eyelid position, velocity, and acceleration, as well as electromyographic and unitary activities. When necessary for quantitative analysis, segments containing conditioned responses were selected exclusively from those obtained during the presentation of the conditioned stimulus alone (Múnera et al., 2001; Caro-Martín et al., 2015).

3.5.5. Histology

Rabbits were pre-anesthetized by intravenous injection of xylazine (Rompun®, 3 mg/kg of animal weight) and ketaminol (Imalgene®, 25 mg/kg of animal weight). When the rabbits showed total absence of reflexes, chloral hydrate (10%. 141975, Panreac Química S.A.U. Barcelona, Spain) was injected intraperitoneally. For the perfusion the following steps were carried out: (1) a U-shaped incision was performed in the thoracic cage of the rabbit expositing his heart; (2) the pericardial tissue was separated and a solution of 0.5 mL of sodium heparin (Sodium Heparin 1000 UI/mL, Chiesi-Spain S.A) was injected in the ventricular cavity; and (3) a cannula was inserted in the right atrium. Finally, with the help of the peristaltic pump (Master Flex® L/S®, Thermo Fisher Scientific Cat. Nº 7524-45, USA) 1 L of saline solution (0.9%) was introduced for cleaning the circulatory system and 2L of paraformaldehyde (4%) were introduced for fixation tissue.

The proper location of eyelid coil and electromyographic electrodes was checked. In order to determine the recording sites in the prefrontal cortex, a small electrolytic lesion (CS-220 stimulator, Cibertec S.A., Madrid, Spain) was carried out in all of the rabbits, their brain was removed and cut into slices (50 µm). The relevant cortical areas were processed for Nissl staining which provides information about the distribution, size, and morphology of cell bodies (cytoarchitecture) with toluidine blue. This

technique stains the cell bodies of all the cells of the tissue, but does not stain the ramifications. Recording sites were adjusted according to the collected stereotaxic coordinates (Girgis and Shih-Hang, 1981; Shek et al., 1986) and with the location of the electrolytic marks.

3.5.6. Data analysis

3.5.6.1. Kinematics and spectral power of conditioned and unconditioned eyelid responses

For the kinematics of the responses were calculated the velocity and acceleration of eyelid movement. The first and second derivative of eyelid position records which correspond to the velocity and acceleration traces were computed digitally, following low-pass filtering of the data (23 dB cutoff at 50 Hz and a zero gain at ≈ 100 Hz) (**Figure 24**). However, the power spectral of eyelid movements was obtained exclusively from the acceleration trace (Domingo et al., 1997; Gruart et al., 2000; Caro-Martín et al., 2015). The power of the spectral density function (or the power spectrum) of the acceleration was calculated using a fast Fourier transform (FFT) to determine the relative strength of the different frequencies present in eyelid displacements. Acceleration segments (1.024 s) containing conditioned responses were selected exclusively from those obtained during the presentation of the conditioned stimulus alone.

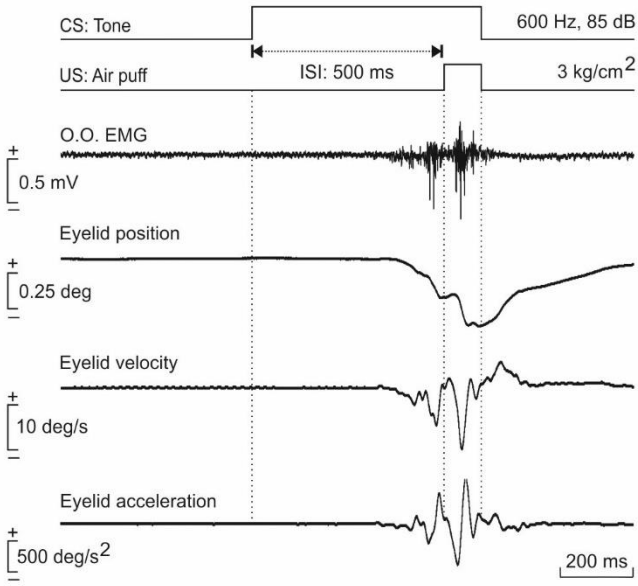

Figure 24. Representative example of a conditioned response recorded during a session of classical eyelid conditioning. From top to bottom are illustrated a conditioning paradigm and representative examples of the electromyographic activity of the orbicularis oculi muscle (O.O. EMG, in mV), eyelid position (in deg.), velocity (in deg./s), and acceleration (in deg./s^2), during the paired presentation of the conditioned stimulus (CS, Tone, 600 Hz, 85 dB) followed 500 ms later by the unconditioned stimulus (US, Air-puff, 3 kg/cm^2).

3.5.6.2. Overlapped firing rates and the spectral analysis of their oscillation profiles

The main characteristics of the firing rate profiles were examined studying the time-locked firings and the maximum firing rates. Different firing rate profiles were first averaged and then overlapped for studied the possible existing oscillations among them. These oscillations were explored through the spectral analysis, which was performed by fitting a trigonometric waveform to the overlapped firing rates. This fit was obtained with the help of the equation $f(t) = a_0 cos(wt)$ where a_0 was the mean value of the dominant peaks of the overlapped firing rates and $w = 2\pi/T$ was the angular frequency. Here T was the average of the latency between the firing rate peaks with respect to conditioned stimulus presentation. The value of T and the corresponding fundamental frequency of the oscillation profile was determined for each CS–US interval. The main goal was to determine the relationship between the period T of the neural oscillation profile and the duration of the CS–US interval (ISI), ─that is, the ratio $\lambda = T/\text{ISI}$.

3.5.6.3. Statistical analysis

Computed results were processed for statistical analysis using the Sigma Plot 11.0 package (Sigma Plot, San Jose, CA, USA) and the MATLAB Toolbox ['Multivariate Statistics' tools] for Windows. For multivariate statistics assessments, both parametric [ANOVA *F*-tests, with or without Repeated Measures (RM)] and non-parametric [ANOVA tests on Ranks, with RM (Friedman RM ANOVA) or without RM (Kruskal-Wallis ANOVA)] methods were used to assess the statistical significance of differences among groups, followed by the appropriate test for all the pairwise multiple-comparison analyses: Holm-Sidak, or Tukey, or Student-Newman-Keuls, in this order of priority.

When the normality (Shapiro-Wilk, or Kolmogorov-Smirnov tests) and equal variance of the errors (Levene Median test) assumptions were satisfied, the statistic, $F_{[(m\text{-}1),(m\text{-}1)\text{x}(n\text{-}1),(l\text{-}m)}$–with its corresponding orders m (number of groups), n (number of animals), and l (number of multivariate observations), was reported (Sánchez-Campusano et al., 2009). For ANOVA *F*-test with/without RM, the first number (m - 1) represents the variability between groups (that is say, the variability due to the differences among the column means) and determines the numerator degree of freedom in the *F*-distribution table. The second and the third numbers in the bracket following the *F* statistic represent the variability within groups (that is say, the variability due to

the differences between the data in each column and the column mean). For ANOVA *F*-test with RM the second number (*m* - 1)x(*n* - 1) determines the denominator degree of freedom in the *F*-distribution table, while the third number informs about the number of multivariate observations. For ANOVA *F*-test without RM, the second number informs about the number of experimental subjects, while the third number (*l* - *m*) determines the denominator degree of freedom in the *F*-distribution table (Hogg and Ledolter, 1987). The factors related to the statistical model proposed here were the training phase and days, corresponding to one-way or two-ways ANOVA *F*-tests.

When the normality assumption was not verified, the significance (*P* value) of *Chi-square* statistic was calculated using the ranks of the data rather than their numeric values. Ranks are found by ordering the data from smallest to largest across all groups, and taking the numeric index of this ordering. The rank for a tied observation is equal to the average rank of all observations tied with it. Note that ANOVA test on Ranks is a non-parametric version of the standard ANOVA *F*-test, and an extension of the Wilcoxon rank sum test to more than two groups. Thus, the usual *F* statistic is replaced by a *Chi-square* statistic (Hollander and Wolfe, 1999). Finally, the parametric and non-parametric methods were also applied to the data taking in to account the sessions/days as repeated measures.

In general, for all the statistical multivariate tests, the significance level (*P*) was indicated. It is common to declare a result significant if the *P* value is less than 0.05 (*), 0.01 (**), or 0.001 (***).

Wilk's lambda criterion and its transformation to the χ^2 distribution used in MATLAB were used to extract significant differences from MANOVA results (cluster analysis for cells–classes–spikes classification) during the spike-sorting problem in the phase space (Porras-García et al., 2010). Unless otherwise indicated, data are represented by the mean ± standard error of mean (SEM).

4. RESULTS

4.1. Testing of the proposed Unsupervised Automatic Algorithm

As explained in the Material and Methods section, an *Unsupervised Automatic Algorithm* for identifying neural spikes was designed in this Doctoral Thesis. Once its development phase was over, there was the need to test the proposed spike-sorting algorithm. Therefore, verification and validation tests were carried out from the start-up of algorithm to the result.

The *Unsupervised Automatic Algorithm* was tested on:

(1) Simulated records with different levels of noise (Asai et al., 2005; Chibiroba et al., 2005), that were ceded by the Neuroheuristic Research Group (Department of Information Science, and LABEX, Faculty of Business and Economics, University of Lausanne, Switzerland).

(2) Real extracellular recordings from neurons in the rostro-medial prefrontal cortex (rmPFC) obtained by us (Caro-Martín et al., 2015) in the laboratory of the Division of Neuroscience (University of Pablo de Olavide, Seville).

4.1.1. Application and validation on simulated records

In order to verify and validate the proposed spike-sorting algorithm, the simulated records, with and without noise, were analyzed.

The first step was to test the *Unsupervised Automatic Algorithm* in the simulated records without noise. Simulated records were sampled at 44 kHz and they had a duration of 180.333 sec (≈ 3 min). To perform the preprocessing in this particular situation (a simulated record without noise, **Figure 25A**), the filtering of the simulated record was not performed, the first-order derivative of this record was not calculated, and the simulated action potentials were directly detected and aligned.

In addition, the detection of the simulated action potentials was performed applying two amplitude thresholds (horizontal dotted lines in **Figure 25A**) that were manually selected because the algorithm was implemented in a no-noise situation.

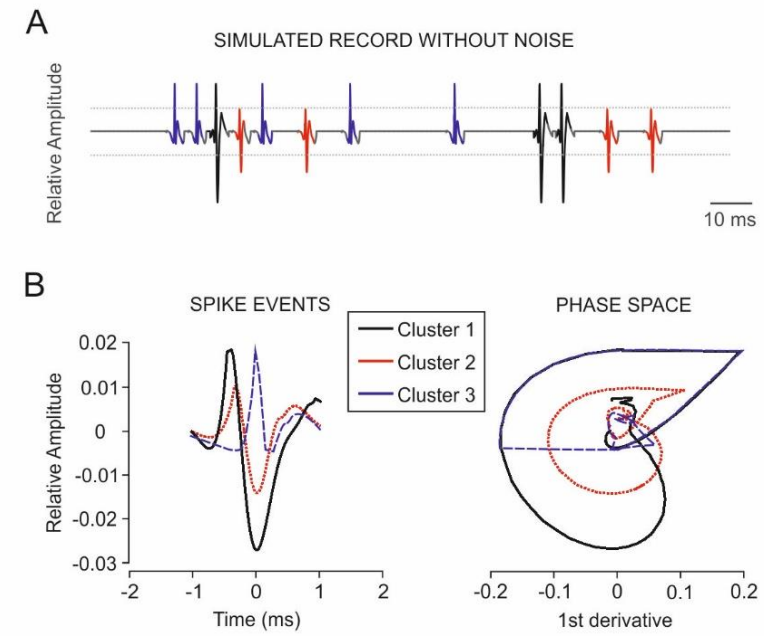

Figure 25. Simulated record without noise illustrating the activity patterns. (**A**) The wide-ranging simulated record was sampled at 44 kHz during 180.333 sec. The time-window of the represented simulated record was of 150 ms. (**B**) At the left, it is represented the three activity patterns (cluster 1, black trace; cluster 2, red trace; and cluster 3, blue trace) of the simulated action potentials clustering using the *Unsupervised Automatic Algorithm*, while the phase space portraits (PSPs; action potential vs. its first derivative) of them are represented at the right part of the panel B. Note that, the simulated action potentials of each cluster are in perfect correspondence to those templates (black, red and blue traces).

For each simulated action potential, a 24D-vector of features was determined and the classification process for all the spike-events was executed. The results allowed to show three activity patterns (cluster 1, 2728 spikes; cluster 2, 2690 spikes; and cluster 3, 2733 in **Figure 25B**). The three activity patterns of the simulated action potentials clustered by the *Unsupervised Automatic Algorithm* are represented in the left part of the **Figure 25B**. In addition, the phase space portraits (PSPs; action potential versus its first derivative) are represented in the right part of **Figure 25B**. Notice that, the simulated action potentials of each cluster were in perfect correspondence to those templates.

For the second validation step, the *Unsupervised Automatic Algorithm* was applied on the same simulated record (sampling frequency, 44 kHz; duration, 180.333 sec) but with a low level of added noise with a signal-to-noise ratio (SNR) of 3.55 dB (see Asai et al., 2005 for details). To perform the preprocessing in this situation (a simulated record with added noise, **Figure 26A**), the simulated record was filtered with a bandpass FIR filter from 450 to 2600 Hz. This frequency range was obtained by applying the ERFo algorithm in the simulated record. In addition, the first-order derivative of the filtered record (**Figure 26B**) was calculated and the spike-events were

detected and aligned. Two amplitude thresholds (horizontal dotted lines in **Figure 26B**) were automatically selected according to the **equation [1]**.

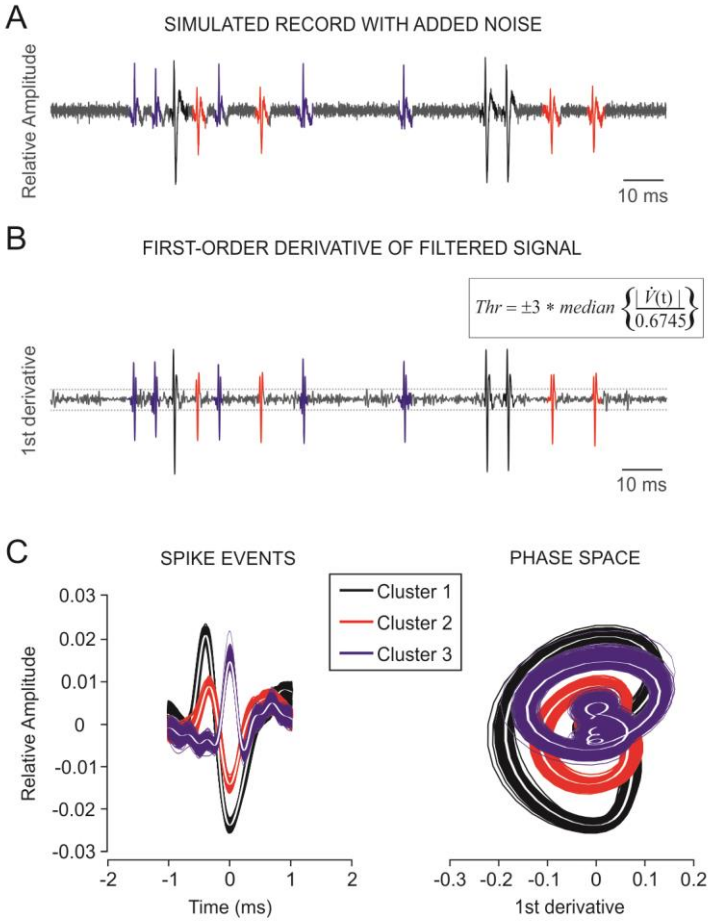

Figure 26. Simulated record with added noise illustrating the activity patterns. (**A**) Simulated record with low added noise and a signal-to-noise (SNR) ratio of 3.55dB. The wide-ranging simulated record was sampled at 44 kHz during 180.333 sec. The time-window of the represented simulated record was of 150 ms. (**B**) First derivative of the band-pass (FIR filter, 450–2600 Hz) filtered record. The horizontal dotted lines indicate the amplitude thresholds for direct spike-event detection (**Equation [1]** is inset). (**C**) At the left, it is represented the three activity patterns (cluster 1, black trace; cluster 2, red trace; and cluster 3, blue trace) of the simulated action potentials clustering using the *Unsupervised Automatic Algorithm*, while the phase space portraits (PSPs; action potential vs. its first derivative) of them are represented at the right part of the panel C. Note that, each white trace (template) represents the mean spike-event of each cluster.

In the same way, for each simulated action potential, a 24D-vector of features was determined and the classification process for all the spike-events was implemented. In this situation (simulated record with added noise), the results allowed to show three activity patterns (cluster 1, 2728 spikes; cluster 2, 2690 spikes; and cluster 3, 2733). At the left of **Figure 26C** are represented the three activity patterns of the simulated action potentials clustered by the *Unsupervised Automatic Algorithm*. In addition, the phase space portraits (PSPs; action potential versus its first derivative) are represented at the

right part of the **Figure 26C**. Gray traces (templates) are indicated the mean spike-events.

The results obtained after performing the two validation tests on simulated records (with and without noise) were similar (i.e., three clusters of activity patterns and the same number of spikes per cluster) to those obtained by other authors (Aksenova et al., 2003; Asai et al., 2005; Chibiroba et al., 2005) who used different feature vectors and other alternative clustering procedures.

4.1.2. Application and validation on extracellular real recordings

Unsupervised Automatic Algorithm was applied on extracellular real recordings of the prefrontal cortex. More precisely, this algorithm was applied and validated to extracellular recordings from the rostro-medial prefrontal cortex (rmPFC) of rabbits during classical eyeblink conditioning with a delay paradigm (Caro-Martín et al., 2015). The rmPFC recordings were obtained during 15 training sessions (two habituation sessions, H01–H02; 10 conditioning session, C01–C10; and three extinction sessions, E01–E03). Each session lasted 1 hour and 10 minutes and was divided in 60 trials of 1.5 sec of duration.

Following the steps described previously in the Data Preprocessing block, each trial was filtered with a bandpass FIR filter from 450 to 2050 Hz. This frequency range was obtained by applying the ERFo algorithm for the rmPFC recordings. ERFo algorithm and the selection of the amplitude thresholds were successfully combined to optimize the preprocessing.

Once the spike-events were detected through the first-order derivative of each filtered recording (**Figure 27A–B**), the spike-events were aligned taking as reference the maximum negative amplitude (**Figure 27C**, left), and the phase space portraits (PSPs; action potential versus its first derivative) were also reconstructed (**Figure 27C**, right).

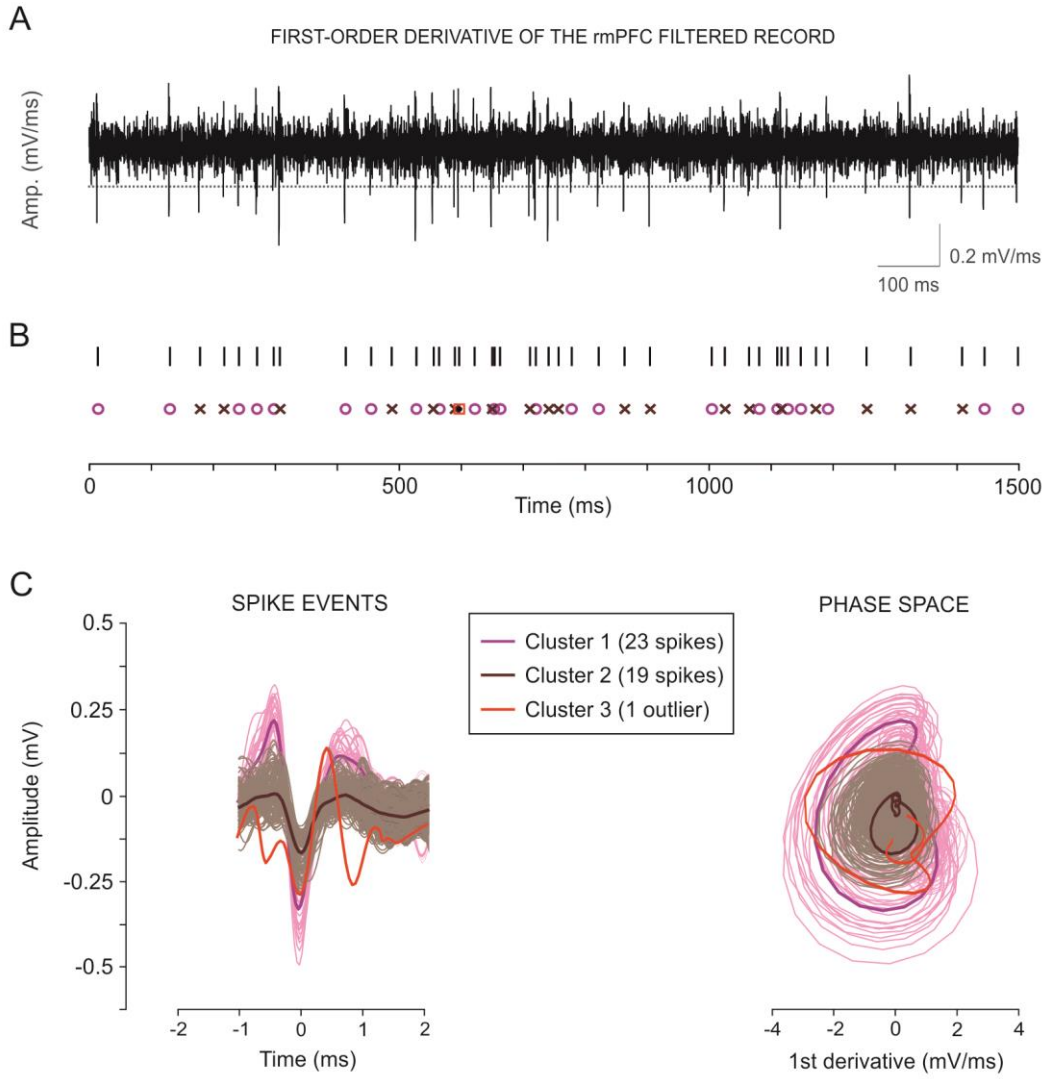

Figure 27. Experimental recording illustrating the neural activity patterns. (**A**) An example of the first derivative of the filtered (band-pass FIR filter, 450–2050 Hz) record (rmPFC, rostro-medial prefrontal cortex). This rmPFC recording was sampled at 25 kHz. The horizontal dotted lines indicate the amplitude threshold for direct spike-event detection. (**B**) For the selected recording (epoch of 1.5 s) three clusters were obtained (cluster 1, 23 spikes; cluster 2, 19 spikes; cluster 3, 1 outlier). (**C**) At the left, the three obtained activity patterns (cluster 1, magenta; cluster 2, brown; and cluster 3, red) are represented in the time domain. At the right, their corresponding phase space portraits (PSPs; action potential vs. its first derivative) are also represented. Note that, the experimental (not simulated) action potentials of each cluster are in perfect correspondence to those templates (magenta, brown and red traces).

Following the procedure described previously in the Spike Classification Block, the twenty-four physiological features based on shape, phase and distribution measures (**Table 2**) were extracted from each spike-event. Special emphasis was placed on determining both the optimal number of clusters (employing the internal validation indices and the *CD*-index; see **Figures 28** and **29**) and the optimal clustering for different feature vectors (applying the *CE*-index; see **Figure 30**).

4.2. Optimal number of clusters, using the validation indices and the *CD*-index

Although the current criterion for the internal validation indices (i.e., maximum values of Silhouette and Dunn indices; minimum value of Davies-Bouldin index) helps to understand better the results of the classification, we corroborated here that the determination of the optimal number of clusters (*K*), applying this criterion, was dependent on the selected distance-metric combination (**Tables 4** and **5**). **Figure 28** illustrates the determination of the optimal number of clusters employing the internal validation indices and the *CD*-index. In this figure are shown the values (in %) of the internal validation indices (Silhouette, Dunn and Davies-Bouldin; see the Material and Methods section for details) for all the combinations (distance versus metric) after applying *K*-means clustering on feature vectors extracted from the neuronal spike-events.

For each selected distance, the resulting number of clusters according to the maximum (for Silhouette and Dunn indices) and minimum (for Davies-Bouldin index) values of the internal validation indices, was different (sqEuclidean, $K = 5$; Cityblock, $K = 3$; Cosine, $K = 5$; Correlation, $K = 4$) and therefore suboptimal, because the goal was to find a single optimal value for the number of final clusters. Moreover, for some combinations (sqEuclidean versus Cosine; sqEuclidean versus Correlation; Cityblock versus sqEuclidean; Cityblock versus Euclidean; Cityblock versus Cityblock; Cosine versus Hamming; Cosine versus Jaccard; Correlation versus Euclidean; and Correlation versus Cityblock) the *maximum-minimum* value criterion was not met (indicated as a failure in the corresponding combination, in **Figures 28B–E** and **29A**).

However, a proper validity measure (*CD*-index) was implemented to obtain the optimal number of clusters among all the distance-metric combinations. The main goal was to make that the three internal validation indices interacted among them according to the three equations shown in **Figure 29B** to produce the maximal cohesion-dispersion of the clustering across all the distance-metric combinations. Success rates of the number of clusters for 60 trials reached 3.17 ± 0.14 in this session. The performance of the internal validation indices (Silhouette, Dunn and Davies-Bouldin) in comparison to the performance of the proposed *CD*-index was showed in the **Figure 29A–C**. Notice that, *CD*-index (**Figure 29C**) always returned definite values (in %) for each distance-metric combination, in contrast with the conventional criterion (for the internal validation indices) that left noticeable gaps in the determination of the number of

clusters when it was not fulfilled (e.g., the failures in Cityblock versus sqEuclidean, and Cityblock versus Cityblock combinations, **Figure 29A**).

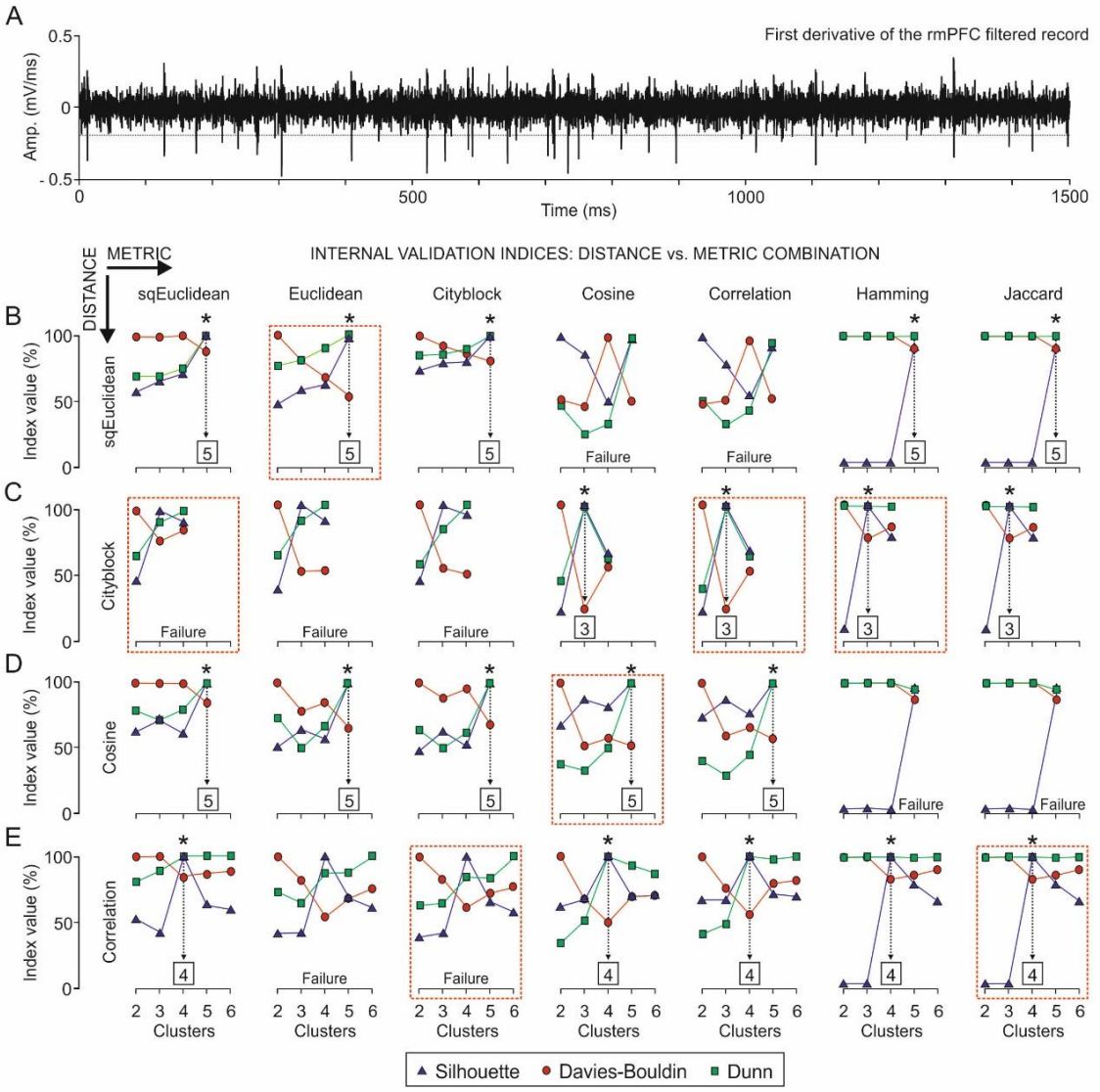

Figure 28. Automatic *K*-means clustering and the internal validation indices. (**A**) An example of the first derivative of the rostro-medial prefrontal cortex (rmPFC) filtered record. The horizontal dotted line indicates the amplitude threshold. (**B-E**) Combination of all possible distances (sqEuclidean, Cityblock, Cosine and Correlation; see **Table 4** for details) and metrics (sqEuclidean, Euclidean, Cityblock, Cosine, Correlation, Hamming and Jaccard; see **Table 5** for details) used by the *K*-means clustering algorithm for the 24D feature vectors (**Table 2**). Each panel indicates the relationship between the value (in %) of the internal validation index (Silhouette, blue triangle; Davies-Bouldin, red circle; or Dunn, green square) and the number of clusters obtained by the unsupervised method. Combinations (distance vs. metric) where the Silhouette and Dunn indices reached their maximum values while the Davies-Bouldin index reached its minimum value were marked with an asterisk (*). In each of these cases, the suboptimal number of clusters was indicated (number inside the square). Red dotted squares enclose some examples (one for each metric) considering different combinations (distance versus. metric) for their comparative analysis in **Figure 29**, employing the cohesion-dispersion index (*CD*-index).

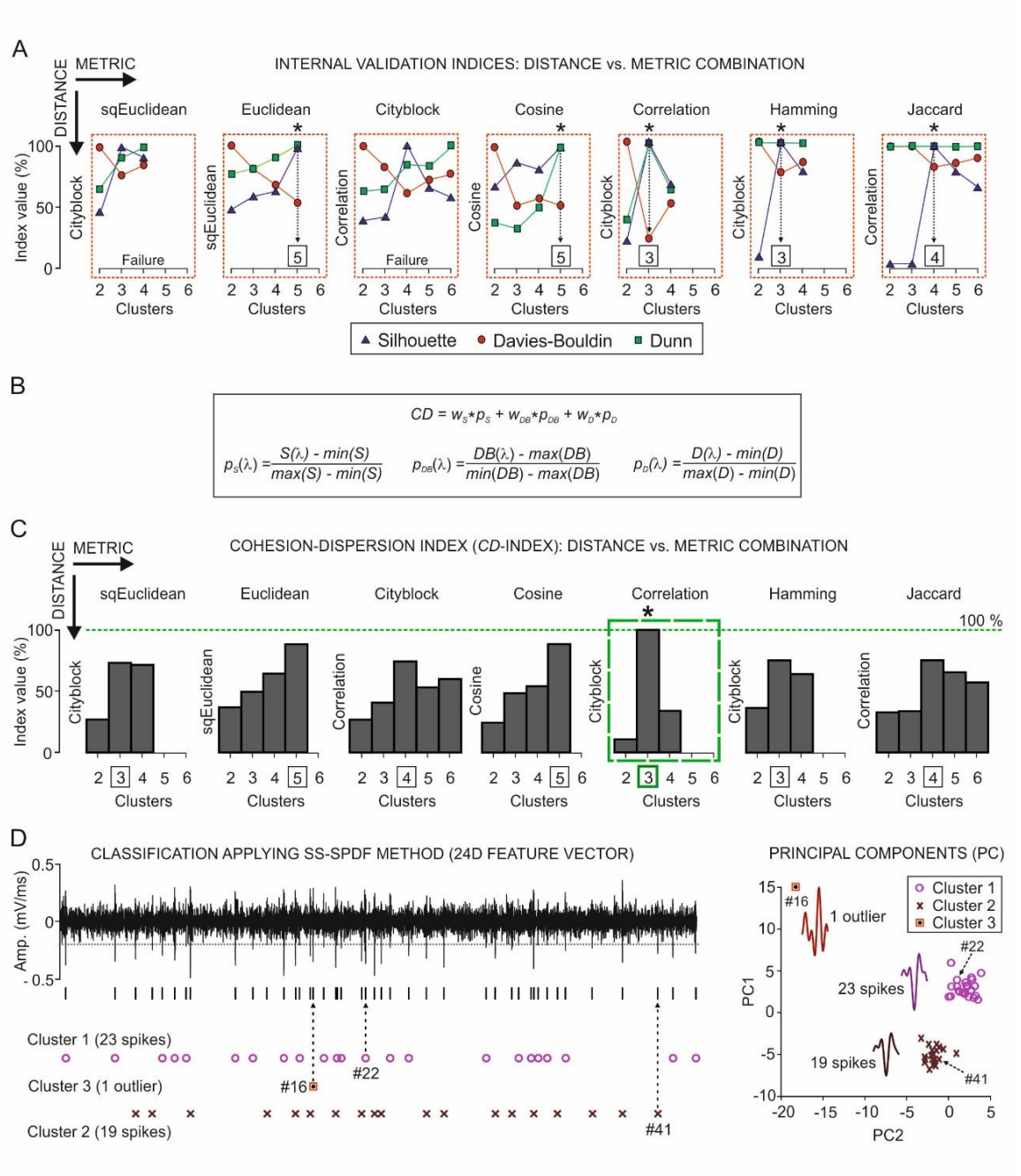

Figure 29. Automatic *K*-means clustering, internal validation indices and cohesion-dispersion index (*CD*-index). (**A**) Some examples of combinations (distance vs. metric) selected from **Figure 28B-E** (red dotted squares) for the 24D feature vectors (**Table 2**). By means of the internal validation indices (Silhouette, Davies-Bouldin, and Dunn) three suboptimal values for the number of clusters were obtained (*K* = 3, 4, or 5). (**B**) Equations for calculating the probability values for each combination (λ, from 1 to 28). The *min* and *max* values were the global extremes of each internal validation index among all the combinations (distance vs. metric). (**C**) *CD*-index value (in %) vs. number of clusters for the seven selected metrics. Note that, the three internal validation indices interact to produce the maximal cohesion-dispersion of the clustering. Therefore, the greatest of all *CD*-index values (i.e., *CD* = 100%, Cityblock vs. Correlation) allowed to obtain the optimal number of clusters (*K* = 3, marked with an asterisk over the green dashed square). (**D**) Classification applying the SS-SPDF method (vectors of 24 features). Note that, for the selected recording epoch (1.5 s; at rmPFC) two clusters were significant (cluster 1, 23 spikes; cluster 2, 19 spikes) in their configurations while the third one was not (cluster 3, 1 outlier). At the bottom right are illustrated the principal components analysis (PC1 vs. PC2 plot) and the waveform templates (magenta, brown, and red profiles) for the resulting clusters.

Finally, the proposed *CD*-index allowed to successfully find the optimal number of clusters (K = 3) which determined the maximal cohesion-dispersion (100%, marked with an asterisk in **Figure 29C**) of the clustering among all the distance-metric combinations. Notice that, for the selected recording trial from the rostro-medial prefrontal cortex (**Figure 29D**) two clusters were significant (cluster 1, 23 spikes; cluster 2, 19 spikes) in their configurations while the other one was not significant (cluster 3, 1 outlier). For this particular example, the number of neurons which was identified and classified as independent clusters of spikes was two. The resulting template of action potentials for each neuron was also represented as result of the principal components analysis (panel at the bottom right in **Figure 29D**).

The next step was to check that the proposed 24D-vector (**Table 2**) of independent and non-redundant features returned the optimal clustering.

4.3. Optimal clustering for different feature vectors employing the *CE*-index

An analysis of the current literature on neuronal spikes pattern recognition revealed a wide variety of feature extraction methods (see **Table 1** of the Introduction section). The proposed *Unsupervised Automatic Algorithm* based on waveform features did not include some of the features proposed by other authors. In this respect, geometric-based features such as areas, energy (E) (Balasubramanian and Obeid, 2011; Bestel et al., 2012), integral transform (IT) (Sonoo and Stalberg, 1993; Zviagintsev et al., 2005; Gibson et al., 2008; 2012), and zero crossing features (ZCF) (Kamboh and Mason, 2013; Saeed and Kamboh, 2013) were rejected, because these features reached a significant ($P < 0.05$) average correlation-coefficient, which value was outside of the confidential interval [$-0.25 < r < 0.25$]. Values of r outside this range indicated that this features were likely not independent among them (multi-collinearity). In additions, for their mathematical formulations was recognized that IT was dependent of the average ZCF, and that E was the square of ZCF. However, the features extraction process of the SS-SPDF method, implemented in the *Unsupervised Automatic Algorithm*, allowed to determine a 24D feature vector whose features were selected for having an average correlation coefficient among them of 0.089 ± 0.02 (mean ± SEM) and *P*-values among them of 0.26 ± 0.01. Notice that, the average correlation coefficient was within the confidential interval [$-0.25 < r < 0.25$] and its value was very close to zero (not significant correlation; *P*-value > 0.05).

In summary, the statistical report indicated that the twenty-four physiological parameters (24D feature vector) of each spike-event were independent features and there was not multi-collinearity among them (see algebraic definitions in **Table 2** of the Material and Methods section).

On the other hand, for checking the relative performance of clustering among different feature vectors, we implemented the *CE*-index (see Material and Methods for details, and **Figure 30**). This alternative error index enabled us to verify the misclassification of clustering.

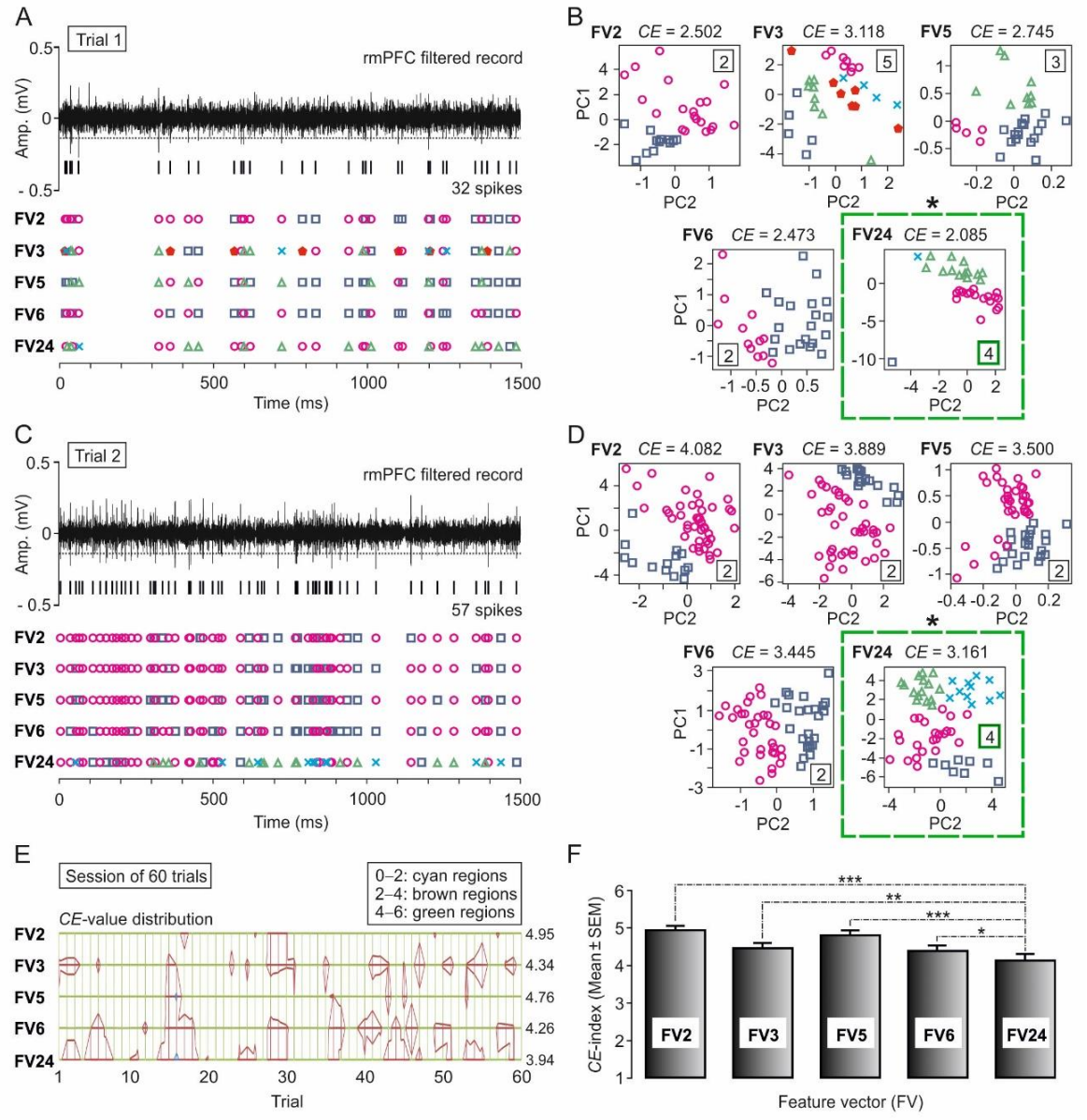

The employed feature vectors (FV) for testing the classification and determining the optimal clustering were the following:

- FV2: Two features were defined in this vector. Zero Crossing Features (ZCF) of the spike [modified of Kamboh and Mason (2013) and Saeed and Kamboh (2013)]. Exactly, the features: ZC1 (the sum of all the values before zero-crossing) and ZC2 (the sum of values after zero-crossing) were extracted of the spike-event of the first derivative.

- FV3: Three features were defined in this vector. The positive peak amplitude (F_{14}) of the spike-event of the first derivative, and the positive (F_{18}) and negative (F_{19}) peaks amplitude of the spike-event of the second derivative. These features were extracted of Paraskevopoulou et al. (2013; 2014).

- FV5: Five features were defined in this vector. The peak-to-valley amplitude, waveform duration, negative Integral Transform (nIT), ratio (nIT/maximum peak) and the logarithm of the maximum rise of the spike-event of the first derivative of the recording. These features were modified of Sonoo and Stalberg (1993), where all the features were directly extracted of the spike waveform.

- FV6: Six features were defined in this vector. Spike peak amplitude, peak roundness, the root-mean-square of pre-spike amplitude, the highest repolarization rate of the spike, the afterhyperpolarization of the spike, and the correlation coefficient between the spike and the reference waveform [modified of Su et al. (2013)]. This modification returned six features equivalent to them, but based on

Figure 30. A comparison of the clustering performance for different feature vectors (FV2, FV3, FV5, FV6, and FV24, with 2, 3, 5, 6 and 24 features, respectively). (**A**), (**C**) Recorded neuronal activities at the rmPFC corresponding to two representative trials (epoch of 1.5 ms). For each trial, the number of identified spike (trial 1 in A, 32 spikes; trial 2 in C, 57 spikes) and the different clusters (spike-events with the same color symbol) are indicated. (**B**), (**D**) shown the process for the determination of the optimal clustering among different feature vectors applying the *CE*-index. For all the principal component (PC) analyses (PC1 vs. PC2 plots), the resulting number of clusters are indicated. In addition, the value of *CE*-index is reported in each panel corresponding to each feature vector. For each selected trial, the lowest value of the *CE*-index (trial 1, *CE* = 2.085; trial 2, *CE* = 3.161) allowed to obtain the optimal clustering among all the classifications (the lowest value of the *CE*-index, marked with an asterisk over the green dashed square, FV24, with *K* = 4). (E) Distribution of the *CE*-index values across the 60 trials in three ranges, which are indicated as contour geometrical regions of different colors (range of 0–2, cyan regions; range of 2–4, brown regions; and range of 4–6, green regions). (F) Multiple comparison analyses. For the pairwise comparisons with significant differences between the mean values of the *CE*-index, the significance level is indicated (*, $P< 0.05$; **, $P < 0.01$; ***, $P< 0.001$; see **Table 8** for details). Data are represented by the Mean ± SEM.

the spike-event of the first or second derivative: negative peak amplitude of the spike-event of the first derivative (amplitude P_2), negative peak amplitude of the spike-event of the second derivative (F_{19}), the root-mean-square of pre-event amplitude of the first derivative (F_8), logarithm of the maximum rise of the spike-event of the first derivative (F_5), positive peak amplitude of the spike-event of the first derivative (amplitude P_4), and the correlation coefficient between the spike-event and the reference waveform of the first derivative (F_4).

– FV24: Twenty-four features were defined in this vector. Description according to the waveform features (shape, phase and distribution measures) proposed in **Table 2** of the Material and Methods section. The twenty-four features were successfully used in Caro-Martín et al. (2015; 2017).

For this purpose, all the rmPFC recordings from different trials in a session and across the different conditioning sessions were analyzed and the corresponding *CE*-index was determined for the feature vector FV24 proposed in this Doctoral Thesis. However, to make the comparisons with the remaining feature vector (FV2, FV3, FV5 and FV6) the neuronal recordings (60 trials, with 1.5 s of duration) corresponding to the 8th conditioning session was selected. To illustrate the results, two representative recordings from the rostro-medial prefrontal cortex were selected (trials of 1.5 sec; **Figure 30A, C**) with different adaptive values of their amplitude thresholds (trial 1, *Thr* = -0.1078 mV; and trial 2, *Thr* = -0.1317 mV). The number of identified spikes in each selected trial was 32 (trial 1), or 57 (trial 2). These identified spike-events (**Figure 30A, C**) were the common start point for the Spike Classification block (**Figure 30B, D**) employing the different feature vectors.

The *Unsupervised Automatic Algorithm* was applied for analyzing these trials (**Figure 30A, C**) and the results revealed that both the resulting number of clusters and the value of the *CE*-index did not depend on the number of features of the vector.

The combination of features used in FV24 returned the lowest value of *CE*-index in trial 1 (*CE*-index = 2.085; $K = 4$; two clusters of neurons and two clusters of outliers with one spike) and in trial 2 (*CE*-index = 3.161; $K = 4$; four clusters of neurons). In the remaining combinations (FV2, FV3, FV5 and FV6) the evaluated clustering (see **Table 7** for details) had a higher *CE*-index value. It seems obvious that a vector of 24 characteristics returns a lower error and therefore the better clustering. However, the

error rate defined in this Doctoral Thesis (see **equation [11]** for the *CE*-index) did not depend on the number of extracted features.

Table 7. Values of the clustering error index (*CE*-index) for different feature vectors (FV). Values of the *CE*-index to check the clustering performance from two representative trials (trials 1 and 2) and from a session of recordings (60 trials, from rmPFC). *CE*-index is reported by the Mean ± SEM (standard error of the mean). The numbers of spikes (*s*) and clusters (*K*) for each trial are also indicated (**Figure 30**).

FV	Feature / Description	*CE*-index value		*CE* = Mean ± SEM
		Trial 1	Trial 2	Session of 60 trial
FV2	Zero Crossing Features (ZCF) of the spike. ZC1 (the sum of all the values before zero-crossing) and ZC2 (the sum of values after zero-crossing). (Kamboh & Mason, 2013; Saeed & Kamboh, 2013).	*CE* = 2.502 *s* = 32 *K* = 2	*CE* = 4.082 *s* = 57 *K* = 2	*CE* = 4.951 ± 0.089
FV3	Positive peak [F_{14}] of the spike FD, and the positive [F_{18}] and negative [F_{19}] peaks of the spike second derivative (SD). (Paraskevopoulou et al., 2013; 2014).	*CE* = 3.118 *s* = 32 *K* = 5	*CE* = 3.889 *s* = 57 *K* = 2	*CE* = 4.340 ± 0.099
FV5	Peak-to-valley amplitude of the spike, waveform duration, negative Integral Transform (nIT), ratio (nIT/maximum peak), and the logarithm of the maximum rise of the spike. (Sonoo & Stalberg, 1993).	*CE* = 2.745 *s* = 32 *K* = 3	*CE* = 3.500 *s* = 57 *K* = 2	*CE* = 4.761 ± 0.088
FV6	Spike peak amplitude, peak roundness (i.e., the spike peak [F_{19}] of the SD), the root-mean-square of pre-spike amplitude, the highest repolarization rate, the afterhyperpolarization (i.e., afterspike minimum), and the correlation coefficient between the spike and the reference waveform. (Su et al., 2013).	*CE* = 2.473 *s* = 32 *K* = 2	*CE* = 3.445 *s* = 57 *K* = 2	*CE* = 4.264 ± 0.103
FV24	Description according to the waveform features (shape, phase and distribution measures) proposed in **Table 3** (Caro-Martín et al., 2015).	*CE* = 2.085 *s* = 32 *K* = 4	*CE* = 3.161 *s* = 57 *K* = 4	*CE* = 3.935 ± 0.108

A lower value of the *CE*-index indicated less misclassified and unclassified events, and therefore a better spike-sorting performance for FV24 (*K* = 4) in comparison with the other selected feature vectors (FV2, FV3, FV5, and FV6). Furthermore, the classification employing the feature vector FV24 had the best arrangement between the value of *CE*-index and the number of clusters (**Table 7**). In this case there were a greater resemblance between the spike waveforms of each cluster and its template.

On the contrary, the classifications employing the feature vectors FV2 (including the zero crossing features ZC1 and ZC2) and FV3 (including the common features F14, F18 and F19) reached the two highest inter-trials values (trial 2; FV2, *CE* = 4.082; FV3, *CE* = 3.889) of the *CE*-index, whereas the number of clusters was the lowest (*K* = 2). For the trial 1 (**Figure 30A, B**), the classification applying the feature vector FV3 had the worst fit between the value of *CE*-index (maximum *CE*-index = 3.118) and the

number of clusters (K = 5). In the case of the trial 2 (**Figure 30C, D**) the classification applying the feature vector FV2 had the worst value of *CE*-index (maximum *CE*-index = 4.082) whereas the number of clusters was the lowest (K = 2). In summary, in the trial 1, the classification employing FV24 successfully identified two clusters of neurons (cluster 1, 17 spikes; cluster 2, 13 spikes) and two outliers, with the lowest value of *CE*-index (*CE*-index = 2.085). In the trial 2 the classification using FV24 successfully identified four clusters of neurons (cluster 1, 15 spikes; cluster 2, 11 spikes, cluster 3, 23 spikes; and cluster 4, 8 spikes), with the lowest value of *CE*-index (*CE*-index = 3.161).

The results for these representative trials indicated that the classification applying a 24D-vector (FV24, with K = 4 clusters of neurons in both trials) had better clustering performance that the classifications employing the other selected feature vectors (FV2, FV3, FV5, and FV6, all with different number of clusters of neurons; **Table 7**).

Furthermore, for each selected feature vector, the values of the *CE*-index for several trials (n = 60) of the representative recording session (8th conditioning session) were calculated (**Table 7**). The range of values for the *CE*-index across the trials and for all the classifications applying the different feature vectors was $1.585 \leq$ *CE*-index ≤ 5.823. In the **Figure 30E** was showed the distribution of the *CE*-index values across the 60 trials in three ranges, which were represented as contour geometrical regions of different colors (range of 0–2, cyan regions; range of 2–4, brown regions; and range of 4–6, green regions). Notice that the proportion of values in the range between 4 and the maximum (5.823) was greater than between 2 and 4 for all feature vectors, except for FV24 for which the proportion was very similar in both ranges.

For these extended datasets, the results also indicated (**Figure 30F**) that the lowest mean value of *CE*-index was obtained for FV24 (*CE*-index = 3.935 ± 0.108). Furthermore, the multiple comparison analyses revealed that there were statistically significant differences ($P \leq 0.03$) between the mean values of the *CE*-index for the pairwise comparisons employing FV24 (*CE*-index = 3.935 ± 0.108) and the other selected feature vectors, whose *CE*-index values (mean ± SEM) were also reported in **Table 7**. However, there were not significant differences in the mean values of *CE*-index for the pairwise comparisons FV2 against FV5 (P = 0.104) and FV3 against FV6 (P = 0.646).

See **Table 8** for more details about these statistical reports.

Table 8. Statistical reports corresponding to the comparison of the mean values of the *CE*-index employing different feature vectors (FV2, FV3, FV5, FV6, and FV24) to check the clustering performance from a session of recordings [n = 60 trials, from the rostro-medial prefrontal cortex (rmPFC)]. Here, the values of the statistics *H* (One-Way ANOVA on Ranks) and *F* (One-Way ANOVA *F*-test) are reported. The significance level (*P*-value) is indicated in each case.

Many Groups (Central Measurement)	**Statistical Test**	**Report**	***P*-value**
FV2 vs. FV3 vs. FV5 vs. FV6 vs. FV24	Kruskal-Wallis One-Way ANOVA on Ranks	H = 62.091 with 4 degrees of freedom	$P < 0.001$; ***
FV2 vs. FV5 vs. FV24	Kruskal-Wallis One-Way ANOVA on Ranks	H = 50.365 with 2 degrees of freedom	$P < 0.001$; ***
FV3 vs. FV6 vs. FV24	Kruskal-Wallis One-Way ANOVA on Ranks	H = 7.049 with 2 degrees of freedom	$P = 0.029$; *
Two Groups (Pairwise comparison)	**Statistical Test**	**Report**	***P*-value**
FV2 vs. FV24	Kruskal-Wallis One-Way ANOVA on Ranks	H = 39.576 with 1 degree of freedom	$P < 0.001$; ***
FV3 vs. FV24	One-Way ANOVA *F*-test	$F_{(1,12,118)} = 7.537$	$P = 0.007$; **
FV5 vs. FV24	Kruskal-Wallis One-Way ANOVA on Ranks	H = 33.550 with 1 degree of freedom	$P < 0.001$; ***
FV6 vs. FV24	One-Way ANOVA *F*-test	$F_{(1,12,118)} = 4.822$	$P = 0.030$; *
FV2 vs. FV3	Kruskal-Wallis One-Way ANOVA on Ranks	H = 18.549 with 1 degree of freedom	$P < 0.001$; ***
FV2 vs. FV5	Kruskal-Wallis One-Way ANOVA on Ranks	H = 2.639 with 1 degree of freedom	$P = 0.104$
FV2 vs. FV6	Kruskal-Wallis One-Way ANOVA on Ranks	H = 22.169 with 1 degree of freedom	$P < 0.001$; ***
FV3 vs. FV5	Kruskal-Wallis One-Way ANOVA on Ranks	H = 11.462 with 1 degree of freedom	$P < 0.001$; ***
FV3 vs. FV6	Kruskal-Wallis One-Way ANOVA on Ranks	H = 0.211 with 1 degree of freedom	$P = 0.646$
FV5 vs. FV6	Kruskal-Wallis One-Way ANOVA on Ranks	H = 16.655 with 1 degree of freedom	$P < 0.001$; ***

Interestingly, the results for an extended datasets (n = 60 trials of the 8th conditioning session) allowed to confirm that both the resulting number of clusters and the value of the *CE*-index did not depend on the number of features used in the *Unsupervised Automatic Algorithm*. Notice that the classification employing FV2 (with two features) and FV5 (with five features) returned similar mean values of the *CE*-index, and the same for the classification applying FV3 (with three features) and FV6 (with six features). In summary, the optimal clustering with the lowest value of the *CE*-index was obtained employing a 24D-vector of features (FV24) proposed in this Doctoral Thesis.

4.4. Pattern recognition of the firing rate profiles

Once the validation testing of the *Unsupervised Automatic Algorithm* was finished and verifying that this algorithm was able to differentiate independent neurons for each trial, a supervised hierarchical clustering method was applied (see section 3.2 of Materials and Methods for more details). This method was used for grouping the different firing rate profiles of each detected neuron and for recognizing neuronal activity patterns of the rostro-medial prefrontal cortex (**Figures 31–33**). For this purpose, the parameters of **Table 6** (**Figure 12**) and the structure of amplitude and latency thresholds (**Figure 13**) were considered. In this Doctoral Thesis, for pattern recognition of the firing rate profiles, all the trials of each conditioning session that are registered at different depths are taken into account: between four and six different recording zones with depths in the range [2.15, 3.0] mm.

In general, during this classification the electrode depth should be considered as an additional parameter of the clustering. However, for the analyses presented here we have not considered the depth factor, because the extracellular records have been acquired with a microelectrode in the V layer of the rostro-medial prefrontal cortex, and it is known from anatomy that although the depth in the above-mentioned range varies discreetly, the same types of principal and non-principal neurons are always being recorded. The activity patterns for the 3rd, 6th and 9th conditioning sessions during a delay paradigm of 250 ms of inter-stimulus interval are shown in the next sections to illustrate the results of the supervised clustering of the firing rate profiles.

4.4.1. Classification of the firing rate profiles for the 3rd conditioning session

The classification of the firing rate profiles for the 3rd conditioning session (**Figure 31**) yields the following results: (1) there was a greater neuronal discharge activity in groups G7 (panel A), G8 (panel D) and G9 (panel G) with respect to the other groups; (2) many peaks of high instantaneous frequencies (peak firing rate > 70 spikes/s) appear throughout the time domain of the recording trial in these same groups; and (3) in group G7 (panel A) of the 3rd conditioning session the highest (133.18 spike/s) of all peak firing rates was reached, although the largest number of trials with significant patterns (see the raster plot) were detected in group G9. These three observations show the diversity in the distribution of the neuronal activity patterns and their corresponding firing rate profiles during the third conditioning session.

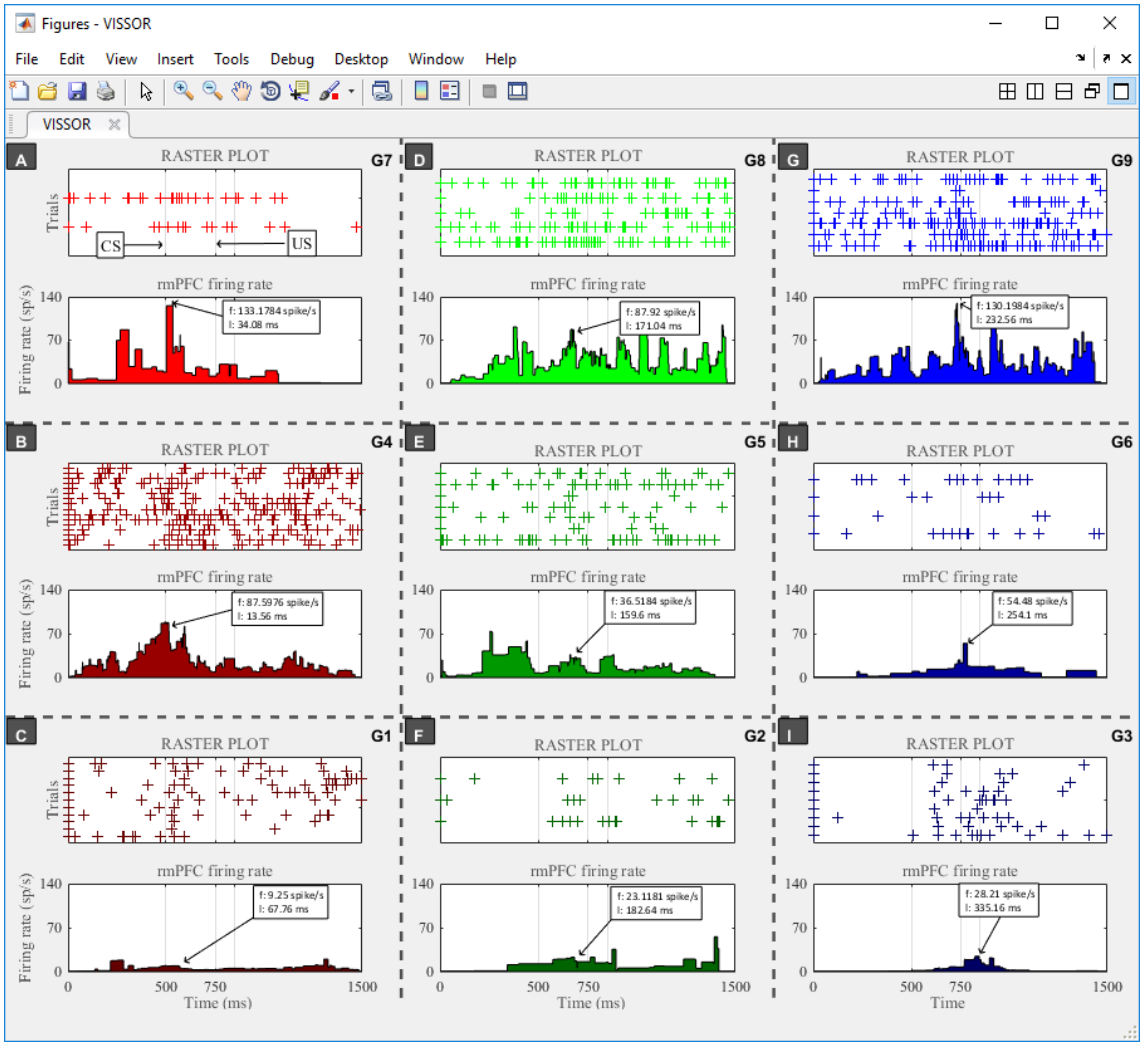

Figure 31. Classification of the firing rate profiles for the 3rd conditioned session. (**A**) Raster plot corresponding to group 7 (G7). The '+' marks (intense red) represent the grouping of the different trials which have a maximum instantaneous frequency higher than the average maximum instantaneous frequency for session. (**B**) Raster plot of the group 4 (G4). The '+' marks (red off) represent the grouping of the different trials which have a maximum instantaneous frequency between the average maximum instantaneous frequency and the average maximum instantaneous frequency minus three times the standard error of the mean. (**C**) Raster plot of the group 1 (G1). The '+' marks (dark red) represent the grouping of the different trials which have a maximum instantaneous frequency lower than the average maximum instantaneous frequency minus three times the standard error of the mean. Groups 7 (G7), 4 (G4) and 1 (G1) have their maximum instantaneous frequency in the interval [CS, CS+100] ms. (**D–I**) The panels D, E and F, as well as the panels G, H and I, are represented with the same scheme described for panels A, B and C, respectively. The difference in the representation consists of the adopted colors (deep green, off green and dark green for the center panels; deep blue, off blue and dark blue for the three panels on the right) and in the temporal distribution of the peak amplitudes of the instantaneous frequency: peaks in the interval [CS+100, CS+200] ms (D, E and F) and in the interval [CS+200, CS+350] ms (G, H and I).

In the remaining groups (from G1–G6) of **Figure 31**, the peak firing rates were significantly lower than in the groups G7–G9, and it should be noted that the instantaneous frequencies were significantly different and had a large variation across trials. However, and as regularity, it was possible to detect three specific moments of occurrence of the peak firing rate, corresponding to three different subinterval of the $ISID_{US}$ time interval (a delay paradigm of 250 ms of inter-stimulus interval, and 100 ms of US duration):

(I) Groups: G1, G4 and G7; subinterval [CS, CS+100] ms.

(II) Groups: G2, G5 and G8; subinterval [CS+100, CS+200] ms.

(III) Groups: G3, G6 and G9; subinterval [CS+200, CS+350] ms.

4.4.2. Classification of the firing rate profiles for the 6th conditioning session

The results of the analysis of neuronal activity patterns in the rostral medial prefrontal cortex during the 6th conditioning session are presented in **Figure 32**. Notice that the highest of all peak firing rates appears in the group G9 (panel G), in the time interval [CS+200, CS+350] ms, specifically at 246.56 ms of the CS, with an average peak value of 142.88 spikes/s.

However, in the remained groups (G6 and G3) of the same interval, the number of action potentials in the $ISID_{US}$ interval was much lower than in G9 and the maximum instantaneous frequencies were of 13.52 and 24.64 spikes/s, respectively.

Classes of profiles grouped in the upper panels of **Figure 32** show peak instantaneous frequencies in the range of 80-150 spikes/s, but the latency corresponding to each peak was in different time subintervals: (I) group G7, subinterval [CS, CS+100] ms; (II) group G8, subinterval [CS+100, CS+200] ms.

In the remaining groups (from G1–G6) of **Figure 32** the neuronal activity patterns was also significantly lower than the groups G7–G9, and the instantaneous frequencies were significantly different were significantly different and had a large variation (in the time domain) across trials. Notice that, the same regularity as mentioned above was observed, which was that the peak firing rates appeared in three well-determined moments within the $ISID_{US}$ time interval.

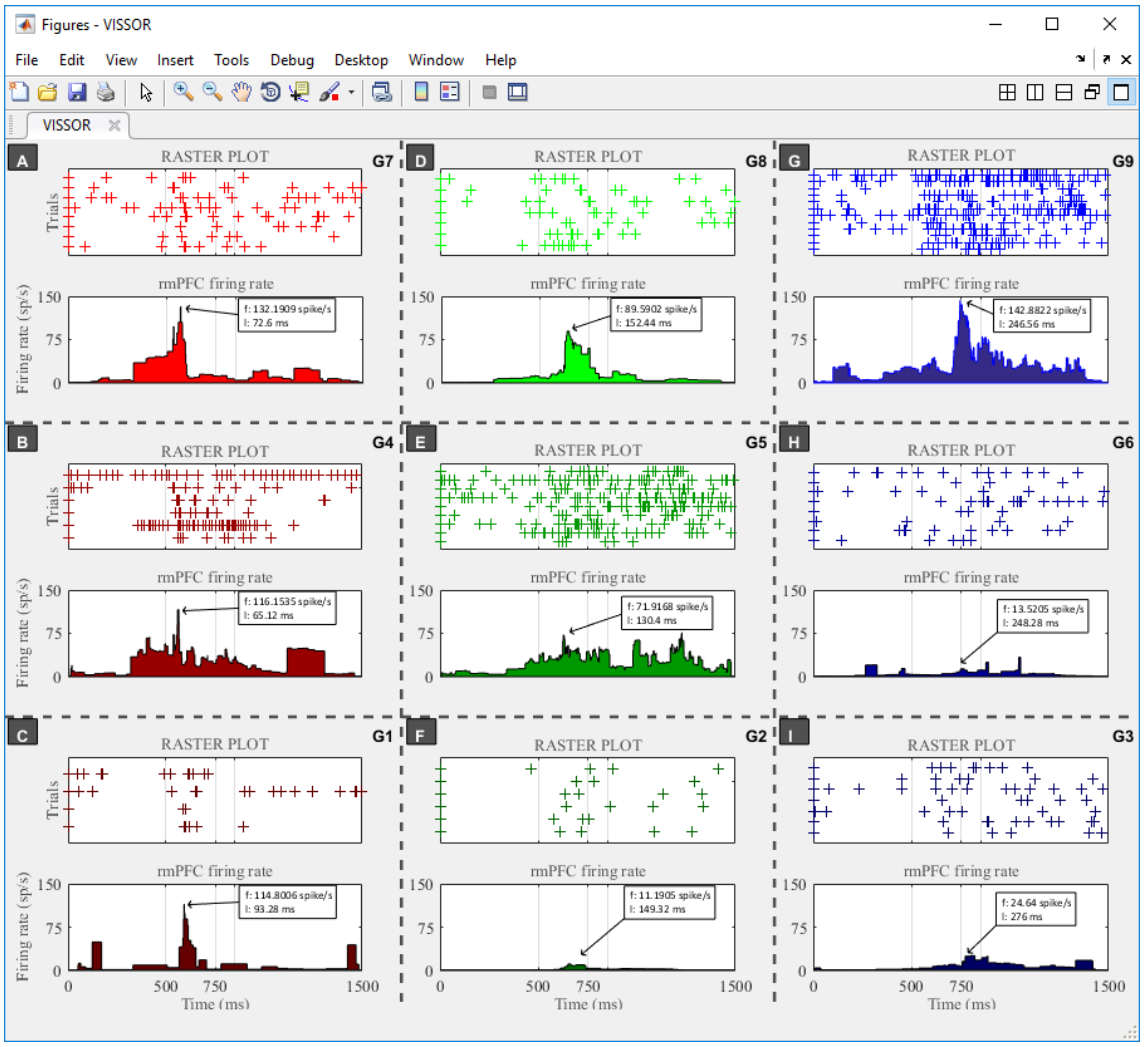

Figure 32. Classification of the firing rate profiles for the 6th conditioned session. (**A**) Raster plot corresponding to group 7 (G7). The '+' marks (intense red) represent the grouping of the different trials which have a maximum instantaneous frequency higher than the average maximum instantaneous frequency for session. (**B**) Raster plot of the group 4 (G4). The '+' marks (red off) represent the grouping of the different trials which have a maximum instantaneous frequency between the average maximum instantaneous frequency and the average maximum instantaneous frequency minus three times the standard error of the mean. (**C**) Raster plot of the group 1 (G1). The '+' marks (dark red) represent the grouping of the different trials which have a maximum instantaneous frequency lower than the average maximum instantaneous frequency for session minus three times the standard error of the mean. Groups 7 (G7), 4 (G4) and 1 (G1) have their maximum instantaneous frequency in the interval [CS, CS + 100] ms. (**D–I**) The panels D, E and F, as well as the panels G, H and I, are represented with the same scheme described for panels A, B and C respectively. The difference in the representation consists of the adopted colors (deep green, off green and dark green for the center panels; deep blue, off blue and dark blue for the three panels on the right), and in the temporal distribution of the peak amplitudes of the instantaneous frequency: peaks in the interval [CS+100, CS+200] ms (D, E and F) and in the interval [CS+200, CS+350] ms (G, H and I).

4.4.3. Classification of the firing rate profiles for the 9th conditioning session

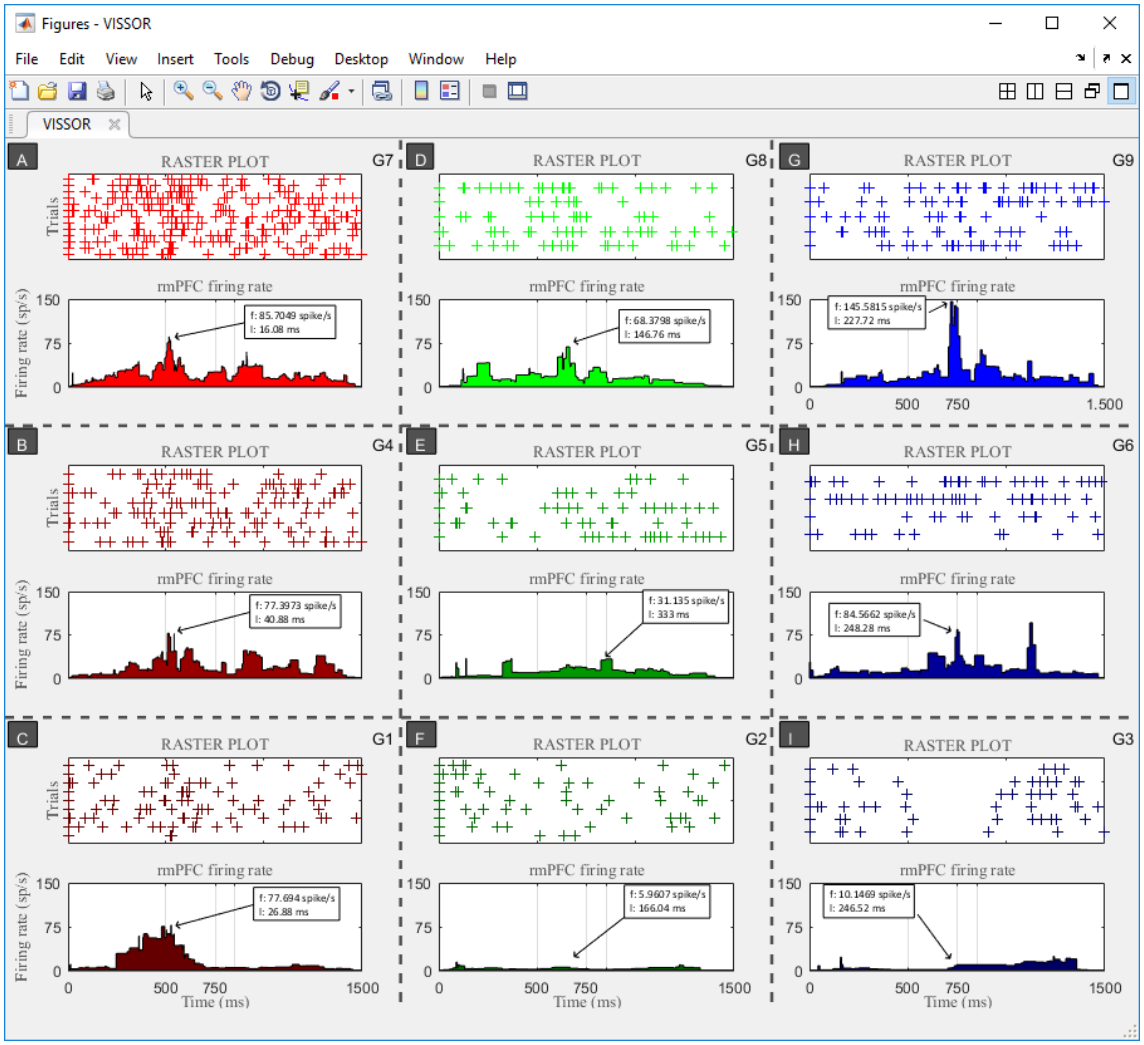

Figure 33. Classification of the firing rate profiles for the 9th conditioned session. (**A**) Raster plot corresponding to group 7 (G7). The '+' marks (intense red) represent the grouping of the different trials which have a maximum instantaneous frequency higher than the average maximum instantaneous frequency for session. (**B**) Raster plot of the group 4 (G4). The '+' marks (red off) represent the grouping of the different trials which have a maximum instantaneous frequency between the average maximum instantaneous frequency and the average maximum instantaneous frequency minus three times the standard error of the mean. (**C**) Raster plot of the group 1 (G1). The '+' marks (dark red) represent the grouping of the different trials which have a maximum instantaneous frequency lower than the average maximum instantaneous frequency for session minus three times the standard error of the mean. Groups 7 (G7), 4 (G4) and 1 (G1) have their maximum instantaneous frequency in the interval [CS, CS + 100] ms. (**D–I**) The panels D, E and F, as well as the panels G, H and I, are represented with the same scheme described for panels A, B and C respectively. The difference in the representation consists in the adopted colors (deep green, off green and dark green for the center panels; deep blue, off blue and dark blue for the three panels on the right), and in the temporal distribution of the peak amplitudes of the instantaneous frequency: peaks in the interval [CS+100, CS+200] ms (D, E and F) and in the interval [CS+200, CS+350] ms (G, H and I).

Finally, the classification of the firing rate profiles for the 9th conditioning session (**Figure 33**) yields the following results: (1) the highest peak firing rates (145.58 spikes/s) was obtained for the group G9 (panel G) in the time interval [CS+200, CS+350] ms (specifically 227.72 ms after CS); (2) the largest number of trials with significant patterns (see the raster plot) were detected in group G7 (panel A); and (3) Group G8 (panel D) had a peak instantaneous frequency whose value was less than the average instantaneous frequency (99.3 spikes/s) among the three groups at the upper level.

Same as during the 3rd and 6th conditioning sessions, during the 9th session the peak firing rates appeared in three well-determined moments, corresponding to the subintervals I, II and III defined above.

After analyzing all the neuronal activity patterns, it was possible to determine that the profiles, whose firing rates were lower than Thr 2 (**Figure 13**), were not significant. **Figure 34** shows the results of the analysis of the firing rate (8th conditioning session) considering only the profiles whose firing rates were between Thr 2 and Thr 1, or were higher than Thr 1.

Similar results to those observed during the 3rd, 6th, and 9th conditioning sessions (regarding nine groups, G1–G9) were obtained during the 8th conditioning session (considering only the six most significant groups, G4–G9).

Therefore, three different neural activity patterns with significant peaks at three well-defined moments of the $ISID_{US}$ interval (350 ms in **Figure 34**) were determined in this Doctoral Thesis during the analysis of the electrophysiological properties of the neurons recorded in the rostro-medial prefrontal cortex of rabbits.

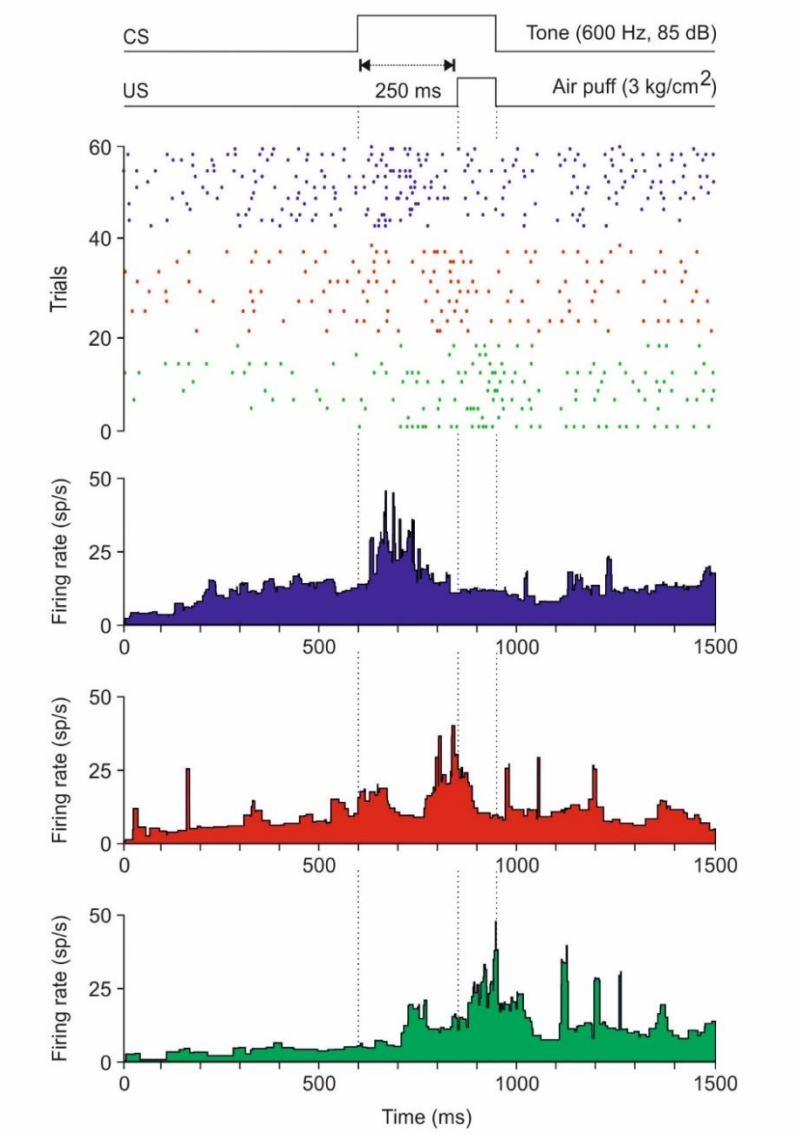

Figure 34. Firing activities of recorded neurons from the rostro-medial prefrontal cortex during classical eyeblink conditioning using a delay conditioning paradigm with 250 ms of inter-stimulus interval. Representative examples of three different types of firing rate recorded during classical eyeblink conditioning. All the illustrated raster displays were collected during the 8th conditioning session (60 trials). The three different firing rates were characterized by having their maximum frequency peaks close to the beginning of the CS (blue raster and firing rate, time to peak 65.3 ms, maximum frequency 47.99 spikes/s); in the center of the CS-US (red raster and firing rate, time to peak 231. ms, maximum frequency 38.15 spikes/s); or next to the end of the US (green raster and firing rate, time to peak 348.99 ms, maximum frequency 49.59 spikes/s).

4.5. Application of *Unsupervised Automatic Algorithm* on recorded neurons from the rostro-medial prefrontal cortex during classical eyeblink conditioning

The main aim of analysing the recorded neurons from the rostro-medial prefrontal cortex was to study how the recorded neuronal activity encoded conditioned eyelid responses in rabbits during a classical eyeblink conditioning. Concretely, how the neurons encoded the oscillatory properties characterizing these conditioned eyelid

responses. For this purpose, five experimental protocols, which depended on different inter-stimulus intervals during classical eyeblink conditioning (**Figure 21**) were designed and carried out in rabbits.

The study of the oscillatory properties of the conditioned eyelid response and recorded neuronal activity during those protocols were carried out as follow:

First, these properties were studied during the classical eyeblink conditioning with a delay paradigm of 250 ms of inter-stimulus interval. The obtained results suggested performing and analyzing a longer inter-stimulus interval during the classical conditioning with the same delay paradigm.

Second, a classical eyeblink conditioning with a delay paradigm of 500 ms of inter-stimulus interval was carried out and analyzed. The performed analysis of the conditioned responses and of the neuronal activity using this protocol (500 ms) and the previous protocol (250 ms) indicated that the neurons could be encoding the duration of the inter-stimulus interval, but not the oscillatory properties of conditioned eyelid responses. Therefore, shorter and longer inter-stimulus intervals than 200-500 ms (Gormezano et al., 1983) were studied and analyzed.

Third, three delay paradigms of 50, 1000 and 2000 ms of inter-stimulus interval were also performed and analyzed to study the limits of the observed effect in the previous protocols (inter-stimulus interval of 250 and 500 ms).

Before analyzing the oscillatory properties in those protocols, the identification of the recorded neurons in the studied area was needed for certifying that the recording sites were limited to the rostro-medial prefrontal cortex.

4.5.1. Histological examination of the recording sites

The histological examination of the recording sites indicated that the studied area was restricted to the rostro-medial prefrontal cortex (AP = 9-11 mm, L = –1 mm, and D = 2.1-3.8 mm from bregma; Girgis and Shih-Chang, 1981; Shek et al., 1986), corresponding to the rostral aspect of Brodman's area 24 or anterior cingulate cortex, and to the rostro dorsal part of Brodman's area 32 or prelimbic cortex (**Figure 35**). Previous histological studies (Benjamin et al., 1978; Leal-Campanario et al., 2007; 2013) had shown that this prefrontal area can be further identified by the preferential projections reaching it from the medial half of the medio dorsal thalamic nucleus.

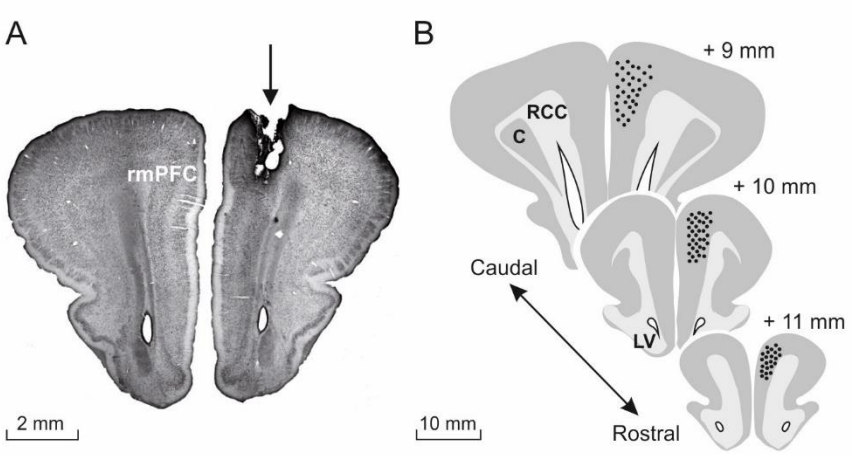

Figure 35. Histological localization of the recording electrode. (**A**) A photomicrograph illustrating an electrolytic lesion (arrow) carried out in the rostro-medial prefrontal cortex (rmPFC) recording sites. (**B**) Schematic diagrams in stereotaxic coordinates from rabbit brain with indication of the recording (black dots) sites. Calibrations for B–D are indicated. Abbreviations: C, claustrum; LV, lateral ventricle; RCC, corpus callosum.

In **Figure 35A**, it is shown a photomicrograph illustrating and electrolytic lesion (arrow) performed in the recordings site. Only recordings obtained throughout electrodes correctly placed in this area were included in the posterior analysis. In **Figure 35B**, it is included a prefrontal cortex drawing indicating with black dots the places where the micropipette tip was located during the electrophysiological recordings in the different sessions and for the different rabbits. All of them where located in the rostro-medial part of 2 mm (in the rostral-caudal axis) of the prefrontal cortex.

4.5.2. Identification of rostro-medial prefrontal cortex neurons

The *Unsupervised Automatic Algorithm* was enabled the proper identification of the recorded unit. Only units with spike duration of > 0.5 ms were considered pyramidal cells and were further analyzed with this algorithm. The spontaneous firing rate of recorded cells ranged from 2 to 15 spikes/s. Characteristically, the neurons presented spontaneous irregular bursts of activity that were similar in duration and profile to those presented by the recorded neurons across conditioning sessions. Because of their firing properties, most of the neurons which were analyzed look similar to the regular-spiking, slow-adapting pyramidal cells described by Dégenètais et al. (2002) —namely, they were capable of generating a tonic firing restricted to a part of the inter-stimulus interval in the presence of conditioned eyelid responses. Spike triggered averaging ($n \geq 3000$ spikes) of recorded neurons did not evoke any identifiable activity in the EMG of the orbicularis oculi muscle, indicating the polysynaptic nature of rmPFC projections to facial motoneurons.

4.5.3. Oscillatory properties of reflex and classically conditioned eyelid responses

As previously indicated, rabbits were prepared for the chronic recording of the electromyography activity of the orbicularis oculi muscle, and of eyelid movements with the help of the magnetic search coil technique. The coil was implanted in the upper lid and the position was recorded for the vertical and horizontal axis. Apart from the eyelid position, the velocity and acceleration profiles of the evoked eyelid responses were also calculated (**Figure 24**). Air-puff-induced blinks consisted of a fast downward movement of the upper eyelid followed by a much slower upward phase until the eyelid's initial position was reached. Mean latency of eyeblinks elicited by 100-ms, 3-kg/cm^2 air puffs was 19.5 ± 4.2 ms (mean ± SD; n = 20). The initial downward phase of evoked eyeblinks presented successive small sags in the direction of closure easily detected in the lid velocity and acceleration profiles.

Provided that all other characteristics of conditioned and unconditioned stimuli were maintained constant, the percentage, profiles, and oscillatory properties of conditioned eyelid responses were highly dependent on conditioned stimulus-unconditioned stimulus time intervals. Rabbits (n = 4) conditioned with a inter-stimulus interval of 250 ms evoked > 50% of conditioned responses by the 3rd conditioning session and reached asymptotic values (> 80% of conditioned responses) by the 4th or 5th conditioning session.

Onset latency of conditioned responses evoked at this conditioned stimulus-unconditioned stimulus time interval decreased through the successive conditioning sessions from 230.3 ± 19.3 ms for the 1st conditioning session to 118.6 ± 18.3 ms for the 10th. As already described (Gruart et al., 2000), evoked conditioned eyelid responses also presented characteristic oscillatory profiles, but with accelerations 1/3 to 1/5 smaller than those reached by reflex eyeblinks.

The optimal conditioned stimulus-unconditioned stimulus time intervals for classical conditioning of nictitating membrane responses in rabbits ranged from 200 ms to 500 ms was showed years ago (Gormezano et al., 1983). In agreement with this early study, rabbits conditioned here with a conditioned stimulus-unconditioned stimulus time interval of 500 ms achieved learning curves slightly lower than those presented by rabbits conditioned with an inter-stimulus interval of 250 ms. Notice that, rabbits (n = 4) conditioned with an inter-stimulus interval of 500 ms evoked > 50% of conditioned responses by the 4th conditioning session and reached asymptotic values (> 80% of conditioned responses) by the 6th conditioning session (**Figure 36**).

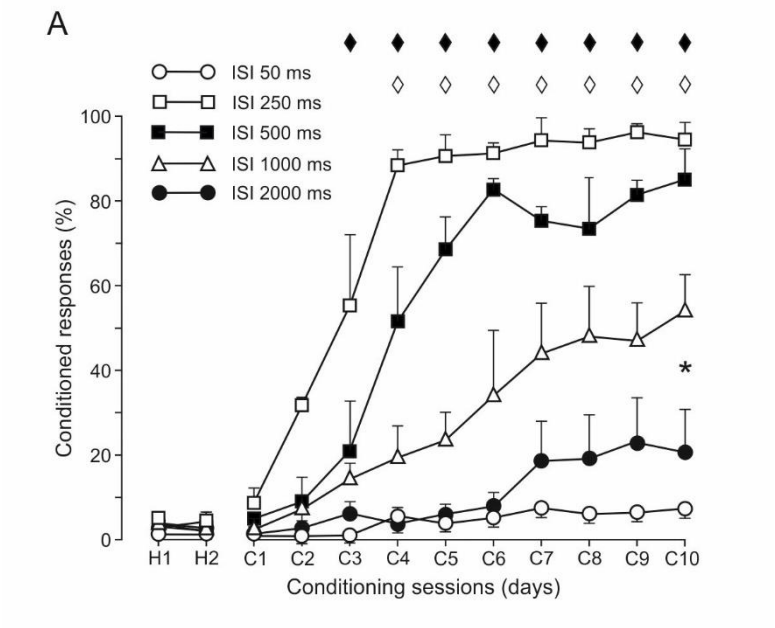

Figure 36. Learning curves during the classical eyeblink conditioning. Evolution of the percentage of conditioned responses (%CRs ± SEM) through the 10 conditioning sessions for five delay conditioning paradigms of different CS-US interval: 50 ms (○), 250 ms (□), 500 ms (■), 1000 ms (Δ), and 2000 ms (●). Note that animals conditioned with 250 ms or 500 ms CS-US intervals reached asymptotic values (80% of CRs) by the 4th to 6th conditioning sessions, but that those trained with the other three intervals failed to reach criterion by the 10th conditioning session. Data collected for intervals of 250 ms and 500 ms were not statistically different, but were significantly ($P < 0.001$) different from those conditionings carried out with the other three CS-US intervals. ♦, $P < 0.001$for (□) vs. (○), (Δ) and (●). ◊, $P < 0.001$ for (■) vs. (○), (Δ) and (●). *, $P < 0.001$ for (Δ) vs. (○) and (●).

In contrast, rabbits conditioned with smaller (50 ms) or larger (1000 or 2000 ms) conditioned stimulus-unconditioned stimulus time intervals presented learning curves significantly (ANOVA on Ranks, $P = 0.170$) lower than those of rabbits trained with inter-stimulus intervals of 250 ms or 500 ms (**Figure 36**). In fact, rabbits trained with inter-stimulus intervals of 50 ms or 2000 ms did not reach the selected criterion (> 40% of conditioned responses by the 10th conditioning session) for the proper acquisition of this type of associative learning task.

A power spectrum analysis was carried out to determine the frequency components of the successive downward waves of air-puff-evoked blinks. The mean power spectra of 30 acceleration records from air-puff-evoked blinks collected from four rabbits showed a dominant peak at 12.6 ± 0.9 Hz over abroad band of frequencies between 7 Hz and 17 Hz (**Figure 37A**). This dominant oscillation for reflexively evoked blinks was slightly faster than that reported in a previous study also in rabbits (4 - 15 Hz; Gruart et al., 2000)

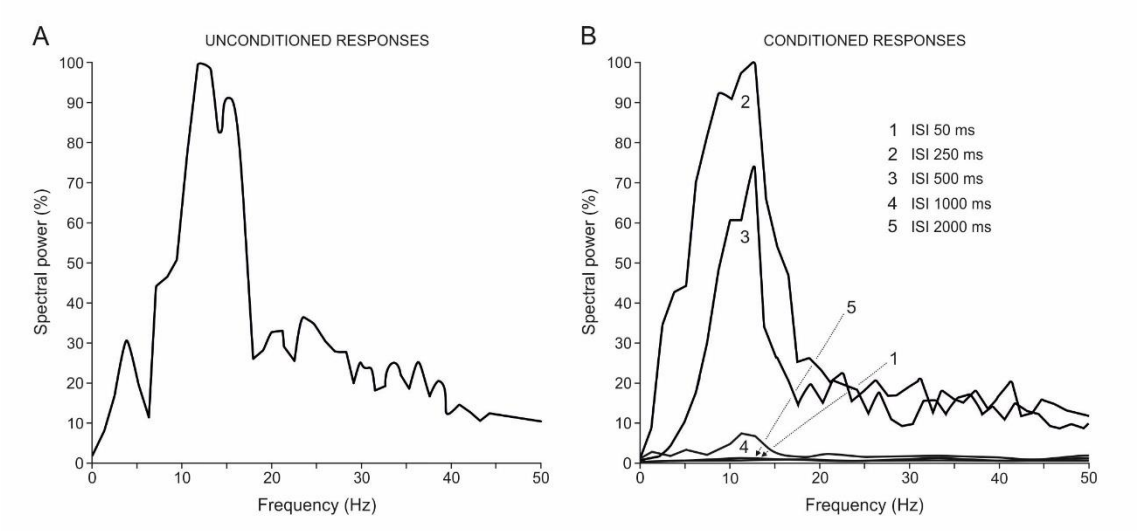

Figure 37. Frequency-component analysis for conditioned responses as a function of CS-US intervals during delay paradigms. (A) Mean spectral power from ≥ 30 acceleration records (n = 4 rabbits) of eyelid reflex responses to air puffs (100 ms, 3 kg/cm^2) presented to the ipsilateral cornea. The 100% value for the illustrated spectral power corresponded to 0.93× 10^7(deg/s^2)^2, with a peak frequency of 12 Hz. (**B**) Mean spectral powers (≥ 10 acceleration profiles) of conditioned responses evoked during the five different CS-US intervals illustrated in **Figure 36** (1, 50 ms; 2, 250 ms; 3, 500 ms; 4, 1000 ms; 5, 2000 ms). Each mean spectral power was obtained from two different rabbits. The 100% value for the illustrated spectral power corresponded to 0.3 × 10^7 (deg/s^2)^2. Peak frequencies for the different CS-US intervals were ≈ 12 Hz.

However, the spectral analysis of frequency components of conditioned eyelid responses evoked with conditioned stimulus-unconditioned stimulus time intervals of 250 ms presented a significant peak at 11.8 ± 0.3 Hz, similar to that presented by reflexively evoked eyeblinks (**Figure 37B**).

Since the amplitude, velocity, and acceleration of conditioned eyelid responses was dependent on the selected conditioned stimulus-unconditioned stimulus time interval, their respective spectral powers should also be different. Indeed, and as illustrated in **Figure 37B**, the spectral powers of conditioned eyeblinks evoked at inter-stimulus intervals of 250 ms and 500 ms were significantly ($P \geq 0.01$) larger than values reached with the other three inter-stimulus intervals, but not different ($F_{(1,1,10)} = 0.391$, $P = 0.546$) one from the other. Interestingly, the dominant frequency was the same (≈ 12 Hz) in the other three cases (**Figure 37B**). The scarce number of conditioned responses (> 10%) evoked during conditioning with 50 ms and 2000 ms of inter-stimulus interval was too small to present any significant peak in the frequency domain (**Figure 37B**). Pseudoconditioned rabbits did not present any identifiable conditioned response.

On the whole, and in accordance with previous reports in rabbits (Gruart et al., 2000) and cats (Domingo et al., 1997), conditioned eyelid responses evoked in behaving rabbits with classical conditioning procedures, using conditioned stimulus-unconditioned stimulus time interval, can be characterized by a ≈ 12 Hz oscillation (Caro-Martín et al., 2015), also present in reflexively evoked blinks.

The next step was to determine whether these oscillatory properties could also be identified in the firing activities of recorded neurons from the rostro-medial prefrontal cortex.

4.5.4. Firing properties of the recorded neurons from the rostro-medial prefrontal cortex during classical eyeblink conditioning with a delay paradigm of 250 ms of inter-stimulus interval

An example of unitary recording in the rostro-medial prefrontal cortex area during delay conditioning using an inter-stimulus interval of 250 ms was illustrated in the **Figure 38A**. For proper isolation and identification, recorded units were filtered, isolated, classified (**Figure 38B**), and prepared for raster displays and the representation of their firing rates. Recordings were carried out during the 9th conditioning session, and the three illustrated neurons were collected from two different rabbits. Although, according to their raster displays (> 40 trials) and their averaged firing rates, the spontaneous firing of the three neurons was fairly similar, they presented a significant peak of activity at different moments of the conditioned stimulus-unconditioned stimulus time interval. Therefore, in blue is represented the raster display and the firing rate of a neuron presenting a peak (≈ 45 spikes/s) of firing ≈ 60 ms after conditioned stimulus onset; in red is represented another neuron whose peak (≈ 37 spikes/s) of firing took place ≈ 185 ms after conditioned stimulus presentation; finally, in green is represented a third neuron whose peak (≈ 48 spikes/s) of firing happened ≈ 300 ms after conditioned stimulus presentation.

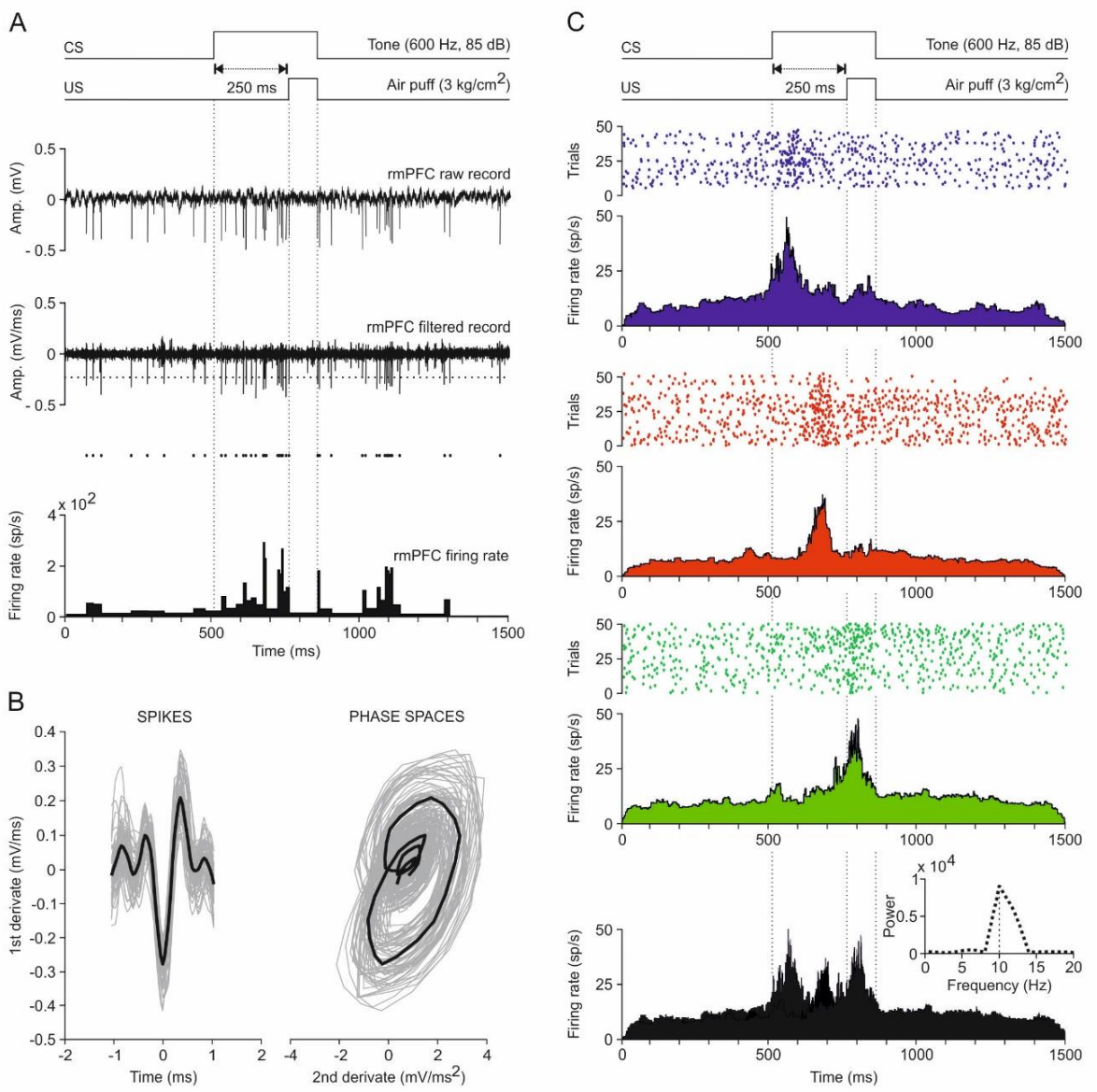

Figure 38. Firing activities of the rostro-medial prefrontal cortex (rmPFC) neurons during classical eyeblink conditioning using a delay conditioning paradigm. (**A**) From top to bottom are illustrated a delay conditioning with indication of CS and US presentations. Below, are illustrated the raw and filtered activity of a representative neuron collected during the 9th conditioning session, as well as a representation of its firing rate. The horizontal dotted line indicates the selected threshold. (**B**) At the left is represented a selection of the spikes detected by the selected threshold, while the phase space portraits (PSPs) of spike waveforms are represented at the right. Black traces indicated the mean value for each representation. (**C**) Representative examples of three different types of firing rate recorded during classical eyeblink conditioning. All the illustrated raster displays were collected during the 9th conditioning session and were averaged from ≥ 40 trials. The three different firing rates were characterized by having their maximum frequency peaks close to the beginning of the CS (blue raster and firing rate, time to peak 59.4 ms, maximum frequency 46.35 spikes/s); in the center of the CS-US (red, time to peak 184.3 ms, maximum frequency 36.99 spikes/s); or next to the end of the US (green, time to peak 302.04 ms, maximum frequency 47.75 spikes/s). The black profile illustrates the overlap of the three firing rates shown above. The inset at the bottom right illustrates the spectral power [10^4(spikes/s)^2, peak frequency of 9.93 Hz] of the black profile. This spectrum was obtained by fitting a waveform with angular frequency $w = 2\pi/T$, where T is the average of the latency between the firing rate peaks with respect to CS presentation ($T = 100.68$ ms).

The firing rate in black illustrated in the bottom part of **Figure 38C** corresponded to the superimposition of the three colored firing rates illustrated above in the same figure. It should be noted that the three peaks of frequency took place during the conditioned stimulus presentation. A spectral analysis of these overlapping peaks of activity showed that peaks took place with a dominant frequency of ≈ 10 Hz (inset at the bottom of **Figure 38C**), which was a value quite close to the dominant frequency (≈ 12 Hz) characteristic of reflex and conditioned eyelid responses.

Representative examples of three different types of recorded neurons from the rostro-medial prefrontal cortex during delay conditioning with an inter-stimulus interval of 250 ms are shown in **Figure 39A**. This panel illustrates the averaged firing rates of neurons recorded across the 10 sessions of a delay conditioning using a conditioned stimulus-unconditioned stimulus time interval of 250 ms. Each represented colored average corresponds to ≥ 2 neurons recorded from the four rabbits included in this group. It is important to note that not a single neuron presented more than one well-defined peak (lasting from 80 ms to 140 ms) of frequency during the inter-stimulus interval or that, as already was showed (Leal-Campanario et al., 2013), none of them (n = 95 neurons, n = 4 rabbits) presented a sustained firing rate for the whole duration of the inter-stimulus interval. In contrast, there was a progressive improvement in the definition of the firing peaks across the successive training sessions.

The evolution in the latency of the three peaks present in the firing rate of the analyzed neurons is represented in **Figure 39B**. As shown, no significant changes in latency with respect to conditioned stimulus onset were observed across conditioning sessions. In **Figure 39C** are represented 10 waveforms fitted to the three dominant peaks in frequency collected for each conditioning session. Notice that the amplitude of the fitted waveforms increased with training, a fact reflected by the different powers of spectra illustrated in **Figure 39D**. In all cases, the average of the fast Fourier analysis of the 10 computed waveforms indicated the presence of a dominant frequency of 12.3 ± 0.3 Hz (inset in **Figure 39D**).

These obtained results suggested to use a longer (500 ms) conditioned stimulus-unconditioned stimulus time interval for classical conditioning to either confirm or rule out that the averaged firing of selected neurons from the rostro-medial prefrontal cortex oscillates at a frequency independent of the inter-stimulus interval, as already was showed for conditioned eyelid responses (**Figure 37B**).

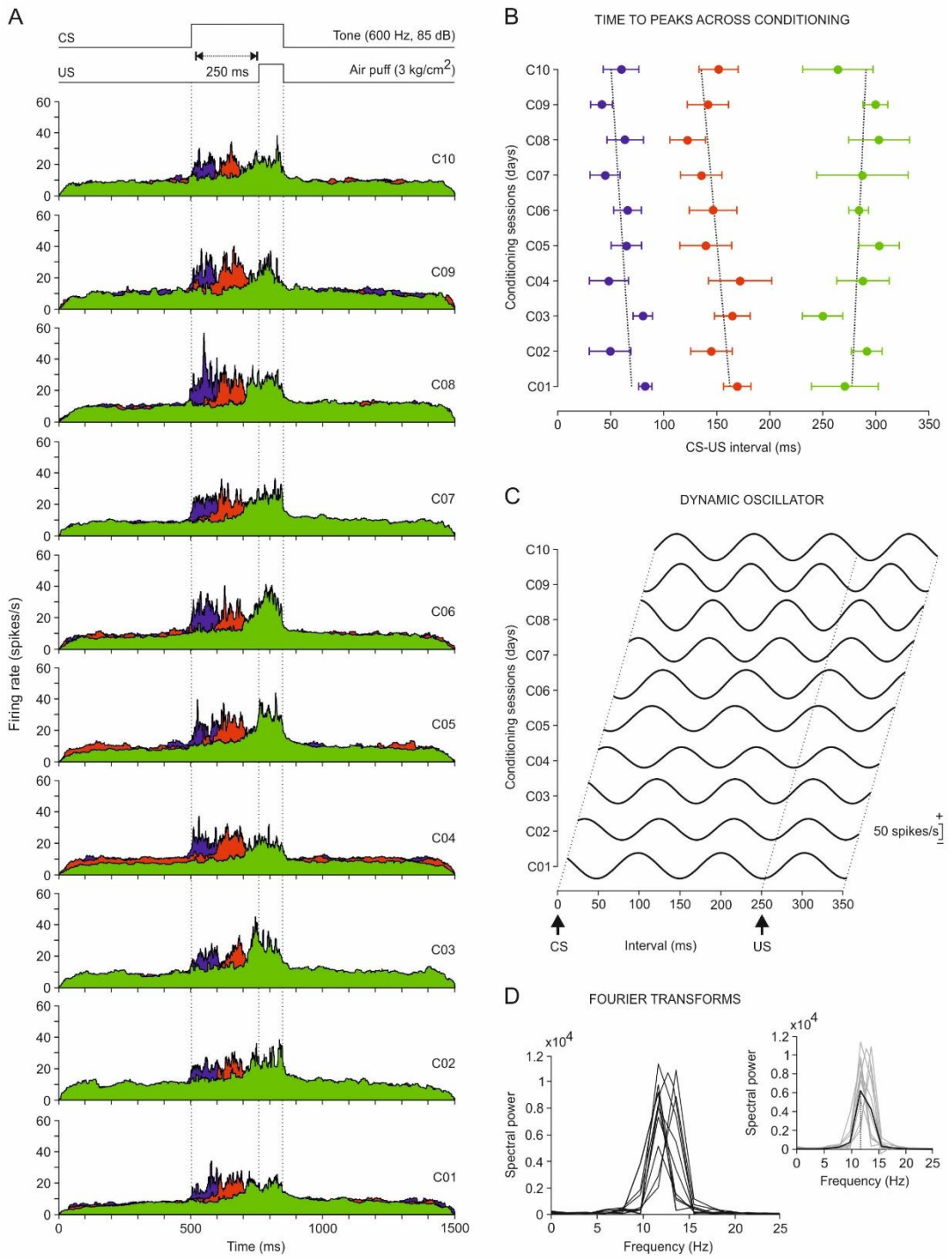

Figure 39. Evolution of the firing rate of the rostro-medial prefrontal cortex (rmPFC) neurons across conditioning sessions with 250 ms of CS-US interval. (**A**) Firing rates of rmPFC neurons recorded from the first (C01) to the tenth (C10) conditioning sessions. Each illustrated profile was averaged from ≥ 2 neurons collected from four different animals. As in **Figure 38C**, the color code indicates the different peak latencies with respect to CS onset of the averaged firing rates. The conditioning paradigm is illustrated at the top. (**B**) Latency evolution for peak firing rates of the three different types of neuron across the 10 conditioning sessions. The corresponding regression lines were: blue group, $y = -2.15x + 71.7$; red group,$y = -3.00x + 165.1$; and green group,$y = 1.47x + 275.7$. (**C**) A dynamic oscillator modeling firing rates. The oscillating curves were computed by fitting a waveform with an angular frequency $w = 2\pi/T$, where Tisthe average of the latency between the three dominant peaks with respect to CS presentation across the 10 conditioning sessions. The scale (in spikes/s) indicates mean firing rates. (**D**) Spectral powers obtained from the10 oscillating curves illustrated in C. On the right is shown the average from these 10 spectral powers. The average presented a maximum power of 0.6×10^4 $(spikes/s)^2$ and a dominant frequency of 11.72 Hz.

4.5.5. Firing properties of the recorded neurons from the rostro-medial prefrontal cortex during classical eyeblink conditioning with a delay paradigm of 500 ms of inter-stimulus interval

The averaged firing rates of neurons recorded across the 10 sessions of a delay conditioning using a conditioned stimulus-unconditioned stimulus time interval of 500 ms is illustrated in **Figure 40A**. Each represented colored average corresponded to ≥ 2 neurons recorded from the four rabbits included in this group. Notice that the dominant peaks presented in the firing rates of neurons recorded during this conditioning task seem to adapt to the longer inter-stimulus interval. Therefore, the duration of the peak increased ≈ 150% (120-200 ms) with respect to peak duration for the 250 ms inter-stimulus interval (80-140 ms). However, none of the recorded neurons (n = 67 neurons, n = 4 rabbits) presented a sustained firing rate for the whole duration of the inter-stimulus interval.

In **Figure 40B** is represented the evolution in the latency of the three peaks present in the firing rate of the analyzed neurons. As shown, no significant changes in latency with respect to conditioned stimulus onset were observed across conditioning sessions. The 10 waveforms fitted to the three dominant peaks in frequency collected for each conditioning session is represented in **Figure 40C**. Notice that the amplitude of the fitted waveforms increased with training, a fact reflected in the different powers of spectra illustrated in **Figure 40D**. In this case, the average of the fast Fourier analysis of the 10 computed waveforms indicated the presence of a dominant frequency of 6.2 ± 0.2 Hz (inset in **Figure 40D**).

In accordance with the above results, the oscillatory properties of recorded neurons from the rostro-medial prefrontal cortex seemed not to be related to the dominant frequency of reflex and conditioned eyeblinks (12 Hz), but do seem to be more related to conditioned stimulus-unconditioned stimulus time intervals (≈12 Hz for 250 ms and ≈6 Hz for 500 ms).

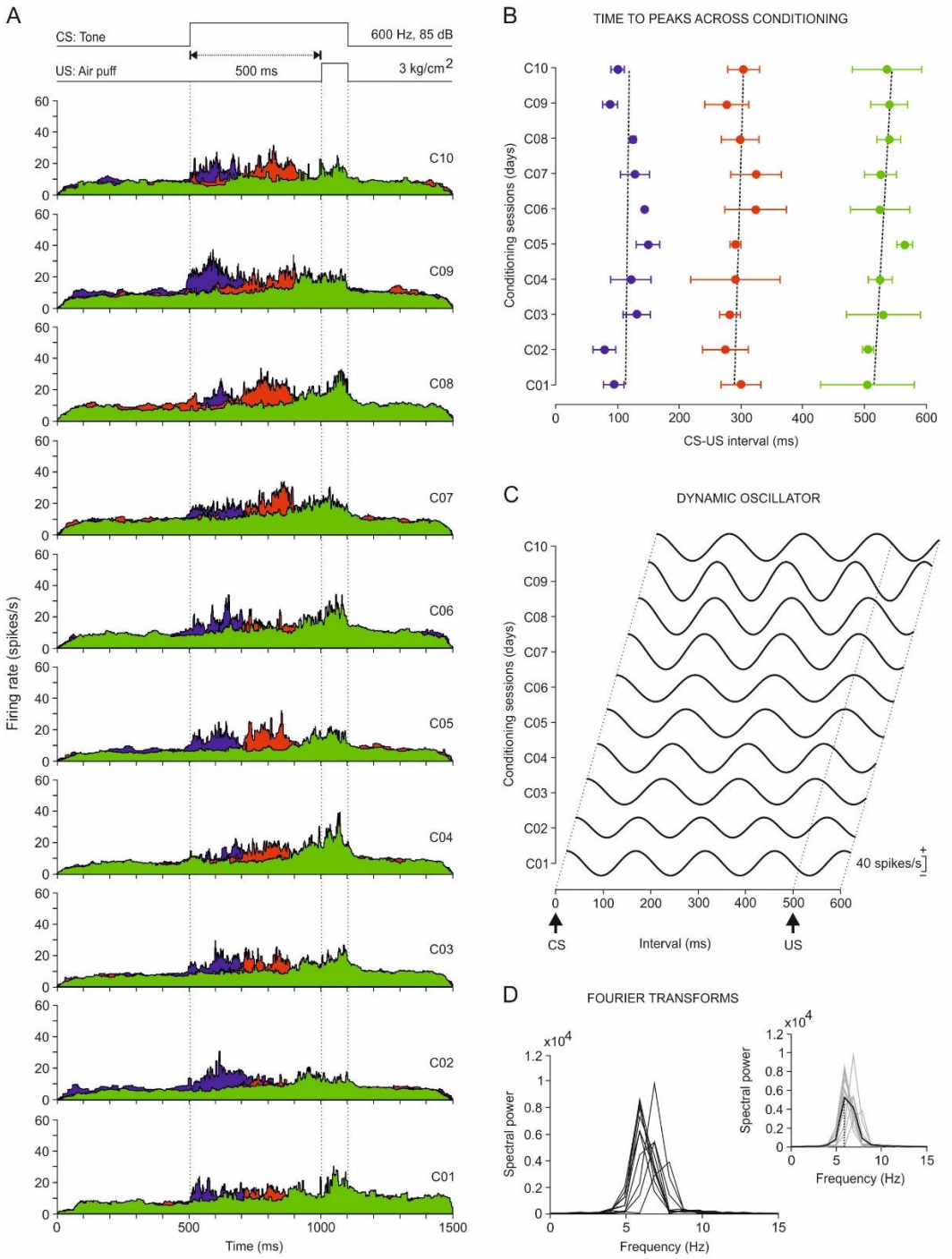

Figure 40. Evolution of the firing rate of the rostro-medial prefrontal cortex (rmPFC) neurons across conditioning sessions with 500 ms of CS-US interval. (**A**) Firing rates of rmPFC neurons recorded from the first (C01) to the tenth (C10) conditioning sessions. Each illustrated profile was averaged from ≥ 2 neurons collected from four different animals. As shown in **Figure 38C**, the color code indicates the different peak latencies with respect to CS onset of the averaged firing rates. Note the progressive definition of the three types of firing rate during CS-US intervals. (**B**) Latency evolution for peak firing rates of the three different types of neuron across the 10 conditioning sessions. The corresponding regression lines were: blue group, $y = 0.65x + 111.9$; red group,$y = 1.64x + 287.3$; and green group,$y = 3.22x + 511.9$. (**C**) A dynamic oscillator modeling firing rates. The oscillating curves were computed by fitting a waveform with an angular frequency $w = 2\pi/T$, where Tisthe average of the latency between the three dominant peaks with respect to CS presentation across the 10 conditioning sessions. The scale (in spikes/s) indicates mean firing rates. (**D**) Spectral powers were obtained from the curves illustrated in C. On the right is shown the average from these 10 spectral powers. The average presented a maximum power of 0.54×10^4 $(spikes/s)^2$ and a dominant frequency of 5.86 Hz.

These obtained results suggested that changes in the firing rate of recorded neurons from the rostro-medial prefrontal cortex could be encoding the duration of the selected time window, and not the oscillatory properties of rabbit eyelids. Indeed, determining the duration of the inter-stimulus interval could be important for the proper timing of the conditioned eyelid response. The difficulty to acquire conditioned eyelid responses with very short or very long inter-stimulus interval (shorter or longer than 200-500 ms) has been reported repeatedly (Gormezano et al., 1983; Gruart et al., 1995; 2000).

4.5.6. Dependence of the oscillatory properties of recorded neurons from the rostro-medial prefrontal cortex on inter-stimulus intervals

Representative examples of averaged of recorded neurons from the rostro-medial prefrontal cortex (≥ 2 collected from ≤ 4 rabbits) is shown in **Figure 41**. Recordings were carried out during the 8th session of delay conditioning of different (50, 250, 500, 1000, and 2000 ms) conditioned stimulus-unconditioned stimulus time interval.

The illustrated data showed that peak firing rates of the averaged neurons occupy the inter-stimulus interval in a definite form for 250 ms and 500 ms of inter-stimulus interval. The firing peaks of the three types of neuron were not so well-defined for the 1000 ms inter-stimulus interval.

Finally, neurons were non-responding to conditioned stimulus-unconditioned stimulus presentations for the shortest (50 ms) and the longest (2000 ms) inter-stimulus interval. In additions, the spectral analysis indicated that the dominant frequency of the peaks in firing rate during the conditioned stimulus-unconditioned stimulus time interval presented an inverse relationship with the inter-stimulus interval: 11.72 Hz for 250 ms, 5.86 Hz for 500 ms, 2.9 Hz for 1000 ms, and 1.5 Hz for 2000 ms.

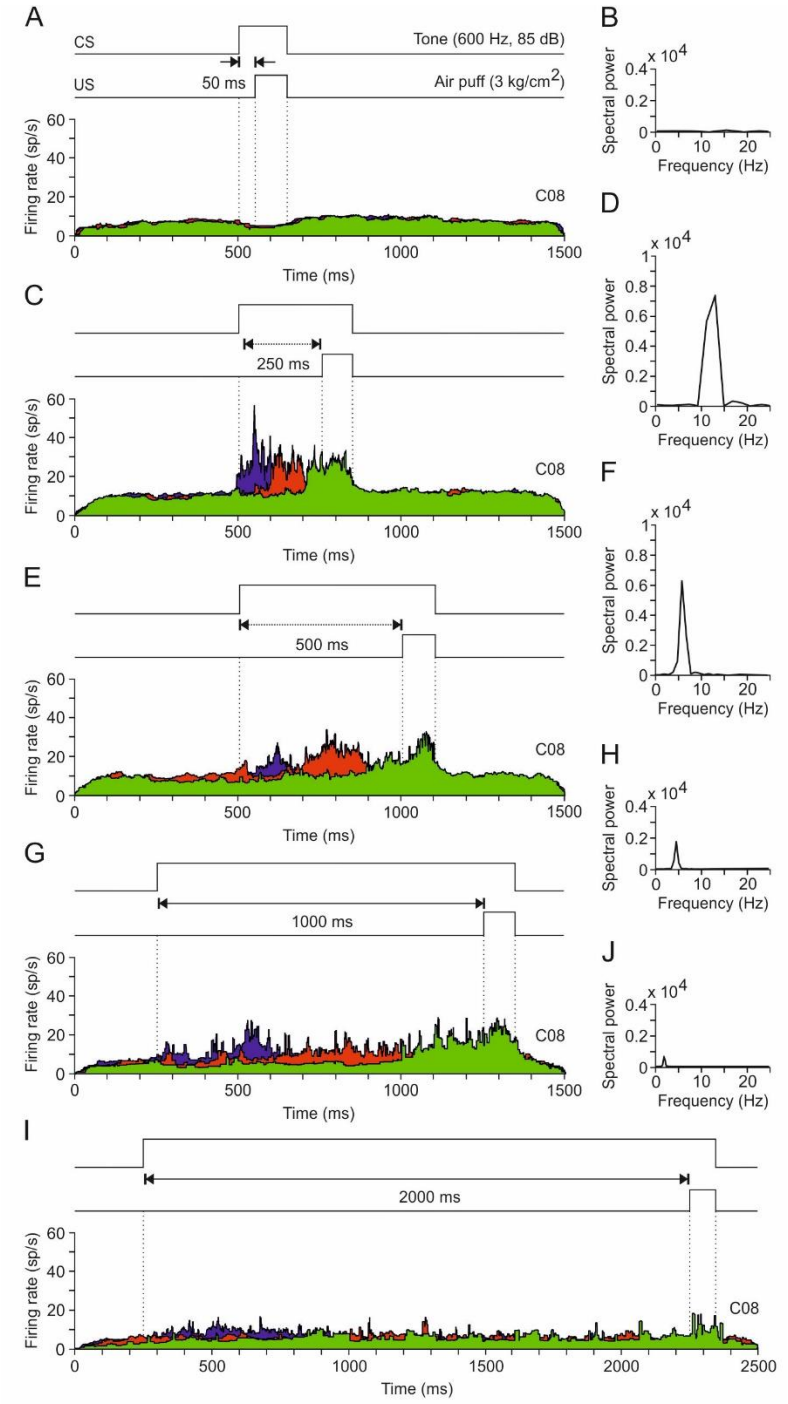

Figure 41. A comparison of the firing rates of the rostro-medial prefrontal cortex (rmPFC) neurons presented during the five different CS-US intervals. (**A**), (**C**), (**E**), (**G**), (**I**) A representation of the three dominant firing rates collected during the 8th conditioning session (C08) for the five CS-US intervals used in this study. (**B**), (**D**), (**F**), (**H**), (**J**) Spectral powers of waveforms computed from the average of the latency between the peaks with respect to CS presentation (see **Figures 39C** and **40C**). (**A**), (**B**) Note that for this CS-US interval (50 ms) there was no activation of rmPFC neurons. (**C**), (**D**) For CS-US intervals of 250 ms, the firing rate of recorded rmPFC neurons presented a dominant frequency of 11.72 Hz [maximum power of 0.73×10^4 (spikes/s)^2]. (**E**), (**F**) In the case of CS-US intervals of 500 ms, the dominant frequency of the firing rate of rmPFC neurons went down to 5.86 Hz (maximum power of 0.59×10^4 (spikes/s^2)). (**G**), (**H**) For CS-US intervals of 1000 ms, the spectral power of the curve fitted to peak firing rates of recorded rmPFC neurons was reduced to 0.21×10^4 (spikes/s)^2 and to a peak frequency of 2.9 Hz.(**I**), (**J**) The firing rate of rmPFC neurons presented a weak modulation for classical eyelid conditioning using a CS-US interval of 2000 ms. The spectral power of the curve fitted to peak firing rates was very low [0.09×10^4 (spikes/s)^2] and the peak frequency was 1.5 Hz.

A summary of the collected results is shown in **Figure 42**. The mean spectral power corresponding to the different timing of peak firing rates as a function of the CS-US interval (**Figure 42A**).

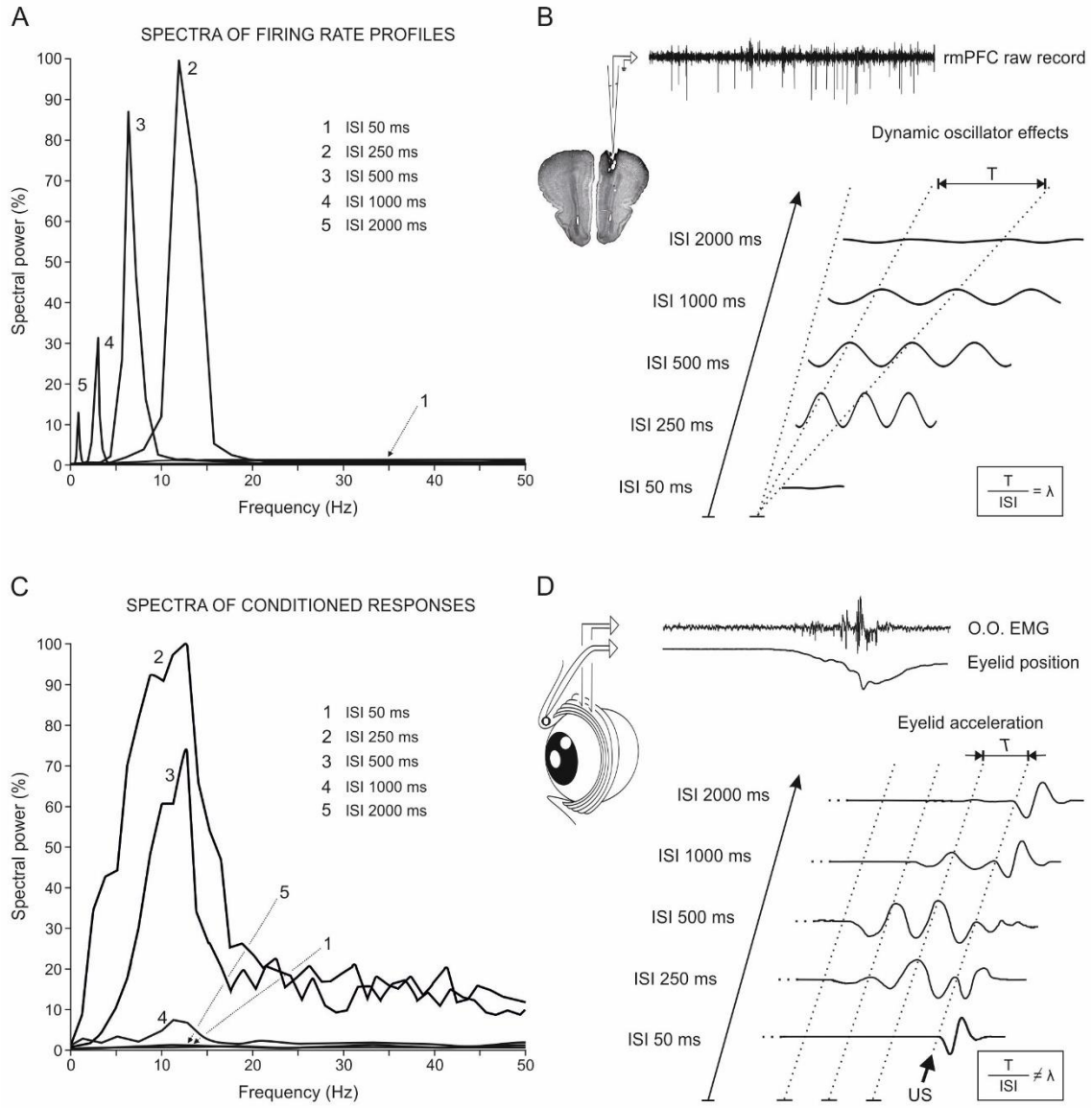

Figure 42. A comparative analysis of the frequency domains for eyelid conditioned responses and for the firing activities of rostro-medial prefrontal cortex (rmPFC) neurons during classical conditioning. (**A**) Mean spectral powers computed from the 10 curves fitted to the dominant peaks present in the firing rates of rmPFC neurons. The five illustrated spectral powers correspond to the following inter-stimulus intervals (CS-US): 50ms (1), 250 ms (2), 500 ms (3), 1000 ms (4), and 2000 ms (5). The 100% value for the illustrated spectral powers corresponds to 0.6×10^4 (spike/s)^2. (**B**) A representation of waveforms corresponding to the five CS-US intervals included in this study. Note that waveforms depend (in amplitude and frequency) on CS-US intervals, and T periods increase with the duration of inter-stimulus interval (ISI), in accordance with a constant $\lambda = \frac{T}{ISI} \approx 0.33$. (**C**) Mean spectral powers of conditioned eyelid responses recorded with the five CS-US intervals indicated in A. Each mean spectral power was obtained from ≥ 10 acceleration profiles recorded in ≥ 2 rabbits. The 100% value for the illustrated spectral powers corresponded to 0.3×10^7 (deg/s^2)^2. The code numbers (1-5) as in A. (**D**) A representation of eyelid acceleration profiles collected from the five CS-US intervals. The beginning of US presentation is indicated. Note that the periods of the accelerations do not depend on CS-US intervals (i.e., $\frac{T}{ISI} \neq \lambda$).

It can be observed that both the power of each oscillation and its frequency decreased with the inter-stimulus interval (**Figure 42B**). In contrast, although the amplitude of acceleration profiles collected from eyelid CRs for the different CS-US intervals decreased with their duration (**Figure 42D**), the dominant frequency (≈12 Hz) remained unchanged (**Figure 42C**).

4.6. Computational complexity

The computational cost of the *Unsupervised Automatic Algorithm* as a function of its execution time at three different levels was examined. The first level was for a single recording (trial of 1.5 sec which not included an inter-stimulus interval during the eyelid classical conditioning). In the **Figure 43** is shown a full implementation of the *Unsupervised Automatic Algorithm* for a single trial of recording, for which the execution time was 51.153 sec. The second level was for a recording conditioning session (C08; n = 60 trials), for which the average execution time was 52.282 ± 1.542 sec by trial and the execution time of the full conditioning session was 52 min and 17 sec. Finally, the third level was for the evolution across the successive conditioning sessions (from C01 to C10), which average execution time was 52.28 ± 0.69 min by session and the execution time of all conditioning sessions was 8 hours, 42 min and 49 sec. Therefore, the *Unsupervised Automatic Algorithm* had a linear complexity order 'O(n)' where the execution time was incremented by n-times, when the number of processed data increased by n. All the computations were developed on a standard personal computer (Inter Core i5-4670 CPU, 3.40 GHz, 4GB-RAM; on Window 8.1 platform) for teaching purposes.

In addition, the execution times of the *Unsupervised Automatic Algorithm* employing the different feature vectors (FV2, FV3, FV5, FV6, and FV24) were compared for the 10th conditioning session (C10). There were not statistically significant differences (One-Way ANOVA *F*-test; $F_{(4,12,295)} = 1.56$; $P = 0.185$) among the mean values of the execution time employing the different feature vectors. Similar results with not significant differences ($P > 0.05$) in the mean values of the execution time were obtained for the other conditioning sessions (C01–C09) during the comparison among the different feature vectors.

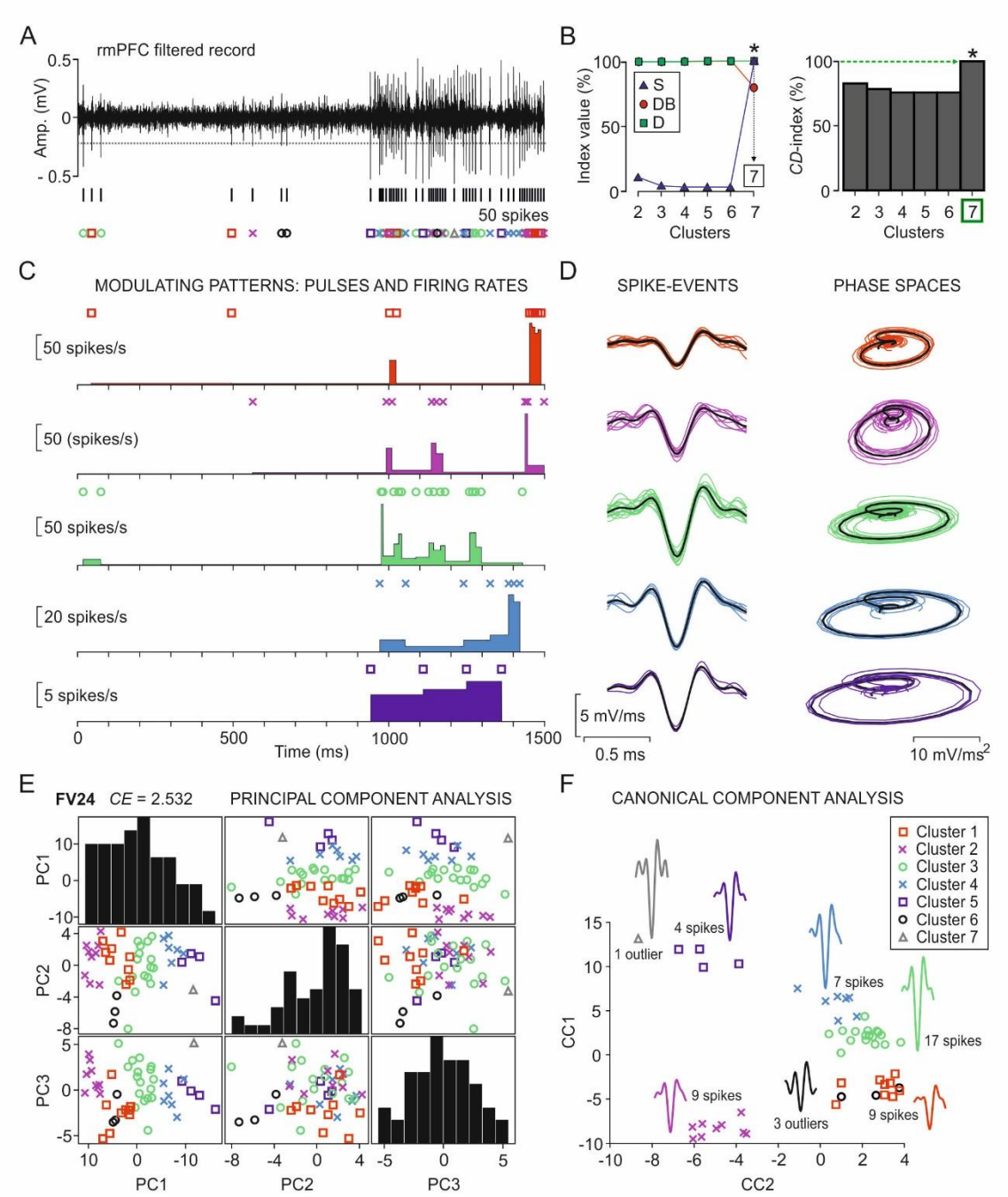

Figure 43. Example of a full implementation of the *Unsupervised Automatic Algorithm* for a single trial. (**A**) A representative single trial of the rostro-medial prefrontal cortex recording and the resulting spike-events (*s* = 50; see the different color symbols, one for each cluster of spike-events). (**B**) Internal validation indices (S, Silhouette; DB, Davies-Bouldin; and D, Dunn) and the *CD*-index (in %) for the optimal distance-metric combination (Cityblock vs. Jaccard). The optimal number of cluster was *K* = 7, corresponding to the maximum value (100%) of the *CD*-index. (**C**) Modulating patterns of the identified neurons (five clusters of neurons), including the pulses (spikes with different color symbol in each panel) and the firing rates (in spikes/s). (**D**) Representation of the spike-events in both time domain and phase space. (**E**) Principal components (PC1, PC2 and PC3) analysis, indicating the value of the *CE*-index (FV24; *CE* = 2.532). Each normalized histogram in the diagonal represents the number of mixed spike-events per band (n = 10) for each principal component. (**F**) Canonical components (CC1 and CC2) analysis. Waveform templates for the resulting clusters (five clusters of neurons, and two clusters of outliers) and their corresponding numbers of spike-events are illustrated.

4.7. *VISSOR* software implementation

The *Unsupervised Automatic Algorithm* was implemented in spike-sorting software *VISSOR* (*Viability of Integrated Spike Sorting of Real Recordings*). Integrated functions included data importing/exporting, preprocessing, spike classification, and visualization. The methods for the spike sorting based on shape, phase and distribution features (SS-SPDF method) and *K*-means clustering with validity and error indices (*CD*-index and *CE*-index) happen to be unique functions provided by this software (**Figure 44**). All functions were integrated into a simple and user-friendly graphical user interface environment designed for easy accessibility. *VISSOR* is software of spike sorting that recognizes specific patterns of neuronal discharges (spikes) present in electrophysiological records. This grouping of spikes is based on the similarity of their profiles, given that, each neuron fires spikes of a particular shape.

Figure 44. Graphical user interface of the *VISSOR* software. This figure shows the four main windows to control the *VISSOR* software by the user. On the left bottom corner is shown the logo (trademark) of this software.

VISSOR software was designed and developed in MATLAB version 7.12.0 / R2011a on Windows platform. For the correct performance of this software was necessary to have the R2011a version of MATLAB Runtime (a standard MATLAB

compiler). This compiler allows to packing *VISSOR* (.mat) functions into an executable (.exe) file. During the installation of the executable *VISSOR* file, MATLAB Runtime will be automatically installed as a mandatory package. For this, an update version of Window and internet access are necessary. Note that in this way, it does not need MATLAB toolboxes installed in the PC.

VISSOR software allows off-line analysis and supports about 25 minutes (approximately) of signals duration. The data file extension can be *.txt* or *.wav* (recognizes both formats). This software offers the original signal visualization and the first-order derivative of this signal without any processing. This visual inspection can be useful to the user for modifying the amplitude thresholds during the spike detection, which can be selected manually or automatically (see the **equations [1]** of Material and Methods section), as well as other parameters such as: the percentage of the artifacts, and the relative refractory period (rrp). In the Spike Classification block of this software is offers the list of the extracted feature (twenty-four independent physiological features) of the spike waveforms (shape, phase and distribution measures), which can be used in the automatic or manual form for the classification of the spike-events.

Finally, the obtained results can be saved with different extensions (for figures: *.tiff, .eps, .jpg, .fig*; for results: *.xlsx, .sdf, .txt*) in a new path, which is generated under the names selected on the experiment details section. Figures and results are presented in two different folders following the automatically created path.

4.8. ERFo software implementation

Extractor of Range for Filtering optimization (ERFo) is a software developed for determining the frequency range boundaries meant to be optimal for the observation of the raw signal power spectrum with the largest value in the range of interest. Integrated functions included data importing/exporting, preprocessing, and visualization with a simple and user-friendly graphical user interface environment (**Figure 45**). ERFo allows knowing the optimal frequency range of the raw signal and which frequency values (extreme values, maximum and minimum) are characteristic of the raw signal power spectrum. It is important to know this range to eliminate frequency components associated with noise and recording artifacts.

ERFo software was designed and developed in MATLAB version 7.12.0 / R2011a on Windows platform. For the correct performance of this software was necessary to have the R2011a version of MATLAB Runtime (a standard MATLAB

compiler). This compiler allows to packing ERFo (.mat) functions into an executable (.exe) file. During the installation of the executable ERFo file, MATLAB Runtime will be automatically installed as a mandatory package. For this, an update version of Window and internet access are necessary. Note that in this way, it does not need MATLAB toolboxes installed in the PC.

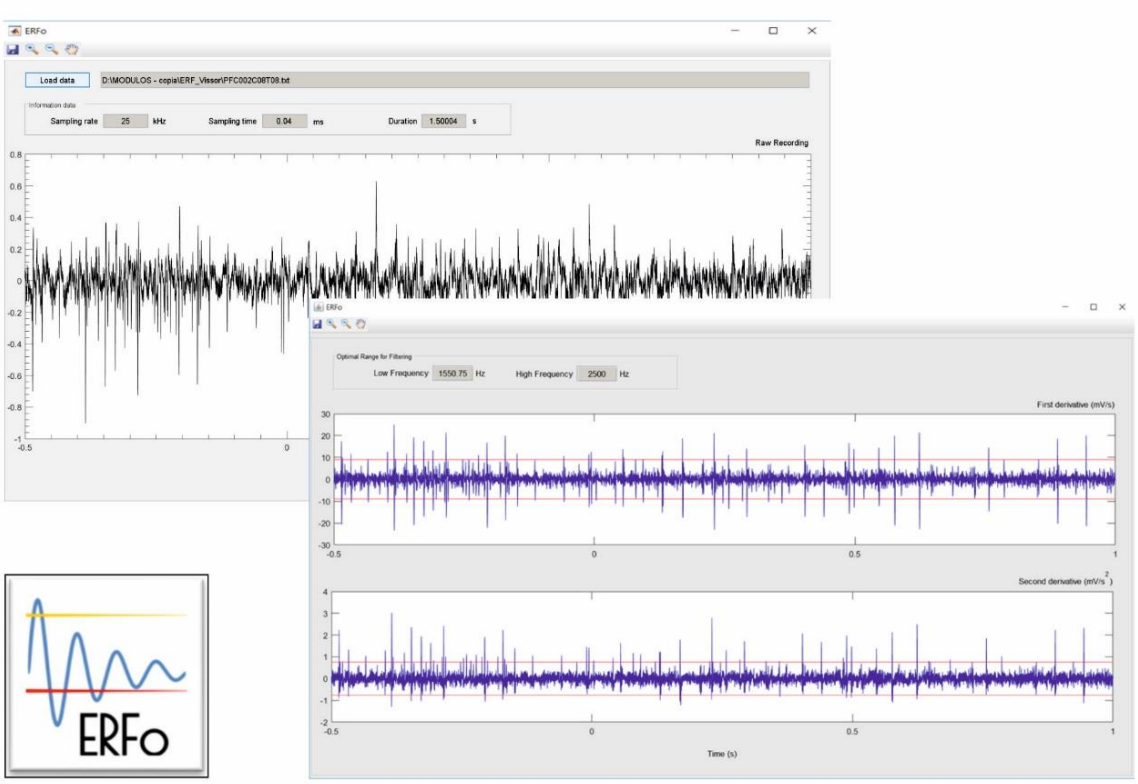

Figure 45. Graphical user interface of the ERFo software. This figure shows the two main windows to control the ERFo software by the user. On the left bottom corner is shown the logo (trademark) of this software.

ERFo software allows off-line analysis and supports/recognizes the data file extensions *.txt* and *.wav*. This software offers the original signal visualization and the first-order and second-order derivatives of this signal by a convolution with a kernel function. This function is a Gaussian curve generated of the standard deviation and mean of the raw signal (see the **equations [15]** of Material and Methods section).

Finally, ERFo software returns the frequency values (extreme values, maximum and minimum) corresponding to the maximum and minimum amplitudes of the waveforms detected by automatically amplitude thresholds and save a log with the date and time of the analysis, the file full path and the optimal frequency range.

The optimal frequency range extracted with ERFo software provides important information about the signal. This value is meant to determine the boundaries between the noise and the best frequencies of the signal. The recommendation when the user

wants to filter is to consider adding 50 Hz (European AC carrier frequency) in the filter creation in order to determine the maximum frequency value for filtering. The optimal minimum frequency of the range is equivalent to the maximum amplitude of the waveform (spike) found in the signal. Therefore, there are not lower frequencies in the signal; the minimum frequency to filter must be less than this frequency and not very close to it. The recommended minimum frequency is obtained by subtracting a value between 500 and 1000 Hz to the optimal minimum frequency suggested by ERFo software.

5. DISCUSSION

The spike-sorting technique is of critical importance in science, especially in electrophysiology, where it is chosen to understand the functional properties of the neural systems through the analysis of real recordings. The neural information extracted from the spike-sorting process should be useful, not only for the identification and for the posterior classification of spikes and neurons, but, also for the objective characterization of the neural activity events under study.

In this sense, specific suboptimal versions of the spike-sorting approach have been successfully applied to study the relationships between kinetic neural commands (spike waveform features and firing modulating rates) and kinematic parameters (performance of learned movements) obtained during classical eyelid conditioning (Sánchez-Campusano et al., 2007; 2009; Porras-García et al., 2010). This neurophysiological characterization allowed studying motor learning as a precise functional state of the cerebellar-interpositus/red-nucleus-motoneuron network in a previous paper by Sánchez-Campusano et al. (2011).

Some authors (Ventura, 2009; Porras-García et al., 2010) have included in their spike-sorting approach some crucial information that not depended only of the waveforms (shape and phase) of the spike events during the spike-sorting process. Ventura (2009) demonstrated that the traditional spike sorting based only in waveform yields biased rate code estimates, because many conventional studies ignore the information on firing rate (rate modulating covariates) during the identification of the neurons. In the same way, Porras-García et al. (2010) applied a similar spike-sorting approach to analyze the multiunitary raw activities from red nucleus and cerebellar/interpositus neurons. This approach also took into account the identification of the standard waveforms, and the classification of probability patterns of spikes in time and frequency domains (Jarvis and Mitra, 2001; Brown et al., 2004; Quiroga et al., 2004; Yang and Mason, 2016), and in the phase space (Aksenova et al., 2003; Chiviroba et al., 2005; Chan et al., 2008).

Trying to improve the methodological approaches used until now for spike-sorting of neural recordings, an *Unsupervised Automatic Algorithm* was applied in this Doctoral Thesis. The spike-pattern classification method (SS-SPDF method), included feature extraction method and unsupervised *K*-means clustering with internal validation indices and cohesion-dispersion index (*CD*-index), to solve the spike-overlapped and amplitude-thresholds problems. In addition, this algorithm took into account the neuronal refractory periods, the inter-spike durations (or firing modulating rates), the

distribution features (kurtosis and asymmetric), and the typical waveform (shape and phase) criteria for spike detection, identification and classification. Therefore, it can be proposed that a proper mixture of spike information in time and frequency domains, and in the phase space (including the distribution measures of the spike), in addition to the neuronal firing rates; could be considered an optimal strategy to determine the actual spike identities and the modulating properties of the involved neurons, beyond the mere calculation of the numbers of cells, classes, and spikes.

5.1. Advantages of the methods and algorithms develop on this Doctoral Thesis

The methods and algorithms presented in this Doctoral Thesis as *Unsupervised Automatic Algorithm* (and implemented in the *VISSOR* software) assemble the following advantages during the classification of the neuronal spike-events and the pattern recognition of the firing rate profiles from real electrophysiological recordings:

1. In this Doctoral Thesis was developed an extractor of frequency range for filtering electrophysiological recordings (implemented in ERFo software). ERFo software provides an optimal frequency range to obtain the best filtering of the electrophysiological recordings. The extraction of the frequency range is a very important step that can be seamlessly integrated into the *VISSOR* preprocessing block. This step comprising the computation of the first-order and second-order derivatives of the recording, and the determination of the minimum and maximum neuronal periods (absolute refractory period of the spike-events). Therefore, ERFo software facilitates the discrimination between principal and non-principal neurons. In addition, the extractor of frequency range and the *Unsupervised Automatic Algorithm* are suitable for both single-microelectrode recordings and for simultaneous recordings of multi-array electrodes.

2. The spike sorting methods that use a non-automatic (manual) procedure for the spike counting under an amplitude threshold are principally based on the user's experience. In the *Unsupervised Automatic Algorithm*, proposed in this Doctoral Thesis, is applied an adaptive and automatic amplitude threshold (Quiroga et al., 2004; Caro-Martín et al., 2015; 2017). This threshold adapts according to the amplitudes of the neuronal spikes and to the basal level of the electrophysiological recording. Therefore, it is able to detect the largest number of significant functional spikes from the electrophysiological recording.

3. The *Unsupervised Automatic Algorithm* recognizes discrete variations of shape, phase and distribution measures of each spike-event with a total of twenty-four independent and non-redundant features (Caro-Martín et al., 2015; 2017), whereas the point sources methods are based only on the detection of peak amplitudes of the spike (McNaughton et al., 1983; Gray et al., 1995).

4. The *Unsupervised Automatic Algorithm* supports unsupervised *K*-means clustering of neuronal spike-events with internal validation indices and a cohesion-dispersion index (*CD*-index). The algorithm is not restricted to the selection of a predetermined number of clusters as others clustering methods, instead it calculates the most relevant clusters according to a maximum of 28 distance-metric combinations and uses the internal validation indices integrated in the cohesion-dispersion index (CD-index) to obtain the most optimal classification. Unlike other authors (Asai et al., 2005; Chibiroba et al., 2005; Aksenova et al., 2003) who used the statistical distributions between the distances from the template of each cluster and all other clustered spike-events. The fits were developed by mean of a probability density function, as for example, the Gamma probability density function.

5. Finally, results from present work incorporates a supervised grouping method of firing rate profiles for raster formation, based on physiological characteristics of the profiles (**Table 6**): peak firing rate and its corresponding peak latency; as well as the number and distribution of spikes in three subintervals defined between the beginning of the CS and the end of the US. This proposed method allows the grouping of three main raster and the identification of three different neuronal activation patterns.

5.2. Efficiency of the methods and algorithms applied on electrophysiological recordings from the rostro-medial prefrontal cortex

In accordance with the results obtained by applying the *Unsupervised Automatic Algorithm* in the recorded neurons from the rostro-medial prefrontal cortex, the rostro-medial prefrontal cortex could be involved in the determination of the conditioned stimulus-unconditioned stimulus time intervals. In the previous work published by Leal-Campanario et al. (2013), the rostro-medial prefrontal cortex is not directly involved in the acquisition process and/or in the proper execution of conditioned eyelid responses.

Moreover, this cortical structure seems to be a potent inhibitor of reflex and conditioned eyeblinks, controlling the release of newly acquired eyelid responses until the acquisition process was established (Leal-Campanario et al., 2013). These results have been also confirmed in this Doctoral Thesis. Indeed, the discharge rate of recorded neurons from the rostro-medial prefrontal cortex was not related to the fixed oscillatory properties of rabbit eyelids, but modified their oscillation as a function of conditioned stimulus-unconditioned stimulus time intervals.

On one hand, the more-definite oscillations presented by the rostro-medial prefrontal cortex during inter-stimulus intervals lasting for 250 ms and 500 ms could explain why these intervals are optimal for classical eyeblink conditioning (Gormezano et al., 1983; Gruart et al., 1995). Therefore, and besides the permissive/modulating role of the rostro-medial prefrontal cortex in the rabbit for the generation of newly acquired motor responses (Leal-Campanario et al., 2007; 2013), the recorded neurons from the rostro-medial prefrontal cortex could play an important role in the rabbit's ability regarding the temporal association between the conditioned stimulus and the unconditioned stimulus. On the other hand, the determination of inter-stimulus intervals by recorded neurons from the rostro-medial prefrontal cortex took place by the participation of three different types of neuron (characterized by their latency of activation to conditioned stimulus presentation).

These results are in contrast with the persistent firing activity of other types of prefrontal neuron. For example, dorsolateral prefrontal cortex neurons show firing activities that persist during the conditioned stimulus-unconditioned stimulus time interval in trace conditioning paradigms, helping in the generation of timed conditioned responses (Weiss and Disterhoft, 2011). In addition, the specific population of neurons from caudal medial prefrontal cortex recorded in rabbits also seems to bridge the temporal gap between the end of the conditioned stimulus and the beginning of the unconditioned stimulus during trace conditioning (Siegel et al., 2012). Therefore, as already reported (Powell et al., 1996), the firing of neurons from medial prefrontal cortex is not directly related to the acquisition of classical eyeblink conditioning. In accord with this latter point, the rostro-medial prefrontal cortex of subprimates is considered to be the highest level of the limbic system, as part of the orbital prefrontal cortex, and therefore involved in the accurate activation or inhibition of selected behaviors and of attentive and cognitive processes (Fuster, 2001; 2008; Kolb et al., 2004).

This is probably the first report on the presence of a neural oscillator underlying the determination of time intervals during associative learning tasks, a neural process that has not been described for neurons located in the same medial prefrontal areas in primates (Fuster, 2008).

5.2.1. Oscillatory properties of the eyelid motor system

The fact that reflex and conditioned nictitating membrane responses present a wavy profile was reported years ago (Berthier, 1992; Welsh, 1992) and was even observed in early classical conditioning experiments in humans (Marquis and Porter, 1939). Illustrations of reflex and conditioned nictitating membrane responses in those previous reports (Berthier, 1992; Welsh, 1992) show noticeable oscillations at 8–10.5 Hz, a value similar to the ≈ 8 Hz reported for eyelid movements in conditioned rabbits (Gruart et al., 2000) and close to values collected here (≈ 12 Hz). The dominant frequency of eyelid responses in the rabbit is about one-third of its resonant frequency (30–35 Hz; Evinger et al., 1984), a fact also seen in cats (Domingo et al., 1997).

As already reported for finger movements in humans (Wessberg and Vallbo, 1995) and further confirmed in this Doctoral Thesis (**Figure 42**), larger conditioned responses in rabbits are achieved by increasing the amplitude and number of waves composing them, but not by modifying the dominant frequency of the movement (Domingo et al., 1997; Gruart et al., 2000). Therefore, the generation of a properly timed conditioned eyelid response could be envisioned as the process of reaching a target in a given time window with the help of a fixed-frequency neuronal oscillating machinery (Domingo et al., 1997).

Because the eyelid is load free, and facial motoneurons receive no proprioceptive feedback signals from the orbicularis muscle (Porter et al., 1989; Trigo et al., 1999), it could be suggested that the oscillatory behavior of the eyelid is the result of the activity of the neuronal mechanisms controlling it. In fact, it has been shown in cats and rats that lid oscillations are an inherent rhythmical property of facial motoneurons innervating the orbicularis oculi muscle (Magariños-Ascone et al., 1999; Trigo et al., 1999). In addition, a noticeable oscillatory behavior has been reported in cat pericruciate cortex neurons during classical eyeblink conditioning (Aou et al., 1992) and in cat cerebellar interpositus neurons during reflexively evoked and classically conditioned eyelid responses (Gruart and Delgado-García, 1994; Jiménez-Díaz et al., 2004).

These data suggested that the eyelid motor system could be controlled by a central neural oscillator tuned to the inertial and viscoelastic needs of moving appendages. However, the present results indicate that the oscillatory properties of the rostro-medial prefrontal cortex reported here are not related to the proper generation of eyelid conditioned responses (**Figure 42**). This point is discussed below in the following section.

5.2.2. A putative role of the oscillatory properties of recorded neurons from the rostro-medial prefrontal cortex as a timing device for inter-stimulus interval association

Comparing the results obtained in this Doctoral Thesis with similar unitary recording and/or lesion studies carried out in more-caudal or more-dorsolateral prefrontal areas, which are thought to determine the increasing relevance of conditioned stimulus presentations or that present firing activities that persist during the whole conditioned stimulus-unconditioned stimulus time interval (Weible et al., 2000; 2003; 2007; Weiss and Disterhoft, 2011; Siegel et al., 2012; Siegel and Mauk, 2013), a differential role of recorded neurons from the rostro-medial prefrontal cortex in the acquisition of classical eyeblink conditioning can be suggested.

The persistent neural activity recorded in both dorsolateral and caudomedial prefrontal cortex during the conditioned stimulus-unconditioned stimulus time interval could be generated by fast-spiking interneurons, but not by projecting pyramidal prefrontal neurons (Povysheva et al., 2006). In contrast, the discharge rate of the neurons from the rostro-medial prefrontal cortex recorded in this Doctoral Thesis was dependent on the activity of a variable oscillator that enabled the determination of inter-stimulus intervals in an optimal range of 250-500 ms by the successive activation of three different groups of prefrontal units. Because of their spike profiles and firing properties, the neurons from the rostro-medial prefrontal cortex recorded here are similar to the pyramidal cells from the rostro-medial prefrontal cortex described by Leal-Campanario et al. (2013). These pyramidal neurons were identified by their antidromic and/or synaptic activation from the medio-dorsal thalamic nucleus. As already reported (Henry et al., 1999; Leal-Campanario et al., 2013), and confirmed here, the activity of recorded neurons from the rostro-medial prefrontal cortex during inter-stimulus intervals was not significantly related to the percentage of conditioned responses and/or to the area of the rectified electromyographic activity of the orbicularis oculi muscle.

The rostro-medial prefrontal cortex of subprimates is homologous with the prefrontal orbital area of primates. Both of them receive a well-defined projection from the medial half of the thalamic medio-dorsal nucleus (Benjamin et al., 1978; Ray et al., 1992; Kronforst-Collins and Disterhoft, 1998; Leal-Campanario et al., 2007). The neurons recorded in this Doctoral Thesis were located in the rostral site of area 24 (anterior cingulate cortex) and the rostro-dorsal part of area 32 (prelimbic cortex), but not in the area 24c involved in facial expression in monkeys (Buchanan et al., 1994; Morecraft et al., 2001; 2012).

Prefrontal cortex, containing Brodmann 24 and 32 areas, project to the caudate nucleus, the claustrum, and other striated areas, from where prefrontal commands can reach many different sensorimotor cortical and subcortical centers (Buchanan et al., 1994; Kronforst-Collins and Disterhoft, 1998; Fuster, 2001). Besides the medio-dorsal thalamic nucleus, rostro-medial prefrontal cortex areas also project to other midline thalamic nuclei, regulating unspecific sensory inputs related to attentive processes and to the presence of novel sensory stimuli. Finally, prefrontal cortex neurons project to different midbrain centers, including the substantia nigra pars reticulata, involved in movement initiation and coordination, and the pontine nuclei projecting heavily to the cerebellar cortex and nuclei (Basso and Evinger, 1996; Basso et al., 1996; Kronforst-Collins and Disterhoft, 1998; Siegel et al., 2012).

However, the peculiar discharge rates of neurons from rostro-medial prefrontal cortex described in this Doctoral Thesis seem to be more related to the cognitive components of classical conditioning than to the generation of conditioned eyeblinks. In this regard, it can be suggested that neural activities shown here could reach other cortical areas more directly involved in non-motor aspects of this type of associative learning. For example, during trace eyeblink conditioning in the rabbit, caudal areas of the anterior cingulate cortex are involved in the salience or relevance of conditioned stimulus presentations (Weible et al., 2003). In addition, caudal medial prefrontal cortex and dorsolateral prefrontal cortex neurons present firing activities that persist during the inter-stimulus interval in trace conditioning paradigms, helping in the generation of timed conditioned eyeblinks (Weiss and Disterhoft, 2011; Siegel and Mauk, 2013). Moreover, the neural signals from the rostro-medial prefrontal cortex can reach the hippocampus either directly or across the thalamic reuniens nucleus (McKenna and Vertes, 2004).

In summary, these collected results is shown in **Figure 42** provide new evidence on the presence in the rostro-medial prefrontal cortex of a variable oscillator that helps to determine time intervals during associative learning tasks. This neural oscillator seems to be particularly adapted to determine inter-stimulus intervals in the range of 250-500 ms—i.e., the optimal values for the proper generation of conditioned nictitating membrane and eyelid responses in behaving rabbits and cats (Gormezano et al., 1983; Domingo et al., 1997; Gruart et al., 2000).

5.3. Proposal of improvement and feasibility for on-line spike-sorting analysis

Implementing the *Unsupervised Automatic Algorithm*, as a new spike-sorting method in which multiple methods of spike sorting and the grouping of neuronal discharges profiles are linked, is an important challenge. This algorithm emerges from the need to detect, identify, classify and cluster different cell groups (principal and non-principal cells) which intervene in brain processes and are distributed across electrophysiological recordings.

Up until today, the *Unsupervised Automatic Algorithm* has been used to detect and cluster principal neurons under an adaptive threshold in the electrophysiological recordings of the rostro-medial prefrontal cortex, which was one of the main objectives of the present work. In addition, thanks to the development of the extractor of optimal frequency range (ERFo software) the non-principal cells could be detected in electrophysiological recordings from any brain process. Currently, the investigation of the possible neuronal patterns of non-principal cells during a classical eyeblink conditioning with a paradigm of delay in the rostro-medial prefrontal cortex is being carried out with this algorithm.

Reached the first group of proposed aims, the improvement of the algorithm (*VISSOR* software) would be:

1. Implementing hierarchical and supervised clustering methods for the classification of the spike-events to compare and justify with the obtained results employing unsupervised *K*-means clustering (the method integrated in the proposed *Unsupervised Automatic Algorithm*). These supervised methods (called *Hierarchical Clusters*) use also validation indices such as the cophenetic correlation and the inconsistency coefficients.

2. Point sources methods, as Principal Component Analysis (PCA) and Fisher Linear Discriminant (FLD), are necessary to reduce the dimensionality of the

features extracted of the spike-events. In the algorithm proposed here was not necessary to reduce the dimensionality, because the independence of the extracted features (non-multi-collinearity) was demonstrated. However, would be interesting to compare the results obtained in this work with the classification and visualization resulting from those methods.

3. Try to reduce the computational cost of the whole algorithm and of the runtimes of each method within the algorithm. In this way, the application of the *Unsupervised Automatic Algorithm* could be extended to the on-line analysis of the neural data with emphasis in spikes detection and classification, as well as in the neurons identification.

4. Extend the *Unsupervised Automatic Algorithm* to off-line analysis of high-density arrays recordings. In this situation, optimizing the spike detection and identification steps (Petrantonakis and Poirazi, 2015) and keeping the relevant spike information during the feature extraction step, it is possible to explore key physiological properties, such as the oscillation patterns (Caro-Martín et al., 2015) of a particular neural event or the neuronal correlates of a specific learning process (Sánchez-Campusano et al., 2007). In addition, with a suitable interface between the experimental data acquisition card (CED 1401) and the developed *VISSOR* software, a full functional tool would be used to compare, analyse and process real electrophysiological recordings on real time.

Future works will be toward those two directions, ─ i.e., to investigate the on-line and multi-array electrodes performances of the proposed *Unsupervised Automatic Algorithm* for both research and clinical applications.

6. THE MAIN FINDING AND CONCLUSIONS

The present Doctoral Thesis was based on the development and implementation of a spike sorting method/algorithm and its application on real electrophysiological recordings for characterizing the detected and identified spike-events and correlate the resulting neural activity patterns with the performance of the behavioral/cognitive process under study.

To address the objectives of the present Doctoral Thesis the following methods and algorithms were developed and carried out: (1) an unsupervised method/algorithm of spike sorting based on shape, phase and distribution features (SS-SPDF) and *K*-means clustering with validity and error indices, which detects, identifies and classifies the neuronal spikes distributed across the real electrophysiological recordings; and (2) a supervised and hierarchical clustering method/algorithm for the classification of the obtained firing rate profiles. In particular, methods and algorithms were applied on real extracellular recordings from the rostro-medial prefrontal cortex of rabbits during classical eyeblink conditioning using delay paradigms with different inter-stimulus intervals (50, 250, 500, 1000 and 2000 ms).

In summary, the main findings of this Doctoral Thesis are the following.

Main Findings:

1. A new algorithm for extract optimal frequency range of electrophysiological recordings was successfully developed and implemented in the ERFo software. This software based on the calculation of the first-order and second-order derivatives of the electrophysiological recording and the determination of the minimum and maximum spike-event periods, reveals important information for the filtering step of the electrophysiological recordings.

2. An efficient alternative method of spike sorting (SS-SPDF method) and its computational algorithm to detect, identify, and classify spike-events from electrophysiological recordings were successfully applied. In contrast to other methods, also based on feature extraction, the proposed method/algorithm is based on shape, phase and distribution features of each spike-event, which reveal significant information of the neural process under study.

3. The uniqueness of the SS-SPDF method and *VISSOR* package is that instead of the reduction of dimensionality adopted in most alternative methods, it carries out spike sorting analyses based on a 24D-vector of independent features for each

spike-event, removing the multi-collinearity among the features to simplify the classification process. Furthermore, the classification technique involves the *K*-means clustering with new and useful validity and error indices to verify both the cohesion-dispersion among spike-events (*CD*-index) and the misclassification of clustering (*CE*-index), respectively. The combination of features used in the proposed feature vector (FV24) returns the highest value of the *CD*-index and the lowest value of *CE*-index, as well as, the best arrangement between them and the optimal number of clusters that determined the maximal cohesion-dispersion of the clustering among all the distance-metric combinations. In this Doctoral Thesis considers that the two proposed indices are proper validity and error measures for quantifying the success of a spike-sorting algorithm.

4. The proposed SS-SPDF method ensured that both the resulting number of clusters and the value of the *CE*-index did not depend on the number of features used during the classification. Therefore, the optimal number of clusters and the optimal clustering were depended strongly on the intrinsic physiological properties of the spike-events and on the neural process as a whole. These physiological properties were explicitly reflected in the proposed 24D-vector of independent features, allowing a greater resemblance between the spike-events of each cluster and its template and the optimal cohesion-dispersion of the clustering.

5. The firing activities of neurons located in the rostro-medial prefrontal cortex recorded in alert behaving rabbits are controlled by a dynamic oscillator. This oscillator generated firing frequencies in a variable band of 3-12 Hz depending on the CS-US intervals (1000, 500 and 250 ms) selected for classical eyeblink conditioning of behaving rabbits. Lower (50 ms) and larger (2000 ms) intervals failed to activate the oscillator and prevented the acquisition of conditioned eyelid responses. This is an unexpected mechanism to generate sustained firing activities in neural circuits generating working memories.

Therefore, in this Doctoral Thesis are extracted the following conclusions.

Conclusions:

1. The better frequency range extracted with the ERFo software allows optimal filtering of the recording and helps to the discrimination between principal and non-principal neurons.

2. The SS-SPDF method based on shape, phase and distribution features, which extracts twenty-four independent features of each spike-event, and *VISSOR* package reveal significant information of the neural processes.

3. The intrinsic physiological properties of the spike-events reflected in these 24 independent features allow a greater similarity between the spike-events of each cluster and its template.

4. The *K*-means clustering technique with the combination of validity and error indices to verify both the cohesion-dispersion among spike-events (*CD*-index) and the misclassification of clustering (*CE*-index), successfully returns an optimal number of clusters in real extracellular recording.

5. The SS-SPDF method and *VISSOR* package ensure that both the resulting number of clusters and the value of the *CE*-index did not depend on the number of features used during the classification.

6. The present methods and algorithms perform better at classifying spikes and neurons, and at assessing their modulating properties compared to other methods also based on feature extraction.

7. The firing activities of neurons located in the rostro-medial prefrontal cortex are controlled by a dynamic oscillator which generated firing frequencies in a variable band of 3-12 Hz depending on the CS-US intervals (1000, 500 and 250 ms).

8. Lower (50 ms) and larger (2000 ms) intervals failed to activate the oscillator and prevented the acquisition of conditioned eyelid responses.

7. REFERENCES

Abeles M, Goldstein MH (1977) Multi-spike train analysis. Proc IEEE 65:762–73

Adamos DA, Kosmidis EK, Theophilidis G (2008) Performance evaluation of PCA-based spike sorting algorithms. Comput Methods Programs Biomed 91:232–244

Aghagolzadeh M, Mohebi A, Oweiss KG (2014) Sorting and tracking neuronal spikes via simple thresholding. IEEE Trans Neural Syst Rehabil Eng 22:858–869

Aksenova TI, Chibirova OK, Dryga OA, Tetko IV, Benabid AL, Villa AEP (2003) An unsupervised automatic method for sorting neuronal spike waveforms in awake and freely moving animals. Methods 30:178–187

Ammann C, Márquez-Ruiz J, Gómez-Climent MA, Delgado-García JM, Gruart A (2016) The Motor Cortex Is Involved in the Generation of Classically Conditioned Eyelid Responses in Behaving Rabbits. J Neurosci 36(26):6988–7001

Aou S, Woody CD, Birt D (1992) Changes in the activity of units of the cat motor cortex with rapid conditioning and extinction of a compound eye blink movement. J Neurosci 12:549–559

Asai Y, Aksenova TI, Villa AEP (2005) On-Line Real-Time Oriented Application for Neuronal Spike Sorting with Unsupervised Learning. In: Duch W, Kacprzyk J, Oja E, Zadrożny S (2005) Eds: ICANN 2005 LNCS 3696:109–114. Springer, Berlin, Heidelberg

Balasubramanian K, Obeid I (2011) Fuzzy logic-based spike sorting system. J Neurosci Methods 198:125–134

Bankman IN, Johnson KO, Schneider W (1993) Optimal detection, classification, and superposition resolution in neural waveform recordings. IEEE Trans Biomed Eng 40:836–841

Barthó P, Hirase H, Monconduit L, Zugaro M, Harris KD, Buzsáki G (2004) Characterization of neocortical principal cells and interneurons by network interactions and extracellular features. J Neurophysiol 92:600–608

Basso MA, Powers AS, Evinger C (1996) An explanation for reflex blink hyperexcitability in Parkinson's disease I Superior colliculus. J Neurosci 16:7308–7317

Basso MA, Evinger C (1996) An explanation for reflex blink hyperexcitability in Parkinson's disease II Nucleus raphe magnus. J Neurosci 16:7318–7330

Benjamin RM, Jackson JC, Golden GT (1978) Cortical projections of the thalamic mediodorsal nucleus in the rabbit. Brain Res 141:251–265

Berthier NE (1992) Muscle activity during unconditioned and conditioned eye blinks in the rabbit. Behav Brain Res 48:21–28

Bestel R, Daus AW, Thielemann C (2012) A novel automated spike sorting algorithm with adaptable feature extraction. J Neurosci Methods 211:168–178

Bezdek JC, Pal NR (1998) Some new indexes of cluster validity. IEEE Trans Syst Man Cybern B Cybern 28:301–315

Biffi E, Ghezzi D, Pedrocchi A, Ferrigno G (2008) Spike detection algorithm improvement, spike waveforms projections with PCA and hierarchical classification. IET Conf Pub 540:122–126

Bishop CM (2006) Pattern recognition and machine learning. New York: Springer-Verlag

Brown EN, Kass RE, Mitra PP (2004) Multiple neural spike train data analysis: state-of-the-art and future challenges. Nat Neurosci 7:456–461

Brychta RJ, Shiavi R, Robertson D, Diedrich A (2007) Spike detection in human muscle sympathetic nerve activity using the kurtosis of stationary wavelet transform coefficients. J Neurosci Methods 160:359–367

Buchanan SL, Thompson RH, Maxwell BL, Powell DA (1994) Efferent connections of the medial prefrontal cortex in the rabbit. Exp Brain Res 100:469–483

Buzsáki G, Kandel A (1998) Somadendritic Back propagation of Action Potentials in Cortical Pyramidal Cells of the Awake Rat. J Neurophysiol 79:1587–1591

Buzsáki G (2004) Large-scale recording of neuronal ensembles. Nat Neurosci 7:446–451

Caro-Martín CR, Delgado-García JM, Gruart A, Sánchez-Campusano R (2017). Spike sorting based on shape, phase and distribution features, and K-means clustering with validity and error indices. Submitted and under reviewed*:* J Neural Eng ID:JNE–101798.

Caro-Martín CR, Leal-Campanario R, Sánchez-Campusano R, Delgado-García JM, Gruart A (2015) A variable oscillator underlies the measurement of time intervals in the rostral medial prefrontal cortex during classical eyeblink conditioning in rabbits. J Neurosci 35:14809–14821

Caro-Martín CR, Leal-Campanario R, Sánchez-Campusano R, Delgado-García JM, Gruart A (2015) A variable oscillator underlies the measurement of time intervals in the medial prefrontal cortex during classical eyeblink conditioning in rabbits. SocNeurosci Meeting S–3524

Caro-Martín CR, Sánchez-Campusano R, Delgado-García JM, Leal-Campanario R, Gruart A (2014) Spike sorting and firing rate distribution of prefrontal cortex neurons during delayed eyeblink conditioning. Acta Physiologica O52: 41–42

Carretero-Guillén A (2015) Functional properties of hippocampal circuitry. Doctoral Thesis: Universidad Pablo de Olavide (Sevilla)

Chan HL, Lin MA, Wu T, Lee ST, Tsai YT, Chao PK (2008a) Detection of neuronal spikes using an adaptive threshold based on the max–min spread sorting method. J Neurosci Methods 172:112–121

Chan HL, Wu T, Lee ST, Fang SC, Chao PK, Lin MA (2008b) Classification of neuronal spikes over the reconstructed phase space. J Neurosci Methods 168:203–211

Charbiwala Z, Karkare V, Gibson S, Marković D, Srivastava M B (2011) Compressive sensing of neural action potentials using a learned union of supports. Conf Proc BSN 53–58

Chen Y, Tsai Y, Chen L (2011) Algorithm and implementation of multi-channel spike sorting using GPU in a home-care surveillance system. ICME IEEE (CFP11) 1–6

Chibirova OK, Aksenova TI, Benabid AL, Chabardes S, Larouched S, Rouatd J, Villa AEP (2005) Unsupervised Spike Sorting of extracellular electrophysiological recording in subthalamic nucleus of Parkinsonian patients. BioSystem 79:159–171

Choi J H, Jung H K, Kim T (2006) A new action potential detector using the MTEO and its effects on spike sorting systems at low signal-to-noise ratios. IEEE Trans Biomed Eng 53:738–746

Clark GA, McCormick DA, Lavond DG, Thompson RF (1984) Effects of lesions of cerebellar nuclei on conditioned behavioral and hippocampal neuronal responses. Brain Res 291:125–136

Constantinidis C, Goldman-Rakic PS (2002) Correlated discharges among putative pyramidal neurons and interneurons in the primate prefrontal cortex. J Neurophysiol 88:3487–3497

Corbit LH, Balleine BW (2003) The role of prelimbic cortex in instrumental conditioning. Behav Brain Res 146:145–157.

Csicsvari J, Hirase H, Czurkó A, Mamiya A, and Buzsáki G (1999) Oscillatory coupling of hippocampal pyramidal cells and interneurons in the behaving rat. Journal of Neuroscience 19:274–287

Damasio AR (1994) Descartes' error: emotion, reason, and the human brain.New York: Grosset/Putnam

Davies DL, Bouldin DW (1979) A cluster separation measure. IEEE Trans Pattern Anal Mach Intell 1:224–227

Davies DL, Bouldin W (1979) A cluster separation measure. IEEE Transactions on Pattern Analysis and Machine Intelligence 1(2):224–227

Deaux EB, Gormezano I (1963) Eyeball retraction: classical and extinction in the albino rabbit. Science 141:630–631

DeCarlo LT (1997) On the meaning and use of kurtosis. Psychol Methods 2:292–307

Dégenètais E, Thierry AM, Glowinski J, Gioanni Y (2002) Electrophysiological properties of pyramidal neurons in the rat prefrontal cortex: an in vivo intracellular recording study. Cereb Cortex 12:1–16

Domingo JA, Gruart A, Delgado-García JM (1997) Quantal organization of reflex and conditioned eyelid responses. J Neurophysiol 78:2518–2530

Donoho DL, Johnstone IM (1994) Ideal spatial adaptation by Wavelet Shrinkage. Biometrika 81:425–455

Dunn JC (1974) A Fuzzy Relative of the ISODATA Process and Its Use in Detecting Compact Well-Separated Clusters. J Cybern 3:32–57

Dunn JC (1974) Well separated clusters and optimal fuzzy partitions. J Cybern 4:95–104,

Einevoll GT, Franke F, Hagen E, Pouzat C, and Harris KD (2012) Towards reliable spike-train recordings from thousands of neurons with multielectrodes. Curr Opin Neurobiol 22:11–17

Ekanadham C, Tranchina D, Simoncelli EP (2014) A unified framework and method for automatic neural spike identification. J Neurosci Methods 222:47–55

Elble RJ (1996) Central mechanisms of tremor. J ClinNeurophysiol 13:133–144

Evinger C, Shaw MD, Peck CK, Manning KA, Baker R (1984) Blinking and associated eye movements in humans, guinea pigs, and rabbits. J Neurophysiol 52:323–339

Fee MS, Mitra PP, Kleinfeld D (1996) Automatic sorting of multiple unit neuronal signals in the presence of anisotropic and non-Gaussian variability. J Neurosci Methods 69:175–188

Fournier J, Mueller CM, Shein-Idelson M, Hemberger M, Laurent G (2016) Consensus-Based Sorting of Neuronal Spike Waveforms. PLoS One 11:e0160494

Fuster JM (1988) The Prefrontal Cortex: anatomy, physiology, and neuropsychology of the frontal lobe. New York: Raven Press.

Fuster JM (1995) Memory in the Cerebral Cortex: Empirical approach to neural networks in the human and nonhuman primate. Cambridge, MA: MIT Press.

Fuster JM (1997) The Prefrontal Cortex: anatomy, physiology, and neuropsychology of the frontal lobe, 3th Edition Lippincott-William and Wilkins Eds, Philadelphia, EE.UU. 1–315

Fuster JM (2001) The Prefrontal Cortex–an update: time is of the essence. Neuron 30:319–333

Fuster JM (2008) The Prefrontal Cortex. 4th Edition London, UK: Academic Press

Gerwig M, Kolb FP, Timmann D (2007) The involvement of the human cerebellum in eyeblink conditioning. *Cerebellum 6*:38-57.

Gibson S, Judy JW, Markovic D (2012) Spike sorting: the first step in decoding the brain. IEEE Signal Process Mag 29:124–143

Gibson S, Judy JW, Markovic D (2008) Comparison of spike-sorting algorithms for future hardware implementation. Conf Proc IEEE Eng Med Biol Soc 5015–5020

Girgis M, Shih-Chang W (1981) A new stereotaxic atlas of the rabbit brain. St Louis: Warren H Green

Gormezano I, Schneiderman N, Deaux EG and Fuentes I (1962) Nictitating membrane: classical conditioning and extinction in the albino rabbit. *Science* 138:33–34.

Gormezano I, Kehoe EJ, Marshall BS (1983) Twenty years of classical conditioning research with the rabbit. Prog Psychobiol Physiol Psychol 10:197–275

Grafen A, Hails R (2002) Modern Statistics for the Life Sciences. New York: Oxford Univ Press

Gray CM, Maldonado PE, Wilson M, McNaughton B (1995) Tetrodes markedly improve the reliability and yield of multiple single-unit isolation from multi-unit recordings in cat striate cortex. J Neurosci Methods 63:43–54

Green JT, Arenos JD (2007) Hippocampal and cerebellar single-unit activity during delay and trace eyeblink conditioning in the rat. Neurobiol Learn Mem 87:269–284

Gruart A (1993) Bases fisiológicas del condicionamiento clásico del reflejo corneal. Tesis doctoral: Universidad Autónoma de Barcelona

Gruart A, Delgado-García JM (1994) Discharge of identified deep cerebellar nuclei neurons related to eye blinks in the alert cat. Neuroscience 61:665–681

Gruart A, Blázquez P, Delgado-García JM (1995) Kinematics of spontaneous, reflex, and conditioned eyelid movements in the alert cat. J Neurophysiol 74:226–248

Gruart A, Pastor AM, Armengol JA and Delgado-García JM (1997) Involvement of cerebellar cortex and nuclei in the genesis and control of unconditioned and conditioned eyelid motor responses. Prog. Brain Res 114:511–528.

Gruart A, Schreurs BG, del Toro ED, Delgado-García JM (2000) Kinetic and frequency-domain properties of reflex and conditioned eyelid responses in the rabbit. J Neurophysiol 83:836–852

Gruart A, Guillazo-Blanch G, Fernández-Mas R, Jiménez-Díaz L, Delgado-García JM (2000) Cerebellar posterior interpositus nucleus as an enhancer of classically conditioned eyelid responses in alert cats. J Neurophysiol 84:2680–2690.

Hair JF, Anderson RE, Tatham RL, Black WC (1998) Multivariate Data Analysis. Englewood Cliffs, N J: Prentice Hall

Handl J, Knowles J, Kell DB (2005) Computational cluster validation in post-genomic data analysis. Bioinformatics 21:3201–3212

Harris KD, Henze DA, Csicsvari J, Hirase H, Buzsáki G (2000) Accuracy of tetrode spike separation as determined by simultaneous intracellular and extracellular measurements. J Neurophysiol 84:401–414

Henry C, Vouimba RM, Garcia R (1999) Plasticity in the mediodorsalthalamo-prefrontal cortical transmission in behaving mice. J Neurophysiol 82:2827–2832

Henze DA, Borhegyi Z, Csicsvari J, Mamiya A, Harris KD, Buzsáki G (2000) Intracellular features predicted by extracellular recordings in the hippocampus in vivo. J Neurophysiol 84:390–400

Horton PM, Nicol AU, Kendrick KM, Feng JF (2007) Spike sorting based upon machine learning algorithms (SOMA). J Neurosci Methods 160:52–68

Hogg RV, Ledolter J (1987) Engineering Statistics. New York: MacMillan

Hollander M, Wolfe DA (1999) Nonparametric Statistical Methods. Hoboken NJ: Wiley

Hulata E, Segev R, Ben-Jacob E (2002) A method for spike sorting and detection based on wavelet packets and Shannon's mutual information. J Neurosci Methods 117:1–12

Ison MJ, Mormann F, Cerf M, Koch C, Fried I, Quian-Quiroga R (2011) Selectivity of pyramidal cells and interneurons in the human medial temporal lobe. J Neurophysiol 106:1713–1721

Jahanmiri-Nezhad F, Barkhaus PE, Rymer WZ, Zhou P (2014) Spike sorting paradigm for classification of multi-channel recorded fasciculation potentials. Comput Biol Med 55:26–35

Jarvis MR, Mitra PP (2001) Sampling properties of the spectrum and coherency of sequences of action potentials. Neural Comput 13:717–749

Jim X, Han J (2010) K-means clustering In Encyclopedia of Machine Learning. Eds Sammut C and Webb G J (Springer US) pp 563–564

Jiménez-Díaz L, Navarro-López J de D, Gruart A, Delgado-García JM (2004) Role of cerebellar interpositus nucleus in the genesis and control of reflex and conditioned eyelid responses. J Neurosci 24:9138–9145

Jurado-Parras MT, Gruart A, Delgado-García JM (2012) Observational learning in mice can be prevented by medial prefrontal cortex stimulation and enhanced by nucleus accumbens stimulation. LearnMem 19:99 –106.

Kamboh AM, Mason AJ (2013) Computationally efficient neural feature extraction for spike sorting in implantable high-density recording systems. IEEE Trans Neural Syst Rehabil Eng 21:1–9

Kapucu FE, Makinen ME, Tanskanen JM, Yla-Outinen L, Narkilahti S, Hyttinen JA (2016) Joint analysis of extracellular spike waveforms and neuronal network bursts. J Neurosci Methods 259:143–155

Karkare V, Gibson S, Marković D (2011) A 130- µW, 64-Channel Neural Spike-Sorting DSP Chip. IEEE J Solid ST Circ 46:1214–1222

Kim KH, Kim SJ (2003) Method for unsupervised classification of multiunit neural signal recording under low signal-to-noise ratio. IEEE Trans Biomed Eng 50:421–431

Kim KH, Kim SJ (2000) Neural spike sorting under nearly 0-dB signal-to-noise ratio using nonlinear energy operator and artificial neural-network classifier. IEEE Trans Biomed Eng 47:1406–1411

Klampfl S, Maass W (2010) A theoretical basis for emergent pattern discrimination in neural systems through slow feature extraction. Neural Comput 22:2979–3035

Klausberger T, Magill PJ, Márton LF, Roberts JD, Cobden PM, Buzsáki G, Somogyi P (2003) Brain-state- and cell-type-specific firing of hippocampal interneurons in vivo. Nature 421:844–848

Knieling S, Sridharan KS, Belardinelli P, Naros G, Weiss D, Mormann F, Gharabaghi A (2016) An Unsupervised Online Spike-Sorting Framework Int. J Neural Syst 26:1550042

Koekkoek SK, Den Ouden WL, Perry G, Highstein SM, De Zeeuw CI (2002) Monitoring kinetic and frequency-domain properties of eyelid responses in mice with magnetic distance measurement technique. J Neurophysiol 88:2124–2133

Kolb B, Whishaw IQ (1999) Fundamentals of Human Neurophychology. New York: Freeman WH.

Kolb B, Pellis S, Robinson TE (2004) Plasticity and functions of the orbital frontal cortex. Brain Cogn 55:104–115

Kronforst-Collins MA, Disterhoft JF (1998) Lesions of the caudal area of rabbit medial prefrontal cortex impair trace eyeblink conditioning. Neurobiol Learn Mem 69:147–162

Leal-Campanario R, Fairen A, Delgado-García JM, Gruart A (2007) Electrical stimulation of the rostral medial prefrontal cortex in rabbits inhibits the expression of conditioned eyelid responses but not their acquisition. Proc Natl Acad Sci USA 104:11459–11464

Leal-Campanario R (2007) Mecanismos corticales del aprendizaje asociativo. Tesis doctoral: Universidad Pablo de Olavide (Sevilla).

Leal-Campanario R, Delgado-García JM, Gruart A (2013) The rostral medial prefrontal cortex regulates the expression of conditioned eyelid responses in behaving rabbits. J Neurosci 33:4378–4386

Leibig C, Wachtler T, Zeck G (2016) Unsupervised neural spike sorting for high-density microelectrode arrays with convolutive independent component analysis. J Neurosci Methods 271:1–13

Letelier JC, Weber PP (2000) Spike sorting based on discrete wavelet transform coefficients. J Neurosci Methods 101:93–106

Lewicki MS (1994) Bayesian modeling and classification of neural signals. Neural Computation 6:1005–1030

Lewicki MS (1998) A review of methods for spike sorting: The detection and classification of neural action potential. Network Computational Neural System 9:R53–R78

Liu Y, Li Z, Xiong H, Gao X, Wu J (2010) Understanding of internal clustering validation measures. IEEE Int Conf Data Mining 911–916

Llinás RR (1991) The noncontinuous nature of movement execution In: Motor Control: Concepts and Issues, edited by DR Humphrey and H-J Freund New York: Wiley, p 223-242

Llinás RR (1988) The intrinsic electrophysiological properties of mammalian neurons: insights into central nervous system function. Science 242:1654–1664

Louis ED (2014) Essential tremor: from bedside to bench and back to bedside. Curr Opin Neurol 27:461–467

MacQueen J (1967) Some methods for classification and analysis of multivariate observations In Proc 5th Berkeley Sym Math Stat Prob (University of California Press, Oakland) pp 281–297

Magariños-Ascone C, Núñez A, Delgado-García JM (1999) Different discharge properties of dorsolateral facial nucleus motoneurons: intracellular in vitro recordings. Neuroscience 94:879–886

Marquis DG, Porter JM (1939) Differential characteristics of conditioned eyelid responses established by reflex and voluntary reinforcement. J ExpPsychol 24:347–365

Maulik U, Bandyopadhyay S (2002) Performance evaluation of some clustering algorithms and validity índices. IEEE Trans Pattern Anal Mach Intell 24:1650–1654

McKenna JT, Vertes RP (2004) Afferent projections to nucleus reuniens of the thalamus. J Comp Neurol 480:115–142

McNaughton BL, O'Keefe J, Barnes CA (1983) The stereotrode: a new technique for simultaneous isolation of several single units in the central nervous system from multiple unit records. J Neurosci Methods 8:391–397

Morecraft RJ, Louie JL, Herrick JL, Stilwell-Morecraft KS (2001) Cortical innervation of the facial nucleus in the non-human primate: a new interpretation of the effects of stroke and related subtotal brain trauma on the muscles of facial expression. Brain 124:176–208

Morecraft RJ, Stilwell-Morecraft KS, Cipolloni PB, Ge J, McNeal DW, Pandya DN (2012) Cytoarchitecture and cortical connections of the anterior cingulate and adjacent somatomotor fields in the rhesus monkey. Brain Res Bull 87:457–497

Moore JW, Gormezano I (1961) Yoked comparisons of instrumental and classical eyelid conditioning. J Exp Psychol 62:552-559

Múnera A, Gruart A, Muñoz MD, Fernández-Mas R, Delgado-García JM (2001) Hippocampal pyramidal cell activity encodes conditioned stimulus predictive value during classical conditioning in alert cats. J Neurophysiol 86:2571–2582

Nguyen T, Khosravi A, Creighton D, Nahavandi S (2014) Spike sorting using locality preserving projection with gap statistics and landmark-based spectral clustering. J Neurosci Methods 238:43–53

Ohberg F, Johansson H, Bergenheim M, Pedersen J, Djupsjobacka M (1996) A neural network approach to real-time spike discrimination during simultaneous recording from several multi-unit nerve filaments. J Neurosci Methods 64:181–187

Oswald B, Knuckley B, Mahan K, Sanders C, Powell DA (2006) Prefrontal control of trace versus delay eyeblink conditioning: role of the unconditioned stimulus in rabbits (Oryctolaguscuniculus). Behav Neurosci 120:1033–1042

Oweiss KG, Anderson DJ (2002) Spike sorting: a novel shift and amplitude invariant technique. Neurocomputing 44:1133–1139

Pacheco-Calderon R, Carretero-Guillen A, Delgado-García JM, Gruart A (2012) Red nucleus neurons actively contribute to the acquisition of classically conditioned eyelid responses in rabbits. J Neurosci 32:12129–12143

Pakhira MK, Bandyopadhyay S, Maulik U (2004) Validity index for crisp and fuzzy clusters. Pattern Recogn 37:487–501

Pal NR, Bezdek JC (1995) On cluster validity for the fuzzy c-means model. IEEE Trans Fuzzy Systems 3:370–379

Paraskevopoulou SE, Wu D, Eftekhar A, Constandinou TG (2014) Hierarchical Adaptive Means (HAM) clustering for hardware-efficient, unsupervised and real-time spike sorting. J Neurosci Methods 235:145–156

Paraskevopoulou SE, Barsakcioglu DI, Saberi MR, Eftekhar A, Constandinou TG (2013) Feature extraction using first and second derivative extrema (FSDE) for real-time and hardware-efficient spike sorting. J Neurosci Methods 215:29–37

Park YG, Park HY, Lee CJ, Choi S, Jo S, Choi H, Kim YH, Shin HS, Llinas RR, Kim D (2010) Ca(V)31 is a tremor rhythm pacemaker in the inferior olive. Proc Natl Acad Sci USA 107:10731–10736

Pavlov I (1927) Conditioned Reflexes: An Investigation of the Physiological Activity of the Cerebral Cortex. Translated and edited by G. V. Anrep. London: Oxford University Press.

Pavlov A, Makarov VA, Makarova I, Panetsos F (2007) Sorting of neural spikes: when wavelet based methods outperform principal component analysis. Natural Comput 6:269–281

Pedreira C, Martinez J, Ison MJ, Quian-Quiroga R (2012) How many neurons can we see with current spike sorting algorithms?. J Neurosci Methods 211:58–65

Petrantonakis PC, Poirazi P (2015) A Simple Method to Simultaneously Detect and Identify Spikes from Raw Extracellular Recordings Front. Neurosci 9:452

Petrovic S (2006) A comparison between the Silhouette index and the Davies-Bouldin index in Labelling IDS Clusters. Proc NordSec06:53–64

Platzer A (2013) Visualization of SNPs with t-SNE. PLoS One 8:e56883

Porras-García E, Sánchez-Campusano R, Martínez-Vargas D, Domínguez-del-Toro E, Cendelin J, Vozeh F, Delgado-García JM (2010) Behavioral characteristics, associative learning capabilities, and dynamic association mapping in an animal model of cerebellar degeneration. J Neurophysiol 104:346–365

Porter JD, Burns LA, May PJ (1989) Morphological substrate for eyelid movements: innervation and structure of primate levatorpalpebraesuperioris and orbicularis oculi muscle. J Comp Neurol 287:64–81

Povysheva NV, Gonzalez-Burgos G, Zaitsev AV, Kröner S, Barrionuevo G, Lewis DA, Krimer LS (2006) Properties of excitatory synaptic responses in fast-spiking interneurons and pyramidal cells from monkey and rat prefrontal cortex. Cereb Cortex 16:541–552

Powell DA, Maxwell B, Penney J (1996) Neuronal activity in the medial prefrontal cortex during pavlovian eyeblink and nictitating membrane conditioning. J Neurosci 16:6296–6306.

Powell DA, Churchwell J, Burris L (2005) Medial prefrontal lesions and Pavlovianeyeblink and heart rate conditioning: effects of partial reinforcement on delay and trace conditioning in rabbits (Oryctolaguscuniculus). Behav Neurosci 119:180–189

Quian -Quiroga R (2012) Spike sorting. Current Biology 22:R45–R46

Quian-Quiroga R, Reddy L, Koch C, Fried I (2007a) Decoding visual inputs multiple neurons in the human temporal lobe. J Neurophysiol 98:1997–2007

Quian-Quiroga R (2007b) Spike sorting. Scholarpedia 2:3583

Quian-Quiroga R (2004) Unsupervised spike sorting with wavelets and superparamagnetic clustering. Neural Computation 16:1661–1687

Quiroga RQ, Nadasdy Z, Ben-Shaul Y (2004) Unsupervised spike detection and sorting with wavelets and superparamagnetic clustering. Neural Comput 16:1661–1687

Ray JP, Russchen PT, Fuller TA, Price JL (1992) Sources of presumptive glutamatergic/aspartatergic afferents to the mediodorsal nucleus of the thalamus in the rat. J CompNeurol 320:435–456

Ray S, Turi RH (1999) Determination of number of clusters in K-means clustering and application in colour image segmentation Proc ICAPRDT'99 Calcutta (India): NarosaPublishing Co:137–143

Regalia G, Coelli S, Biffi E, Ferrigno G, Pedrocchi A (2016) A framework for the comparative assessment of neuronal spike sorting algorithms towards more accurate off-line and on-line microelectrode arrays data analysis. Comput Intell Neurosci 8416237

Rescorla RA (1988) Pavlovian conditioning. It's not what you think it is. American Psychologist 43(3):151–160

Rey HG, Pedreira C, Quian Quiroga R (2015) Past, present and future of spike sorting techniques. Brain Res Bull 119:106–117

Romo R, Brody CD, Hernández A, Lemus L (1999) Neuronal correlates of parametric working memory in the prefrontal cortex. Nature 3:470–473.

Rousseeuw PJ (1987) Silhouettes: a graphical aid to the interpretation and validation of cluster analysis. J Comput Appl Math 20:53–65

Rutishauser U, Schuman EM, Mamelak AN (2006) Online detection and sorting of extracellularly recorded action potentials in human medial temporal lobe recordings, in vivo. J Neurosci Methods 154:204–224

Saeed M, Kamboh AM (2013) Hardware architecture for on-chip unsupervised online neural spike sorting. Proc IEEE EMBS Conf Neural Eng 1319–1322

Salganicoff M, Sarna M, Sax L, Gerstein GL (1988) Unsupervised waveform classification for multi-neuron recordings: A real-time, software-based system I Algorithms and implementation. J Neurosci Methods 25:181–187

Sánchez-Campusano R (2007) Métodos analíticos y experimentales optimizados para el control neuromuscular de las respuestas motoras aprendidas: El sistema motor palpebral. Tesis doctoral: Universidad Pablo de Olavide (Sevilla).

Sánchez-Campusano R, Gruart A, Delgado-García JM (2007) The cerebellar interpositus nucleus and the dynamic control of learned motor responses. J Neurosci 27:6620–6632

Sánchez-Campusano R, Gruart A, Delgado-García JM (2009) Dynamic associations in the cerebellar-motoneuron network during motor learning. J Neurosci 29:10750–10763

Sánchez-Campusano R, Gruart A, Delgado-García JM (2011) Dynamic changes in the cerebellar-interpositus/red-nucleus-motoneuron pathway during motor learning. Cerebellum 10:702–710

Sánchez-Campusano R, Delgado-García JM, Gruart A (2012) Cerebelo, aprendizaje motor y biomecánica palpebral: una aproximación analítico-experimental. Saarbrücken, SB: EAE–LAP LAMBERT Academic Publishing GmbH & Co. KG [*ISBN: 978-3-8473-6740-6*] pp:1–364

Sato T, Suzuki T, Mabuchi K (2007) Fast automatic template matching for spike sorting based on Davies-Bouldin validation índices. Conf Proc IEEE Eng Med Biol Soc 3200–3203

Sauerland EK, Knauss T, Nakamura Y, Clemente CD (1967) Inhibition of monosynaptic and polysynaptic reflexes and muscle tone by electrical stimulation of the cerebral cortex. Exp Neurol 17:159–171.

Scanziani M, Häusser M (2009) Electrophysiology in the age of light. Nature 461:930–939

Schmidt EM (1984) Computer separation of multi-unit neuroelectric data: a review. J Neurosci Methods 12:95–111

Schneiderman N, Fuentes I, Gormezano I (1962) Acquisition and extinction of the classically conditioned eyelid response in the albino rabbit. *Science* 136:650–652.

Shek JW, Wen GY, Wisniewski HM (1986) Atlas of the rabbit brain and spinal cord. Zurich, Switzerland: Karger

Shoham S, Fellows MR, Normann RA (2003) Robust, automatic spike sorting using mixtures of multivariate t-distributions. J Neurosci Methods 127:111–122

Siegel JJ, Kalmbach B, Chitwood RA, Mauk MD (2012) Persistent activity in a cortical-to-subcortical circuit: bridging the temporal gap in trace eyelid conditioning. J Neurophysiol 107:50–64

Siegel JJ, Mauk MD (2013) Persistent activity in prefrontal cortex during trace eyelid conditioning: dissociating responses that reflect cerebellar output from those that do not. J Neurosci 33:15272–15284

Silva GA (2011) The need for the emergence of mathematical neuroscience: beyond computation and simulation. Front Comput Neurosci 5:51

Sonoo M, Stalberg E (1993) The ability of MUP parameters to discriminate between normal and neurogenic MUPs in concentric EMG: analysis of the MUP "thickness" and the proposal of "size index". Electroencephalogr Clin Neurophysiol 89:291–303

Stevenson IA, Kording KP (2011) How advances in neural recording affect data analysis. Nature Neuroscience 14:139–142

Stewart CM, Newlands SD, Perachio AA (2004) Spike detection, characterization, and discrimination using feature analysis software written in LabVIEW. Comput Methods Programs Biomed 76:239–251

Su CK, Chiang CH, Lee CM, Fan YP, Ho CM, Shyu LY (2013) Computational solution of spike overlapping using data-based subtraction algorithms to resolve synchronous sympathetic nerve discharge. Front Comput Neurosci 7:149

Swadlow HA (2003) Fast-spike interneurons and feedforward inhibition in awake sensory neocortex. Cerebral Cortex 13:25–32

Swindale NV, Spacek MA (2016) Verification of multichannel electrode array integrity by use of cross-channel correlations. J Neurosci Methods 263:95–102

Takehara-Nishiuchi K, Kawahara S, Kirino Y (2005) NMDA receptor-dependent processes in the medial prefrontal cortex are important for acquisition and the early stage of consolidation during trace, but not delay eyeblink conditioning. Learn Mem 12:606–614

Takekawa T, Isomura Y, Fukai T (2010) Accurate spike sorting for multi-unit recordings. Eur J Neurosci 31:263–272

Takekawa T, Isomura Y, Fukai T (2012) Spike sorting of heterogeneous neuron types by multimodality-weighted PCA and explicit robust variational. Bayes Front Neuroinform 6:5

Takens F (1981) Detecting strange attractors in turbulence. Lect Notes Math 898:366–381

Thakur PH, Lu H, Hsiao SS, Johnson KO (2007) Automated optimal detection and classification of neural action potentials in extra-cellular recordings. J Neurosci Methods 162:364–376

Thompson RF (2005) In search of memory traces. Annu. Rev. Psychol 56:1-23.

Thompson RF, Steinmetz JE (2009) The role of the cerebellum in classical conditioning of discrete behavioral responses. Neuroscience 162:732-755.

Thorbergsson PT, Garwicz M, Schouenborg J, Johansson AJ (2014) Strategies for high-performance resource-efficient compression of neural spike recordings. PLoS One 9:e93779

Tou JT, Gonzalez RC (1974) Pattern Recognition Principles. Massachusetts: Addixon-Wesley

Trigo JA, Gruart A, Delgado-García JM (1999) Discharge properties of abducens, accessory abducens, and orbicularis oculi motoneurons during unconditioned and conditioned eye blinks in the alert cat. J Neurophysiol 81:1666–1684

Trigo JA, Roa L, Gruart A, Delgado-García JM (2003) A kinetic study of blinking responses in cats. J Physiology 549:195–205

Vargas-Irwin C, Donoghue JP (2007) Automated spike sorting using density grid contour clustering and subtractive waveform decomposition. J Neurosci Methods 164:1–18

Ventura V (2009a) Automatic spike sorting using tuning information. Neural Comput 21:2466–2501

Ventura V (2009b) Traditional waveform based spike sorting yields biased rate code estimates. Proc Natl Acad Sci *U S A* 106:6921–6926

Viskontas IV, Ekstrom AD, Wilson CL, Fried I (2007) Characterizing interneuron and pyramidal cells in the human medial temporal lobe in vivo using extracellular recordings. Hippocampus 17:49–57

Vogelstein RJ, Murari K, Thaku PH, Diehl C, Chakrabartty S, Cauwenberghs G (2004) Spike sorting with support vector machines. IEEE EMBS 4009–4012

Volkmann J, Joliot M, Mogilner A, Ioannides AA, Lado F, Fazzini E, Ribary U, Llinás R (1996) Central motor loop oscillations in parkinsonian resting tremor revealed by magnetoencephalography. Neurology 46:1359–1370

Wang GL, Zhou Y, Chen AH, Zhang PM, Liang PJ (2006) A robust method for spike sorting with automatic overlap decomposition. IEEE Trans Biomed Eng 53:1195–1198

Weible AP, McEchron MD, Disterhoft JF (2000) Cortical involvement in acquisition and extinction of trace eyeblink conditioning. Behav Neurosci 114:1056–1067

Weible AP, O'Reilly JA, Weiss C, Disterhoft JF (2007) Comparisons of dorsal and ventral hippocampus cornuammonis region 1 pyramidal neuron activity during trace eye-blink conditioning in the rabbit. Neuroscience 141:1123–1137

Weible AP, Weiss C, Disterhoft JF (2003) Activity profiles of single neurons in caudal anterior cingulate cortex during trace eyeblink conditioning in the rabbit. J Neurophysiol 90:599–612

Weiss C, Disterhoft JF (2011) Exploring prefrontal cortical memory mechanisms with eyeblink conditioning. Behav Neurosci 125:318–326

Welsh JP and Harvey JA (1991). Pavlovian conditioning in the rabbit during inactivation of the interpositus nucleus. J Physiology 444:459–480

Welsh JP (1992) Changes in the motor pattern of learned and unlearned responses following cerebellar lesions: a kinematic analysis of the nictitating membrane reflex. Neuroscience 47:1–19

Werner T, Vianello E, Bichler O, Garbin D, Cattaert D, Yvert B, De Salvo B, Perniola L (2016) Spiking Neural Networks Based on OxRAM Synapses for Real-Time Unsupervised Spike Sorting. Front Neurosci 10:474

Wessberg J, Vallbo AB (1995) Coding of pulsatile motor output by human muscle afferents during slow finger movement. J Physiol (Lond) 485:271–282

Weiss C, Disterhoft JF (2011) Exploring prefrontal cortical memory mechanisms with eyeblink conditioning. Behav Neurosci 125:318–326.

Wiskott L, Sejnowski TJ (2002) Slow feature analysis: unsupervised learning of invariances. Neural Comput 14:715–770

Wood F, Goldwater S, Black MJ (2006) A Non-Parametric Bayesian Approach to Spike Sorting Proceedings of the 28th. IEEE EMBS Annual International Conference ThBP78:1165–1168

Wood F, Fellows M, Donoghue J, Black M (2004) Automatic spike sorting for neural decoding. Conf Proc IEEE Eng Med Biol Soc 6:4009–4012

Woody CD, Wang XF, Gruen E, Landeira-Fernandez J (1992). Unit activity to click CS changes in dorsal cochlear nucleus after conditioning. NeuroReport 3(5):385–388

Woodruff-Pak DS, Lavond DG, Thompson RF (1985) Trace conditioning: abolished by cerebellar nuclear lesions but not lateral cerebellar cortex aspirations. Brains Research 348:249–260

Yang Y, Boling S, Eftekhar A, Paraskevopoulou SE, Constandinou TG, Mason AJ (2014) Computationally efficient feature denoising filter and selection of optimal features for noise insensitive spike sorting. Conf Proc IEEE Eng Med Biol Soc 1251–1254

Yang Z, Chen TC, Liu W (2008) A neuron signature based spike feature extraction algorithm for on-chip implementation. Conf Proc IEEE Eng Med Biol Soc 1716–1719

Yuan Y, Yang C, Si J (2012) The M-Sorter: an automatic and robust spike detection and classification system. J Neurosci Methods 210:281–290

Zamani M, Demosthenous A (2014) Feature extraction using extrema sampling of discrete derivatives for spike sorting in implantable upper-limb neural prostheses. IEEE Trans Neural Syst Rehabil Eng 22:716–726

Zhang PM, Wu JY, Zhou Y, Liang PJ, Yuan JQ (2004) Spike sorting based on automatic template reconstruction with a partial solution to the overlapping problema. J Neurosci Methods 135:55–65

Zouridakis G, Tam DC (2000) Identification of reliable spike templates in multi-unit extracellular recordings using fuzzy clustering. Comput Methods Programs Biomed 61:91–98

Zviagintsev A, Perelman Y, Ginosar R (2005) Low–Power Architectures for Spike Sorting Proc 2nd Int. IEEE EMBS Conf Neural Eng 162–165

8. ANNEXES

8.1. Intellectual property directly related to the doctoral thesis

VISSOR (*Viability of Integrated Spike Sorting of Real Recordings*):

A SOFTWARE FOR THE DETECTION, IDENTIFICATION AND CLASSIFICACION OF THE ACTION POTENTIALS DISTRIBUTED ACROSS NEURAL DATA.

Intellectual property reference number: SE-386-17
Mark reference number: M3664133
Version: 1.0. January 2017

Authors

Carmen Rocío Caro Martín, Raudel Sánchez Campusano, Agnès Gruart i Massó, José María Delgado García.

Pablo de Olavide University
Department of Physiology, Anatomy and Cell Biology.
Carretera de Utrera, km. 1. 41013-Sevilla. España.

Description

VISSOR: Software for spike sorting analysis of neural time series data. Available functions include data importing/exporting, preprocessing, spike classification, and visualization. The software for spike sorting based on shape, phase and distribution features and *K*-means clustering with validity and error indices are unique functions provided by this toolbox. *VISSOR* recognizes specific patterns of neuronal discharges (spikes) present in electrophysiological records. This grouping of spikes is based on the similarity of their profiles, given that, each neuron fires spikes of a particular shape. All functions have been integrated into a simple and user-friendly graphical user interface environment designed for easy accessibility.

Reference and acknowledgement

VISSOR was developed by Carmen Rocío Caro Martín (PhD Student) under the supervision of Drs. Raudel Sánchez Campusano (PhD) and Agnès Gruart i Massó (PhD). This study was supported by grants from the Spanish MINECO (BFU2011-29286) and Junta de Andalucía (BIO122, CVI 2487, and P07-CVI-02686) to Agnès Gruart i Massò and José María Delgado García. Caro Martín had a Predoctoral fellowship from MINECO during this period (reference number BES-2012-052748).

ERFO (Extractor of Range for Filtering optimization):

A SOFTWARE FOR DETERMINING THE FREQUENCY RANGE BOUNDARIES (EXTREME VALUES, MAXIMUM AND MINIMUM) MEANT TO BE OPTIMAL FOR THE OBSERVATION OF THE RECORDING POWER SPECTRUM WITH THE LARGEST POWER IN THE RANGE OF INTEREST.

Intellectual property reference number: pending of OEPM
Mark reference number: pending of OEPM
(Oficina Española de Patentes y Marcas)
Version: 1.0. January 2017

Authors

Carmen Rocío Caro Martín, Alessandro E.P. Villa, Agnès Gruart i Massó, José María Delgado García.

Pablo de Olavide University
Department of Physiology, Anatomy and Cell Biology.
Carretera de Utrera, km. 1. 41013-Sevilla. España.

Description

The application "Extracting the Range for Filtering optimization (ERFo)" determines the frequency range boundaries meant to be optimal for the observation of the raw signal power spectrum with the largest power in the range of interest. This software is important to eliminate frequency components associated with noise and possible recorded artefacts and for performing the most optimal filtering of the neural recording. All functions have been integrated into a simple and user-friendly graphical user interface environment designed for easy accessibility.

Reference and acknowledgement

ERFo was developed by Carmen Rocío Caro Martín (PhD Student - Pablo de Olavide University, Seville, Spain) and supervised by Alessandro E.P. Villa (Professor - University of Lausanne, Switzerland) under the research project awarded by the Spanish Ministry of Economy and Competitiveness (reference number: BFU2011-29286) granted to Agnès Gruart i Massó and José María Delgado García (both Full Professors - University Pablo de Olavide, Seville, Spain). Rocío Caro received a short-term training fellowship (EEBB-I-16-10562) to visit Dr. Villa's laboratory.

8.2. Papers directly related to the doctoral thesis

Behavioral/Cognitive

A Variable Oscillator Underlies the Measurement of Time Intervals in the Rostral Medial Prefrontal Cortex during Classical Eyeblink Conditioning in Rabbits

C. Rocío Caro-Martín, Rocío Leal-Campanario, Raudel Sánchez-Campusano, José M. Delgado-García, and Agnès Gruart

Division of Neurosciences, Pablo de Olavide University, Seville-41013, Spain

We were interested in determining whether rostral medial prefrontal cortex (rmPFC) neurons participate in the measurement of conditioned stimulus–unconditioned stimulus (CS-US) time intervals during classical eyeblink conditioning. Rabbits were conditioned with a delay paradigm consisting of a tone as CS. The CS started 50, 250, 500, 1000, or 2000 ms before and coterminated with an air puff (100 ms) directed at the cornea as the US. Eyelid movements were recorded with the magnetic search coil technique and the EMG activity of the orbicularis oculi muscle. Firing activities of rmPFC neurons were recorded across conditioning sessions. Reflex and conditioned eyelid responses presented a dominant oscillatory frequency of ≈12 Hz. The firing rate of each recorded neuron presented a single peak of activity with a frequency dependent on the CS-US interval (i.e., ≈12 Hz for 250 ms, ≈6 Hz for 500 ms, and≈3 Hz for 1000 ms). Interestingly, rmPFC neurons presented their dominant firing peaks at three precise times evenly distributed with respect to CS start and also depending on the duration of the CS-US interval (only for intervals of 250, 500, and 1000 ms). No significant neural responses were recorded at very short (50 ms) or long (2000 ms) CS-US intervals. rmPFC neurons seem not to encode the oscillatory properties characterizing conditioned eyelid responses in rabbits, but are probably involved in the determination of CS-US intervals of an intermediate range (250–1000 ms). We propose that a variable oscillator underlies the generation of working memories in rabbits.

Key words: **delay conditioning; neural oscillators; prefrontal cortex; rabbits; unitary recordings**

Significance Statement

The way in which brains generate working memories (those used for the transient processing and storage of newly acquired information) is still an intriguing question. Here, we report that the firing activities of neurons located in the rostromedial prefrontal cortex recorded in alert behaving rabbits are controlled by a dynamic oscillator. This oscillator generated firing frequencies in a variable band of 3–12 Hz depending on the conditioned stimulus–unconditioned stimulus intervals (1 s, 500 ms, 250 ms) selected for classical eyeblink conditioning of behaving rabbits. Shorter (50 ms) and longer (2 s) intervals failed to activate the oscillator and prevented the acquisition of conditioned eyelid responses. This is an unexpected mechanism to generate sustained firing activities in neural circuits generating working memories.

Introduction

Motor tremor should not be taken as an admonitory symptom of a pathological condition, as an unwanted byproduct of movement performance, or as the exclusive result of the inertial and viscoelastic properties of moving body parts, but rather as the necessary background for the coordinated execution of spontaneous and acquired movements (Llinás, 1991; Elble, 1996; Volkmann et al., 1996; Park et al., 2010; Louis, 2014). In a previous study of the kinematic properties of cat eyelids, Gruart et al. (1995) suggested the existence of a 20–25 Hz oscillator underlying reflex and classical eyeblink responses. Indeed, published records note the easily seen presence of oscillations in eyelid movements or in the EMG activity of involved facial or retractor bulbi muscle (Berthier, 1992; Welsh, 1992). In particular, eyelid oscillations in rabbits present a dominant frequency of 4–15 Hz (Gruart et al., 2000). It was shown previously that oscillatory

Received June 14, 2015; revised Sept. 15, 2015; accepted Sept. 29, 2015.

Author contributions: R.S.-C., J.M.D.-G., and A.G. designed research; C.R.C.-M., R.L.-C., R.S.-C., J.M.D.-G., and A.G. performed research; C.R.C.-M., R.L.-C., R.S.-C., J.M.D.-G., and A.G. analyzed data; J.M.D.-G. and A.G. wrote the paper.

This work was supported by the Spanish Ministry of Economy and Competitiveness (Grant BFU2014-56692-R to A.G. and J.M.D.-G.) and Junta de Andalucía (Grants BIO122, CVI 2487, and P07-CVI-02686 to A.G. and J.M.D.-G.). We thank Roger Churchill for help in manuscript editing.

The authors declare no competing financial interests.

Correspondence should be addressed to Prof. Agnès Gruart, Division of Neurosciences, Pablo de Olavide University, Ctra. de Utrera, Km. 1, Seville-41013, Spain. E-mail: agrumas@upo.es.

DOI:10.1523/JNEUROSCI.2285-15.2015

 0270-6474/15/3514809-13$15.00/0

activities of the eyelid are tuned to its size and viscoelastic properties, as determined in different (mouse, rat, rabbit, cat, and human) species of mammals (Domingo et al., 1997; Gruart et al., 2000; Koekkoek et al., 2002).

Oscillations in a range similar to those presented by the lids have also been described in the resting membrane potentials and firing properties of cat facial motoneurons (Trigo et al., 1999) and motor cortex neurons (Aou et al., 1992) during the performance of conditioned eyeblinks. In a recent study of the firing activities of rostral medial prefrontal cortex (rmPFC) neurons in rabbits during the classical conditioning of eyelid responses, we reported the presence of dominant peaks in the discharge rate of recorded neurons at different latencies with respect to CS presentations, but always within the CS-US interval (Leal-Campanario et al., 2013). This observation raised the possibility that neural firing of rmPFC neurons could be related to the oscillatory properties and timing of conditioned eyeblinks or, on the contrary, could be involved in the determination of CS-US intervals, associative strength of conditioning stimuli, or related matters.

We recorded the firing activities of rmPFC neurons during classical eyeblink conditioning of behaving rabbits. For conditioning, we used a delay because it has been reported that cerebral cortical areas are not involved in its proper acquisition and retrieval (Clark et al., 1984; Takehara-Nishiuchi et al., 2005; Oswald et al., 2006). In this way, we could determine whether rmPFC activity during this type of associative learning is engaged in additional neural processing of associative learning tasks. To properly determine the oscillatory properties of conditioned eyelid responses, lid movements were recorded with the magnetic search coil technique (Gruart et al., 2000). The EMG activity of the ipsilateral orbicularis oculi muscle was also recorded. Firing activities of contralateral pyramidal rmPFC neurons were recorded across the successive conditioning sessions. Collected results suggest that the rmPFC plays an important role in cognitive processes related to associative learning tasks, such as the determination of CS-US intervals. In contrast, the rmPFC does not seem to be involved directly in the acquisition process or in the execution of the acquired eyelid responses.

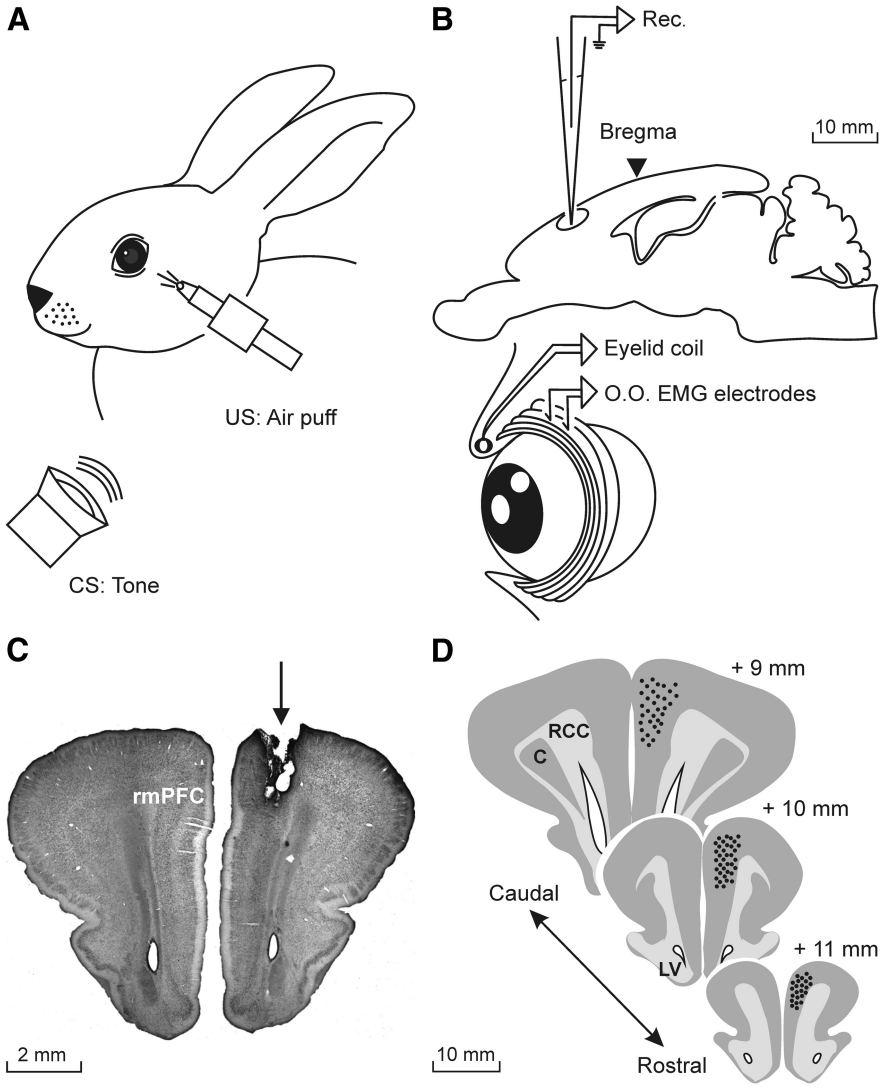

Figure 1. Experimental design. ***A***, For the classical conditioning of eyelid responses with a delay paradigm, rabbits were presented with a tone (600 Hz, 85 dB) as a CS. The tone was followed at different CS-US intervals (100, 250, 500, 1000, or 2000 ms) by an air puff (100 ms, 3 kg/cm^2) directed at the left cornea as a US. The two stimuli terminated simultaneously. ***B***, Diagram illustrating the rmPFC recording (Rec.) area. Eyelid movements were recorded using the magnetic field search coil technique with the help of a coil chronically implanted in the left upper lid. Animals were also implanted with EMG recording electrodes in the ipsilateral orbicularis oculi (O.O.) muscle. ***C***, Photomicrograph illustrating an electrolytic lesion (arrow) performed in the rmPFC recording sites. ***D***, Schematic diagrams in stereotaxic coordinates from rabbit brain with indication of the recording (black dots) sites. Calibrations for ***B***–***D*** are indicated. C, Claustrum; LV, lateral ventricle; RCC, corpus callosum.

Materials and Methods

Experimental animals. Experiments were performed on adult male rabbits (New Zealand white albino) weighing 2.5–3 kg on arrival obtained from an authorized supplier (Isoquimen). Animals were housed in individual cages for the whole experiment and kept on a 12/12 h light/dark cycle with constant ambient temperature (21 ± 1°C) and humidity (50 ± 7%). Food and water were available *ad libitum*. All experimental procedures were performed in accordance with European Union (2010/63/EU) guidelines and Spanish (BOE 34/11370-421, 2013) regulations for the use of laboratory animals in chronic experiments. Experimental protocols were also approved by the local University Ethics Committee.

Surgery. Animals were anesthetized with intramuscular injections of a ketamine–xylazine mixture (Ketaminol, 50 mg/ml; Rompun, 20 mg/ml; and atropine sulfate, 0.5 mg/kg). The anesthesia dosage was 0.35 ml/kg and was maintained by intravenous perfusion of the mixture at a flow rate of 10 mg/kg/h. As illustrated in Figure 1, all of the animals ($n = 24$) were implanted with a 5-turn coil (3 mm in diameter) into the center of the left upper eyelid close to the lid margin. Coils were made from Teflon-coated stainless steel wire (A-M Systems) with an external diameter of 50 μm and weight of 10–15 mg. Animals were also implanted with recording bipolar hook electrodes in the ipsilateral orbicularis oculi muscle. These electrodes were made from the same stainless steel wire. In addition, a 5 × 5 mm window was drilled in the frontal bone centered above the right rmPFC (Girgis and Shih-Chang, 1981; Shek et al., 1986). The dura mater was removed and an acrylic recording chamber was

constructed around the window. The brain surface was protected with a piece of silicone sheet and the chamber was filled with sterile gauze and capped with a plastic cover. A needle tip was implanted stereotaxically in one corner of the chamber for reference purposes during unitary recordings. Finally, a head-holding system consisting of three bolts cemented to the skull perpendicular to the stereotaxic plane was implanted. A silver electrode (1 mm in diameter) was attached to the skull as a ground. Terminals of the coil and EMG and ground electrodes were soldered to a six-pin socket. All wire connections were covered with cyanoacrylate glue and the whole system was attached to the skull with the aid of three small screws fastened and cemented with an acrylic resin to the bone (for details, see Leal-Campanario et al., 2007, 2013).

Recording and stimulation procedures. Recording sessions began 2 weeks after surgery. Each rabbit was placed in a Perspex restrainer specially designed for limiting the animal's movements (Gruart et al., 2000). The box was placed on the recording table and was surrounded by a black cloth. The recording room was kept softly illuminated and a 60 dB background white noise was switched on during the experiments. For all subjects, the first two recording sessions consisted of adapting the rabbit to the restrainer and to the experimental conditions; no stimulus was presented during these two sessions.

Eyelid movements were recorded with the magnetic field search coil technique (coil system from C-N-C Engineering). Eyelid coils were calibrated with a transparent protractor placed sagittally to the animal's head and with its center located at the external canthus of the lids. Eyelid closures were evoked with air puffs. Upper eyelid maximum opening ranged from 30° to 40° for the 24 animals. For the sake of homogeneity, the gain of the recording system was adjusted to yield 1 V per 10° (Gruart et al., 2000). The EMG activity of the orbicularis oculi muscle was recorded using a Grass P511 differential amplifier with a bandwidth of 0.1 Hz to 10 kHz.

Neuronal electrical activity was recorded in the rmPFC area with the help of a NEX-1 preamplifier (Biomedical Engineering). These recordings were performed with glass micropipettes filled with 2 M NaCl (3–6 MΩ of resistance) and filtered in a bandwidth of 1 Hz to 10 kHz. The recording area was approached with the help of stereotaxic coordinates (Girgis and Shih-Chang, 1981; Shek et al., 1986). At the end of each recording session, the recording micropipette was always removed and the recording chamber sterilized and closed.

Tones were applied from a loudspeaker located 80 cm below the animal's head. Air puffs directed at the left cornea were delivered through the opening of a plastic pipette (3 mm in diameter) attached to a metal holder fixed to the animal's nine-pin socket (dual-channel air-puff device; Biomedical Engineering).

Classical conditioning. Classical eyeblink conditioning was achieved by the use of a delay conditioning paradigm as described in detail previously (Leal-Campanario et al., 2007, 2013). For this, animals were presented with a tone (600 Hz, and 85 dB) as the CS, followed 50, 250, 500, 1000, or 2000 ms from its beginning by an air puff (100 ms, 3 kg/cm^2) as the US (Fig. 1*A*). The two stimuli terminated at the same time. Four animals were used for each of these five CS-US time intervals. The conditioning session consisted of 66 CS-US trials separated at random by intervals of 50–70 s. Six of the 66 trials were test trials in which the CS was presented alone. A conditioning session lasted for ≈70 min and animals were trained on 10 successive days. We considered a conditioned response (CR) the presence during the CS–US interval of EMG activity initiated >50 ms after CS onset and with a peak amplitude at least 2 times greater than the EMG amplitude recorded 50 ms before the CS onset. In addition, an animal was considered conditioned when it was able to produce 80% of CRs per session to the CS-US paired presentation (Gruart et al., 2000; Leal-Campanario et al., 2007, 2013). For the two habituation sessions, animals were presented with the CS alone for the same number of trials/session and at the same time intervals. Pseudoconditioning sessions, performed in four additional animals, also consisted of 66 trials separated at random by intervals of 50–70 s. For each trial, the CS was presented unpaired in relation to the US, the only restriction being that no more than two CS or US trials occurred sequentially (Gruart et al., 2000). The total training per session for pseudoconditioning was the same as for conditioning.

Unitary recordings in the rmPFC area were made during habituation, conditioning, and pseudoconditioning sessions (Fig. 1*B*). The recording micropipette was approached to the selected recording site with the help of the implanted reference needle. The recording site was changed in the horizontal plane in steps of 0.1 mm until a suitable unit was recorded and identified (Leal-Campanario et al., 2007, 2013; Pacheco-Calderón et al., 2012). Neuron isolation was performed during the time intervals in which CS-US pairs of stimuli were not presented. Usually, a range of 1–6 neurons was recorded per conditioning session.

Histology. At the end of the experiments, animals were deeply anesthetized with sodium pentobarbital (50 mg/kg, i.p.) and perfused transcardially with saline and 4% paraformaldehyde. The proper location of eyelid coil and EMG electrodes was checked. To determine the recording sites in the prefrontal cortex a small electrolytic lesion (CS-220 stimulator; Cibertec) was performed in all of the animals, their brain was removed and cut into slices (50 μm), and the relevant cortical areas were processed for Nissl staining (Fig. 1*C*). Recording sites were adjusted according to the collected stereotaxic coordinates and with the location of the electrolytic marks (Fig. 1*D*).

Data collection and analysis. The horizontal and vertical position of the upper eyelid, the unrectified EMG activity of the orbicularis oculi muscle, the unitary activity recorded in the rmPFC, and 1 V rectangular pulses corresponding to CS and US presentations were acquired online through an 8-channel analog-to-digital converter (1401-plus; CED), and transferred to a computer for quantitative offline analysis. Data were sampled at 5000 Hz (for EMG recordings) or 25000 Hz (for unitary recordings), with an amplitude resolution of 12 bits. Computer programs (Spike2 and SIGAVG from CED) were used to display eyelid position, velocity, and acceleration, as well as EMG and unitary activities (Figs. 2, 3). When necessary for quantitative analysis, segments containing CRs were selected exclusively from those obtained during the presentation of the CS alone. The programs also allowed the representation of the firing rate of the recorded neurons (Múnera et al., 2001; Leal-Campanario et al., 2007, 2013).

Velocity and acceleration traces were computed digitally as the first and second derivative of eyelid position records after low-pass filtering of the data (23 dB cutoff at 50 Hz and a zero gain at ≈100 Hz; Fig. 2*A*). As explained in detail previously (Domingo et al., 1997), the power of the spectral density function (i.e., the power spectrum) of selected data were calculated using a fast Fourier transform to determine the relative strength of the different frequencies present in eyelid displacements. The power spectra of eyelid movements were calculated exclusively from the corresponding acceleration (Domingo et al., 1997; Gruart et al., 2000). Acceleration segments (1.024 s) containing CRs were selected exclusively from those obtained during the presentation of the CS alone. This design allowed the complete CR to be contained in the segment with a spectral resolution of 0.97 Hz (Fig. 2*C*,*D*).

For unitary analysis, we designed and developed a customized spike-sorting algorithm called *VISSOR* (Viability of Integrated Spike Sorting of Real Recordings) on a MATLAB (The MathWorks) platform, which determined the number of neuronal spikes distributed across time with up to 22 physiological parameters characterizing each action potential (Fig. 3*A*,*B*; Porras-García et al., 2010; Caro-Martín et al., 2014, 2015). In short, a total of eight parameters of spike shapes in time domain (e.g., spike duration, peak-to-peak amplitude, negative and positive deflections), nine parameters from spike trajectory in phase space (e.g., negative and positive peaks of the first and second derivatives), and five parameters in relation to the distribution measures (e.g., interquartiles metrics, kurtosis coefficient, Fisher asymmetry) were determined from each recorded unit. Spikes were automatically grouped by *k*-means clustering (Paraskevopoulou et al., 2013), followed by an index of validation (e.g., silhouette) to verify the homogeneity and dissimilarity between spikes during classification (Su et al., 2013). For raster plots, we examined the firing-rate patterns (peak firing rate and time-locked firing) for all spiking events. Finally, we clustered the spiking events by means of an unsupervised procedure (hierarchical clustering analysis) of patterns rec-

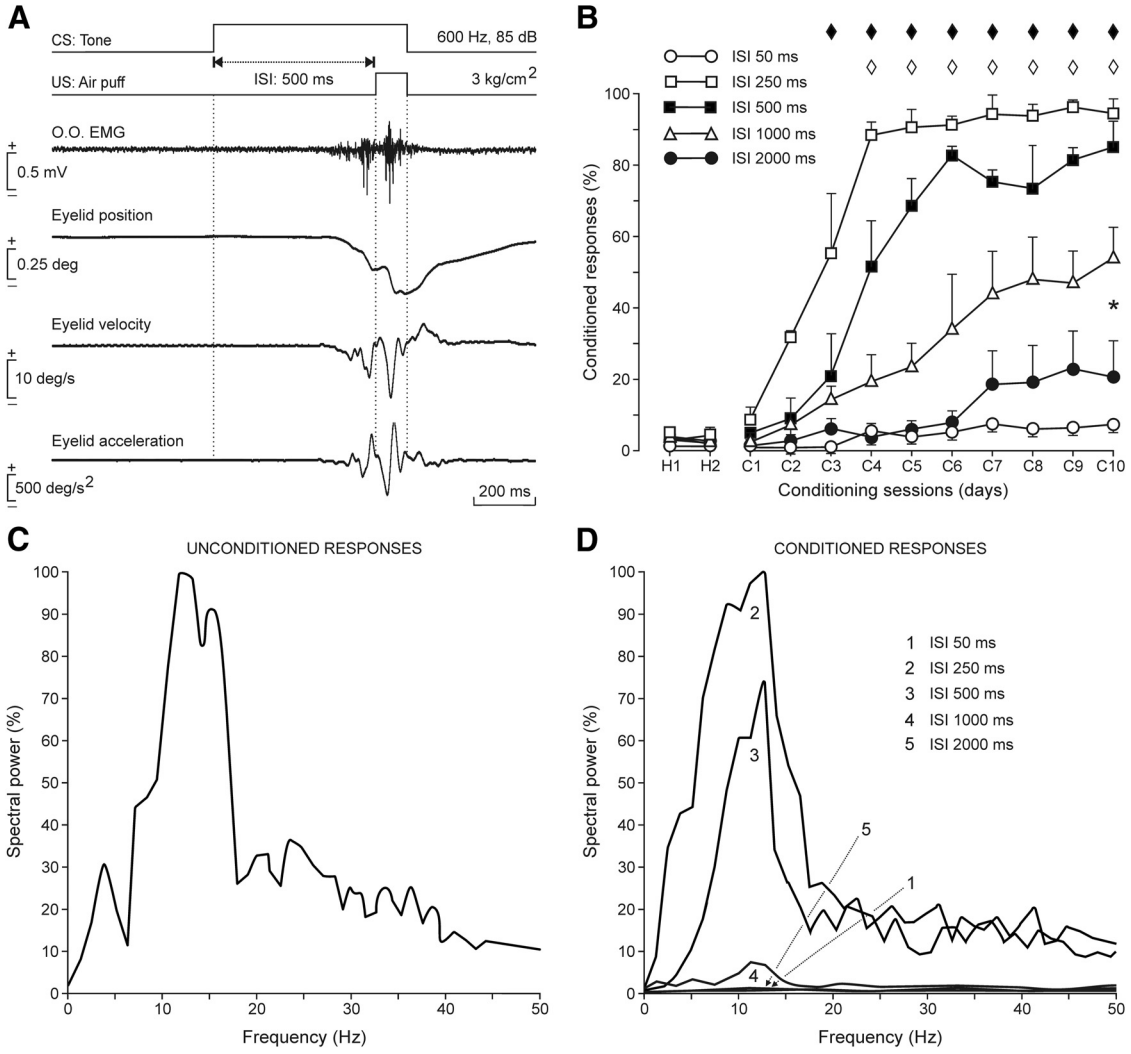

Figure 2. Frequency-component analysis for CRs as a function of CS-US intervals in a delay paradigm. ***A***, From top to bottom are illustrated the conditioning paradigm, representative examples of the EMG activity of the orbicularis oculi muscle (O.O. EMG), and eyelid position, velocity, and acceleration during the paired presentation of the CS followed 500 ms later by the US. ***B***, Evolution of the percentage of CRs (% CRs ± SEM) through the 10 conditioning sessions for five delay conditioning paradigms of different CS-US interval: 50 ms (○), 250 ms (□), 500 ms (■), 1000 ms (△), and 2000 ms (●). Note that animals conditioned with 250 or 500 ms CS-US intervals reached asymptotic values (80% of CRs) by the fourth to sixth conditioning sessions, but that those trained with the other three intervals failed to reach criterion by the 10th conditioning session. Data collected for intervals of 250 and 500 ms were not statistically different, but were significantly (one-way ANOVA on ranks, $p = 0.17$) different from those conditionings performed with the other three CS-US intervals. Pairwise multiple-comparison analysis, Holm–Sidak method: ♦ $p < 0.001$ for □ versus ○, △, and ●. ◊ $p < 0.001$ for ■ versus ○, △, and ●. *$p < 0.001$ for △ versus ○ and ●. ***C***, Illustration of the mean spectral power from ≥30 acceleration records ($n = 4$ rabbits) of eyelid reflex responses to air puffs (100 ms, 3 kg/cm^2) presented to the ipsilateral cornea. The 100% value for the illustrated spectral power corresponded to 0.93×10^7 (deg/s^2)^2, with a peak frequency of 12 Hz. ***D***, Mean spectral powers (≥10 acceleration profiles) of CRs evoked during the five different CS-US intervals illustrated in ***B*** (1, 50 ms; 2, 250 ms; 3, 500 ms; 4, 1000 ms; 5, 2000 ms). Each mean spectral power was obtained from two different rabbits. The 100% value for the illustrated spectral power corresponded to 0.3×10^7 (deg/s^2)^2. Peak frequencies for the different CS-US intervals were ≈12 Hz.

ognition and averaged the firing rate with similar time-locked firing and peak firing rates.

The spectral power of overlapped firing rate profiles was calculated by fitting a waveform with the help of the equation $f(t) = \alpha_0 \cos(wt)$, where α_0 is the mean value of the three dominant peaks in the averaged firing rates. Each waveform was calculated for the angular frequency $w = 2\pi/T$ where T is the average of the latency between the firing rate peaks with respect to CS presentation. The value of T was determined for each CS-US interval after the analysis of recorded firing rate profiles (Figs. 4, 5).

Computed results were processed for statistical analysis using the Statistics MATLAB Toolbox and SigmaPlot 11.0 package. As statistical inference procedures, both one- and two-way ANOVA (estimate of within-group and between-group variance on the basis of one dependent measure) and MANOVA (estimate of variance in multiple dependent parameters across groups) were used to assess the statistical significance of differences between groups. When the normality (Shapiro–Wilk or Kolmogorov–Smirnov tests) and equal variance of the errors (Levene Median test) assumptions were satisfied, the corresponding statistical significance test [i.e., the $F_{[(m-1),\,(m-1)\times(n-1),\,(l-m)]}$ statistics and the resulting probability $P < p$ at the predetermined significance level $p < 0.05$] was performed with sessions as repeated measures and coupled with contrast analysis when appropriate. The orders m (number of groups), n (number of rabbits), and l (number of multivariate observations) were reported accompanying the F-statistic values (Sánchez-Campusano et al., 2007). When the normality assumption was not confirmed, the significance (p value) of the χ^2 statistic was calculated using the ranks of the data rather than their numeric values. ANOVA test on ranks is a nonparametric version of the classical ANOVA F test and an extension of the Wilcoxon rank-sum test to more than two groups.

Wilk's lambda criterion and its transformation to the χ^2 distribution (MATLAB) were used to extract significant differences from MANOVA

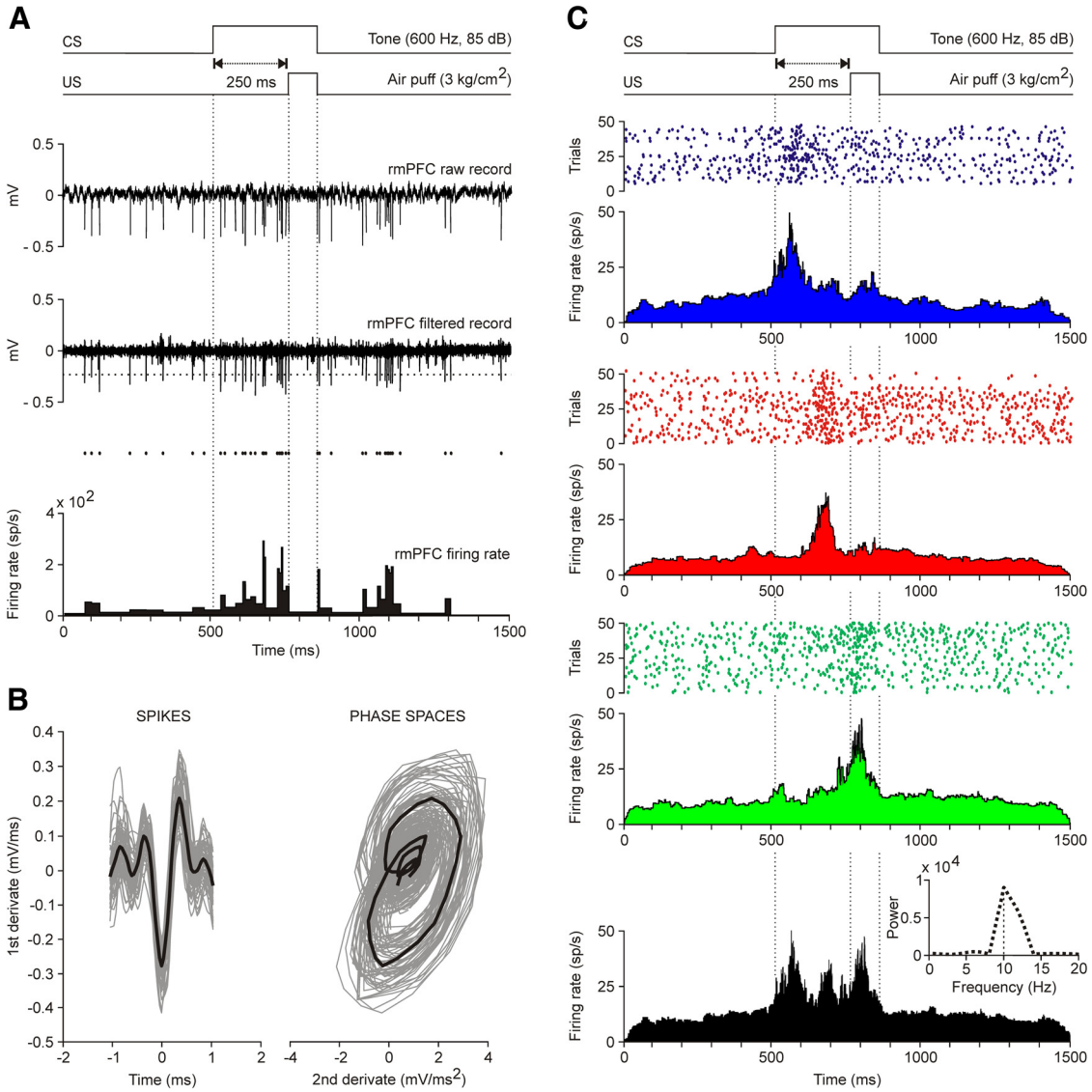

Figure 3. Firing activities of rmPFC neurons during classical eyeblink conditioning using a delay conditioning paradigm. ***A***, From top to bottom are illustrated a delay conditioning with indication of CS and US presentations. Below are illustrated the raw and filtered activity of a representative neuron collected during the ninth conditioning session, as well as a representation of its firing rate. The horizontal dotted line indicates the selected threshold. ***B***, At the left is represented a selection of the spikes detected by the selected threshold, while the phase space portraits (PSPs) of spike waveforms are represented at the right. Black traces indicated the mean value for each representation. ***C***, Representative examples of three different types of firing rate recorded during classical eyeblink conditioning. All of the illustrated raster displays were collected during the ninth conditioning session and were averaged from ≥40 trials. The three different firing rates were characterized by having their maximum frequency peaks close to the beginning of the CS (blue raster and firing rate, time to peak 59.4 ms, maximum frequency 46.35 spikes/s), in the center of the CS-US (red, time to peak 184.3 ms, maximum frequency 36.99 spikes/s), or next to the end of the US (green, time to peak 302.04 ms, maximum frequency 47.75 spikes/s). The black profile illustrates the overlap of the three firing rates shown above. The inset at the bottom right illustrates the spectral power [10^4(spikes/s)^2, peak frequency of 9.93 Hz] of the black profile. This spectrum was obtained by fitting a waveform with angular frequency $w = 2\pi/T$, where T is the average of the latency between the firing rate peaks with respect to CS presentation ($T = 100.68$ ms).

results (cluster analysis for cells–classes–spikes classification) during the spike-sorting problem in the phase space (Porras-García et al., 2010). Unless otherwise indicated, data are represented by the mean ± SEM.

Results

Oscillatory properties of reflex and classically conditioned eyelid responses

As illustrated in Figure 1, *A* and *B*, animals were prepared for the chronic recording of the EMG activity of the orbicularis oculi muscle and of eyelid movements with the help of the magnetic search coil technique. In Figure 2*A* is shown a representative example of reflex and conditioned eyelid responses during the eighth conditioning session recorded with the EMG electrodes and the coil implanted in the upper lid. Position, velocity, and acceleration profiles of the evoked eyelid responses are also illustrated. Air-puff-induced blinks consisted of a fast downward movement of the upper eyelid, followed by a much slower upward phase until the eyelid's initial position was reached (Fig. 2*A*). Mean latency of eyeblinks elicited by 100 ms, 3 kg/cm^2 air puffs was 19.5 ± 4.2 ms (mean ± SD; $n = 20$). The initial downward phase of evoked eyeblinks presented successive small sags in the direction of closure easily detected in the lid velocity and acceleration profiles. A power spectrum analysis was performed to determine the frequency components of the successive downward waves of air-puff-evoked blinks. The mean power spectra of 30 acceleration records from air-puff-evoked blinks collected from four rabbits showed a dominant peak at 12.6 ± 0.9 Hz over

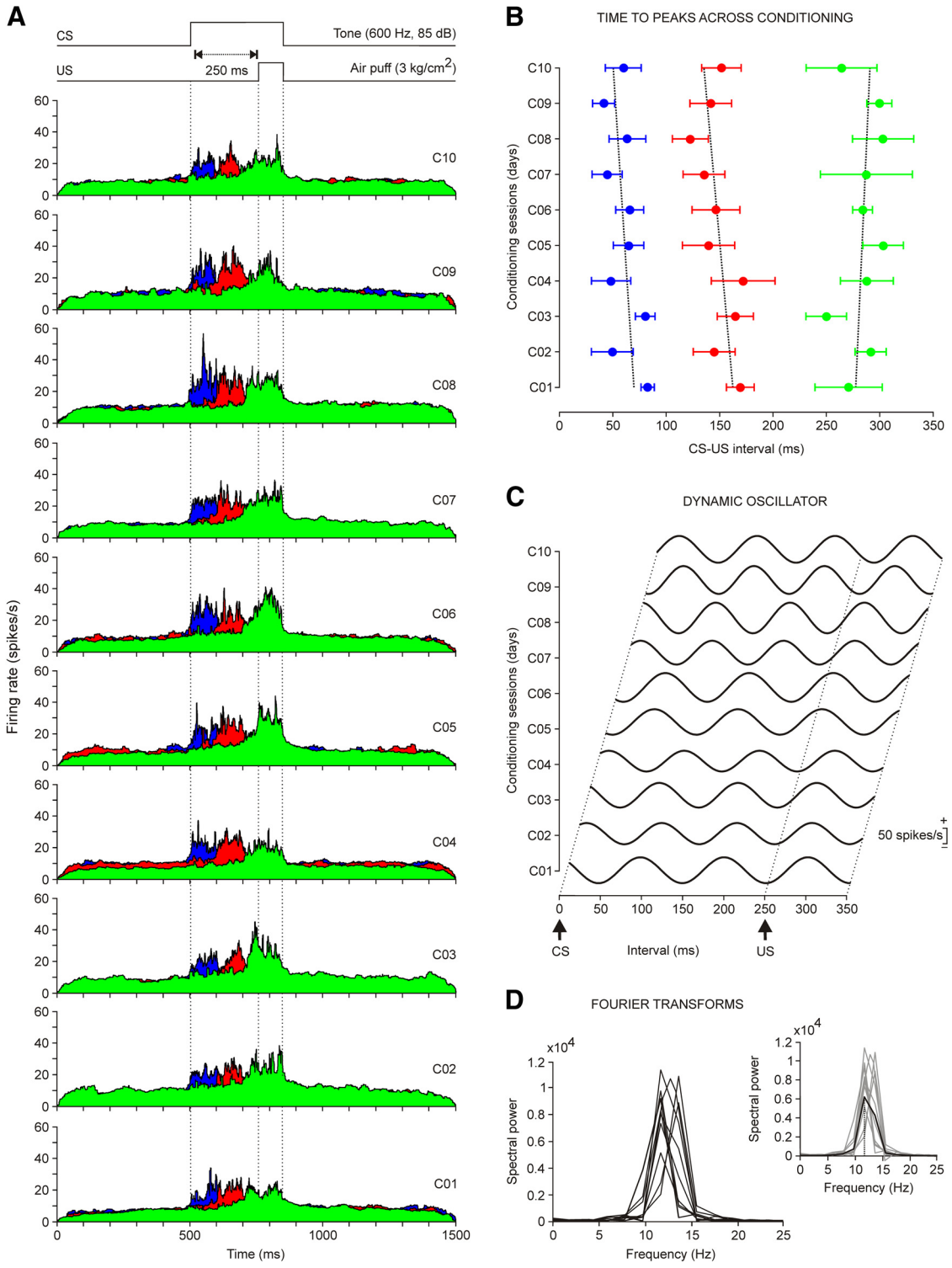

Figure 4. Evolution of the firing rate of rmPFC neurons across conditioning sessions with 250 ms of CS-US interval. ***A***, Firing rates of rmPFC neurons recorded from the first (C01) to the tenth (C10) conditioning sessions. Each illustrated profile was averaged from at least two neurons collected from four different animals. As in Figure 3*C*, the color code indicates the different peak latencies with respect to CS onset of the averaged firing rates. The conditioning paradigm is illustrated at the top. ***B***, Latency evolution for peak firing rates of the three different types of neuron across the 10 conditioning sessions. The corresponding regression lines were as follows: blue group, $y = -2.15x + 71.7$; red group, $y = -3.00x = 165.1$; and green group, $y = -1.47x + 275.7$. ***C***, Dynamic oscillator modeling firing rates. The oscillating curves were computed by fitting a waveform with an angular frequency $w = 2\pi/T$, where T is the average of the latency between the three dominant peaks with respect to CS presentation across the 10 conditioning sessions. The scale (in spikes/s) indicates mean firing rates. ***D***, Spectral powers obtained from the 10 oscillating curves illustrated in ***C***. On the right is shown the average from these 10 spectral powers. The average presented a maximum power of 0.6×10^4(spikes/s)^2 and a dominant frequency of 11.72 Hz.

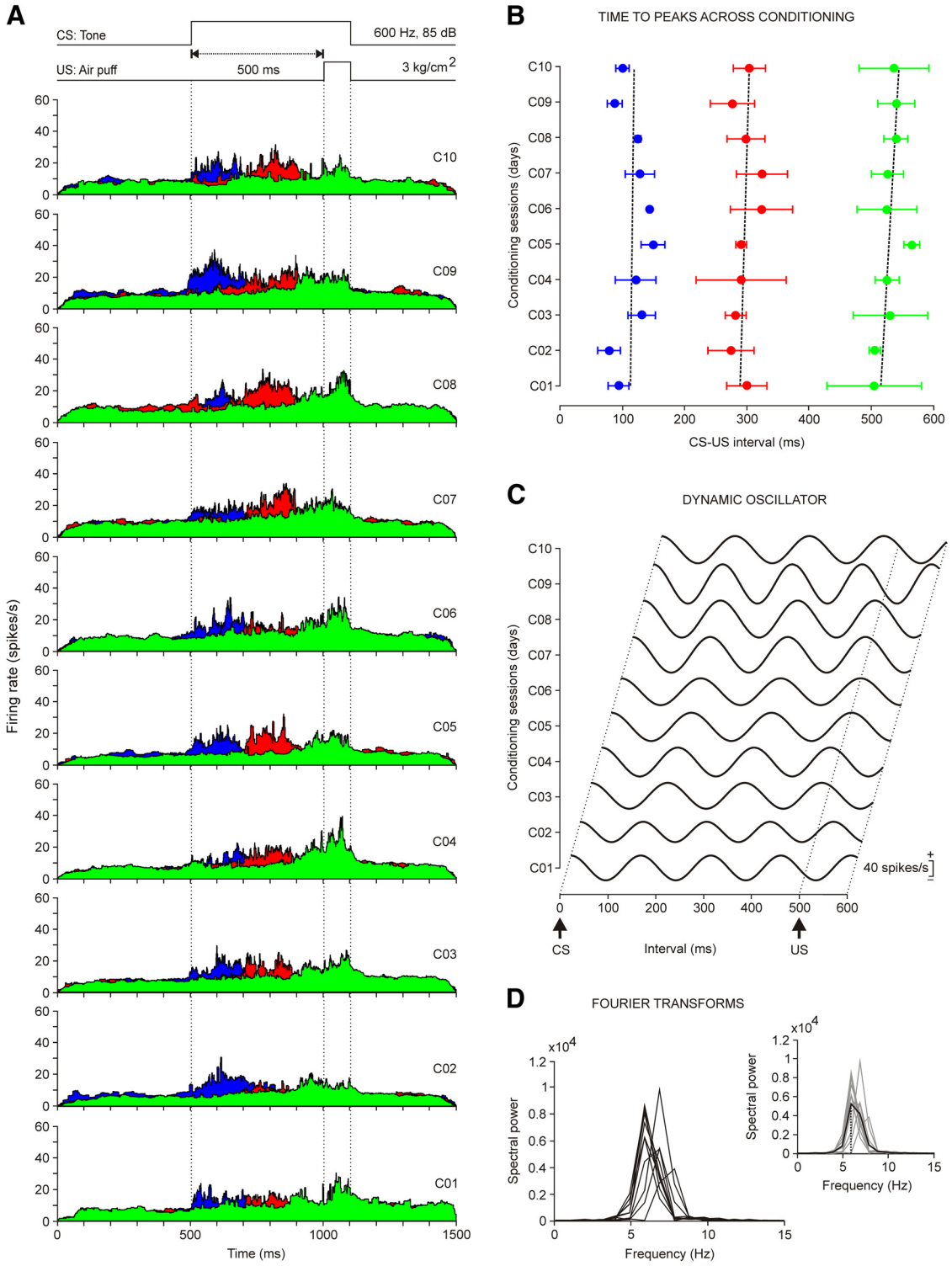

Figure 5. Evolution of the firing rate of rmPFC neurons across conditioning sessions with 500 ms of CS-US interval. ***A***, Firing rates of rmPFC neurons recorded from the first (C01) to the tenth (C10) conditioning sessions. Each illustrated profile was averaged from ≥2 neurons collected from four different animals. As shown in Figure 3*C*, the color code indicates the different peak latencies with respect to CS onset of the averaged firing rates. Note the progressive definition of the three types of firing rate during CS-US intervals. ***B***, Latency evolution for peak firing rates of the three different types of neuron across the 10 conditioning sessions. The corresponding regression lines were as follows: blue group, $y = 0.65x + 111.9$; red group, $y = 1.64x + 287.3$; and green group, $y = 3.22x + 511.9$. ***C***, Dynamic oscillator modeling firing rates. The oscillating curves were computed by fitting a waveform with an angular frequency $w = 2\pi/T$, where T is the average of the latency between the three dominant peaks with respect to CS presentation across the 10 conditioning sessions. The scale (in spikes/s) indicates mean firing rates. ***D***, Spectral powers were obtained from the curves illustrated in ***C***. On the right is shown the average from these 10 spectral powers. The average presented a maximum power of 0.54×10^4 (spikes/s)^2 and a dominant frequency of 5.86 Hz.

a broad band of frequencies between 7 and 17 Hz (Fig. 2*C*). This dominant oscillation for reflexively evoked blinks was slightly faster than that reported in a previous study, also in rabbits (4–15 Hz; Gruart et al., 2000).

Provided that all other characteristics of CS and US were maintained constant (see Materials and Methods), the percentage, profiles, and oscillatory properties of conditioned eyelid responses were highly dependent on CS-US intervals. Animals ($n = 4$) conditioned with a CS-US interval of 250 ms evoked >50% of CRs by the third conditioning session and reached asymptotic values (> 80% of CRs) by the fourth or fifth conditioning session (Fig. 2*B*). Onset latency of CRs evoked at this CS-US interval decreased through the successive conditioning sessions from 230.3 ± 19.3 ms for the first conditioning session to 118.6 ± 18.3 ms for the 10th. As described previously (Gruart et al., 2000), evoked conditioned eyelid responses also presented characteristic oscillatory profiles, but with accelerations 1/3 to 1/5 smaller than those reached by reflex eyeblinks (Fig. 2*A*). However, the spectral analysis of frequency components of conditioned eyelid responses evoked with CS-US intervals of 250 ms presented a significant peak at 11.8 ± 0.3 Hz— i.e., similar to that presented by reflexively evoked eyeblinks (Fig. 2*C*,*D*).

It was shown years ago that the optimal CS-US intervals for classical conditioning of nictitating membrane responses in rabbits ranged from 200 to 500 ms (Gormezano et al., 1983). In agreement with this early study, animals conditioned here with a CS-US interval of 500 ms achieved learning curves slightly lower than those presented by animals conditioned with an interstimulus interval of 250 ms (Fig. 2*B*). In contrast, animals conditioned with smaller (50 ms) or larger (1000 or 2000 ms) CS-US intervals presented learning curves significantly (one-way ANOVA on ranks; $p = 0.170$) lower than those of animals trained with CS-US intervals of 250 or 500 ms (Fig. 2*B*). In fact, animals trained with interstimulus intervals of 50 or 2000 ms did not reach the selected criterion (>40% of CRs by the 10th conditioning session) for the proper acquisition of this type of associative learning task.

Because the amplitude, velocity, and acceleration of conditioned eyelid responses was dependent on the selected CS-US interval (not illustrated), their respective spectral powers should also be different. Indeed, and as illustrated in Figure 2*D*, the spectral powers of conditioned eyeblinks evoked at CS-US intervals of 250 and 500 ms were significantly ($p \geq 0.01$) larger than values reached with the other three interstimulus intervals, but not different (one-way ANOVA F test; $F_{(1,1,10)} = 0.391$, $p = 0.546$) from one another. Interestingly, the dominant frequency was the same (≈12 Hz) in the other three cases (Fig. 2*D*). The scarce number of CRs (<10%) evoked during conditioning with 50 and 2000 ms of CS-US interval was too small to present any significant peak in the frequency domain (Fig. 2*D*). Pseudoconditioned animals did not present any identifiable CR.

On the whole, and consisent with previous reports in rabbits (Gruart et al., 2000) and cats (Domingo et al., 1997), conditioned eyelid responses evoked in behaving rabbits with classical conditioning procedures using delay paradigms of increasing CS-US interval can be characterized by an ≈12 Hz oscillation that is also present in reflexively evoked blinks. The next step was to determine whether these oscillatory properties could also be identified in the firing activities of rmPFC neurons.

Identification of rmPFC recorded neurons

As illustrated in Figure 1*B*, animals were prepared for unitary recordings in the rmPFC area. The histological examination of the recording sites indicated that the studied area was restricted to the rmPFC (AP = 9–11 mm, L = −1 mm, and D = 2.1–3.8 mm from bregma; Girgis and Shih-Chang, 1981; Shek et al., 1986), corresponding to the rostral aspect of Brodman's area 24 or anterior cingulate cortex and to the rostrodorsal part of Brodman's area 32 or prelimbic cortex (Fig. 1*C*,*D*). Previous histological studies (Benjamin et al., 1978; Leal-Campanario et al., 2007, 2013) have shown that this prefrontal area can be further identified by the preferential projections reaching it from the medial half of the mediodorsal thalamic nucleus.

In Figure 3*A* is illustrated an example of unitary recording in the rmPFC area during delay conditioning using a CS-US interval of 250 ms. For proper isolation and identification, recorded units were filtered, isolated, classified, and prepared for raster displays and the representation of their firing rates. The spike-sorting tools used here enabled the proper identification of the recorded unit (Fig. 3*B*). Only units with spike duration of >0.5 ms were considered pyramidal cells and further analyzed. The spontaneous firing rate of recorded cells ranged from 2 to 15 spikes/s. Characteristically, they presented spontaneous irregular bursts of activity that were similar in duration and profile to those presented by the recorded neurons across conditioning sessions. Because of their firing properties, most of the neurons analyzed here look similar to the regular-spiking, slow-adapting pyramidal cells described by Dégenètais et al. (2002)—namely, they were capable of generating a tonic firing restricted to a part of the CS-US interval in the presence of conditioned eyelid responses. Spike-triggered averaging ($n \geq 3000$ spikes) of recorded neurons did not evoke any identifiable activity in the EMG of the orbicularis oculi muscle, indicating the polysynaptic nature of rmPFC projections to facial motoneurons (not illustrated).

Firing properties of rmPFC neurons during classical eyeblink conditioning with a delay paradigm of 250 ms of CS-US interval

In Figure 3*C* are shown representative examples of three different types of rmPFC neuron recorded during delay conditioning with a CS-US interval of 250 ms. Recordings were performed during the ninth conditioning session and the three illustrated neurons were collected from two different animals. Although, according to their raster displays (>40 trials) and their averaged firing rates, the spontaneous firing of the three neurons was fairly similar, they presented a significant peak of activity at different moments of the CS-US interval. Therefore, in blue is represented the raster display and the firing rate of a neuron presenting a peak (≈45 spikes/s) of firing ≈60 ms after CS onset; in red is represented another neuron with a peak (≈37 spikes/s) of firing that happened ≈185 ms after CS presentation; finally, in green is represented a third neuron with a peak (≈48 spikes/s) of firing that happened ≈300 ms after CS presentation.

The firing rate in black illustrated in the bottom part of Figure 3*C* corresponds to the superimposition of the three colored firing rates illustrated above in the same figure. It should be noted that the three peaks of frequency took place during the CS presentation. A spectral analysis of these overlapping peaks of activity showed that peaks took place with a dominant frequency of ≈10 Hz (Fig. 3*C*, inset, bottom); that is, a value quite close to the dominant frequency (≈12 Hz) characteristic of reflex and conditioned eyelid responses (Fig. 2*A*,*C*,*D*).

In Figure 4*A* are illustrated the averaged firing rates of neurons recorded across the 10 sessions of a delay conditioning using a CS-US interval of 250 ms. Each represented colored average corresponds to ≥2 neurons recorded from the four animals included in this group. It is important to note that not a single neuron

presented more than one well defined peak (lasting from 80 to 140 ms) of frequency during the CS-US interval or that, as already shown (Leal-Campanario et al., 2013), none of them ($n = 95$ neurons, $n = 4$ rabbits) presented a sustained firing rate for the whole duration of the interstimulus interval. In contrast, there was a progressive improvement in the definition of the firing peaks across the successive training sessions (see below). In Figure 4*B* is represented the evolution in the latency of the three peaks present in the firing rate of the analyzed neurons (first peak, 29 neurons; second peak, 28 neurons; third peak, 38 neurons). As shown, no significant changes in latency with respect to CS onset were observed across conditioning sessions. In Figure 4*C* are represented 10 waveforms fitted to the three dominant peaks in frequency collected for each conditioning session. Note that the amplitude of the fitted waveforms increased with training—a fact reflected by the different powers of spectra illustrated in Figure 4*D*. In all cases, the average of the fast Fourier analysis of the 10 computed waveforms indicated the presence of a dominant frequency of 12.3 ± 0.3 Hz (Fig. 4*D*, inset).

These results prompted us to use a longer (500 ms) CS-US interval for classical conditioning to either confirm or rule out that the averaged firing of selected rmPFC neurons oscillates at a frequency independent of the interstimulus interval, as already shown for conditioned eyelid responses (Fig. 2*D*).

Firing properties of rmPFC neurons during classical eyeblink conditioning with a delay paradigm of 500 ms of CS-US interval

In Figure 5*A* are illustrated the averaged firing rates of neurons recorded across the 10 sessions of a delay conditioning using a CS-US interval of 500 ms. Each represented colored average corresponds to ≥2 neurons recorded from the four animals included in this group. Note that the dominant peaks present in the firing rates of neurons recorded during this conditioning task seem to adapt to the longer CS-US interval. Therefore, the duration of the peak increased ≈150% (120–200 ms) with respect to peak duration for the 250 ms interstimulus interval (80–140 ms). However, none of the recorded neurons ($n = 67$ neurons, $n = 4$ rabbits) presented a sustained firing rate for the whole duration of the interstimulus interval. In Figure 5*B* is represented the evolution in the latency of the three peaks present in the firing rate of the analyzed neurons (first peak, 18 neurons; second peak, 21 neurons; third peak, 28 neurons). As shown, no significant changes in latency with respect to CS onset were observed across conditioning sessions. In Figure 5*C* are represented 10 waveforms fitted to the three dominant peaks in frequency collected for each conditioning session. Note that the amplitude of the fitted waveforms increased with training, a fact reflected in the different powers of spectra illustrated in Figure 5*D*. In this case, the average of the fast Fourier analysis of the 10 computed waveforms indicated the presence of a dominant frequency of 6.2 ± 0.2 Hz (Fig. 5*D*, inset).

Consistent with the above results, the oscillatory properties of rmPFC neurons do not seem to be related to the dominant frequency of reflex and conditioned eyeblinks (i.e., 12 Hz), but do seem to be more related to CS-US intervals (≈12 Hz for 250 ms and ≈6 Hz for 500 ms). These results suggested that changes in the firing rate of rmPFC neurons could encode the duration of the selected time window and not the oscillatory properties of rabbit eyelids. Indeed, determining the duration of the CS-US interval could be important for the proper timing of the conditioned eyelid response. The difficulty to acquire conditioned eyelid responses with very short or very long CS-US (i.e., shorter or longer than 200–500 ms) has been reported repeatedly (Gormezano et al., 1983; Gruart et al., 1995, 2000).

Dependence of the oscillatory properties of rmPFC neurons on CS-US intervals

In Figure 6 are shown representative examples of averaged rmPFC neurons (≥2 collected from ≤4 animals). Recordings were performed during the eighth session of delay conditioning of different (50, 250, 500, 1000, and 2000 ms) CS-US intervals. The illustrated data show that peak firing rates of the averaged neurons occupy the CS-US interval in a definite form for 250 and 500 ms of interstimulus interval. The firing peaks of the three types of neuron ($n = 55$, $n = 4$ animals) were not so well defined for the 1000 ms CS-US interval (first peak, 17 neurons; second peak, 15 neurons; third peak, 23 neurons). Finally, neurons were nonresponding to CS-US presentations for the shortest (50 ms; $n = 41$ neurons, $n = 4$ rabbits) and the longest (2000 ms; $n = 43$ neurons, $n = 4$ rabbits) interstimulus interval. In addition, the spectral analysis indicated that the dominant frequency of the peaks in firing rate during the CS-US interval presented an inverse relationship with the interstimulus interval: 11.72 Hz for 250 ms, 5.86 for 500 ms, 2.9 Hz for 1000 ms, and 1.5 Hz for 2000 Hz. A summary of the collected results is shown in Figure 7. The mean spectral power corresponding to the different timing of peak firing rates as a function of the CS-US interval (Fig. 7*A*). It can be observed that both the power of each oscillation and its frequency decreased with the interstimulus interval (Fig. 7*B*). In contrast, although the amplitude of acceleration profiles collected from eyelid CRs for the different CS-US intervals decreased with their duration (Fig. 7*D*), the dominant frequency (≈12 Hz) remained unchanged (Fig. 7*C*).

Discussion

Main findings of the present study

Consistent with the present results, the rmPFC cortex could be involved in the determination of CS-US intervals, but as described previously (Leal-Campanario et al., 2013) and confirmed here, it is not directly involved in the acquisition process and/or in the proper execution of conditioned eyelid responses. Indeed, the discharge rate of rmPFC neurons was not related to the fixed oscillatory properties of rabbit eyelids, but modified their oscillation as a function of CS-US intervals. The more-definite oscillations presented by the rmPFC during CS-US intervals lasting for 250 and 500 ms could explain why these intervals are optimal for classical eyeblink conditioning (Gormezano et al., 1983; Gruart et al., 1995). Therefore, and in addition to the permissive/modulating role of the rmPFC in the rabbit for the generation of newly acquired motor responses (Leal-Campanario et al., 2007, 2013), rmPFC neurons could play an important role in the rabbit's ability regarding the temporal association between the CS and the US. Conversely, the determination of CS-US intervals by rmPFC neurons took place by the participation of three different types of neuron (characterized by their latency of activation to CS presentation). These results are in contrast with the persistent firing activity of other types of prefrontal neuron. For example, dorsolateral prefrontal cortex neurons show firing activities that persist during the CS-US interval in trace conditioning paradigms, helping in the generation of timed CRs (Weiss and Disterhoft, 2011). In addition, the specific population of caudal mPFC neurons recorded in rabbits also seems to bridge the temporal gap between the end of the CS and the beginning of the US during trace conditioning (Siegel et al., 2012). Therefore, as described previously (Powell et al., 2005), the firing of medial PFC

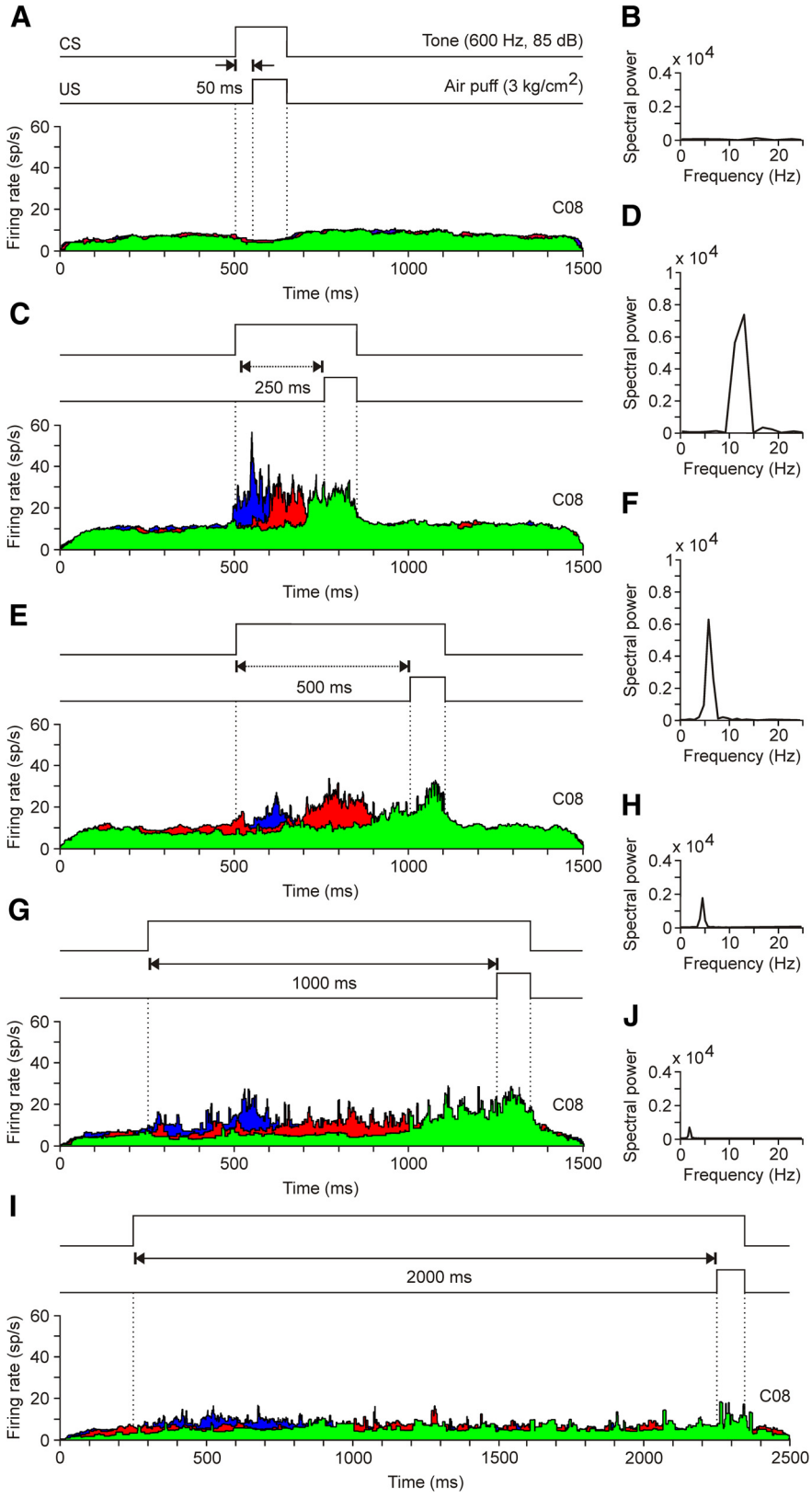

Figure 6. A comparison of the firing rates of rmPFC neurons presented during the five different CS-US intervals. ***A***, ***C***, ***E***, ***G***, ***I***, Representation of the three dominant firing rates collected during the eighth conditioning session (C08) for the five CS-US intervals used in this study. ***B***, ***D***, ***F***, ***H***, ***J***, Spectral powers of waveforms computed from the average of the latency between the peaks with respect to CS presentation (Figs. 4*C* and 5*C*). ***A***, ***B***, Note that, for this CS-US interval (50 ms), there was no activation of rmPFC neurons. ***C***, ***D***, For CS-US intervals of 250 ms, the firing rate of recorded rmPFC neurons presented a dominant frequency of 11.72 Hz [maximum power of 0.73×10^4 (spikes/s)^2]. ***E***, ***F***, In the case of CS-US intervals of 500 ms, the dominant frequency of the firing rate of rmPFC neurons went down to 5.86 Hz [maximum power of 0.59×10^4(spikes/s^2)]. ***G***, ***H***, For CS-US intervals of 1000 ms, the spectral power of the curve fitted to peak firing rates of recorded rmPFC neurons was reduced to 0.21×10^4(spikes/s)^2 and to a peak frequency of 2.9 Hz. ***I***, ***J***, The firing rate of rmPFC neurons presented a weak modulation for classical eyelid conditioning using a CS-US interval of 2000 ms. The spectral power of the curve fitted to peak firing rates was very low [0.09×10^4 (spikes/s)^2] and the peak frequency was 1.5 Hz.

neurons is not directly related to the acquisition of classical eyeblink conditioning. Consistent with this latter point, the rmPFC of subprimates is considered to be the highest level of the limbic system, as part of the orbital prefrontal cortex, and therefore involved in the accurate activation or inhibition of selected behaviors and of attentive and cognitive processes (Fuster, 2001, 2008; Kolb et al., 2004). This is probably the first report on the presence of a neural oscillator underlying the determination of time intervals during associative learning tasks, a neural process that has not been described for neurons located in the same medial prefrontal areas in primates (Fuster, 2008). This neural mechanism could also underlie the generation of hippocampal time cells (Eichenbaum, 2014; Howard and Eichenbaum, 2015).

Oscillatory properties of the eyelid motor system

The fact that reflex and conditioned nictitating membrane responses present a wavy profile was reported years ago (Berthier, 1992; Welsh, 1992) and was even observed in early classical conditioning experiments in humans (Marquis and Porter, 1939). Illustrations of reflex and conditioned nictitating membrane responses in those previous reports (Berthier, 1992; Welsh, 1992) show noticeable oscillations at 8–10.5 Hz, a value similar to the ≈8 Hz reported for eyelid movements in conditioned rabbits (Gruart et al., 2000) and close to values collected here (≈12 Hz). The dominant frequency of eyelid responses in the rabbit is ~1/3 of its resonant frequency (30–35 Hz; see Evinger et al., 1984), a finding also seen in cats (Domingo et al., 1997).

As already reported for finger movements in humans (Wessberg and Vallbo, 1995) and further confirmed here (Fig. 7*D*), larger CRs in rabbits and cats are achieved by increasing the amplitude and number of waves composing them, but not by modifying the dominant frequency of the movement (Domingo et al., 1997; Gruart et al., 2000). Therefore, the generation of a properly timed conditioned eyelid response could be envisioned as the

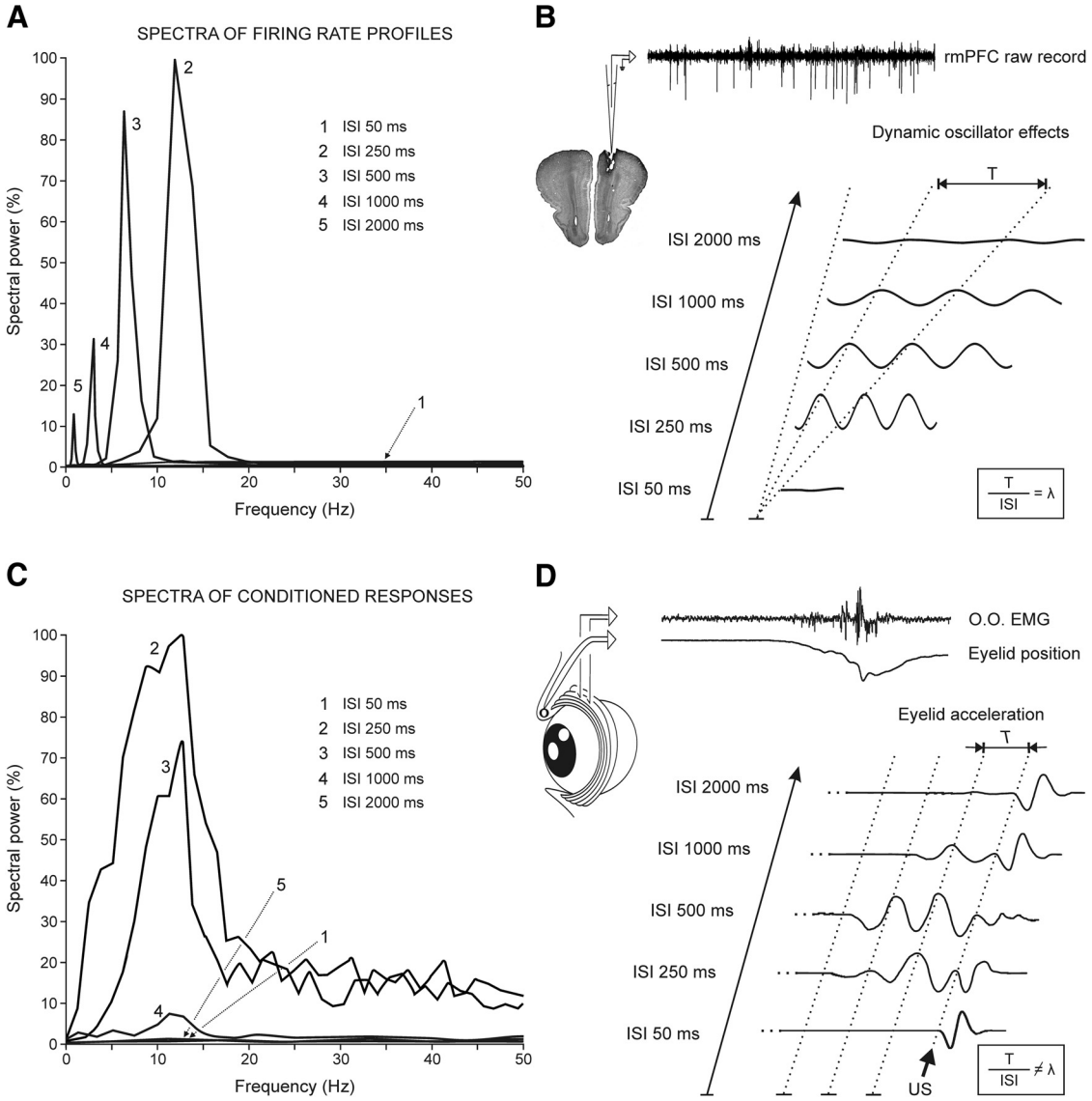

Figure 7. Comparative analysis of the frequency domains for eyelid CRs and for the firing activities of rmPFC neurons during classical conditioning. ***A***, Mean spectral powers computed from the 10 curves fitted to the dominant peaks present in the firing rates of rmPFC neurons. The five illustrated spectral powers correspond to the following CS-US intervals: 50 ms (1), 250 ms (2), 500 ms (3), 1000 ms (4), and 2000 ms (5). The 100% value for the illustrated spectral powers corresponds to 0.6×10^4 (spike/s)^2. ***B***, Representation of waveforms corresponding to the five CS-US intervals included in this study. Note that waveforms depend (in amplitude and frequency) on CS-US intervals, and *T* periods increase with the duration of interstimulus interval (ISI), consistent with a constant $\lambda = \frac{T}{ISI} \approx 0.33$. ***C***, Mean spectral powers of conditioned eyelid responses recorded with the five CS-US intervals indicated in ***A***. Each mean spectral power was obtained from ≥10 acceleration profiles recorded in ≥2 rabbits. The 100% value for the illustrated spectral powers corresponded to 0.3×10^7 (deg/s^2)^2. The code numbers (1–5) are as in ***A***. ***D***, Representation of eyelid acceleration profiles collected from the five CS-US intervals. The beginning of US presentation is indicated. Note that the periods of the accelerations do not depend on CS-US intervals $\left(\text{i.e., } \frac{T}{ISI} \neq \lambda\right)$.

process of reaching a target in a given time window with the help of a fixed-frequency neuronal oscillating machinery (Domingo et al., 1997).

Because the eyelid is load free and facial motoneurons receive no proprioceptive feedback signals from the orbicularis muscle (Porter et al., 1989; Trigo et al., 1999), it could be suggested that the oscillatory behavior of the eyelid is the result of the activity of the neuronal mechanisms controlling it. In fact, it has been shown recently in cats and rats that lid oscillations are an inherent rhythmical property of facial motoneurons innervating the orbicularis oculi muscle (Magariños-Ascone et al., 1999; Trigo et al., 1999). In addition, a noticeable oscillatory behavior has been reported in cat pericruciate cortex neurons during classical eyeblink conditioning (Aou et al., 1992) and in cat cerebellar interpositus neurons during reflexively evoked and classically conditioned eyelid responses (Gruart and Delgado-García, 1994; Jiménez-Díaz et al., 2004). These data suggested that the eyelid motor system could be controlled by a central neural oscillator tuned to the inertial and viscoelastic needs of moving appendages. However, the present results indicate that the oscillatory properties of the rmPFC reported here are not related to the proper generation of eyelid CRs, a point that is discussed below.

Putative role of the oscillatory properties of rmPFC neurons as a timing device for CS-US association

Comparing our results with similar unitary recording and/or lesion studies performed in more caudal or dorsolateral prefrontal areas, which are thought to determine the increasing relevance of

CS presentations or that present firing activities that persist during the whole CS-US interval (Weible et al., 2000, 2003, 2006; Weiss and Disterhoft, 2011; Siegel et al., 2012; Siegel and Mauk, 2013), we can suggest a differential role of rmPFC neurons in the acquisition of classical eyeblink conditioning. The possibility that the persistent neural activity recorded in both dorsolateral and caudomedial PFC during the CS-US interval could be generated by fast-spiking interneurons, but not by projecting pyramidal prefrontal neurons (Povysheva et al., 2006), should be discarded because of the low percentage (6–8%) of putative interneurons present in the rmPFC (Barthó et al., 2004; Insel and Barnes, 2015). Nevertheless, visual observation of neural discharge rates illustrated in those reports (Fig. 4*A* in Siegel et al., 2012; Fig. 4 in Siegel and Mauk, 2013; Fig. 4*A–C* in Hattori et al., 2014) indicates the presence of evident peaks and valleys in the illustrated firing profiles. Therefore, a spectral analysis of those firing profiles could perhaps present dominant frequencies similar to those reported here.

In contrast, the discharge rate of rmPFC neurons recorded in the present study was dependent on the activity of a variable oscillator that enabled the determination of CS-US intervals in an optimal range of 250–500 ms by the successive activation of three different groups of prefrontal units. Because of their spike profiles and firing properties, rmPFC neurons recorded here are similar to the rmPFC pyramidal cells described by Leal-Campanario et al. (2013). These pyramidal neurons were identified by their antidromic and/or synaptic activation from the mediodorsal thalamic nucleus. As described previously (Herry et al., 1999; Leal-Campanario et al., 2013) and confirmed by the present results, the activity of recorded rmPFC neurons during CS-US intervals was not significantly related to the percentage of CRs and/or to the area of the rectified EMG activity of the orbicularis oculi muscle.

The rmPFC of subprimates is homologous to the prefrontal orbital area of primates. Both of them receive a well defined projection from the medial half of the thalamic mediodorsal nucleus (Benjamin et al., 1978; Ray et al., 1992; Kronforst-Collins and Disterhoft, 1998; Leal-Campanario et al., 2007). The neurons recorded here are located in the rostral site of area 24 (anterior cingulate cortex) and the rostrodorsal part of area 32 (prelimbic cortex), but not in the area 24c involved in facial expression in monkeys (Buchanan et al., 1994; Morecraft et al., 2001, 2012).

Prefrontal areas 24 and 32 project to the caudate nucleus, the claustrum, and other striated areas from which prefrontal commands can reach many different sensorimotor cortical and subcortical centers (Buchanan et al., 1994; Kronforst-Collins and Disterhoft, 1998; Fuster, 2001). In addition to the mediodorsal thalamic nucleus, rmPFC areas also project to other midline thalamic nuclei, regulating unspecific sensory inputs related to attentive processes and to the presence of novel sensory stimuli. Finally, PFC neurons project to different midbrain centers, including the substantia nigra pars reticulata, which is involved in movement initiation and coordination, and the pontine nuclei projecting heavily to the cerebellar cortex and nuclei (Basso and Evinger, 1996; Basso et al., 1996; Kronforst-Collins and Disterhoft, 1998; Siegel et al., 2012). However, the peculiar discharge rates of rmPFC neurons described in this study seem to be more related to the cognitive components of classical conditioning than to the generation of conditioned eyeblinks. Neural activities shown here could reach other cortical areas more directly involved in nonmotor aspects of this type of associative learning. For example, during trace eyeblink conditioning in the rabbit, caudal areas of the anterior cingulate cortex are involved in the salience or relevance of CS presentations (Weible et al., 2003). In addition, caudal mPFC and dorsolateral PFC neurons present firing activities that persist during the CS-US interval in trace conditioning paradigms, helping in the generation of timed conditioned eyeblinks (Weiss and Disterhoft, 2011; Siegel and Mauk, 2013). Moreover, rmPFC neural signals can reach the hippocampus either directly or across the thalamic reuniens nucleus (McKenna and Vertes, 2004).

In summary, these results provide new evidence on the presence in the rmPFC of a variable oscillator that helps to determine time intervals during associative learning tasks. This neural oscillator seems to be particularly adapted to determine CS-US intervals in the range of 250–500 ms, the optimal values for the proper generation of conditioned nictitating membrane and eyelid responses in behaving rabbits and cats (Gormezano et al., 1983; Domingo et al., 1997; Gruart et al., 2000).

References

Aou S, Woody CD, Birt D (1992) Changes in the activity of units of the cat motor cortex with rapid conditioning and extinction of a compound eye blink movement. J Neurosci 12:549–559. Medline

Barthó P, Hirase H, Monconduit L, Zugaro M, Harris KD, Buzsáki G (2004) Characterization of neocortical principal cells and interneurons by network interactions and extracellular features. J Neurophysiol 92:600–608. CrossRef Medline

Basso MA, Evinger C (1996) An explanation for reflex blink hyperexcitability in Parkinson's disease. II. Nucleus raphe magnus. J Neurosci 16:7318–7330. Medline

Basso MA, Powers AS, Evinger C (1996) An explanation for reflex blink hyperexcitability in Parkinson's disease. I. Superior colliculus. J Neurosci 16:7308–7317. Medline

Benjamin RM, Jackson JC, Golden GT (1978) Cortical projections of the thalamic mediodorsal nucleus in the rabbit. Brain Res 141:251–265. CrossRef Medline

Berthier NE (1992) Muscle activity during unconditioned and conditioned eye blinks in the rabbit. Behav Brain Res 48:21–28. CrossRef Medline

Buchanan SL, Thompson RH, Maxwell BL, Powell DA (1994) Efferent connections of the medial prefrontal cortex in the rabbit. Exp Brain Res 100:469–483. CrossRef Medline

Caro-Martín CR, Sánchez-Campusano R, Delgado-García JM, Leal-Campanario R, Gruart A (2014) Spike sorting and firing rate distribution of prefrontal cortex neurons during delayed eyeblink conditioning. Acta Physiologica 52:41–42.

Caro-Martín CR, Leal-Campanario R, Sánchez-Campusano R, Delgado-García JM, Gruart A (2015) A variable oscillator underlies the measurement of time intervals in the medial prefrontal cortex during classical eyeblink conditioning in rabbits. Soc Neurosci Abstr 41:3534.

Clark GA, McCormick DA, Lavond DG, Thompson RF (1984) Effects of lesions of cerebellar nuclei on conditioned behavioral and hippocampal neuronal responses. Brain Res 291:125–136. CrossRef Medline

Dégenètais E, Thierry AM, Glowinski J, Gioanni Y (2002) Electrophysiological properties of pyramidal neurons in the rat prefrontal cortex: an in vivo intracellular recording study. Cereb Cortex 12:1–16. CrossRef Medline

Domingo JA, Gruart A, Delgado-García JM (1997) Quantal organization of reflex and conditioned eyelid responses. J Neurophysiol 78:2518–2530. Medline

Eichenbaum H (2014) Time cells in the hippocampus: a new dimension for mapping memories. Nat Rev Neurosci 15:732–744. CrossRef Medline

Elble RJ (1996) Central mechanisms of tremor. J Clin Neurophysiol 13:133–144. CrossRef Medline

Evinger C, Shaw MD, Peck CK, Manning KA, Baker R (1984) Blinking and associated eye movements in humans, guinea pigs, and rabbits. J Neurophysiol 52:323–339. Medline

Fuster JM (2001) The prefrontal cortex–an update: time is of the essence. Neuron 30:319–333. CrossRef Medline

Fuster JM (2008) The prefrontal cortex, Ed 4. London: Academic.

Girgis M, Shih-Chang W (1981) A new stereotaxic atlas of the rabbit brain. St. Louis: Warren H. Green.

Gormezano I, Kehoe EJ, Marshall BS (1983) Twenty years of classical conditioning research with the rabbit. Prog Psychobiol Physiol Psychol 10:197–275.

Gruart A, Delgado-García JM (1994) Discharge of identified deep cerebellar nuclei neurons related to eye blinks in the alert cat. Neuroscience 61:665–681. CrossRef Medline

Gruart A, Blázquez P, Delgado-García JM (1995) Kinematics of spontaneous, reflex, and conditioned eyelid movements in the alert cat. J Neurophysiol 74:226–248. Medline

Gruart A, Schreurs BG, del Toro ED, Delgado-García JM (2000) Kinetic and frequency-domain properties of reflex and conditioned eyelid responses in the rabbit. J Neurophysiol 83:836–852. Medline

Hattori S, Yoon T, Disterhoft JF, Weiss C (2014) Functional reorganization of a prefrontal cortical network mediating consolidation of trace eyeblink conditioning. J Neurosci 34:1432–1445. CrossRef Medline

Herry C, Vouimba RM, Garcia R (1999) Plasticity in the mediodorsal thalamo-prefrontal cortical transmission in behaving mice. J Neurophysiol 82:2827–2832. Medline

Howard MW, Eichenbaum H (2015) Time and space in the hippocampus. Brain Res 1621:345–354. CrossRef Medline

Insel N, Barnes CA (2015) Differential activation of fast-spiking and regular-firing neuron populations during movement and reward in the dorsal medial frontal cortex. Cereb Cortex 25:2631–2647. CrossRef Medline

Jiménez-Díaz L, Navarro-López Jde D, Gruart A, Delgado-García JM (2004) Role of cerebellar interpositus nucleus in the genesis and control of reflex and conditioned eyelid responses. J Neurosci 24:9138–9145. CrossRef Medline

Koekkoek SK, Den Ouden WL, Perry G, Highstein SM, De Zeeuw CI (2002) Monitoring kinetic and frequency-domain properties of eyelid responses in mice with magnetic distance measurement technique. J Neurophysiol 88:2124–2133. Medline

Kolb B, Pellis S, Robinson TE (2004) Plasticity and functions of the orbital frontal cortex. Brain Cogn 55:104–115. CrossRef Medline

Kronforst-Collins MA, Disterhoft JF (1998) Lesions of the caudal area of rabbit medial prefrontal cortex impair trace eyeblink conditioning. Neurobiol Learn Mem 69:147–162. CrossRef Medline

Leal-Campanario R, Fairén A, Delgado-García JM, Gruart A (2007) Electrical stimulation of the rostral medial prefrontal cortex in rabbits inhibits the expression of conditioned eyelid responses but not their acquisition. Proc Natl Acad Sci U S A 104:11459–11464. CrossRef Medline

Leal-Campanario R, Delgado-García JM, Gruart A (2013) The rostral medial prefrontal cortex regulates the expression of conditioned eyelid responses in behaving rabbits. J Neurosci 33:4378–4386. CrossRef Medline

Llinás RR (1991) The noncontinuous nature of movement execution. In: Motor control: concepts and issues (Humphrey DR, Freund HJ, eds), pp 223–242. New York: Wiley.

Louis ED (2014) Essential tremor: from bedside to bench and back to bedside. Curr Opin Neurol 27:461–467. CrossRef Medline

Magariños-Ascone C, Núñez A, Delgado-García JM (1999) Different discharge properties of dorsolateral facial nucleus motoneurons: intracellular in vitro recordings. Neuroscience 94:879–886. CrossRef Medline

Marquis DG, Porter JM (1939) Differential characteristics of conditioned eyelid responses established by reflex and voluntary reinforcement. J Exp Psychol 24:347–365. CrossRef

McKenna JT, Vertes RP (2004) Afferent projections to nucleus reuniens of the thalamus. J Comp Neurol 480:115–142. CrossRef Medline

Morecraft RJ, Louie JL, Herrick JL, Stilwell-Morecraft KS (2001) Cortical innervation of the facial nucleus in the non-human primate: a new interpretation of the effects of stroke and related subtotal brain trauma on the muscles of facial expression. Brain 124:176–208. CrossRef Medline

Morecraft RJ, Stilwell-Morecraft KS, Cipolloni PB, Ge J, McNeal DW, Pandya DN (2012) Cytoarchitecture and cortical connections of the anterior cingulate and adjacent somatomotor fields in the rhesus monkey. Brain Res Bull 87:457–497. CrossRef Medline

Múnera A, Gruart A, Muñoz MD, Fernández-Mas R, Delgado-García JM (2001) Hippocampal pyramidal cell activity encodes conditioned stimulus predictive value during classical conditioning in alert cats. J Neurophysiol 86:2571–2582. Medline

Oswald B, Knuckley B, Mahan K, Sanders C, Powell DA (2006) Prefrontal control of trace versus delay eyeblink conditioning: role of the unconditioned stimulus in rabbits (Oryctolaguscuniculus). Behav Neurosci 120:1033–1042. CrossRef Medline

Pacheco-Calderón R, Carretero-Guillén A, Delgado-García JM, Gruart A (2012) Red nucleus neurons actively contribute to the acquisition of classically conditioned eyelid responses in rabbits. J Neurosci 32:12129–12143. CrossRef Medline

Paraskevopoulou SE, Barsakcioglu DY, Saberi MR, Eftekhar A, Constandinou TG (2013) Feature extraction using first and second derivative extrema (FSDE) for real time and hardware-efficient spike sorting. J Neurosci Methods 215:29–37. CrossRef Medline

Park YG, Park HY, Lee CJ, Choi S, Jo S, Choi H, Kim YH, Shin HS, Llinas RR, Kim D (2010) Ca(V)3.1 is a tremor rhythm pacemaker in the inferior olive. Proc Natl Acad Sci U S A 107:10731–10736. CrossRef Medline

Porras-García E, Sánchez-Campusano R, Martínez-Vargas D, Domínguez-del-Toro E, Cendelín J, Vozeh F, Delgado-García JM (2010) Behavioral characteristics, associative learning capabilities, and dynamic association mapping in an animal model of cerebellar degeneration. J Neurophysiol 104:346–365. CrossRef Medline

Porter JD, Burns LA, May PJ (1989) Morphological substrate for eyelid movements: innervation and structure of primate levator palpebrae superioris and orbicularis oculi muscle. J Comp Neurol 287:64–81. CrossRef Medline

Povysheva NV, Gonzalez-Burgos G, Zaitsev AV, Kröner S, Barrionuevo G, Lewis DA, Krimer LS (2006) Properties of excitatory synaptic responses in fast-spiking interneurons and pyramidal cells from monkey and rat prefrontal cortex. Cereb Cortex 16:541–552. Medline

Powell DA, Churchwell J, Burriss L (2005) Medial prefrontal lesions and Pavlovian eyeblink and heart rate conditioning: effects of partial reinforcement on delay and trace conditioning in rabbits (Oryctolaguscuniculus). Behav Neurosci 119:180–189. CrossRef Medline

Ray JP, Russchen FT, Fuller TA, Price JL (1992) Sources of presumptive glutamatergic/aspartatergic afferents to the mediodorsal nucleus of the thalamus in the rat. J Comp Neurol 320:435–456. CrossRef Medline

Sánchez-Campusano R, Gruart A, Delgado-García JM (2007) The cerebellar interpositus nucleus and the dynamic control of learned motor responses. J Neurosci 27:6620–6632. CrossRef Medline

Shek JW, Wen GY, Wisniewski HM (1986) Atlas of the rabbit brain and spinal cord. Zurich: Karger.

Siegel JJ, Mauk MD (2013) Persistent activity in prefrontal cortex during trace eyelid conditioning: dissociating responses that reflect cerebellar output from those that do not. J Neurosci 33:15272–15284. CrossRef Medline

Siegel JJ, Kalmbach B, Chitwood RA, Mauk MD (2012) Persistent activity in a cortical-to-subcortical circuit: bridging the temporal gap in trace eyelid conditioning. J Neurophysiol 107:50–64. CrossRef Medline

Su CK, Chiang CH, Lee CM, Fan YP, Ho CM, Shyu LY (2013) Computational solution of spike overlapping using data-based subtraction algorithms to resolve synchronous sympathetic nerve discharge. Front Comp Neurosci 7:149. CrossRef Medline

Takehara-Nishiuchi K, Kawahara S, Kirino Y (2005) NMDA receptor-dependent processes in the medial prefrontal cortex are important for acquisition and the early stage of consolidation during trace, but not delay eyeblink conditioning. Learn Mem 12:606–614. CrossRef Medline

Trigo JA, Gruart A, Delgado-García JM (1999) Discharge properties of abducens, accessory abducens, and orbicularis oculi motoneurons during unconditioned and conditioned eye blinks in the alert cat. J Neurophysiol 81:1666–1684. Medline

Volkmann J, Joliot M, Mogilner A, Ioannides AA, Lado F, Fazzini E, Ribary U, Llinás R (1996) Central motor loop oscillations in parkinsonian resting tremor revealed by magnetoencephalography. Neurology 46:1359–1370. CrossRef Medline

Weible AP, McEchron MD, Disterhoft JF (2000) Cortical involvement in acquisition and extinction of trace eyeblink conditioning. Behav Neurosci 114:1058–1067. Medline

Weible AP, Weiss C, Disterhoft JF (2003) Activity profiles of single neurons in caudal anterior cingulate cortex during trace eyeblink conditioning in the rabbit. J Neurophysiol 90:599–612. CrossRef Medline

Weible AP, O'Reilly JA, Weiss C, Disterhoft JF (2006) Comparisons of dorsal and ventral hippocampus cornu ammonis region 1 pyramidal neuron activity during trace eye-blink conditioning in the rabbit. Neuroscience 141:1123–1137. Medline

Weiss C, Disterhoft JF (2011) Exploring prefrontal cortical memory mechanisms with eyeblink conditioning. Behav Neurosci 125:318–326. CrossRef Medline

Welsh JP (1992) Changes in the motor pattern of learned and unlearned responses following cerebellar lesions: a kinematic analysis of the nictitating membrane reflex. Neuroscience 47:1–19. CrossRef Medline

Wessberg J, Vallbo AB (1995) Coding of pulsatile motor output by human muscle afferents during slow finger movement. J Physiol 485:271–282. CrossRef Medline